

Electronic Thesis and Dissertation Repository

5-18-2011 12:00 AM

Mechanisms of Atrial Arrhythmia: Investigations of the Neuro-Myogenic Interface in the Mouse

Jari Michael Tuomi, *University of Western Ontario*

Supervisor: Dr. Doug Jones, *The University of Western Ontario*

A thesis submitted in partial fulfillment of the requirements for the Doctor of Philosophy degree in Physiology

© Jari Michael Tuomi 2011

Follow this and additional works at: <https://ir.lib.uwo.ca/etd>



Part of the [Circulatory and Respiratory Physiology Commons](#), and the [Physiological Processes Commons](#)

Recommended Citation

Tuomi, Jari Michael, "Mechanisms of Atrial Arrhythmia: Investigations of the Neuro-Myogenic Interface in the Mouse" (2011). *Electronic Thesis and Dissertation Repository*. 181.
<https://ir.lib.uwo.ca/etd/181>

This Dissertation/Thesis is brought to you for free and open access by Scholarship@Western. It has been accepted for inclusion in Electronic Thesis and Dissertation Repository by an authorized administrator of Scholarship@Western. For more information, please contact wlsadmin@uwo.ca.

**MECHANISMS OF ATRIAL ARRHYTHMIA: INVESTIGATIONS OF THE
NEURO-MYOGENIC INTERFACE IN THE MOUSE**

(Spine title: Investigations of Atrial Arrhythmia in the Mouse)

(Thesis format: Integrated Article)

by

Jari Michael Tuomi

Graduate Program in Physiology

A thesis submitted in partial fulfillment
of the requirements for the degree of
Doctor of Philosophy

The School of Graduate and Postdoctoral Studies
The University of Western Ontario
London, Ontario, Canada

© Jari Tuomi 2011

THE UNIVERSITY OF WESTERN ONTARIO
School of Graduate and Postdoctoral Studies

CERTIFICATE OF EXAMINATION

Supervisors

Dr. Doug Jones

Dr. Stephen Sims (Co-Supervisor)

Supervisory Committee

Dr. Peter Chidiac

Dr. Gerard Guiraudon

Dr. Stan Leung

Examiners

Dr. Qingping Feng

Dr. Dale Laird

Dr. Subrata Chakrabarti

Dr. Peter Backx

The thesis by

Jari Michael Tuomi

entitled:

Mechanisms of Atrial Arrhythmia: Investigations of the Neuro-Myogenic Interface in the Mouse

is accepted in partial fulfillment of the
requirements for the degree of
Doctor of Philosophy

Date _____

Chair of the Thesis Examination Board

Abstract

Arrhythmia mechanisms rely on multiple factors including structural (myogenic), nervous (neurogenic), and interrelated (the neuro-myogenic interface) factors. I hypothesized that due to this neuro-myogenic interface, the intrinsic cardiac autonomic nervous system (ICANS) is involved in most atrial arrhythmias. This thesis also provides a "Threshold Model" as a tool to assess the role of different physiological factors influencing arrhythmia. This model allows relative comparison and interpretation of the role of various factors influencing arrhythmogenesis. The mouse allows relatively simple manipulation of genes to determine their role in arrhythmia. This thesis determined what atrial arrhythmias are inducible in the mouse (in vivo) and how to systematically study those arrhythmias. I found that atrial tachycardia/fibrillation (AT/F) and junctional tachycardia (JT) are inducible in the mouse. AF and JT pose significant clinical challenges as many patients do not respond well to current interventions. Neurogenic AF relies on acetylcholine, while myogenic AF relies, in part on gap junctions formed by connexins (Cxs). The atria has muscarinic M2 and M3 receptors. The duration of M2R/M3R G protein signalling is regulated by GTP hydrolysis, a process accelerated by the regulators of G protein signalling (RGS). RGS2 deficient ($RGS2^{-/-}$) mice had reduced refractory periods that were normalized with a selective M3R blocker (Darifenacin) and increased susceptibility to AT/F induction compared to littermates. For the first time, this showed a role of M3 and RGS in atrial arrhythmia. Cx40 deficient ($Cx40^{-/-}$) mice were protected from carbachol induced AT/F, while Cx43 G60S mutant ($Cx43^{G60S/+}$) mice, with an 80% reduction in phospho-Cx43 in the atria were highly susceptible to AT/F that was terminated by darifenacin. This shows a novel neurogenic component to what was previously described as myogenic arrhythmia. Another novel finding was that JT has a neurogenic component, resulting from inappropriate AV nodal pacemaker activation initiated

by autonomics. Ivabradine hydrochloride, a selective pacemaker channel blocker, prevented JT and may be useful in patients with JT.

In conclusion, this thesis has provided novel findings of the vital role of the neuro-myogenic interface in atrial arrhythmias and has provided the basis for future investigations of potential therapeutic options for patients.

STATEMENT OF CO-AUTHORSHIP

The studies performed in **Chapters 2-4** were performed by Jari Tuomi in the laboratory of Dr. Doug Jones, with the assistance of the co-authors listed below.

Dr. Doug Jones contributed to experimental design, data interpretation, and manuscript preparation for all the studies in this thesis. My advisory committee consisting of Dr. Stephen Sims, Dr. Peter Chidiac, Dr. Gerard Guiraudon, and Dr. Stan Leung provided intellectual guidance during my studies.

Chapter 2: Dr. Chidiac provided the RGS2^{-/-} mice, provided intellectual guidance and contributed to manuscript preparation.

Chapter 3: Dr. Karl Tysl provided the Cx40^{-/-} mice and critically reviewed the manuscript before publication.

Chapter 4: Sarah Detombe performed the CT imaging of catheter location in the lab of Dr. Maria Drangova.

ACKNOWLEDGEMENTS

I would like to thank my supervisor and mentor Dr. Doug Jones for giving me freedom to grow, for always being available to discuss various issues, and for his constant support and guidance. My experience working with Doug as a 4th year undergraduate thesis student drove my interest to pursue graduate studies. You are one of the most patient individuals I have ever met. I have learned much from your example. Not only did you help me grow as an independent scientist, you helped me see the world. Thank you for everything you have done for me.

I would like to thank Dr. Peter Chidiac who always had an open door to discuss G protein signalling with me. Dr. Chidiac opened his lab to me, supported my travel to the American Heart Association conference in Orlando Florida, and acted as an unofficial co-supervisor to my studies. He is one of the kindest people I have met, an excellent scientist, and a great example.

Thank you to my advisory committee Dr. Stephen Sims, Dr. Peter Chidiac, Dr. Gerard Guiraudon, and Dr. Stan Leung for your valuable input and suggestions throughout my studies.

I would also like to thank all the members of the department who have made my thesis possible. Thank you Dr. Gerald Kidder for providing the Cx43^{G60S/+} mutant mice. Thank you Dr. Robert Gros for your assistance performing the blood pressure measurements in the conscious Cx40^{-/-} mice.

Finally, I want to thank all of my friends for your support and for all the great times we shared during our studies.

DEDICATION

I dedicate my thesis to my family who for my entire life have supported and encouraged me in all my pursuits.

To my mother, Margaret Tuomi, and father, Chris Tuomi, thank you for being my example of hard work, providing the environment where I could grow my curiosity, and always pushing me to be better than I am. I love you both.

To Jonathan Tuomi, my older brother, you are my trail blazer always going first and showing me what life can and should be. I hope I can one day have the same loving family you do. To my nephew, Mitchell Tuomi, I hope your life is filled with happiness, and that you are passionate and successful in whatever you pursuit

Finally, I would like to include some words my late grandfather, Mike Anich, left me in a card on my graduation from elementary school. His words were a great source of inspiration to me.

Dear Jari, I hope you do well in years to come. I know you will. I didn't have the opportunity to continue my education as my father couldn't afford to send me to University.. I do hope you make it. Here is a little poem.

"I slept and dreamt that life was beauty;
I woke, and found that life was duty.
Was thy dream than a shadowy lie?
Toil on, poor heart unceasingly;
And thou shalt find thy life to be
A truth and noon day light to thee."

Life of Duty, Ellen Sturgis Hooper

Table of contents

TITLE PAGE.....i

CERTIFICATE OF EXAMINATIONii

ABSTRACT.....iii

STATEMENT OF CO-AUTHORSHIP..... v

ACKNOWLEDGEMENTS..... vi

DEDICATION.....vii

TABLE OF CONTENTSviii

LIST OF TABLES.....xiii

LIST OF FIGURES.....xiv

LIST OF ABBREVIATION, SYMBOLS AND NOMENCLATURExvi

CHAPTER 1: LITERATURE REVIEW..... 1

1.0 OVERVIEW 1

1.1 ELECTRICITY IN THE HEART 2

1.1.1 The Fast Response Cardiac Action Potential..... 2

1.1.2 The Slow Response Cardiac Action Potential 4

1.1.3 Determinants Of Cardiac Excitability..... 5

1.1.4 Determinants Of Cardiac Conduction 8

1.2 AUTONOMIC REGULATION OF CARDIAC ACTIVITY 11

1.2.1 Anatomy Of Cardiac Autonomic Innervation 11

1.2.2 G Protein-Coupled Receptor Signalling 12

1.2.3 Atrial Muscarinic Acetylcholine Receptors And Effectors..... 14

1.2.4 Atrial Regulators of G Protein Signalling (RGS) Proteins 18

1.3 CLASSIFICATION OF SUPRAVENTRICULAR TACY-ARRHYTHMIAS 21

1.4 ABNORMAL IMPULSE INITIATION 22

1.5 ABNORMAL IMPULSE PROPAGATION (REENTRY)	24
1.6 ATRIAL TACHYCARDIA/FIBRILLATION	28
1.7 RATIONALE	34
1.8 SUMMARY OF HYPOTHESES AND OBJECTIVES	37
<i>1.8.1 Hypotheses</i>	37
<i>1.8.2 Objectives</i>	37
1.9 REFERENCES	37
CHAPTER 2: Evidence for enhanced M3 muscarinic receptor function and sensitivity to atrial arrhythmia in the RGS2 deficient mouse	49
2.0 CHAPTER SUMMARY	49
2.1 INTRODUCTION	50
2.2 METHODS	52
<i>2.2.1 Animals And Preoperative Procedures</i>	52
<i>2.2.2 Surface Limb Lead Electrocardiograms (ECG)</i>	53
<i>2.2.3 In Vivo Intracardiac Electrophysiology Studies</i>	53
<i>2.2.4 Catheter Positioning</i>	53
<i>2.2.5 Pacing Protocols</i>	54
<i>2.2.6 Arrhythmia Induction</i>	54
<i>2.2.7 Effects of muscarinic receptor drugs</i>	54
<i>2.2.8 RNA Isolation And Real Time RT-PCR</i>	56
<i>2.2.9 Statistical Analysis</i>	56
2.3 RESULTS	57
<i>2.3.1 Atrial Effective Refractory Periods</i>	57
<i>2.3.2 Atrial Tachyarrhythmia Induction</i>	59
<i>2.3.3 Mechanism Of Arrhythmia (Evidence For Re-Entry)</i>	62
<i>2.3.4 Expression Of M2, M3 And M4 Receptors And RGS2 And RGS4 mRNA</i>	64
<i>2.3.5 Effects Of Body Temperature</i>	64

2.4 DISCUSSION.....	67
2.5 CLINICAL RELEVANCE.....	71
2.6 LIMITATIONS.....	71
2.7 REFERENCES	72
CHAPTER 3: Atrial Tachycardia/Fibrillation in the Connexin 43 G60S Mutant (Oculodentodigital Dysplasia) Mouse	77
3.0 CHAPTER SUMMARY.....	77
3.1 INTRODUCTION	78
3.2. METHODS.....	80
<i>3.2.1 Animals And Preoperative Procedures</i>	<i>80</i>
<i>3.2.2 Surface Limb Lead Electrocardiograms (ECG)</i>	<i>81</i>
<i>3.2.3 Blood Pressure And Conscious Restrained Heart Rates.....</i>	<i>81</i>
<i>3.2.4 In Vivo Intracardiac Electrophysiology Studies</i>	<i>81</i>
<i>3.2.5 Pacing Protocols.....</i>	<i>81</i>
<i>3.2.6 Arrhythmia Induction Protocols</i>	<i>82</i>
<i>3.2.7 Epicardial Left Atrial Recordings.....</i>	<i>82</i>
<i>3.2.8 Statistical Analysis</i>	<i>84</i>
3.3 RESULTS.....	84
<i>3.3.1 Standard Electrophysiological Parameters.....</i>	<i>84</i>
<i>3.3.2 Effective Refractory Periods.....</i>	<i>84</i>
<i>3.3.3 Cardiac Hypertrophy/Hypertension.....</i>	<i>85</i>
<i>3.3.4 Atrial Tachyarrhythmia Induction</i>	<i>85</i>
<i>3.3.5 Electrogram Analysis</i>	<i>91</i>
<i>3.3.6 Left Atrial Recordings</i>	<i>93</i>
3.4 DISCUSSION.....	96
3.5 LIMITATIONS.....	101
3.6 REFERENCES	101

CHAPTER 4: Junctional Tachycardia in the Mouse is Prevented by Pacemaker

Channel (If) Blockade.....	106
4.0 CHAPTER SUMMARY.....	106
4.1 INTRODUCTION	107
4.2 METHODS	111
4.2.1 <i>Animals.....</i>	<i>111</i>
4.2.2 <i>In Vivo Intracardiac Electrophysiology Studies</i>	<i>111</i>
4.2.3 <i>Blood Pressure.....</i>	<i>112</i>
4.2.4 <i>Pharmacological Tests</i>	<i>113</i>
4.2.5 <i>Statistical analysis.....</i>	<i>113</i>
4.3 RESULTS.....	113
4.3.1 <i>Antegrade AV nodal conduction</i>	<i>113</i>
4.3.2 <i>Functional Longitudinal Dissociation Of The His Bundle (FP vs SP conduction)</i>	<i>115</i>
4.3.3 <i>Junctional arrhythmia</i>	<i>116</i>
4.3.4 <i>Diagnostic Pacing Studies.....</i>	<i>116</i>
4.3.5 <i>Blood Pressure Measurements</i>	<i>119</i>
4.3.6 <i>AV Nodal Conduction Times</i>	<i>122</i>
4.3.7 <i>Subthreshold Stimulation.....</i>	<i>122</i>
4.3.8 <i>Vagal Nerve Stimulation.....</i>	<i>122</i>
4.3.9 <i>Pharmacological Tests Of Baroreflex Involvement</i>	<i>123</i>
4.3.10 <i>His Bundle Electrograms Amplitude Alterations During JT vs Sinus Rhythm.</i>	<i>123</i>
4.3.11 <i>Activation Patterns During JT.....</i>	<i>124</i>
4.3.12 <i>Pharmacological Tests Of Pacemaking</i>	<i>124</i>
4.3.13 <i>RGS2 Deficient Mice.....</i>	<i>126</i>
4.4 DISCUSSION.....	127
4.5 REFERENCES	132
CHAPTER 5: DISCUSSION	137

5.1 SUMMARY AND MAJOR FINDINGS.....	Error! Bookmark not defined.138
5.2 LIMITATIONS.....	145
5.3 REFERENCES	Error! Bookmark not defined.147
APPENDIX I.....	150
APPENDIX II	185
CURRICULUM VITAE.....	186

LIST OF TABLES

Table 2.1: Intracardiac electrophysiological values recorded in the absence and presence of carbachol and atropine in 1 month old male RGS2 ^{-/-} and wild type mice.	58
Table 2.2: Incidence of AT/F induced by PES or burst pacing and maximum duration of induced AT/F with either PES or burst pacing induction.	63
Table 3.1: Intracardiac electrophysiological values recorded in the absence and presence of carbachol in 6-mo-old male Cx40 ^{-/-} and C57BL/6 wild-type mice.	86
Table 3.2: Intracardiac electrophysiological values recorded from 6-mo-old male Cx43 ^{G60S/+} and Cx43 ^{+/+} mice	86
Table 4.1: Basic electrophysiological values (in ms) in 6-mo-old male C57BL/6 mice recorded in the absence and presence of: Carbachol; Atropine, and Propranolol	121

LIST OF FIGURES

Figure 1.1: The Cycle of Arrhythmogenesis.....	32
Figure 2.1: Photograph of the 2F octapolar stimulation / recording / drug infusion catheter (CIB'ER Mouse®, NuMED Inc., Hopkinton, NY) used for intracardiac electrophysiological studies in the mouse.....	55
Figure 2.2: Atrial effective refractory period (AERP) was measured using programmed electrical stimulation (PES) with a 100ms drive train in 1-mo-old male wild type compared RGS2 ^{-/-} mice.....	60
Figure 2.3: Atrial tachycardia/fibrillation (AT/F) induced with burst pacing (Burst) of the mid right atrium (MRA) in a 1-mo-old wild-type (WT) mouse	61
Figure 2.4: Programmed electrical stimulation (PES)-induced atrial tachycardia/fibrillation (AT/F) with a single extrastimulus (S2) in a 1-mo-old RGS2 ^{-/-} mouse	65
Figure 2.5: Quantitative real time reverse transcriptase polymerase chain reaction (qRT-PCR) determination of M2 and M3 receptor mRNA content in the atria of 1-mo-old wild-type (WT) mice	66
Figure 2.6: Relative mRNA expression as a ratio of the normalized gene of interest (GOI) relative to a house keeper gene (GAPDH) compared to either RGS4 (A) or M3R (B) in the left atrium, using the following equation: $[N0(GOI)/N0(GAPDH)]/[N0(M3R \text{ or } RGS4)]$..	68
Figure 3.1: induction of atrial fibrillation (AT/F) with a single atrial stimulus (SAS) delivered during sinus rhythm in a 6-mo-old male Cx43 ^{G60S/+} mouse	83
Figure 3.2: Incidence of AT/F-induced PES or burst pacing in 6-mo-old male wild-type (WT) and Cx40 ^{-/-} mice	88
Figure 3.3: Incidence of AT/F induced by a SAS, PES, and burst pacing in 6-mo-old male Cx43 ^{+/+} littermate and Cx43 ^{G60S/+} mice.....	90
Figure 3.4: Morphology of fractionated bipolar electrograms (FEs) in mice recorded during sinus rhythm and electrically induced AT/F	92
Figure 3.5: Classification of electrogram activation patterns during AT/F in Cx43 ^{G60S/+} , Cx43 ^{+/+} , and WT mice with carbachol-induced AT/F.....	94
Figure 3.6: Recording from epicardial electrodes during AT/F in mechanically ventilated Cx43 ^{G60S/+} mice	95
Figure 4.1: A diagrammatic representation of the structure of the atrial inputs to the AV node from optical mapping data adapted from Wu & Zipes.....	108

Figure 4.2: Photograph of the 2F octapolar recording catheter used for intracardiac pacing and recording experiments in the mouse	114
Figure 4.3: An antegrade AV nodal conduction curve in a mouse with discontinuous AV nodal conduction	117
Figure 4.4: Single AV nodal reentrant beats were observed during recording of antegrade AV nodal conduction.....	118
Figure 4.5: Ventricular Burst Pacing induced Junctional Arrhythmia in a mouse	120
Figure 4.6: Evidence for a shifting junctional pacemaker locus along the slow pathway region in the mouse	125

LIST OF ABBREVIATIONS, SYMBOLS AND NOMENCLATURE

AC	adenylyl cyclase
AERP	atrial effective refractory period
AF	atrial fibrillation
AH ₁₀₀	drive cycle length of 100 ms
AHERP	high right atrial effective refractory period
AH	atrial hisian interval
AMERP	mid right atrium efficiency refractory period
AT/F	atrial tachycardia/fibrillation
AVNERP	AV nodal effective refractory period
AVN	artioventricular node
AVNRT	atrioventricular nodal re-entrant tachycardia
cAMP	cyclic AMP
CCh	carbachol
CFAE	complex fractionated atrial electrograms
CI	confidence interval
CL	cycle length
Cx43 ^{-/-}	Cx43 deficient
Cx43 ^{G60S/+}	Cx43 G60S
Cxs	Connexins
DPCPX	8-cyclopentyl-1,3-dipropylxanthine
ECG	electrocardiograms
ERP	the effective refractory period

FE	fractional electrograms
FP	fastpathway
GIRK4 ^{-/-}	GIRK3.4 knock out
Gj	junctional conductance
GOI	gene of interest
GPCR	G-protein coupled receptors
HBE	his bundle region electrogram
HRA	high right atrial/superior vena cava region
HV	his ventricular
ICANS	intrinsic cardiac autonomic nervous system
IP	intermediate pathway
JT	junctional tachycardia
LL1	limb lead I
M3R	G α q-coupled M3 muscarinic receptors
M2R	G α i/o-coupled M2 receptors
MRA	mid right atrium
ODDD	<i>Oculodentodigital dysplasia</i>
PES	programmed electrical stimulation
PNE	peripheral nodal extension
PUFA	n3-polyunsaturated fatty acids
RA	right atrium
REST	relative expression software tool
RGS	regulator of G protein signalling
RGS2 ^{-/-}	regulator of G protein signalling 2 knock out

RV	right ventricle
RVP	rapid ventricular pacing
S1	drive train stimuli
S2	single extra stimulus
S1S2	coupling interval of the S1 and S2 stimuli
SAN	sinoatrial nodal
SAS	single atrial stimuli
SIU5	stimulus isolation unit
SP	slow pathway
VERP	ventricle effective refractory period
WCL	Wenkebach cycle length
WT	wild type

CHAPTER 1: LITERATURE REVIEW

1.0 OVERVIEW

The focus of this thesis is the study of atrial arrhythmia (in vivo) in the mouse. An adequate understanding of the various mechanisms of arrhythmia necessitates a brief discussion of the electrical origins of the cardiac action potential, with the interspecies variation in the expression levels and subtypes of ion channels and transporters being of particular interest. These differences are responsible for the different morphology of action potentials within different areas of the heart and between species. The interspecies differences in cardiac action potential morphology (due to differences in underlying currents) may obscure the extrapolation to humans of data such as that obtained from phenotyping genetically altered mice. Not only does the mouse heart beat ~10 times faster than the human heart, the action potential morphology is more triangular in shape and is almost 10 times shorter in duration. However, the ease of performing genetic alterations in the mouse provides a unique and powerful tool for extrapolating the function of specific genes in regulating cardiac excitability and arrhythmogenesis to the human, that is not yet readily available in other model organisms (sheep, dog, pig, rabbit, rat). However, the question has been raised as to whether or not the mouse is an appropriate model for investigating cardiac arrhythmia⁹³. At the cellular level attempts have been made to anthropomorphize the mouse cardiomyocyte action potential, using a novel dynamic patch clamp method¹, to behave like human cardiomyocytes. While this has potential for bridging the gap between studies in mouse and human at the cellular level, results gained from whole animal studies, while potentially informative, must be interpreted with caution. This however, has not stopped research into arrhythmia mechanisms using mouse models, as evidenced by an ever

expanding scientific literature on the subject. This thesis attempted to hone the use of whole animal (mouse) electrophysiological investigations, while exploring specific genetic factors influencing the neurogenic and myogenic components and their interrelationship, (the neuro-myogenic interface) in atrial arrhythmia. In the following section, the electricity in the heart will be discussed with a focus on the major ionic constituents of the cardiac action potential, cardiac excitability and impulse conduction. Detailed comparisons of mouse and human cardiac action potentials are available elsewhere⁹³.

1.1 ELECTRICITY IN THE HEART

1.1.1 The Fast Response Cardiac Action Potential

Cardiac action potentials (AP) can be divided into two types, the fast response and the slow response types. Fast response action potentials occur in atrial, ventricular and Purkinje cells. Slow response action potentials are observed in the sinoatrial (SA) and atrioventricular (AV) nodes and will be discussed in the next section. The cardiac action potential has 5 phases which are characterized by the dominant ion channel conductance during that phase. The action potential is initiated during phase 0, where the upstroke velocity (V_{max}) of the AP characterizes the specific cardiac cell type as having either a fast or slow response. Fast response human and mouse myocardial cells have a rapid upstroke (human= 216 V/s^{27} , mouse= 278 V/s^{94}) produced by high conductance sodium channels (I_{Na}). The membrane potential becomes maximally depolarized ($\sim 20\text{mV}$) during phase 1 which is followed by a brief rapid repolarization due to activation of the transient outward potassium current (I_{to}). The plateau phase (phase 2) is determined by a balance of inward calcium depolarizing current ($I_{Ca,L}$) and outward potassium hyperpolarizing currents (I_{Ks} , I_{Kr} , I_{K1}). The interspecies variation in AP morphology is primarily due to these differences in the duration of the calcium

mediated plateau phase⁹³ which is an important component of the long action potential duration (APD) observed in human ($APD_{90} = 297 \text{ ms}^{27}$), relative to the mouse ($APD_{90} = 37.4 \text{ ms}^{94}$). Rapid repolarization occurs during phase 3 as calcium channels close, allowing the outward conducting potassium channels to act unopposed. The delayed rectifier potassium channels (I_{Ks} , I_{Kr}) in humans close during phase 3 and I_{K1} becomes the dominant current at the end of phase 3 returning the cell to its resting membrane potential (RMP, phase 4). At the RMP, myocardial cells are almost exclusively permeable to potassium ions K^+ , which drive the RMP close to the equilibrium potential for K^+ ($E_k = -94 \text{ mV}$). The RMP of the human atrial myocardial cell was found to be -81.2 mV^{27} , while the mouse is -76.8 mV^{94} . During phase 4, the sodium channels inactivation gates move to the permissive position due to the hyperpolarized RMP and thus are prepared to fire another action potential. Following activation, all excitable cells enter a period in which another activation is impossible, known as the refractory period. The refractory period is divided into an absolute and a relative refractory period. No action potential can be generated during the absolute refractory period no matter the stimulus intensity due to the closure of the Na channels inactivation gate. The relative refractory period is determined by the time frame in which an action potential can be generated by a supernormal stimulus, and results from an incomplete recovery of Na^+ channel from their inactivated state and a greater than normal (at rest) outward potassium conductance. All phases of the atrial cardiac action potential are sensitive to autonomic regulation by acetylcholine. Importantly phase 4 is modified by activation of M2 muscarinic receptors and downstream G protein gated inward rectifier potassium channels ($GIRK1/4$ or $I_{K, ACh}$). $I_{K, ACh}$ activation hyperpolarizes the resting membrane potential, having significant effects on the refractory period and thereby the duration of the AP. The autonomic "neurogenic" regulation of the cardiac action potential is an important factor regulating

electrophysiological properties and susceptibility to atrial arrhythmia and will be discussed in great detail in coming sections as well as in **Chapter 2** of this thesis.

1.1.2 The Slow Response Cardiac Action Potential

Slow response cardiac action potentials of SA and AV nodal cells are so named due to the slow rate of rise (V_{max}) of the action potential in phase 0, relative to that of fast response cells. Slow response cells have limited Na^+ channel expression and so phase 0 responses are "slow" as they are carried by low conductance L-Type and T-Type Calcium (Ca^{2+}) Channels ($I_{Ca,L}$) ($I_{Ca,T}$). Patch-clamp studies in isolated AVN cells show that $I_{Ca,L}$ is a major constituent of the action potential (AP) upstroke^{63, 86}, while I_{Kr} contributes to both AP repolarization and diastolic depolarization. The maximal diastolic potential of slow response SA and AV nodal cells are variable ranging from about -50 to -65 mV. In the rabbit, two morphologically distinct populations of AVN cells were identified: ovoid cells which had Nodal or Nodal-His-like AP configurations, and rod-shaped cells that are Atrial-Nodal-like⁸⁶. The rapid inward sodium current (I_{Na}) was found in all rod-shaped cells but in only 30% of ovoid cells. The diastolic membrane potential of SA and AV nodal cells is unstable and spontaneously depolarizes at rest, forming the basis of the intrinsic cardiac pacemaking activity. Genetic markers of pacemaking tissue (high: Cx30.2/Cx45/ HCN4/Tbx3, low: Cx40/Cx43/SCN5a) are expressed in both the mouse SA and AV node²¹. The I_f channel density is much greater in the SAN¹², than the dominant AVN pacemaker region⁷², located in the posterior nodal extension³⁵. This suggests that I_f channel expression density correlates with intrinsic pacemaker rate. The human AVN also contains HCN4, with little HCN4 detected in the surrounding atrium¹³². Diastolic depolarization occurs in 2 phases, the early and late phase. A net inward current at rest is generated during these phases by two biological clocks named the membrane clock and the intracellular calcium clock. Interaction

between these two clocks (mutual entrainment) is the foundation of the proposed coupled clock pacemaker system⁷⁰, allowing membrane events to regulate cytosolic function and vice versa. The membrane clock (M clock) initiates the early phase 4 diastolic depolarization due to the interplay of many time and voltage dependent ion channels. The M clock is formed by L-type Ca^{2+} channels (I_{CaL}), T-type Ca^{2+} channels (I_{CaT}), delayed rectifier K^+ channels (I_{K}), Na/ Ca^{2+} exchanger (NCX) (I_{NCX}), and Na/K ATPase (I_{NaK}) and importantly the hyperpolarization-activated cyclic nucleotide-gated pacemaker funny channel (I_{f}). The Ca^{2+} clock operates based on the rhythmic oscillation of local Ca^{2+} release from the sarcoplasmic reticulum (SR) due to the interplay and status/function of SR calcium pumps (SERCA), calcium release channels, and ryanodine receptors (RyR)⁷⁰. Spontaneous release of calcium raises cytosolic calcium levels to regulate activation of an inward $\text{Na}^+/\text{Ca}^{2+}$ exchange current (I_{NCX}) which greatly contributes to the exponential rise in membrane potential during the late diastolic depolarization⁷⁰. Autonomic nervous regulation of these 2 mechanisms is important for normal heart rate control and response during rest and exercise⁷⁰. The role of the autonomic/neurogenic influences in pacemaking will be discussed in following sections as well as in **Chapter 4** of this thesis.

1.1.3 Determinants Of Cardiac Excitability

Cardiac excitability can be defined as the ability of a cell to fire an action potential. Excitability is characterized by "the threshold response elicited by a square-wave stimulus of appropriate amplitude (strength) and time (=duration or pulse width)"⁴⁴. Excitability of cardiac cells was examined by Cabo and Rosenbaum¹⁶ using the DiFrancesco-Nobel cardiac membrane model²⁹. Excitability was determined by plotting combinations of values of electrical stimulus strength versus duration to form a "strength-duration curve", where values above the curve indicate the cell is excited. This concept becomes important when

considering source-sink relationships (due to excitatory inward currents and passive electrical properties respectively) and local current responses involved in influencing excitability and impulse propagation.

The level of cell excitability changes during the action potential, decreasing upon depolarization and gradually increasing upon repolarization. Excitability is therefore ". . . a measure of the current condition of the cell and how easy it is to generate an action potential"¹⁶. This effect of: ". . . the current condition of a cell . . ." can be observed by changing the timing of delivery of successive cardiac impulses, which illustrates the existence of a "rate-dependence" of cardiac electrical function (e. g. decremental conduction) and arrhythmia susceptibility, which is discussed throughout this thesis. Similar to the strength-duration curve, excitability can be measured by plotting the minimum current stimulus required to elicit an action potential against the timing or coupling interval of the previous action potential, forming the "strength-interval curve". Following complete repolarization to a steady-state level the strength-interval curve is near flat; however ". . . as the time interval decreases, stimulation threshold first decreases during the supranormal period and then sharply increases during the absolute refractory period"¹⁶. Biophysically this response can be understood in terms of the steady state voltage and time dependence of inactivation of the sodium channel⁵³(which forms the upstroke of the action potential), and the changes in membrane conductance during the relative refractory period (increased K^+ permeability) which increases the threshold for eliciting an action potential. The supranormal period occurs because during the late phase of repolarization the difference between membrane voltage and threshold are smaller, reducing the current necessary to generate an action potential. The frequency of action potential firing causes changes in action potential duration and amplitude. A decrease in both the amplitude and duration of the action potential

are observed with an increase in firing frequency, imposing a rate dependence on refractoriness¹⁶. This rate dependence of APD is commonly described by the "cardiac restitution curve", where APD is plotted against the basic cycle length of the stimulation.

The level of cardiac excitability is of critical importance as it determines how a propagating electrical wave front in the electrical medium of the heart will respond after breaking into two wavelets following the interaction with an electrical or anatomical obstacle. Due to the importance of excitability in the mechanisms of arrhythmia the interrelation of these concepts will be discussed briefly here and then again in **Section 1.5**. When an electrical wave breaks it has the potential to curl and rotate around the broken ends forming a circularly conducting spiral wave. These high frequency circularly conducting waves forms the basis of many rapid heart rates or tachycardias. Whether or not a broken wave will begin to rotate depends on the level of cardiac excitability. If excitability is too high, the broken waves will refuse. If excitability is too low, the broken wave will shrink as they propagate away and disappear (a phenomenon known as decremental conduction). However, if excitability is relatively low a broken wave can form counter rotating spirals thus generating a rapid arrhythmia⁵⁸.

How individual cardiac cells are activated within the cardiac milieu depends on current transfer from one cell to another via gap junction channels and this is another component of cardiac excitability¹⁰⁶. The degree and orientation (anisotropy) of cell-to-cell coupling regulates the source to sink relationships (cable properties) within the heart and is critically important to propagation of the action potential. The interrelation of cardiac excitability, gap junction channel conductance and impulse conduction are considered in the following section.

1.1.4 Determinants Of Cardiac Conduction

The propagation of the cardiac action potential is determined by current source (Phase 0) and sink factors (passive electrical properties/ I_{K1}), where a modification of either component alters the cardiac conduction velocity. These factors are considered in a model where two cells are connected end to end by intracellular gap junction channels. The current source is determined by the level of excitability while the passive electrical properties (important for current transfer between cells) include the cytoplasmic resistance and the gap junction channel resistance. As such gap junction discussed below are a critical determinant of cardiac conduction.

Gap junction channels are composed of 4 transmembrane domain proteins, connexins (Cxs), which oligomerize in the Golgi apparatus to form hexamers called connexons⁶⁹. Connexons from adjacent cells dock, primarily at the intercalated disc forming low resistance channels that allow rapid propagation of electrical signals¹⁷. While 4 primary isoforms of Cxs are found in cardiomyocytes (mouse Cx30.2/ human Cx31.9, Cx40, Cx43, Cx45), only Cx40 and Cx43 are abundant in the working myocardium. The atrium expresses similar amounts of Cx40 and Cx43⁷¹. Thus atrial gap junctions may have varying stoichiometry of connexin oligomerization. In a homomeric gap junction both connexons are formed by the same type of connexins. Heteromeric gap junctions have connexons with different types of connexins. Homotypic gap junctions have connexons are the same while heterotypic indicates they are different. In **Chapter 3**, the functional consequences of coexpression of Cx40 and Cx43, as well as their individual influences in determining the susceptibility to atrial tachycardia/fibrillation, will be discussed. Here I will summarize the role of gap junction channels in determining cardiac conduction velocity (θ) which include the degree of gap junction conductance and functional status of the channel (whether it is open or not).

These properties have been detailed by Robert Weingart in a recent text⁴⁹ which was used as the primary source for the following summary.

As gap junctions form an intracellular connection between adjacent cells they allow the conductance of electrical current from cell to cell. The degree of junctional conductance is determined by composition of the channel, and the regulation of that channel by intrinsic gating mechanisms. These gates close in a voltage and time dependent manner upon exposure to a voltage gradient across the junction (transjunctional voltage)⁴⁹. These properties have been investigated utilizing dual patch clamp of cell pairs connected by gap junctions. With this dual patch clamp technique, the membrane potential of each cell (V_1 and V_2) can be controlled thereby setting up a voltage gradient across the gap junction (V_j)⁴⁹. The current passing through the gap junction (I_j) can be determined at different transjunctional voltages (V_j), and both the junctional conductance ($g_j = I_j/V_j$) and voltage gating mechanism of various gap junctions (composed of different connexins) can be determined⁴⁹. The results of these studies indicate that cardiac gap junctions tend to be open at rest ($V_j = 0$ mV), and close in a voltage and time-dependent manner during the course of the action potential⁴⁹. Depending on the stoichiometry of oligomerization, gap junctions can have unique gating and conductance properties²⁵ which are discussed below. There are two phases of the junctional conductance that occurs upon exposure to a transjunctional voltage gradient. Initially a large instantaneous current ($I_{j,inst}$) passes through the gap junction which rapidly decays to a second "steady state" current ($I_{j,ss}$) value⁴⁹. The steady state junctional conductance ($g_{j,ss}$) decays in a voltage dependent manner depending on the composition of the gap junction. This voltage dependent decay has a negative effect on cardiac conduction following a hierarchy where $Cx45 > Cx40 > Cx43 > Cx30$.²⁴⁹ The time-dependent gating of gap junctions during the action potential also results in a reduction in conduction velocity⁴⁹. This

inactivation follows a rank order where the effect of inactivation is greater for channels composed of Cx40<Cx43<Cx45<<Cx30.2⁴⁹. As such it is likely that the voltage and time dependent gating will impose greater limitations on conductance for Cx40 containing channels then Cx43 containing channels in the atrium⁴⁹. This has important implications which must be considered when interpreting the results of the studies in **Chapter 3**.

The above discussion described results for cell pairs connected by many gap junction channels, however studies have also been performed describing the properties of single channels. These single channel properties are investigated using induced cell pairs where the experimenter will patch individual cells and position them next to one another. The first occurrence of cell-to-cell conductance represents a single newly formed gap junction channel. It was found that the single channel conductance (γ_j) fluctuates between a main state ($\gamma_{j,\text{main}}$) and a residual state ($\gamma_{j,\text{residual}}$) where $\gamma_{j,\text{main}}$ is greater than $\gamma_{j,\text{residual}}$ ⁴⁹. The comparison of results from many studies of homomeric-homotypic gap junction channels has revealed that $\gamma_{j,\text{main}}$ and $\gamma_{j,\text{residual}}$ follow a rank order where Cx40>Cx43>Cx45>Cx30.2⁴⁹.

The contribution of different gap junctions in determining cardiac conduction velocity will rely on their static and their dynamic properties. In general, reduced channel number (structural change), or either reduced channel conductance or increased voltage sensitivity (functional changes) will reduce conduction velocity. The dynamic factors have been describes as being more complex depending on a number of parameters including the interplay of voltage and time dependent gating properties of individual channels⁴⁹.

Within the heart, the effect gap junctions have on the propagation velocity of a cardiac action potential will depend on a number of factors including cell geometry, tissue architecture and the action potential characteristics. Conduction velocity depends critically on the length of the AP upstroke, the voltage gradient along the tissue axis, the number of

gap junctions sensing the voltage gradient, and the actual voltage across single gap junctions⁴⁹. There is a complex interrelation between the cardiac action potential (**sections 1.1.1-1.1.3**) and the composition and functional status of gap junction channels in determining conduction velocity. These concepts are worth noting because, in general, reduced cardiac conduction velocity and excitability promotes arrhythmia. In the following section I discuss the role of the autonomic innervation of the heart, neural transmitters and the associated G-protein coupled receptors, G proteins, and regulator of G protein signalling (RGS) proteins that regulate the downstream effectors (ion channels, adenylyl cyclase) that influence cardiac electrical properties and arrhythmia.

1.2 AUTONOMIC REGULATION OF CARDIAC ACTIVITY

1.2.1 Anatomy Of Cardiac Autonomic Innervation

This thesis is mostly concerned with the role of the parasympathetic autonomic nervous system's influences on cardiac arrhythmia susceptibility. However, the heart receives both sympathetic and parasympathetic efferent innervations as well as having the ability to process information internally via an intrinsic intracardiac autonomic nervous system (ICANS). The ICANS may interact with the efferent nerve supply in a complex fashion to regulate cardiac function and is thought to act as a "mini-brain" on the heart. Subpopulations of intrinsic cardiac neurons express multiple neurotransmitters⁵⁰; however, in Guinea pig posterior ganglia, choline acetyltransferase immunostaining of all neurons indicates major parasympathetic cholinergic input to the myocardium⁷⁹. These neurons of the ICANS are primarily located in 5 groups of atrial ganglionated plexi (GPs) which have been described by Arora et al.⁶ and may represent areas of local control of cardiac muscle. The heterogeneous distribution of GPs could be considered the first level of the heterogeneous

autonomic regulation of cardiac function. These factors are important in promoting arrhythmia and will be discussed in **Section 1.5** on atrial tachycardia/fibrillation. Although close contact of the neuron with muscle does not mean exclusive control of the adjacent area, it is an important consideration. The necessity of close proximity for neural control is consistent with the “local brain” in the intestinal tract⁴⁰. This postulate has been examined using subthreshold stimulation of cardiac GPs and has revealed local control over the duration of refractory periods. Below I discuss the function and role of acetylcholine-activated muscarinic G protein-coupled receptors and their effectors in the heart.

1.2.2 G Protein-Coupled Receptor Signalling

G protein-coupled receptors (GPCRs) are 7 transmembrane domain cell surface receptors that bind extracellular ligands (hormones, neurotransmitters, and drugs) and transduce signals into the intracellular environment. There are approximately 864 genes in the human which encode for GPCRs⁸¹. These GPCRs control most physiological process in the body¹²⁶ and are targets of >60% of the available pharmaceutical agents^{44, 71}. Most sympathetic and parasympathetic receptors are members of the GPCR superfamily which couple to various downstream signalling cascades including those controlling adenylyl cyclase, Ca²⁺ homeostasis, and ion channels¹²⁶. In the heart, GPCRs control chronotropic (rate of contraction), inotropic (strength of contraction), lusitropic (speed of relaxation), and dromotropic (velocity of conduction) responses to acetylcholine and adrenaline¹²⁶. Ligand binding will either stabilize or induce a conformational change in its GPCR that will activate a coupled intracellular heterotrimeric G protein (G $\alpha\beta\gamma$). There are 4 families of mammalian heterotrimeric G proteins including G_s α , G_{i/o} α , G_{q/11} α , and G_{12/13} α with various subtypes, effectors and expression profiles⁸¹. When in an inactive state, the G protein is bound to GDP, forming a G α -GDP-G $\beta\gamma$ complex. The G α -GDP conformation is stabilized by the G $\beta\gamma$

subunit, which acts as a GDP dissociation inhibitor (GDI), explaining the slow release of bound GDP from the complex. The release of GDP and activation of the $G\alpha$ subunit is accelerated by guanine nucleotide exchange factors (GEFs) which catalyse GDP/GTP exchange at heterotrimeric G proteins ($G\alpha\beta\gamma$). The GEFs for most G proteins are GPCRs; however, intracellular GEFs have been identified¹³⁰. Activation promotes a conformational rearrangement, or potentially dissociation of the heterotrimer into a free, GTP-liganded $G\alpha$ and the $G\beta\gamma$ dimer¹²⁴, both of which can regulate downstream effectors. Whereas GTP binding promotes activation, the on-switch of G protein signalling, GTP hydrolysis (GTP to GDP + P) controls the rate at which G protein signalling is switched off. The hydrolysis of bound GTP by the intrinsic catalytic activity of the $G\alpha$ subunit is slow ($t_{1/2} = \sim 9$ seconds to a few minutes). In order to maintain fast and efficient signal transduction, this deactivating step can be accelerated by GTPase activating proteins (GAPs) more than 1000 fold. The GAPs for G proteins are effector proteins such as phospholipase C β (PLC β) and the regulators of G protein signalling (RGS) proteins. The efficiency of GAP activity on G proteins can be so high that G protein signalling and downstream effector activation can be completely suppressed¹⁰⁴. Studies of the kinetics of these reactions indicate that in order for downstream effectors of G-proteins to be activated in the presence of a GAP, the GAP must potentiate both the rate of GTP hydrolysis and the rate of receptor stimulated GTP binding, supporting the general concept of GAPs as accelerators¹⁰⁴. As such, understanding how the timing of the activation and hydrolysis reactions are regulated is fundamental to understanding the role of G protein signalling in disease. For instance, an increased activity of an effector (such as GIRK1/4) downstream from a GPCR (M2 Muscarinic receptor) that promotes a disease state (Atrial Fibrillation) could be caused by multiple events such as: 1) increased ligand (acetylcholine) availability (by stimulating the vagal nerve or inhibiting acetylcholine

esterase); 2) mutation in the GPCR that increases its intrinsic activity of the receptor (such as in precocious puberty); 3) increased levels of GPCRs, G proteins or effectors, or 4) reduced content or activity of GAPs (RGS proteins). In the following sections, the atrial muscarinic receptors, associated effectors, and their regulation by RGS proteins are discussed.

1.2.3 Atrial Muscarinic Acetylcholine Receptors And Effectors

Five different types of muscarinic acetylcholine receptors (mAChRs) have been cloned. M1, M3, and M5 receptors are $G_{\alpha q}$ coupled receptors, while M2 and M4 receptors are $G_{\alpha i/o}$ coupled. The classical notion is that the cardiac mAChR are exclusively of the M2 subtype; however, there is increasing evidence supporting an important functional role of M3 receptors^{111, 123}. M3 muscarinic receptors were first identified in human atria in 2000 by Hellgren and coworkers⁵¹. In 2002 a Czech group attempted quantification of M1-M5 muscarinic subtype mRNAs in rat atria utilizing the older competitive RT-PCR. Their results indicated that M2 mRNA represented more than 90% of the total muscarinic mRNA in the atria, while M3 was less than 3%⁶⁸. More recent studies using quantitative PCR have also reported low level expression of M1, M4 and M5 muscarinic receptors in the atria, but this may be due to low level DNA contamination as RNA in most studies was not treated with DNase⁶⁵. The functional consequence of co-expression of multiple muscarinic receptor types has been the focus of many studies discussed below, the most compelling of which use genetic M2 and M3 receptor knockout mice.

In the heart, the muscarinic type 2 (M2) receptors inhibit adenylyl cyclase (AC) activation and induce activation of the G protein-coupled inward rectifier K^+ channel ($GIRK_{3.1/3.4}$ or $I_{K, ACh}$)⁶⁷ by $G\beta\gamma$ released from $G_{\alpha i}$. Inhibition of adenylyl cyclase production of cAMP reduces the activity of I_f (a cAMP dependent current) and the L-type Ca^{2+} current

($I_{Ca,L}$) through $G_{\alpha o}$. $I_{Ca,L}$ is also regulated by $G_{\alpha i}$ and nitric oxide^{13, 14}. It was also found that Adenylyl cyclase 5 deficient mice have a reduced $I_{Ca,L}$ activity⁹⁷. Further more, studies in $G_{\alpha i 2}$ knockout mice found that these mice lack muscarinic regulation of $I_{Ca,L}$ ¹⁹. In the atria, activation of $I_{K, ACh}$ increases membrane K^+ permeability, facilitating an outward current that hyperpolarizes the cell and reduces the action potential duration. There is a gradient of $I_{K, ACh}$ current in the mouse atria that, when combined with the heterogeneous distribution of parasympathetic ganglia (**section 1.2.1**), may augment the dispersion of atrial refractoriness⁷⁴. The dispersion of atrial refractoriness was mapped optically in mouse⁹⁶. These studies revealed that APD was shorter in the left than the right⁹⁶ atrium and that CCh could reduce APD in all areas except the left atrial appendage. The role of $I_{K, ACh}$ in the atrium was also determined using $GIRK4$ knock out ($GIRK4^{-/-}$) mice which lack functional $I_{K, ACh}$ channels. $GIRK4^{-/-}$ mice have abnormal heart rate regulation¹²⁵ and are resistant to CCh-induced atrial fibrillation⁶⁷. In the SAN, $I_{K, ACh}$ hyperpolarizes the membrane potential, and decreases the pacemaker pre-potential slope, which contributes approximately 50% to the *in vivo* bradycardic response. M2 receptor activation of $G_{\alpha i}$ inhibits adenylyl cyclase, decreasing cyclic adenosine monophosphate (cAMP) production, which reduces protein kinase A (PKA) activation⁶⁷. PKA, through phosphorylation, increases the activity of $I_{Ca,L}$ and the rapid delayed rectifier potassium channel (I_{Kr}), which promotes repolarization during the plateau phase of cardiac action potential (AP)¹¹⁶. The inhibition of I_{Kr} prolongs AP duration²³. In summary, the functions of the M2 receptor include activation of $I_{K, ACh}$ (hyperpolarization), inhibition of I_{Kr} (prolonging repolarization), and inhibition of I_f (negative chronotropy)⁴⁹.

On the other hand, M3 muscarinic receptors couple to $G_{\alpha q}$ to activate PLC, PKC and $I_{K, M3}$ ¹¹¹. To date, $I_{K, M3}$ is the only identified K^+ channel activated by $G_{\alpha q}$. $I_{K, M3}$ current is

highly selective for K^+ . $I_{K, M3}$ has delayed rectifier properties with a relatively slow activation time constant (approximately 150 ms at +50 mV), which is followed by a partial and slower decay¹²³. The tail current is characterized by an initial rapid rising phase followed by a slow decay with a mean time constant of ~170 ms¹¹². The waveform is similar to that of I_{Kr} ; however, it is insensitive to the I_{Kr} blockers dofetilide and E-4031, and to the slow delayed rectifier K^+ current (I_{Ks}) inhibitor, chromanol 293B. $I_{K, M3}$ is blocked by the non-selective muscarinic antagonist, atropine¹²³ and the M3 selective antagonist, Darifenicin (used in **Chapter 2** and **Chapter 3** experiments)^{122, 123}.

Of special note, M3 receptor distribution was more confined to the intercalated disk region¹²³, and thus was suggested to regulate ventricular gap junction-mediated cell-to-cell conduction¹²². Yue et al. (2006)¹²⁹ found physical and functional interactions between M3 and connexin 43 (Cx43) in rat ventricular myocytes, which were impaired during myocardial ischemia. Gap junction remodelling is an essential component promoting atrial as well as lethal ventricular tachyarrhythmias^{28, 32, 33, 46, 113}. The functions of the cardiac M3 receptors suggested so far include: [1] depressed inotropy; [2] protection against myocardial ischemia; [3] regulation of cell-to-cell communication, and [4] participation in the generation and maintenance of AF¹²³. Using the M3 receptor antagonist 4-DAMP, Wang et al., (2004)¹²³, concluded that the M3 receptor does mediate, in part, the bradycardic response to vagal stimulation. However, the pKb of 4-DAMP for M3 is 8.9-9.3, only one order of magnitude greater the pKb for M2 receptors (7.8-8.4). Perhaps the weak inhibition of vagal bradycardia with high dose 4-DAMP used in Wang's study was due to blockade of M2 rather than M3 receptors. Vagal induced bradycardia was completely abolished in M2 muscarinic receptor ($M2^{-/-}$) deficient mice but was not affected in M3 muscarinic receptor ($M3^{-/-}$) deficient

mice³⁷. However, this does not exclude a role for M3-mediated modulation of atrial or AVN function, as analysis of atrial or AVN function was not done.

The functional consequence of co-expression of M2 and M3 receptors in the atria was studied in M2^{-/-}, M3^{-/-} and M2/M3 double deficient (M2^{-/-}/M3^{-/-}) mice. In wild type mouse atria, CCh induces a negative inotropic response followed by a sustained positive inotropic response. M3^{-/-} mice were devoid of the positive inotropic phase while M2^{-/-} mice had only a positive inotropic response to CCh. M2^{-/-}/M3^{-/-} double knockout mice were devoid of any inotropic response⁶⁵. The susceptibility to arrhythmia was not studied in these mice. These results strongly indicate that functional M3 muscarinic receptors are present in the atria.

The well known vagal modulation of AV nodal function^{24, 80} has long been attributed to M2 coupled I_{K, ACh}^{24, 35}. In the AVN, it is suggested that activation of I_{K, ACh} causes hyperpolarization mediated inhibition of voltage-gated I_{Ca, L}⁶³. However, there is conflicting evidence in the literature on muscarinic regulation of AVN function. Tertiapin-Q, a bee venom derived peptide⁴³, potently inhibits the I_{K, ACh} current⁶⁰. In isolated guinea pig hearts, tertiapin abolished CCh-induced prolongation of PR interval³¹. However, His bundle electrograms were not measured, which is important for determining the site of block within the node, and neither were AVN effective refractory periods (AVNERP), nor Wenkebach cycle lengths (WCL). Kir3.4 deficient mice which lack functional I_{K, ACh} channels, were primarily developed to determine the role of I_{K, ACh} in AF⁶⁷. When challenged with CCh, no significant difference in the changes in the AV interval, WCL, or AVNERP were found in the knock out compared to wild type (WT) mice. This suggests that I_{K, ACh} is not involved in autonomic control of AV nodal conduction. These conflicting observations have neither been explained nor previously discussed. It must be asked, "how is autonomic mediated

modulation of AV nodal conduction accomplished if $I_{K, ACh}$ is not involved?". Studies in mice deficient in Cav1.3, the atrial selective $I_{Ca, L}$ isoform, have been found to have prolonged AVN conduction and loss of isoproterenol-induced enhancement of AVN conduction⁷⁸. These observations, taken together, suggest that autonomic regulation of AVN conduction may principally involve modification of $I_{Ca, L}$. Regulation of $I_{Ca, L}$ occurs: [1] through phosphorylation by PKA and PKC¹²⁸; [2] by the voltage dependence of $I_{Ca, L}$, and [3] through modulation by Ca^{2+} -calmodulin. If M3 muscarinic receptors are involved in regulating AV nodal function it could be through a PKC mediate modulation of $I_{Ca, L}$ ¹²⁸.

In the following section I consider the role regulators of G protein signalling play in autonomic regulation of atrial function and arrhythmia.

1.2.4 Atrial Regulators of G Protein Signalling (RGS) Proteins

Regulators of G Protein Signalling (RGS) proteins were first identified as GTPase activating proteins (**GAPs**), accelerating the intrinsic GTPase activity of $G\alpha$ subunits, as the duration of G protein activation is primarily controlled by GTP hydrolysis. Also, RGS proteins can interfere with G-protein binding to effector proteins, separate from their regulation of hydrolysis⁵⁵. Thus RGS proteins are important regulators of GPCR signalling. Currently, 20 different genes encoding RGS proteins have been identified. The RGS proteins have been divided into 4 subfamilies, based on sequence and structural similarities: **RZ/A** (RGS17, 19 and 20); **R4/B** (RGS1–5, 8, 13, 16 and 21); **R7/C** (RGS6, 7, 9 and 11), and **R12/D** (RGS10, 12 and 14)⁸. The majority of RGS proteins are GAPs for $G_{\alpha i/o}$ and many also act on $G_{\alpha q/11}$ ⁸⁹; however, none are GAPs for $G_{\alpha s}$ but some RGS-like proteins such as p115RhoGEF do have GAP activity on the $G_{\alpha 11/12}$ subfamily. RGS2, 3, 4, 6, 10, RGSZ2 and GAIP are all found in atrial cardiomyocytes³⁰. To investigate the role of RGS proteins in regulating the chronotropic effects of adrenergic, muscarinic and purinergic receptor

stimulation, mutant Gai and Gao proteins were generated that are insensitive to binding of all RGS proteins³⁹. Knockin cells expressing the Gai2GS/GS insensitive mutant had an enhanced responses to M2 muscarinic but not A1 adenosine receptor stimulation, while the GaoG184S insensitive mutant had enhanced A1 adenosine and M2 receptor mediated responses³⁹. Interestingly, Gas stimulation of beating rate was almost completely abolished in the Gai2GS/GS insensitive mutant cells. Gai2GS/GS insensitive mutant mice also displayed pronounced (5 fold greater) muscarinic mediated bradycardia and 3rd degree AV nodal block³⁸. These data from Gai2-RGS-insensitive mutant mice indicate that in the SAN and AVN, M2 receptors primarily couple through Gai2 to inhibit cAMP production and activation of PKA^{38, 39}. Adenosine 1 and 3 receptor overexpressing mice have also have prolonged AVN conduction^{36, 64}, which may involve receptor-mediated inhibition of adenylyl cyclase 5/6 (AC5/6), primarily coupling through Gao^{38, 39}. Susceptibility to atrial arrhythmia has not been examined in these mice. It is currently believed that specific RGS proteins may couple to specific signalling pathways within the cell. To explore the specific role of RGS proteins in regulating various signal transduction pathways in vivo, knockout mice for 3 (RGS2, RGS4 and RGS6) of the 7 atrial RGS proteins (RGS2, 3, 4, 6, 10, RGSZ2 and GAIP) have been developed. These mice have revealed the critically important role of RGS proteins in regulating the specific autonomic responses in the atria. These functions are discussed below with attention paid to RGS2 as study of atrial arrhythmia in the RGS2 deficient (RGS2^{-/-}) mouse is the topic of **Chapter 2** of this thesis.

RGS2, a member of the R4/B subfamily, is the second most highly expressed RGS protein in the heart³⁰. RGS2 is a unique RGS protein as it is a selective GAP for Gαq¹³⁴, and has little to no GAP activity on Gai/o. RGS2 has also been identified as a regulator of AC signalling¹¹⁴. In HEK 293 cell culture, RGS2 inhibited Gas stimulation of AC5 and AC6¹⁰⁵.

¹⁰⁸. The mechanism was not through its GAP activity, but rather through a physical interaction of the N-terminus of RGS2 with the C1 catalytic loop of AC5^{9, 108}. Increases in cAMP levels produced by forskolin treatment increased RGS2 expression⁹⁹. The potential for a role of RGS2 inhibition of AC signalling in the AV node is considered in **Chapter 4**. Removal of RGS2's inhibitory effect on Gαq signalling increases the activity of Gαq-dependent signalling. Interestingly, RGS2 has also been revealed as an important target in cardiovascular disease¹¹⁸ (cardiac hypertrophy and hypertension). RGS2^{-/-} mice have a hypertensive phenotype^{52, 98} that is suggested to be mediated by vascular changes, possibly through angiotensin II, endothelin and/or α-adrenergic receptors, rather than cardiac alterations. However, direct analysis of cardiac “contractility”, by measuring left ventricular *dP/dt*, was not done in these mice^{52, 98}. Chronic telemetry found an increase in mean arterial pressure of ~10 mm Hg, while heart rate was unchanged, indicating a resetting of the baroreceptor reflex⁴⁵. This was confirmed by directly measuring baroreflex sensitivity calculated by cross-spectral analysis of heart rate variability. Heart rate variability was not different in RGS2^{-/-} compared to RGS2^{+/+} mice⁴⁵. This indicates that any observed cardiac phenotype cannot be explained by a baroreflex mediated enhancement of vagal nerve activity. As RGS2 is a specific regulator of Gαq signalling, it is possible that it is an important regulator of M3 muscarinic signalling in the atria. This indeed seems to be the case and is discussed in detail in **Chapter 2**.

Recently, RGS4 was demonstrated to be an important regulator of SAN function²². RGS4 in the SAN inhibited parasympathetic signalling and I_{K, ACh} activity. In mice expressing LacZ under control of the RGS4 promoter, high expression of LacZ-RGS4 was found in the SAN with little expression in the surrounding right atrium. RGS4-null (RGS4^{-/-}) mice had lower baseline heart rates and a greater increase in heart rate following administration of atropine, a

non-selective parasympathetic antagonist. High expression of RGS4 was also present in the AVN (demonstrated using LacZ staining) suggesting that altered dromotropic responses (increased PR interval) might be observed in RGS4^{-/-} mice. This was found to be the case as RGS4^{-/-} mice were highly susceptible to AVN conduction block when treated with isoproterenol; however, there is limited electrophysiological data describing this phenotype (location of conduction block) and results were obtained principally in Langendorff hearts (removed from in vivo autonomic influences).

As RGS4 was found only in the SA and AV nodal region, the RGS protein regulating parasympathetic signalling and I_{K, ACh} activity in the atrium remained, until recently, unknown. RGS6-deficient (RGS6^{-/-}) atrial myocytes exhibited a significant reduction in the time course of I_{K, ACh} activation and deactivation. RGS6^{-/-} mice also displayed bradycardia and AV nodal conduction block indicating that there is at least partial redundancy in RGS protein function in vivo. It would be interesting to compare the susceptibility to atrial arrhythmia between the RGS-insensitive-Gai2 knockin, RGS4^{-/-} and RGS6^{-/-} mice, however studies of this nature have not yet been published.

1.3 CLASSIFICATION OF SUPRAVENTRICULAR TACY-ARRHYTHMIAS

Cardiac arrhythmias (abnormal heart rhythms) can be organized and slow (*bradycardia*), organized and fast (*tachycardia*) or disorganized and fast (fibrillation). These arrhythmias are further classified by where they occur in the heart, i.e., either in the ventricles, or above the ventricles (supraventricular arrhythmia).

Supraventricular tachycardias (SVT) are commonly seen in clinical settings. The different types of SVTs have been classified based on their anatomic location (sinus node, atrio-ventricular node, and atrial myocardium) and the apparent mechanism of the arrhythmia

(abnormal impulse initiation (focal) or abnormal impulse conduction (reentry)). The following is a non-exhaustive list of supraventricular tachy-arrhythmias, many of which will be discussed in this thesis: atrial tachycardia (AT, atrial myocardium/focal or multifocal arrhythmia), inappropriate sinus tachycardia (IST, sinus node/focal arrhythmia), junctional tachycardia (JT, AV node/focal arrhythmia, also called junctional ectopic tachycardia, JET), atrial flutter (AFL, atrial myocardium/anatomic re-entry), atrio-ventricular nodal re-entrant tachycardia (AVNRT, AV node/functional anatomic re-entry), and atrial fibrillation (AF, atrial myocardium/both focal and functional re-entrant mechanisms proposed). All atrial arrhythmias are produced by abnormalities of either cardiac impulse initiation, impulse conduction or both. In the following sections, the mechanisms of abnormal impulse initiation and impulse conduction will be discussed.

1.4 ABNORMAL IMPULSE INITIATION

Abnormal impulse initiation falls into three categories; enhanced normal automaticity, abnormal automaticity and triggered activity. Within the atrium, SA and AV nodal cells have an intrinsic ability to self activate (pacemaker activity/automaticity). A hierarchy of pacemaking activity exists within the human atrium, where firing rate is fastest in the SA node, 60-100 beats per minute (bpm), and slower in the subsidiary AV node pacemaker (40-60 bpm). This normal automaticity is tightly regulated by autonomic influences. Parasympathetic vagal stimulation (primarily acetylcholine) leads to a decrease in the slope of phase 4, the action potential upstroke velocity and thus heart rate (<60 bpm). Enhancement of normal automaticity occurs during parasympathetic withdrawal and sympathetic activation, which results in an increase in the slope of phase 4 with increases in rate to over 200 bpm. Metabolic abnormalities such as hypoxia (inhibits Na⁺-K⁺ pump) and

low extracellular K^+ concentration can increase the slope of phase 4 depolarization causing enhancement of normal automaticity. As discussed above, SA and AV nodal cells have automaticity, whereas normally, contractile atrial myocardium does not, and thus automaticity there is considered abnormal. Abnormal automaticity arises from atrial cells when they are depolarized to levels between -60 to -10 mV. Depolarization induced abnormal automaticity may result from a decrease in K^+ conductance allowing a net inward depolarizing current⁵⁸.

Triggered activity is a mechanism of abnormal impulse generation that is caused by afterdepolarizations of the cardiac action potential. Afterdepolarizations can be defined as depolarizing oscillations in membrane potential that are dependent on the preceding action potential and can give rise to a new action potential¹²⁰. Two types of afterdepolarization have been described, delayed afterdepolarizations (DADs) and early after depolarizations (EADs), named in relation to the phase of the action potential in which they occur. DADs are oscillations in membrane potential that occur following repolarization of the action potential while EADs occur during the action potential plateau (phase 2) or during the late phase 3 repolarization¹²⁰. Whether or not an afterdepolarization will "trigger" an action potential depends on the level of the membrane potential in which they are generated as well as the electrotonic interactions between inexcitable tissue with areas that have already recovered from refractoriness⁵⁸. In general, DADs are caused by conditions that lead to intracellular Ca^{2+} overload, and have found to be inducible by β -adrenergic stimulation (sympathetic response). β -adrenergic stimulation, among other things, increases the L-Type Ca^{2+} current which can lead to Ca^{2+} overload and activation of the transient inward current (I_{TI}) through a Ca^{2+} -dependent non-specific ion channel. I_{TI} activation forms the major component of the DAD. EADs can result from factors that prolong action potential duration or result in a net

increase in inward current⁵⁸. The latter can occur through β -adrenergic augmentation of the L-type Ca^{2+} current while cholinergic (parasympathetic/vagal) stimulation can suppress EADs and triggered activity⁵⁸.

The abnormal initiation of a cardiac impulse is the "trigger" of many arrhythmias that involve the abnormal propagation of the cardiac impulse (reentry). The factors leading to abnormal impulse propagation are discussed in the following section.

1.5 ABNORMAL IMPULSE PROPAGATION (REENTRY)

Abnormal impulse propagation occurs due to the slow conduction of cardiac impulses or when the same electrical activation front repetitively reactivates an area of tissue. The reactivation of tissue by the same wavefront or the reentry of an impulse into an area can be due to circular conduction around a circuit or the reflection of cardiac impulses along a linear pathway. Reentry along a linear pathway, called reflection reentry, requires the presence of severely impaired conduction or a narrow gap of refractory tissue⁵. Reflection is the back and forth activation of tissue across this gap due to passive electrotonic depolarizations.

Reflection, within the accessory (atrio-ventricular) pathway of patients with manifest pre-excitation in Wolff-Parkinson-White (WPW) syndrome, is a suggested mechanism of AF initiation and may explain the propensity of AF in this patient population¹⁰⁹. Circular conduction, a more common form of reentry, can occur when electrical impulses propagate around a circuit and is also called circus movement reentry. Due to the rapidity of the circular conduction, which is dependent on the conduction velocity of the impulse and the size of the circuit, reentry results in high frequency repetitive activation of the myocardial substrate. Circular reentry often involves the conduction of a cardiac impulse around a predetermined circuit formed by an anatomic obstacle. Reentry that occurs in the absence of a

predetermined circuit is called functional reentry. Two examples of reentrant arrhythmia requiring an anatomic obstacle is that of AV reciprocating tachycardia (AVRT) in WPW syndrome, and atrial flutter (AFL). The anatomical circuit in AVRT involves conduction between the normal conduction system (atrium, AV node and ventricle) and an abnormal accessory pathway that directly links the atrium to the ventricle (AV pathway). Interrupting the circuit in WPW by destroying the accessory AV pathway surgically or by application of radiofrequency energy with a transvenous "ablation" catheter cures AVRT. In the anatomic circuit of typical AFL, a "critical isthmus" exists between the tricuspid valve annulus, the inferior vena caval orifice, the eustachian ridge, and the coronary sinus ostium. This isthmus is critical because ablation of this region terminates AFL. The rest of the circuit is bound by the tricuspid valve ring, and the venae cavae. Reentry in AFL is not purely anatomic in origin as functional lines of block between the vena cavae or in the sinus venous region is important in the arrhythmia mechanism.

A number of conditions must be met in order to achieve circus movement reentry around an anatomic circuit including: unidirectional block; slow conduction in one part of the circuit; and a wavelength that is shorter than the length of the circuit. These conditions are true of AVNRT which is discussed in **Chapter 4** of this thesis. These conditions can usually be promoted by the abnormal "early" initiation of a cardiac impulse (**Section 1.4**). Blocked conduction in one direction (unidirectional) of an anatomic circuit allows circular conduction to be initiated, and in most cases occurs in the region with the longest refractory period (uncovered by the premature impulse). Slow conduction in one part of the circuit also facilitates the initiation of reentry as it allows other parts of the pathway to recover from refractoriness so that they can be re-activated by the reentrant impulse.

If the conduction time around the circuit is not long enough, the wavefront will collide with the refractory tail of the previous activation cycle and reentry will be terminated. This fact indicates an important concept in reentry known as the wavelength. The wavelength (λ) describes the minimum length of an electrical activation wave (from wave front to wave tail) within a predetermined circuit, necessary for reentrant activation to occur and is a product of the conduction velocity (CV) of the electrical impulse and the effective refractory period (ERP) of the tissue where, " $\lambda = CV \times ERP$ "². If the wavelength is shorter than the length of the circuit, reentry will be stable and a gap of excitable tissue will be present between the wave front (depolarizing tissue) and the wave tail (repolarizing tissue). An externally delivered stimulus (from a electrode catheter) has the ability to invade this excitable gap and advance the time of the next cycle (entrainment) or terminate reentry by advancing the wavefront to a point at which it collides with refractory tissue. Clinical diagnostic catheter based electrophysiological studies rely on the concept of an excitable gap, where premature pacing that terminates an arrhythmia or demonstrates entrainment confirms a reentrant arrhythmia mechanism. This concept is used in studies throughout this thesis (**Chapter 2, Chapter 3 and Chapter 4**)

Reentrant activation occurring in the absence of a predetermined anatomic circuit is known as functionally determined reentry. Investigation of the leading circle model² of functional reentry was the first to present experimental evidence for the presence of reentry in the absence of an anatomical obstacle. In this experiment, a reentrant tachycardia was initiated in an isolated rabbit left atrium using programmed electrical stimulation with 20 impulses delivered at a coupling interval of 500 ms (the S1 stimuli) followed by an extrastimulus (the S2) delivered with an S1S2 coupling interval near the refractory period of the atrium. This technique is also used throughout this thesis (**Chapter 2 and Chapter 3**) to

induced and study atrial tachycardia/fibrillation (AT/F) in the mouse. By compiling electrogram recordings from over 300 sites, functional circus movement reentrant activation was observed for the first time². The leading circle model attempted to explain this finding by hypothesizing that a functional zone of refractory tissue was present at the centre of rotation due to a continual electronic depolarization². In this leading circle model, the wavefront must propagate through relatively refractory tissue where there is no fully excitable gap and the wavelength will be close to the length of the circuit. As a result of a lack of an excitable gap, this type of reentry would be very difficult to terminate with an externally delivered electrical stimuli. This model was found to not adequately describe many of the properties of functional reentry⁵⁸, including reentry in mouse atria (where the calculated wavelength is larger than the size of the atria), and the susceptibility to termination with electrical pacing (requiring an excitable gap). The leading circle hypothesis was however of great influence, driving research that led to the concept of rotors and the spiral wave hypothesis of functional re-entry. A rotor in the context of functional re-entry is the organizing source (driver) of functional re-entrant activity. It is described as "the structure immediately surrounding the pivot of a rotating wave in two or three dimensions"⁵⁸. A rotor is the source of spiral waves of excitation that propagate around the rotation centre. Rotors form when a propagating electrical wave "breaks" on an anatomical or electrophysiological heterogeneity, and under appropriate conditions of excitability (not too high or not too low, **Section 1.1.3**), begins to rotate^{59, 119}. The spiral wave hypothesis explains many properties of functional reentry which are not easily resolved by the leading circle hypothesis including, among other things, the presence of an excitable gap and functional reentry in the atria of mice (**Chapter 2** and **Chapter 3**).

Importantly, many modifiable factors have been identified which may explain the initiation of reentrant tachy-arrhythmias in the atrium including the dispersion of refractoriness, altered conduction velocity/current source-sink relationships, and the degree of myocardial excitability. In the following section I will discuss in depth two specific supraventricular tachyarrhythmias, atrial tachycardia and atrial fibrillation, which rely on abnormal impulse initiation and conduction for their initiation and maintenance.

1.6 ATRIAL TACHYCARDIA/FIBRILLATION

AT/F have distinct clinical diagnoses but as I will discuss these two arrhythmias may lie amongst a progressive mechanistic spectrum. Clinically, the major difference between the two arrhythmias is that the electrical activity of AT on the ECG is rapid and organized while AF is rapid and disorganized. This simple observation suggests that the underlying mechanisms of AT are deterministic while the presumed complexity and dynamic nature of AF alludes to a stochastic mechanistic nature. The stochastic mechanistic view was predominant for over 50 years and proposed that AF relied on multiple reentrant wavelets⁹⁰. However, optical mapping studies of AF in isolated sheep atria have found that AF may involve both deterministic (a high frequency "mother rotor") and stochastic components (fibrillatory conduction of multiple wavelets spawned from the deterministic driver)^{56, 66}. Remodelling of the atria may promote stochastic fibrillatory conduction (the propagation of multiple wavelets) as "AF begets AF" indicating that atria remodelling promotes sustained disorganized activity. In fact atrial tachycardia remodelling with rapid electronic pacemakers is commonly used experimentally to induce a fibrillatory substrate, indicating that AT and AF may belong to a progressive spectrum^{85, 110} of arrhythmogenesis. Atrial fibrillation relies on the interaction of triggers, perpetuators and substrate for initiation and maintenance of the

arrhythmia³. Triggers combined with dynamic substrates of structural heterogeneities, reduced refractoriness, enhanced spatial dispersion of refractoriness and abnormal impulse conduction, to initiate and perpetuate the arrhythmia⁹². As AT and AF may be related it is not surprising that focal atrial tachycardia originating from the pulmonary veins accounts for 16% of focal AT, 78% of left atrial ATs and more than 90% of AF triggers⁴⁸.

Abnormal impulse initiation and conduction contribute to the mechanism of AT, but are also involved in the initiation and maintenance of AF. Atrial tachycardia is an uncommon cause of supraventricular tachycardia, occurring in only 5% of adult and 10-15% of paediatric patients⁴⁹. Atrial tachycardia in patients depends on increased automaticity, triggered activity and micro-reentry²⁰. Various observations suggest that the autonomic nervous system may play a role in AT. For instance, automatic AT in patients (7/36) can be initiated by isoproterenol infusion but not by programmed electrical stimulation²⁰. Also, DADs observed from monophasic action potential recordings in patients with triggered activity (9/36) were terminated with propranolol and vagal manoeuvres (Valsalva manoeuvre and carotid sinus massage)²⁰. However, the majority of patients (20/36) have AT caused by micro-circuit reentry that is readily initiated and terminated by atrial pacing and do not display DADs²⁰. Clearly there is a role for autonomic influences in focal arrhythmias. In **Chapter 4**, I study the role of abnormal autonomic (baroreflex) influences in a focal arrhythmia initiated in the AV node, Junctional Tachycardia.

While AT is relatively uncommon, AF is the most common cardiac arrhythmia seen in general clinical practice^{10, 62}. AF increases with age with a prevalence of 0.02% of people 18-39 years of age to 11.6% of people over 75 years of age⁹⁵. These observations suggest that fibrillatory conduction at rapid atrial activation rates is a more likely state of the atria than uniform conduction at rapid rates. There is a rate-dependence of these arrhythmias,

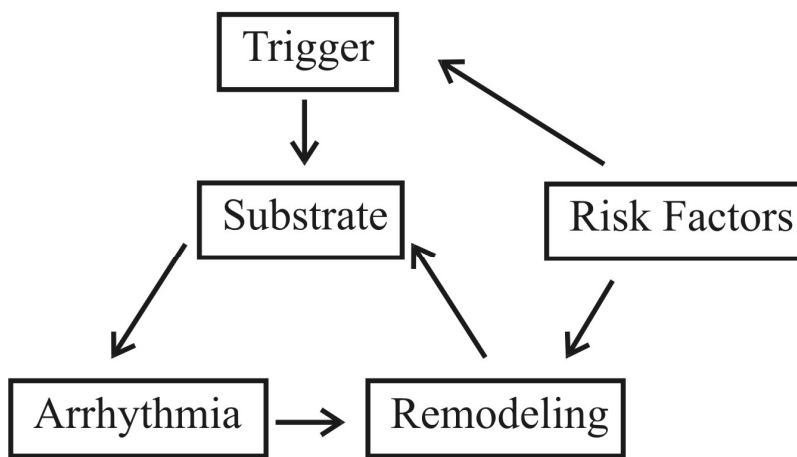
where AT is presumed to occur at rates below the "breakdown frequency" necessary for fibrillatory conduction, which is a hallmark of AF. AT rates are generally reported between 100-250 bpm while local activation rates during AF can exceed 400-600 bpm⁹⁰. The breakdown frequency is an important electrical substrate of AF as a lower breakdown frequency promotes fibrillatory conduction at slower rates. As discussed above the rapid rates during AF promotes remodelling of the atria that potentiates AF duration (AF begets AF). There are however a number of factors that cause the pre-arrhythmia remodelling of the atrial substrate that is required for AF to occur in the first place. These factors "prime" the initial substrate state, promoting the rapid triggers (e.g., pulmonary vein ectopy) and susceptibility to fibrillatory conduction necessary for AF. These "clinical risk factors"¹⁰³ for the onset and development of AF are listed in **Figure 1.1**, which is a simple representation of the cycle of arrhythmogenesis. In this model, AF risk factors induce the pre-arrhythmia remodelling of the atria that may promote arrhythmogenic triggers and a substrate which is susceptible to fibrillatory conduction and AF maintenance. The breakdown frequency of conduction is, however, not an independent predictor of an atrial substrate that will maintain AF. For instance, Cx40^{-/-} mice have a lower pacing induced breakdown frequency of 1-1 right atrial impulse conduction than wild type mice but did not present with AF⁷. This indicates that the factors that promote fibrillatory conduction may not necessarily contribute to the mechanism driving AF and even oppose it. However, in **Chapter 3**, I present data showing that reduced Cx43 content in the atria not only promotes AF initiation and maintenance but the conduction disturbances which are the hallmark of an AF substrate.

The rapid rates during AF cause remodelling of the atria that promotes long lasting permanent AF¹¹⁷. This process generally referred to as "AF begets AF" describes how new onset paroxysmal AF, will eventually become persistent AF, with the final state being

permanent AF. This classification system divides AF into groups based on the duration of AF episodes and the therapeutic history^{95, 127}. Paroxysmal AF has episodes that last less than 1 week and terminates spontaneously without electrical or pharmacological cardioversion. Persistent AF episodes last longer than 1 week or are susceptible to electrical or pharmacologic cardioversion. A patient is said to be in permanent AF when AF is continually present and a strategy of rhythm control has been abandoned or never tried^{95, 127}. It must be recognized that as these divisions are based on the effectiveness of current medical interventions and as there can be significant overlap of clinical diagnoses amongst patient populations they may not be indicative of underlying mechanisms.

Lone and paroxysmal AF has been shown to be primarily initiated from the pulmonary veins and posterior left atrial regions^{47, 85}. These venous segments are where most of the ganglionated plexi are in contact with the left atrium (**Section 1.2.1**). Both alterations in vagal responses and a significant increase in AF control^{87-89, 100-102} were found in patients where the ganglionated plexi (GPs) were targeted¹⁰⁷ or inadvertently modified during catheter ablation of AF sources in the pulmonary veins. This observation demonstrates the importance of the intrinsic cardiac autonomic nervous system in AF, which is commonly referred to as neurogenic AF^{18, 26, 54, 73, 91, 133}. Neurogenic AF relies extensively on the action of acetylcholine (**Section 1.2.2**) and is also referred to as vagal AF⁴².

The role of acetylcholine in setting the stage for rotor development and stabilization of the leading sources of AF have been reviewed³⁴. Acetylcholine has been found to promote left to right frequency gradients and enhance the dominant frequency of the AF driver⁷⁷. These responses were also dependent on acetylcholine concentration, with higher concentrations resulting in faster dominant frequencies. AF studies commonly focus on



Classic Risk Factors

- Heart Failure
- Coronary Artery Disease
- Valvular Heart Disease
- Diabetes
- Hypertension
- Genetic Factors

New Risk Factors

- Metabolic Syndrome
- Sleep Apnea
- Inflammation
- Alcohol
- Extreme Exercise

Figure 1.1: The Cycle of Arrhythmogenesis.

acetylcholine concentration dependence and the expression profiles of receptors and downstream effectors while ignoring the regulators of the G protein signalling cascades (**Section 1.2.2**). **Chapter 2** of this thesis attempts to address this issue by studying neurogenic atrial tachycardia/fibrillation in the RGS2 deficient mouse.

Persistent AF is associated with diffuse macroscopic and histological atrial myocardial changes, referred to as remodelling. Atrial arrhythmia can also cause ventricular remodelling and, if protracted, cardiac failure. This in turn, feeds back on the atria and produces irreversible interstitial atrial fibrosis⁶¹. Such remodelling is associated with multiple changes in the atrial myocardium, such as altered signalling, fibrosis, and ion channels consistent with a "myogenic" hypothesis of AF. Myogenic AF is generally considered to be distinct from Neurogenic AF and is suggested to involve all mechanistic components unrelated to neurogenic components. However, the neurogenic and myogenic components of AF mechanisms are not easily separable, and there may be an important neuro-myogenic interface in AF mechanisms. The study of the involvement of the neuro-myogenic interface in mechanism of atrial arrhythmia is a central goal of this thesis and is discussed below.

The comparison of multiple interrelated factors that promote AF can be discussed utilizing a simplistic "Threshold Model" of arrhythmogenesis, which I propose in this thesis. The complexity of AF lies in the nature of the interaction that occurs between the electrical and physiological medias of the heart. A two media conceptual perspective is useful when thinking of arrhythmia as it allows the simple recognition that there are multiple physiological factors which can allow the same electrical phenomena to occur. In other words, many potentially unrelated changes in the physiology of the atria can allow the same electrical phenomena to occur in the atria's electrical media. An example of this would be that both decreased upstroke velocity (reduced Na⁺ channel conductance) of the action

potential and decreased junctional conductance slow the propagation velocity of electrical waves in the heart (**Section 1.1.4**). The proposed "threshold model" of arrhythmogenesis is useful as it allows for the simple relative comparison of multiple physiological factors which can have complimentary or opposing roles in promoting an electrical AF substrate. A substrate that is susceptible to AF initiation by an appropriate trigger would be said to be above the threshold for promoting AF. If the atrial substrate is well below the AF threshold a single arrhythmogenic perturbation (low concentration acetylcholine) might not bring the atria close enough to threshold to allow a trigger to initiate AF. If however the atria is well above the threshold for AF, and is in permanent AF, than an antiarrhythmic treatment (such as electrical cardioversion) might not terminate AF if it cannot force the atria below threshold. These concepts form the basis of the studies performed in this thesis and will be discussed in the following section outlining the rationale, objectives and hypotheses.

1.7 RATIONALE

When experimental work began, utilization of the mouse for AF studies was in its infancy with only a few published papers demonstrating long lasting sustained AF in the mouse. AF studies have commonly utilized the sheep, the pig and the dog as models due to anatomic similarity with the human (critical mass hypothesis)⁴¹. To date, the mouse is the most commonly utilized organism where single genes can be manipulated to determine their role in arrhythmia. As such, an objective of this thesis was to determine what atrial arrhythmias are inducible in the mouse and how to systematically and reproducibly elicit and study those arrhythmias. Following this, I wanted to use the mouse to study the molecular factors involved in arrhythmia susceptibility and substrate formation. Genetic alterations in mice allow the investigation of single factors which can promote arrhythmia in vivo. One of

the greatest challenges in studying AF has been the difficulty of dissociating fibrillatory activation from its mechanism¹¹ where it has been said that “atrial fibrillation has prevented the study of atrial fibrillation”¹¹. Due to this limitation, most molecular data published to date is correlative and does not describe the initial substrate state that lead to AF development (the pre-arrhythmia remodelling). Studies in genetically manipulated mice may address both issues as "induced pre-arrhythmia substrate remodelling", thereby allow for investigations of the initial state dissociated from fibrillatory activation and thus yield causative mechanistic insights. This information will provide mechanistic insights into what physiological alterations will allow the excitable media to sustain arrhythmia. Based on such findings, novel interventions can be developed. The study of arrhythmia mechanism in the mouse with an eye toward the development of novel antiarrhythmic interventions is an objective of this thesis.

Both neurogenic^{18, 26, 54, 73, 91, 133} and myogenic^{75, 121, 41, 4, 57, 76, 82-84, 115, 131} hypotheses have been proposed to account for arrhythmia mechanisms. The separation of AF mechanisms into strictly neurogenic and myogenic types is difficult as there can be interactions between the two. Also, in considering a two media (physiological and electrical) perspective of the heart and arrhythmogenesis, where multiple unrelated factors can promote the same electrical phenomena, it can be seen that a neuro-myogenic interface is important. The central hypothesis of this thesis is that there is an interface of neuro-myogenic influences in arrhythmia mechanism. As such it is proposed that the intrinsic cardiac autonomic nervous system has a role in most atrial arrhythmias. In **Chapter 2** I investigated the role of the regulator of G-protein signalling 2 (RGS2) protein in modifying G-protein signalling cascades (neurogenic AF) utilizing an RGS2 knockout mouse. It was hypothesized that, as a selective regulator of Gαq-mediated signalling, RGS2^{-/-} mice would have enhanced M3

muscarinic receptor signalling and an increased susceptibility to electrically induced atrial tachycardia/fibrillation. In **Chapter 3** Cx40 deficient and Cx43^{G60S/+} mutant mice, with an 80% reduction in atrial phospho-Cx43, were studied to determine the role of altered connexin content in promoting myogenic AF. Based on a comparative analysis of literature, it was hypothesized that Cx40 deficient mice would be protected from AF while the Cx43^{G60S/+} mutant would have severe AF. By identifying a model of AF promoted by structural alterations in gap junctions, the role of the ICANS in myogenic AF could be studied. Finally, by utilizing the threshold Model of arrhythmogenesis, the relative role or interface of disparate neurogenic (role of M3 muscarinic receptors) and myogenic factors (role of altered connexin content) in promoting AF were analyzed in the reasonably controlled context of induced pre-arrhythmia substrate remodelling. In **Chapter 4** I identified another atrial arrhythmia which is inducible in the mouse that involves the ICANS, junctional tachycardia. Junctional tachycardia is most prevalent among children following cardiac surgery (~10%) and can increase the risk of mortality up to 15%, however the mechanism of the arrhythmia is unknown. I tested the hypothesis that JT is caused by inappropriate activation of the AV node pacemaker initiated by abnormal autonomic influences. The final objective of this thesis was to develop the proposed "Threshold Model" of arrhythmogenesis and use it to analyze results and make relative comparisons of observations obtained from the different experiments performed in **Chapters 2-4**. In **Chapter 5**, the discussion section of this thesis, the Threshold Model will be used to explain the role of the ICANS in studies examining the neuro-myogenic interface of atrial arrhythmia. I will also present this simple relative comparison Threshold Model as a useful tool to make predictions of the outcomes of clinical arrhythmia interventions.

1.8 SUMMARY OF HYPOTHESES AND OBJECTIVES

1.8.1 Hypotheses

- 1.** There is an interface of neuro-myogenic influences on arrhythmia mechanism. Therefore the intrinsic cardiac autonomic nervous system has a role in most atrial arrhythmias.
- 2.** RGS2^{-/-} mice have enhanced M3 muscarinic receptor signalling and an increased susceptibility to electrically induced atrial tachycardia/fibrillation.
- 3.** Cx40 deficient mice will be protected from, but the Cx43^{G60S/+} mutant will have severe AT/F.
- 4.** Junctional tachycardia is caused inappropriate activation of the AV nodal pacemaker initiated by abnormal autonomies.

1.8.2 Objectives

- 1.** To determine what atrial arrhythmias are inducible in the mouse and how to systematically elicit and study those arrhythmias.
- 2.** Determine the mechanisms of the induced atrial arrhythmias in the mouse to provide the basis for future investigations of potential therapeutic options for patients.
- 3.** Develop the proposed "Threshold Model" of arrhythmogenesis and use it to analyze results and make relative comparisons of observations obtained from the different experiments performed in this thesis.

1.9 REFERENCES

1. Ahrens-Nicklas RC, Christini DJ. Anthropomorphizing the mouse cardiac action potential via a novel dynamic clamp method. *Biophys J* 97:2684-92. 18-11-2009.
2. Allesie MA, Bonke FI, Schopman FJ. Circus movement in rabbit atrial muscle as a mechanism of tachycardia. *Circ Res* 33:54-62. 1973.
3. Allesie MA, Boyden PA, Camm AJ, Kleber AG, Lab MJ, Legato MJ, Rosen MR, Schwartz PJ, Spooner PM, Van Wagoner DR, Waldo AL. Pathophysiology and prevention of atrial fibrillation. *Circulation* 103:769-77. 6-2-2001.
4. Allesie MA, Lammers W, Bonke F. Experimental evaluation of Moe's multiple wavelet hypothesis of atrial fibrillation. In: Zipes DP, Jarife J, eds. *Cardiac Electrophysiology and Arrhythmias*. New York, NY, USA: Grune & Stratton Inc; 1985. p. 265-75.
5. Antzelevitch C. Clinical application of new concepts of parasystole, reflection, and tachycardia. *Cardiol Clin* 1:39-50. 1983.
6. Arora RC, Waldmann M, Hopkins DA, Armour JA. Porcine intrinsic cardiac ganglia. *Anat Rec* 271A:249-58. 2003.
7. Bagwe S, Berenfeld O, Vaidya D, Morley GE, Jalife J. Altered right atrial excitation and propagation in connexin40 knockout mice. *Circulation* 112:2245-53. 11-10-2005.
8. Bansal G, Druey KM, Xie Z. R4 RGS proteins: regulation of G-protein signaling and beyond. *Pharmacol Ther* 116:473-95. 2007.
9. Beazely MA, Watts VJ. Regulatory properties of adenylate cyclases type 5 and 6: A progress report. *Eur J Pharmacol* 535:1-12. 27-3-2006.
10. Benjamin EJ, Wolf PA, D'Agostino RB, Silbershatz H, Kannel WB, Levy D. Impact of atrial fibrillation on the risk of death: the Framingham Heart Study. *Circulation* 98:946-52. 8-9-1998.
11. Bernard C. *An Introduction to the Study of Experimental Medicine*. New York, New York: Dover Publications, Inc.; 1957.
12. Brioschi C, Micheloni S, Tellez JO, Pisoni G, Longhi R, Moroni P, Billeter R, Barbuti A, Dobrzynski H, Boyett MR, DiFrancesco D, Baruscotti M. Distribution of the pacemaker HCN4 channel mRNA and protein in the rabbit sinoatrial node. *J Mol Cell Cardiol* 47:221-7. 2009.

13. Burger DE, Lu X, Lei M, Xiang FL, Hammoud L, Jiang M, Wang H, Jones DL, Sims SM, Feng Q. Neuronal nitric oxide synthase protects against myocardial infarction-induced ventricular arrhythmia and mortality in mice. *Circulation* 120:1345-54. 6-10-2009.
14. Burger DE, Xiang FL, Hammoud L, Jones DL, Feng Q. Erythropoietin protects the heart from ventricular arrhythmia during ischemia and reperfusion via neuronal nitric-oxide synthase. *J Pharmacol Exp Ther* 329:900-7. 2009.
15. Calo LA, Pagnin E, Davis PA, Sartori M, Ceolotto G, Pessina AC, Semplicini A. Increased expression of regulator of G protein signaling-2 (RGS-2) in Bartter's/Gitelman's syndrome. A role in the control of vascular tone and implication for hypertension. *J Clin Endocrinol Metab* 89:4153-7. 2004.
16. Candido C, Rosenbaum DS. *Quantitative Cardiac Electrophysiology*. New York: Marcel Dekker, Inc.; 2002.
17. Caspar DL, Goodenough DA, Makowski L, Phillips WC. Gap junction structures. I. Correlated electron microscopy and x-ray diffraction. *J Cell Biol* 74:605-28. 1977.
18. Chang CM, Wu TJ, Zhou S, Doshi RN, Lee MH, Ohara T, Fishbein MC, Karagueuzian HS, Chen PS, Chen LS. Nerve sprouting and sympathetic hyperinnervation in a canine model of atrial fibrillation produced by prolonged right atrial pacing. *Circulation* 103:22-5. 2001.
19. Chen F, Spicher K, Jiang M, Birnbaumer L, Wetzel GT. Lack of muscarinic regulation of Ca(2+) channels in G(i2)alpha gene knockout mouse hearts. *Am J Physiol Heart Circ Physiol* 280:H1989-H1995. 2001.
20. Chen SA, Chiang CE, Yang CJ, Cheng CC, Wu TJ, Wang SP, Chiang BN, Chang MS. Sustained atrial tachycardia in adult patients. Electrophysiological characteristics, pharmacological response, possible mechanisms, and effects of radiofrequency ablation. *Circulation* 90:1262-78. 1994.
21. Christoffels VM, Smits GJ, Kispert A, Moorman AF. Development of the pacemaker tissues of the heart. *Circ Res* 106:240-54. 5-2-2010.
22. Cifelli C, Rose RA, Zhang H, Voigtlaender-Bolz J, Bolz SS, Backx PH, Heximer SP. RGS4 Regulates Parasympathetic Signaling and Heart Rate Control in the Sinoatrial Node. *Circ Res*. 24-7-2008.
23. Clark RB, Mangoni ME, Lueger A, Couette B, Nargeot J, Giles WR. A rapidly activating delayed rectifier K⁺ current regulates pacemaker activity in adult mouse sinoatrial node cells. *Am J Physiol Heart Circ Physiol* 286:H1757-H1766. 2004.
24. Clemo HF, Belardinelli L. Effect of adenosine on atrioventricular conduction. I: Site and characterization of adenosine action in the guinea pig atrioventricular node. *Circ Res* 59:427-36. 1986.

25. Cottrell GT, Burt JM. Heterotypic gap junction channel formation between heteromeric and homomeric Cx40 and Cx43 connexons. *Am J Physiol Cell Physiol* 281:C1559-C1567. 2001.
26. Coumel P, Attuel P, Lavallee J, Flammang D, Leclercq JF, Slama R. [The atrial arrhythmia syndrome of vagal origin]. *Arch Mal Coeur Vaiss* 71:645-56. 1978.
27. Courtemanche M, Ramirez RJ, Nattel S. Ionic mechanisms underlying human atrial action potential properties: insights from a mathematical model. *Am J Physiol* 275:H301-H321. 1998.
28. Danik SB, Liu F, Zhang J, Suk HJ, Morley GE, Fishman GI, Gutstein DE. Modulation of cardiac gap junction expression and arrhythmic susceptibility. *Circ Res* 95:1035-41. 12-11-2004.
29. DiFrancesco D, Noble D. A model of cardiac electrical activity incorporating ionic pumps and concentration changes. *Philos Trans R Soc Lond B Biol Sci* 307:353-98. 10-1-1985.
30. Doupnik CA, Xu T, Shinaman JM. Profile of RGS expression in single rat atrial myocytes. *Biochim Biophys Acta* 1522:97-107. 3-12-2001.
31. Drici MD, Diochot S, Terrenoire C, Romey G, Lazdunski M. The bee venom peptide tertiapin underlines the role of I(KACh) in acetylcholine-induced atrioventricular blocks. *Br J Pharmacol* 131:569-77. 2000.
32. Dupont E, Ko Y, Rothery S, Coppens SR, Baghai M, Haw M, Severs NJ. The gap-junctional protein connexin40 is elevated in patients susceptible to postoperative atrial fibrillation. *Circulation* 103:842-9. 13-2-2001.
33. Dupont E, Matsushita T, Kaba RA, Voizzi C, Coppens SR, Khan N, Kaprielian R, Yacoub MH, Severs NJ. Altered Connexin Expression in Human Congestive Heart Failure. *J Mol Cell Cardiol* 33:359-71. 2001.
34. Efimov IR, Fedorov VV. Chessboard of atrial fibrillation: reentry or focus? Single or multiple source(s)? Neurogenic or myogenic? *Am J Physiol Heart Circ Physiol* 289:H977-H979. 2005.
35. Efimov IR, Nikolski VP, Rothenberg F, Greener ID, Li J, Dobrzynski H, Boyett M. Structure-function relationship in the AV junction. *Anat Rec A Discov Mol Cell Evol Biol* 280:952-65. 2004.
36. Fabritz L, Kirchhof P, Fortmuller L, Auchampach JA, Baba HA, Breithardt G, Neumann J, Boknik P, Schmitz W. Gene dose-dependent atrial arrhythmias, heart block, and brady-cardiomyopathy in mice overexpressing A(3) adenosine receptors. *Cardiovasc Res* 62:500-8. 1-6-2004.

37. Fisher JT, Vincent SG, Gomeza J, Yamada M, Wess J. Loss of vagally mediated bradycardia and bronchoconstriction in mice lacking M2 or M3 muscarinic acetylcholine receptors. *FASEB J* 18:711-3. 2004.
38. Fu Y, Huang X, Piao L, Lopatin AN, Neubig RR. Endogenous RGS proteins modulate SA and AV nodal functions in isolated heart: implications for sick sinus syndrome and AV block. *Am J Physiol Heart Circ Physiol* 292:H2532-H2539. 2007.
39. Fu Y, Huang X, Zhong H, Mortensen RM, D'Alecy LG, Neubig RR. Endogenous RGS proteins and Galpha subtypes differentially control muscarinic and adenosine-mediated chronotropic effects. *Circ Res* 98:659-66. 17-3-2006.
40. Furness JB, Jones C, Nurgali K, Clerc N. Intrinsic primary afferent neurons and nerve circuits within the intestine. *Prog Neurobiol* 72:143-64. 2004.
41. Garrey WE. The nature of fibrillary contraction of the heart. Its relations to tissue mass and form. *Am J Physiol* 33:397-414. 1914.
42. Garrey WE. Auricular fibrillation. *Physiol Rev* 4:215-50. 1924.
43. Gauldie J, Hanson JM, Shipolini RA, Vernon CA. The structures of some peptides from bee venom. *Eur J Biochem* 83:405-10. 1978.
44. Geivers H, Schaper W, Servaes J, Xhonneux R. Cardiac excitability determined by electronic computer. *Pflugers Arch Gesamte Physiol Menschen Tiere* 298:185-90. 1967.
45. Gross V, Tank J, Obst M, Plehm R, Blumer KJ, Diedrich A, Jordan J, Luft FC. Autonomic nervous system and blood pressure regulation in RGS2-deficient mice. *Am J Physiol Regul Integr Comp Physiol* 288:R1134-R1142. 2005.
46. Gutstein DE, Morley GE, Tamaddon H, Vaidya D, Schneider MD, Chen J, Chien KR, Stuhlmann H, Fishman GI. Conduction slowing and sudden arrhythmic death in mice with cardiac-restricted inactivation of connexin43. *Circ Res* 88:333-9. 16-2-2001.
47. Haissaguerre M, Jais P, Shah DC, Takahashi A, Hocini M, Quiniou G, Garrigue S, Le Mouroux A, Le Metayer P, Clementy J. Spontaneous initiation of atrial fibrillation by ectopic beats originating in the pulmonary veins. *N Engl J Med* 339:659-66. 3-9-1998.
48. Haissaguerre M, Shah DC, Jais P, Hocini M, Yamane T, Deisenhofer I, Garrigue S, Clementy J. Mapping-guided ablation of pulmonary veins to cure atrial fibrillation. *Am J Cardiol* 86:9K-19K. 2-11-2000.
49. Hashimoto N, Yamashita T, Tsuruzoe N. Tertiapin, a selective IKACH blocker, terminates atrial fibrillation with selective atrial effective refractory period prolongation. *Pharmacol Res* 54:136-41. 2006.
50. Hassall CJ, Burnstock G. Immunocytochemical localisation of neuropeptide Y and 5-hydroxytryptamine in a subpopulation of amine-handling intracardiac neurones that do

- not contain dopamine beta-hydroxylase in tissue culture. *Brain Res* 422:74-82. 29-9-1987.
51. Hellgren I, Mustafa A, Riazi M, Suliman I, Sylven C, Adem A. Muscarinic M3 receptor subtype gene expression in the human heart. *Cell Mol Life Sci* 57:175-80. 20-1-2000.
 52. Heximer SP, Knutsen RH, Sun X, Kaltenbronn KM, Rhee MH, Peng N, Oliveira-dos-Santos A, Penninger JM, Muslin AJ, Steinberg TH, Wyss JM, Mecham RP, Blumer KJ. Hypertension and prolonged vasoconstrictor signaling in RGS2-deficient mice. *J Clin Invest* 111:445-52. 2003.
 53. Hille B. *Ionic Channels of Excitable Membranes*. Sinauer Associates Inc.; 1984.
 54. Hoffa M, Ludwig C. Einige neueversuche uber herzbewegung. *Zeitschrift Rationellen Medizin* 9:107-44. 1850.
 55. Hollinger S, Hepler JR. Cellular regulation of RGS proteins: modulators and integrators of G protein signaling. *Pharmacol Rev* 54:527-59. 2002.
 56. Jalife J. Rotors and spiral waves in atrial fibrillation. *J Cardiovasc Electrophysiol* 14:776-80. 2003.
 57. Jalife J, Berenfeld O, Skanes A, Mandapati R. Mechanisms of atrial fibrillation: mother rotors or multiple daughter wavelets, or both? *J Cardiovasc Electrophysiol* 9:S2-12. 1998.
 58. Jalife J, Delmar M, Anumonwo J, Berenfeld O, Kalifa J. *Basic Cardiac Electrophysiology for the Clinician*. 2 ed. Hoboken, NY: Wiley-Blackwell; 2009.
 59. Jalife J, Pandit SV. Ionic mechanisms of wavebreak in fibrillation. *Heart Rhythm* 2:660-3. 2005.
 60. Jin W, Lu Z. A novel high-affinity inhibitor for inward-rectifier K⁺ channels. *Biochem* 37:13291-9. 22-9-1998.
 61. Kalifa J, Jalife J, Zaitsev AV, Bagwe S, Warren M, Moreno J, Berenfeld O, Nattel S. Intra-atrial pressure increases rate and organization of waves emanating from the superior pulmonary veins during atrial fibrillation. *Circulation* 108:668-71. 12-8-2003.
 62. Kannel WB, Abbott RD, Savage DD, McNamara PM. Epidemiologic features of chronic atrial fibrillation: the Framingham study. *N Engl J Med* 306:1018-22. 29-4-1982.
 63. Katz AM. *Physiology of the Heart*. Philadelphia: Lippincott Williams & Wilkins; 2006.
 64. Kirchhof P, Fabritz L, Fortmuller L, Matherne GP, Lankford A, Baba HA, Schmitz W, Breithardt G, Neumann J, Boknik P. Altered sinus nodal and atrioventricular nodal

- function in freely moving mice overexpressing the A1 adenosine receptor. *Am J Physiol Heart Circ Physiol* 285:H145-H153. 2003.
65. Kitazawa T, Asakawa K, Nakamura T, Teraoka H, Unno T, Komori S, Yamada M, Wess J. M3 muscarinic receptors mediate positive inotropic responses in mouse atria: a study with muscarinic receptor knockout mice. *J Pharmacol Exp Ther* 330:487-93. 2009.
 66. Kleber AG. The fibrillating atrial myocardium. What can the detection of wave breaks tell us? *Cardiovasc Res* 48:181-4. 2000.
 67. Kooroor P, Wickman K, Maguire CT, Pu W, Gehrman J, Berul CI, CLAPHAM DE. Evaluation of the role of I(KACh) in atrial fibrillation using a mouse knockout model. *J Am Coll Cardiol* 37:2136-43. 15-6-2001.
 68. Krejci A, Tucek S. Quantitation of mRNAs for M(1) to M(5) subtypes of muscarinic receptors in rat heart and brain cortex. *Mol Pharmacol* 61:1267-72. 2002.
 69. Laird DW. The life cycle of a connexin: gap junction formation, removal, and degradation. *J Bioenerg Biomembr* 28:311-8. 1996.
 70. Lakatta EG, Maltsev VA, Vinogradova TM. A coupled SYSTEM of intracellular Ca²⁺ clocks and surface membrane voltage clocks controls the timekeeping mechanism of the heart's pacemaker. *Circ Res* 106:659-73. 5-3-2010.
 71. Lin X, Gemel J, Glass A, Zemlin CW, Beyer EC, Veenstra RD. Connexin40 and connexin43 determine gating properties of atrial gap junction channels. *J Mol Cell Cardiol* 48:238-45. 1-1-2010.
 72. Liu J, Noble PJ, Xiao G, Abdelrahman M, Dobrzynski H, Boyett MR, Lei M, Noble D. Role of pacemaking current in cardiac nodes: insights from a comparative study of sinoatrial node and atrioventricular node. *Prog Biophys Mol Biol* 96:294-304. 2008.
 73. Liu L, Nattel S. Differing sympathetic and vagal effects on atrial fibrillation in dogs: role of refractoriness heterogeneity. *Am J Physiol* 273:H805-H816. 1997.
 74. Lomax AE, Rose RA, Giles WR. Electrophysiological evidence for a gradient of G protein-gated K⁺ current in adult mouse atria. *Br J Pharmacol* 140:576-84. 2003.
 75. MacWilliam JA. Fibrillar contraction of the heart. *J Physiol* 8:296. 1887.
 76. Mandapati R, Skanes A, Chen J, Berenfeld O, Jalife J. Stable microreentrant sources as a mechanism of atrial fibrillation in the isolated sheep heart. *Circulation* 101:194-9. 18-1-2000.
 77. Mansour M, Mandapati R, Berenfeld O, Chen J, Samie FH, Jalife J. Left-to-right gradient of atrial frequencies during acute atrial fibrillation in the isolated sheep heart. *Circulation* 103:2631-6. 29-5-2001.

78. Matthes J, Yildirim L, Wietzorrek G, Reimer D, Striessnig J, Herzig S. Disturbed atrio-ventricular conduction and normal contractile function in isolated hearts from Cav1.3-knockout mice. *Naunyn Schmiedebergs Arch Pharmacol* 369:554-62. 2004.
79. Mawe GM, Talmage EK, Lee KP, Parsons RL. Expression of choline acetyltransferase immunoreactivity in guinea pig cardiac ganglia. *Cell Tissue Res* 285:281-6. 1996.
80. Mazgalev T, Dreifus LS, Michelson EL, Pelleg A. Vagally induced hyperpolarization in atrioventricular node. *Am J Physiol* 251:H631-H643. 1986.
81. Milligan G, Kostenis E. Heterotrimeric G-proteins: a short history. *Br J Pharmacol* 147 Suppl 1:S46-S55. 2006.
82. Moe GK. On the multiple wavelet hypothesis of atrial fibrillation. *Arch Int Pharmacodyn* 40:183-9. 1962.
83. Moe GK, Abildskov JA. Atrial fibrillation as a self-sustaining arrhythmia independent of focal discharge. *Am Heart J* 58:59-70. 1959.
84. Moe GK, RHEINBOLDT WC, Abildskov JA. A computer model of atrial fibrillation. *Am Heart J* 67:200-20. 1964.
85. Morillo CA, Klein GJ, Jones DL, Guiraudon CM. Chronic rapid atrial pacing. Structural, functional, and electrophysiological characteristics of a new model of sustained atrial fibrillation. *Circulation* 91:1588-95. 1-3-1995.
86. Munk AA, Adjemian RA, Zhao J, Ogbaghebriel A, Shrier A. Electrophysiological properties of morphologically distinct cells isolated from the rabbit atrioventricular node. *J Physiol* 493 (Pt 3):801-18. 15-6-1996.
87. Nademanee K, McKenzie J, Kosar E, Schwab M, Sunsaneewitayakul B, Vasavakul T, Khunnawat C, Ngarmukos T. A new approach for catheter ablation of atrial fibrillation: mapping of the electrophysiologic substrate. *J Am Coll Cardiol* 43:2044-53. 2-6-2004.
88. Nakagawa H, Sherlag BJ, Lockwood D, Wolf RK, Peyton M, Wu R, Yokoyama K, PO SS, Herring L, Lazzara R, Jackmann WK, Armour JA. Localization of left atrial ganglionated plexuses using endocardial and epicardial high frequency stimulation in patients with atrial fibrillation. *Heart Rhythm* 2:S 10-S11. 2005.
89. Nakagawa H, Sherlag BJ, Wu AW, Lockwood D, Yokoyama K, Herring L, Lazzara R, Jackman WM. Addition of Selective ablation of Autonomic Ganglia to Pulmonary Vein Antrum Ablation for Treatment of Paroxysmal and Persistent Atrial Fibrillation. *Circulation* 110:III-543. 2005.
90. Nattel S. New ideas about atrial fibrillation 50 years on. *Nature* 415:219-26. 10-1-2002.
91. Nattel S. Age, gender, and supraventricular arrhythmias: roles of ion channels, connexins, and tissue architecture? *Heart Rhythm* 1:397-8. 2004.

92. Nattel S, Allessie M, Haissaguerre M. Spotlight on atrial fibrillation-the 'complete arrhythmia'. *Cardiovasc Res* 54:197-203. 2002.
93. Nerbonne JM. Studying cardiac arrhythmias in the mouse--a reasonable model for probing mechanisms? *Trends Cardiovasc Med* 14:83-93. 2004.
94. Nishimaru K, Makuta R, Tanaka Y, Tanaka H, Shigenobu K. Pharmacological properties of excitation-contraction mechanisms in isolated mouse left atria. *Pharmacology* 62:87-91. 2001.
95. Nixon JV. *The AHA Clinical Cardiac Consult*. 3 ed. Philadelphia: Lippincott Williams & Wilkins; 2011.
96. Nygren A, Lomax AE, Giles WR. Heterogeneity of action potential durations in isolated mouse left and right atria recorded using voltage-sensitive dye mapping. *Am J Physiol Heart Circ Physiol* 287:H2634-H2643. 2004.
97. Okumura S, Kawabe J, Yatani A, Takagi G, Lee MC, Hong C, Liu J, Takagi I, Sadoshima J, Vatner DE, Vatner SF, Ishikawa Y. Type 5 adenylyl cyclase disruption alters not only sympathetic but also parasympathetic and calcium-mediated cardiac regulation. *Circ Res* 93:364-71. 22-8-2003.
98. Oliveira-dos-Santos AJ, Matsumoto G, Snow BE, Bai D, Houston FP, Whishaw IQ, Mariathasan S, Sasaki T, Wakeham A, Ohashi PS, Roder JC, Barnes CA, Siderovski DP, Penninger JM. Regulation of T cell activation, anxiety, and male aggression by RGS2. *Proc Natl Acad Sci U S A* 97:12272-7. 24-10-2000.
99. Pabarcus MK, Casida JE. Kynurenine formamidase: determination of primary structure and modeling-based prediction of tertiary structure and catalytic triad. *Biochim Biophys Acta* 1596:201-11. 29-4-2002.
100. Pappone C, Rosanio S, Oreto G, Tocchi M, Gugliotta F, Vicedomini G, Salvati A, Dicandia C, Mazzone P, Santinelli V, Gulletta S, Chierchia S. Circumferential radiofrequency ablation of pulmonary vein ostia: A new anatomic approach for curing atrial fibrillation. *Circulation* 102:2619-28. 21-11-2000.
101. Pappone C, Santinelli V, Manguso F, Vicedomini G, Gugliotta F, Augello G, Mazzone P, Tortoriello V, Landoni G, Zangrillo A, Lang C, Tomita T, Mesas C, Mastella E, Alfieri O. Pulmonary vein denervation enhances long-term benefit after circumferential ablation for paroxysmal atrial fibrillation. *Circulation* 109:327-34. 27-1-2004.
102. 2004Platt M, Mandapati R, Sherlag BJ, Yamanashi WS, Nagakawa H, Lazzara R, Jackman WM. Limiting the number and extend of radiofrequency applications to terminate atrial fibrillation and subsequently prevent its inducibility. *Heart Rhythm* 1, S11, 2004.
103. Rosiak M, Dziuba M, Chudzik M, Cygankiewicz I, Bartczak K, Drozd J, Wranicz JK. Risk factors for atrial fibrillation: Not always severe heart disease, not always so 'lonely'. *Cardiol J* 17:437-42. 2010.

104. Ross EM. Coordinating speed and amplitude in G-protein signaling. *Curr Biol* 18:R777-R783. 9-9-2008.
105. Roy AA, Lemberg KE, Chidiac P. Recruitment of RGS2 and RGS4 to the plasma membrane by G proteins and receptors reflects functional interactions. *Mol Pharmacol* 64:587-93. 2003.
106. Saffitz JE, Laing JG, Yamada KA. Connexin expression and turnover : implications for cardiac excitability. *Circ Res* 86:723-8. 14-4-2000.
107. Sakamoto S, Schuessler RB, Lee AM, Aziz A, Lall SC, Damiano RJ, Jr. Vagal denervation and reinnervation after ablation of ganglionated plexi. *J Thorac Cardiovasc Surg* 139:444-52. 2010.
108. Salim S, Sinnarajah S, Kehrl JH, Dessauer CW. Identification of RGS2 and type V adenylyl cyclase interaction sites. *J Biol Chem* 278:15842-9. 2-5-2003.
109. Schwieler JH, Zlochiver S, Pandit SV, Berenfeld O, Jalife J, Bergfeldt L. Reentry in an accessory atrioventricular pathway as a trigger for atrial fibrillation initiation in manifest Wolff-Parkinson-White syndrome: a matter of reflection? *Heart Rhythm* 5:1238-47. 2008.
110. Shen MJ, Choi EK, Tan AY, Han S, Shinohara T, Maruyama M, Chen LS, Shen C, Hwang C, Lin SF, Chen PS. Patterns of baseline autonomic nerve activity and the development of pacing-induced sustained atrial fibrillation. *Heart Rhythm* 8:583-9. 2011.
111. Shi H, Wang H, Yang B, Xu D, Wang Z. The M3 receptor-mediated K(+) current (IKM3), a G(q) protein-coupled K(+) channel. *J Biol Chem* 279:21774-8. 21-5-2004.
112. Shi H, Yang B, Xu D, Wang H, Wang Z. Electrophysiological characterization of cardiac muscarinic acetylcholine receptors: different subtypes mediate different potassium currents. *Cell Physiol Biochem* 13:59-74. 2003.
113. Shiroshita-Takeshita A, Sakabe M, Haugan K, Hennen JK, Nattel S. Model-dependent effects of the gap junction conduction-enhancing antiarrhythmic peptide rotigaptide (ZP123) on experimental atrial fibrillation in dogs. *Circulation* 115:310-8. 23-1-2007.
114. Sinnarajah S, Dessauer CW, Srikumar D, Chen J, Yuen J, Yilma S, Dennis JC, Morrison EE, Vodyanoy V, Kehrl JH. RGS2 regulates signal transduction in olfactory neurons by attenuating activation of adenylyl cyclase III. *Nature* 409:1051-5. 22-2-2001.
115. Skanes AC, Mandapati R, Berenfeld O, Davidenko JM, Jalife J. Spatiotemporal periodicity during atrial fibrillation in the isolated sheep heart. *Circulation* 98:1236-48. 22-9-1998.
116. Tamargo J, Caballero R, Gomez R, Valenzuela C, Delpon E. Pharmacology of cardiac potassium channels. *Cardiovasc Res* 62:9-33. 1-4-2004.

117. Thijssen VL, Ausma J, Liu GS, Alessie MA, van Eys GJ, Borgers M. Structural changes of atrial myocardium during chronic atrial fibrillation. *Cardiovasc Pathol* 9:17-28. 2000.
118. Tsang S, Woo AY, Zhu W, Xiao RP. Deregulation of RGS2 in cardiovascular diseases. *Front Biosci (Schol Ed)* 2:547-57. 2010.
119. Vaquero M, Calvo D, Jalife J. Cardiac fibrillation: from ion channels to rotors in the human heart. *Heart Rhythm* 5:872-9. 2008.
120. Volders PG, Vos MA, Szabo B, Sipido KR, de Groot SH, Gorgels AP, Wellens HJ, Lazzara R. Progress in the understanding of cardiac early afterdepolarizations and torsades de pointes: time to revise current concepts. *Cardiovasc Res* 46:376-92. 2000.
121. Vulpain A. Note sur les effets de la faradisation directe des ventricules du coeur le chien. *Archives de Physiologie* 1:975. 1874.
122. Wang H, Lu Y, Wang Z. Function of cardiac M3 receptors. *Auton Autacoid Pharmacol* 27:1-11. 2007.
123. Wang Z, Shi H, Wang H. Functional M3 muscarinic acetylcholine receptors in mammalian hearts. *Br J Pharmacol* 142:395-408. 2004.
124. Wess J. G-protein-coupled receptors: molecular mechanisms involved in receptor activation and selectivity of G-protein recognition. *FASEB J* 11:346-54. 1997.
125. Wickman K, Nemej J, Gendler SJ, CLAPHAM DE. Abnormal heart rate regulation in GIRK4 knockout mice. *Neuron* 20:103-14. 1998.
126. Wieland T, Lutz S, Chidiac P. Regulators of G protein signalling: a spotlight on emerging functions in the cardiovascular system. *Curr Opin Pharmacol* 7:201-7. 2007.
127. Yan GX, Kowey PR. *Management of Cardiac Arrhythmias*. 2 ed. New York: Humana Press; 2011.
128. Yang L, Liu G, Zakharov SI, Morrow JP, Rybin VO, Steinberg SF, Marx SO. Ser1928 is a common site for Cav1.2 phosphorylation by protein kinase C isoforms. *J Biol Chem* 280:207-14. 7-1-2005.
129. Yue P, Zhang Y, Du Z, Xiao J, Pan Z, Wang N, Yu H, Ma W, Qin H, Wang WH, Lin DH, Yang B. Ischemia impairs the association between connexin 43 and M3 subtype of acetylcholine muscarinic receptor (M3-mAChR) in ventricular myocytes. *Cell Physiol Biochem* 17:129-36. 2006.
130. Zhao P, Nguyen CH, Chidiac P. The proline-rich N-terminal domain of G18 exhibits a novel G protein regulatory function. *J Biol Chem* 285:9008-17. 19-3-2010.
131. Zipes DP. The seventh annual Gordon K. Moe Lecture. Atrial fibrillation: from cell to bedside. *J Cardiovasc Electrophysiol* 8:927-38. 1997.

132. 2009 Zipes DP, Jalife J. Cardiac electrophysiology: from cell to bedside, 5th ed. 2009.
133. Zipes DP, Mihalick MJ, Robbins GT. Effects of selective vagal and stellate ganglion stimulation of atrial refractoriness. *Cardiovasc Res* 8:647-55. 1974.
134. Zou MX, Roy AA, Zhao Q, Kirshenbaum LA, Karmazyn M, Chidiac P. RGS2 is upregulated by and attenuates the hypertrophic effect of alpha1-adrenergic activation in cultured ventricular myocytes. *Cell Signal* 18:1655-63. 2006.

CHAPTER 2: Evidence for enhanced M3 muscarinic receptor function and sensitivity to atrial arrhythmia in the RGS2 deficient mouse

A version of this chapter has been published:

Tuomi JM, Chidiac P, Jones DL. Evidence for enhanced M3 muscarinic receptor function and sensitivity to atrial arrhythmia in the RGS2 deficient mouse. *Am J Physiol Heart Circ Physiol*. 2010 Feb;298(2):H554-61. Epub 2009 Dec 4.

2.0 CHAPTER SUMMARY

The role of the intrinsic cardiac autonomic nervous system in promoting neurogenic AF is well recognized, especially in patients with lone AF that develops nocturnally. Nocturnal AF in particular highlights an important vagal parasympathetic component of AF mechanisms. Studies in vagally mediated AF commonly focus on acetylcholine concentration dependence and the expression profiles of receptors and downstream effectors while ignoring the important regulators of the G protein signalling cascades. The amplitude of G protein effector signalling is strongly regulated by GTP hydrolysis, a process greatly accelerated (1000 fold) by GTPase activating proteins, such as the regulator of G protein signalling. The studies performed in this chapter attempts to address this issue by studying neurogenic atrial tachycardia/fibrillation in the RGS2 deficient mouse. These studies have also identified important anatomical and methodological considerations that must be adhered to in order to obtain systematic and reproducible data on arrhythmia susceptibility in the mouse. By using His bundle electrograms as a landmark of catheter positioning I have determined that AF induction in the mouse requires pacing in the Mid-Right Septal atrium (MRA). Also, I suggest that AF induction with single premature extra stimuli during

programmed electrical stimulation is more physiologically relevant than high frequency burst pacing (50Hz) with important mechanistic implications (re-entry). Overall, these studies find for the first time, a role for RGS proteins in atrial arrhythmia, showing that RGS2 deficiency in the mouse raises the substrate above the threshold for AF induction.

2.1 INTRODUCTION

Atrial fibrillation (AF) is the most common cardiac arrhythmia seen in general clinical practice⁵. It is characterized by abnormal, disorganized and very rapid atrial electrical activation. AF is a common health problem in the developed world³⁵, and its prevalence increases from about 0.5% of people in their 50s to nearly 10% of those over 80 years of age⁵. As the population ages, AF thus will place an increasing burden on health care resources, not only for its treatment and ongoing therapeutic management, but also because of the two most serious complications of AF, heart failure and stroke¹⁰. The generation of AF requires two critical components: 1) a trigger that initiates the event, and 2) a susceptible or vulnerable substrate that maintains the arrhythmia once initiated. AF can be triggered by ectopic foci firing¹⁵ from areas such as the pulmonary vein region¹³ or posterior left atrium²⁹. Maintenance of AF may depend on rotor formation, which is the organizing source (driver) of functional re-entrant activity (spiral waves). Rotors form when a propagating electrical wave “breaks” on an anatomical or electrophysiological heterogeneity, and under appropriate conditions of excitability, begins to rotate^{17, 41}. The wavelength of excitation (which is equal to the product of the conduction velocity and the refractory period), is also important in re-entry, with shorter wavelengths resulting in more stable rotors. For a review of rotors in cardiac fibrillation see Vaquero 2008⁴¹.

The pathogenesis of AF is complex, involving not only remodelling of the atrium, but also effects mediated via the intrinsic cardiac autonomic nervous system (ICANS)²⁵. Subpopulations of intrinsic cardiac neurons express multiple neurotransmitters¹⁴; however, in Guinea pig posterior ganglia, choline acetyltransferase immunostaining of all neurons indicates major parasympathetic cholinergic input to the myocardium²⁸. Rhythm management after catheter ablation of arrhythmogenic tissue in the pulmonary veins tends to be more successful when these autonomic ganglia are knowingly or inadvertently modified³⁶. Recently, we demonstrated that selective surgical left atrial neuroablation blocked the ability to electrically induce AF in the anaesthetized pig²⁰. The abrogation of parasympathetic signals may underlie the anti-arrhythmogenic effects of ICANS manipulation, since the development of AF can be promoted by cholinergic input to the atrium. ICANS-derived ACh activates multiple muscarinic receptor subtypes present in the atria including Gai/o-coupled M2 receptors (M2R) as well as Gαq-coupled M3 muscarinic receptors (M3R). These receptor subtypes activate distinct potassium currents including the G protein activated inward rectifier potassium current (GIRK3.1/3.4 or $I_{K, ACh}$) by M2R, and delayed rectifier potassium ($I_{K, M3}$) channels via the M3R³⁸.

Muscarinic receptors are GPCRs (G-protein coupled receptors), and as such they activate heterotrimeric G proteins by catalyzing GDP dissociation from the Gα subunit and consequently promoting GTP binding. This activating step leads to conformational changes and possibly also subunit dissociation within the G protein, thus enabling both Gα-GTP and the Gβγ dimer to regulate downstream effectors⁴⁴. Gα proteins are turned off by their intrinsic ability to hydrolyze GTP, however in vivo this step may be facilitated by an RGS (Regulator of G protein signalling) protein, thus shortening the duration of G protein activation. Most RGS proteins appear to be expressed in cardiac tissue³² and 7 distinct

isoforms (RGS2, RGS3, RGS4, RGS6, RGS10, RGS19 (GAIP) and RGS17 (RGSZ2) have been specifically localized to atrial myocytes⁹. Nearly all RGS proteins are GAPs for G α i/o, and about half also act on G α q/11¹. RGS2 is one of the most highly expressed RGS proteins in the heart²⁴, and it is a uniquely selective GAP for G α q with limited potency on G α i/o^{1,7}. Thus, RGS2 is potentially an important regulator of atrial G α q-coupled M3 receptors

Since RGS proteins limit GPCR signalling, we hypothesized that they may limit atrial arrhythmogenesis by keeping in check parasympathetic signals mediated via atrial muscarinic receptors. To test this, I compared RGS2^{-/-} and wild type mice for atrial electrophysiological properties and susceptibility to the induction of atrial tachyarrhythmias. To determine if the loss of RGS2 would enhance susceptibility to tachyarrhythmia induction, we performed in vivo electrophysiological pacing and recording studies in both strains. Overall, our results suggest that removing the inhibitory effect of RGS2 on M3-activated G α q renders the knockout mice more susceptible to electrically-induced atrial tachyarrhythmia.

2.2 METHODS

2.2.1 Animals And Preoperative Procedures

The generation and genotyping of RGS2 knock out (RGS2^{-/-}) mice have been described (Oliviera-Dos-Santos³⁰). Mice were provided with ad libitum food and water and held on a standard (12h:12h) light:dark cycle. The studies were approved by the Animal Use and Care Committee of the University of Western Ontario (protocol #2006-121-12) and complied with the guidelines of the Canadian Council on Animal Care and the Guide to the Care and Use of Laboratory Animals published by the US National Institutes of Health (Institution #A5527-01). One month old male RGS2^{-/-} and control C57BL/6 wild type (WT) mice were

anaesthetized with an i.p injection of a mixture of ketamine (150 mg/kg) and xylazine (10 mg/kg), and fixed in a supine position over a heated water blanket. Body temperature was monitored with a YSI-402 (Yellow Springs Instruments, Yellow Springs, Ohio) small animal rectal probe inserted approximately 1 cm past the anal sphincter, and maintained within the normal physiological range (36.5-38°C)⁸. Hair was removed from the neck with Nair® cream hair remover (Church & Dwight, Co, Inc., Mississauga, ON). With a cut down approach, a 23 ga Teflon endotracheal tube was inserted and ligated in place to keep the airway dry and open.

2.2.2 Surface Limb Lead Electrocardiograms (ECG)

Measurements were obtained using 4 subcutaneous 25 ga platinum electrodes (Grass Instrument Inc., Quincy, Mass.) placed at the base of each limb. ECG tracings were filtered between 0.05 to 100 Hz, digitized and sampled at 1.5 kHz, with an ECG 100 preamplifier connected to a MP100 recording system (BIOPAC Systems, Biolynx, Montreal, PQ).

2.2.3 In Vivo Intracardiac Electrophysiology Studies

A 2F octapolar stimulation / recording / drug infusion catheter (CIB'ER Mouse®, NuMED Inc., Hopkinton, NY) was inserted through the right jugular vein and advanced into the right atrium and ventricle (Fig. 1). Intracardiac electrograms were sampled at 1.5 kHz, and filtered at 100 to 5000 Hz (DA 100 amplifier, BIOPAC Systems). All data were recorded using Acknowledge software (BIOPAC Systems).

2.2.4 Catheter Positioning

Stimulation sites within the heart is known to influence the effective refractory period (ERP)²⁷. In the present study we used His bundle potential recordings (Fig. 1) to establish catheter positioning within the right atrium (RA) and ventricle (RV). Based on the size of the

RA and the spacing of the catheter electrodes, the two pairs of bipolar RA electrodes were located at the mid right atrium (MRA) and the high right atrium / superior vena cava region (HRA) above the crista terminalis.

2.2.5 Pacing Protocols

Bipolar pacing used 2 ms pulses at twice the diastolic threshold, delivered through a Grass SIU5 stimulus isolation unit, connected to a Grass S99 stimulator, programmed with a custom-built timer. Atrial (AERP), ventricular (VERP), and AV nodal (AVNERP) effective refractory periods were assessed with programmed electrical stimulation (PES)²⁷ using a drive train of 9 stimuli (S1) at cycle lengths of 150 and 100 ms followed by delivery of an extra stimulus (S2). Atrial pacing with 1 ms decrements were used to determine the Wenkebach cycle length (WCL).

2.2.6 Arrhythmia Induction

Both PES¹⁹ and burst pacing¹⁸ (2 ms pulses at 50 Hz, 400 ms burst duration) were used to determine susceptibility to atrial arrhythmia induction. Burst pacing used up to 30 bursts of pacing in both atrial locations. Atrial fibrillation in the mouse was implied to be distinguishable from atrial tachycardia based on the surface electrograms: lack of regular P waves, irregularly irregular ventricular responses, in combination with intracardiac electrograms having fractionation and/or intracardiac activation heterogeneities between the mid- and high-right atrium.

2.2.7 Effects of muscarinic receptor drugs

Pharmacological agents were purchased from Sigma, (Mississauga, ON), unless otherwise stated. Muscarinic receptor drugs, including the nonselective agonist carbachol (0.5 mg/kg), and the nonselective antagonist atropine (1 mg/kg) were injected

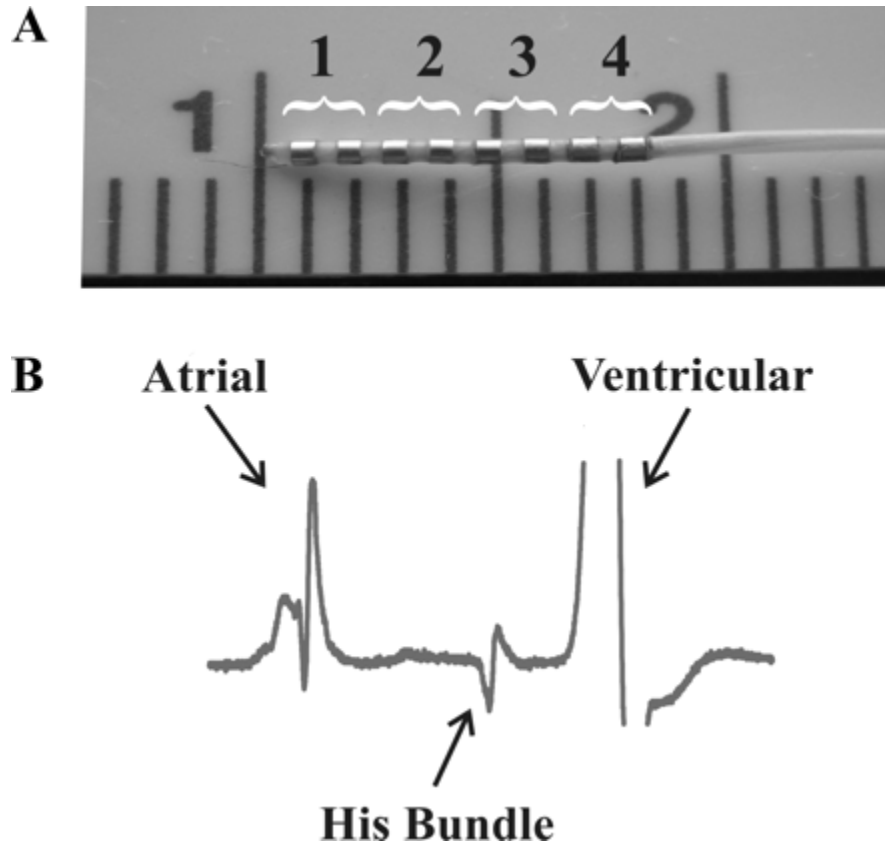


Figure 2.1: A. Photograph of the 2F octapolar stimulation / recording / drug infusion catheter (CIB'ER Mouse®, NuMED Inc., Hopkinton, NY) used for intracardiac electrophysiological studies in the mouse. Note the 0.5 mm spacing of the electrodes. Each bracketed electrode pair was used for recording and electrical stimulation. Numbers indicates the position within the heart: 1=right ventricle, 2=His bundle, 3=mid right atrium, 4=high right atrium / superior vena cava. B. Representative recording from electrode pair 2 showing the atrial, ventricular and His deflections.

intraperitoneally. The M3R-selective antagonist darifenacin hydrobromide (Cedar Lane labs, Markham, ON, 1 mg/kg) was administered intravenously. Electrophysiological measurements were made sequentially in the absence of drug, and then in the presence of carbachol, followed either by atropine or by darifenacin and then atropine. Effects of vagal stimulation (10V, 30 Hz, 3 s) on heart rate were measured prior to and after darifenacin and atropine administration.

2.2.8 RNA Isolation And Real Time RT-PCR

RNA was isolated using a Trizol kit (Qiagen Inc., Invitrogen, Burlington, ON). RNA concentration was determined using a spectrophotometer (Beckman Coulter, Mississauga, ON). Isolated RNA was converted to cDNA using the High-Capacity cDNA Reverse Transcription Kit (Applied Biosystems Inc., Carlsbad, CA). Real time analyses were carried out using Taqman gene expression Assays-on-Demand from Applied Biosystems and normalized to levels of the endogenous control, GAPDH. Relative expression of M2R, M3R, M4R, RGS2 and RGS4 mRNA were determined using 40 cycles on the ABI Prism 7900 HT sequence detector (Perkin Elmer Life Sciences, Woodbridge, ON). All samples were amplified in 3 parallel reactions per trial. To determine real time amplification efficiencies (E) and starting concentration (N0) of the amplicon, non-baseline corrected raw input data from the ABI Prism 7900 HT sequence detector was analyzed by linear regression analysis with LinRegPCR (2009) software³⁴.

2.2.9 Statistical Analysis

Group wise comparison of gene expression ratios were calculated using the relative expression REST software³¹, with efficiency and Ct deviations calculated by LinRegPCR. Discrete data were analyzed using Chi Square analysis³⁹. Drug and strain comparisons used

2-way ANOVA and the Bonferoni post-hoc test with GraphPad Prism 4 software. A P-value of <0.05 was be considered statistically significant.

2.3 RESULTS

2.3.1 Atrial Effective Refractory Periods

PES revealed a regional heterogeneity in refractory period, with longer AERPs in the HRA region compared to the MRA, and this difference was observed in both RGS2^{-/-} and WT mice (**Table 2.1**). AERPs were significantly lower in the RGS2^{-/-} mice in both the HRA (34±2 vs 30±1 ms, P<0.05) and MRA (23±1 vs. 21±1 ms, P<0.05) regions compared to WT mice (**Table 2.1**). Strain-related differences remained after carbachol administration, which reduced AERPs in both strains. In contrast, the nonselective muscarinic antagonist atropine increased AERPs to similar levels in both strains (**Table 2.1**). To determine the role of the M3R in the RGS2^{-/-} mouse we used the selective M3R blocker darifenacin hydrobromide (**Fig. 2.2**). Darifenacin increased the AERP from 20±2 to 30±1 of the MRA in the RGS2^{-/-} mouse (P<0.05, n=5) and from 25±1 to 30±1, in WT mice (n=6, P<0.05), which eliminated the strain-related differences. Two-way ANOVA revealed a significant interaction between strain and drug (darifenacin), suggesting that increased signalling through the M3 receptor may underlie the lower AERPs measured in animals lacking RGS2.

Since it has been established that vagally-induced bradycardia is mediated via M2R but not M3R¹¹, we compared the effects of darifenacin and atropine on heart rate changes following vagus nerve stimulation. Stimulating the vagus (10V, 30 Hz, 3 s) decreased heart rate by 38±6.8% in WT animals. This decrease was abolished by atropine but was unaltered in the presence of darifenacin (35±4.5%, n=4, P>0.5). This provided evidence that this dose

Table 2.1: Intracardiac electrophysiological values recorded in the absence and presence of carbachol and atropine in 1 month old male RGS2^{-/-} and wild type mice.

	Vehicle				Carbachol				Atropine			
	Wild Type		RGS2 ^{-/-}		Wild Type		RGS2 ^{-/-}		Wild Type		RGS2 ^{-/-}	
AhERP ₁₅₀	34±1	17	30±1	14*	29±1	11	26±2	7*				
AmERP ₁₅₀	24±1	19	21±1	19†	23±1	11	20±1	11*				
AhERP ₁₀₀	33±1	20	30±1	15*	29±1	12	25±2	8*	48±1	12	48±3	9
AmERP ₁₀₀	23±1	20	21±1	19*	22±1	12	19±1	10*	38±1	12	39±2	9
WCL	91±1	20	90±1	20	98±1	12	101±3	10	92±2	12	85±1	10†
AVNERP ₁₅₀	59±1	15	60±1	17	61±2	10	70±4	9*				
AVNERP ₁₀₀	66±1	20	65±1	20	72±2	12	79±3	10*	65±2	12	60±2	10*
AH ₁₅₀	21±1	7	21±1	6	21±1	10	23±1	7				
AH ₁₀₀	26±1	11	26±1	8	30±1	11	29±2	7	26±1	10	25±1	8
VERP ₁₅₀	37±1	15	39±1	15	43±2	11	44±2	7				
VERP ₁₀₀	41±1	18	43±1	20	45±1	12	45±2	9	42±1	12	42±2	10

Values are means ± SE; n (no. of mice) indicated beside value. AhERP, high atrial effective refractory period; AmERP, mid atrial effective refractory period; VERP, ventricular effective refractory period; AVNERP, atrial-ventricular effective refractory period; WCL, Wenkebach cycle length. Subscripts 100 and 150 refer to drive cycle lengths of 100 and 150 ms, respectively.

* 95% Confidence interval (CI) and

† 99% CI for difference in RGS2^{-/-} vs. wild type within drug group.

of darifenacin did not affect M2R signalling.

2.3.2 Atrial Tachyarrhythmia Induction

Atrial burst pacing (**Fig. 2.3**), and PES (**Fig. 2.4**)¹⁸ induced atrial tachyarrhythmias which demonstrated properties of AF; however, validating AF would require high density mapping and recording from the left atrium which often is the driver of regular rhythms recorded from the right atrium²⁹. Thus these have generally been labelled AT/F. PES-induction is thought to mimic physiological initiations of AF, as premature atrial beats often precede AF episodes¹⁵. On the other hand, burst pacing, although thought to be a non-physiological provocation, will reliably induce AF via cardiac electrical instability¹⁸. AF is very rarely induced by single extrastimuli in large animal and human studies and was thus anticipated to be even less provokable in mice, due to their small size. Thus AT/F sensitivity to single extrastimuli in the mouse implies a highly vulnerable myocardial substrate. The duration of induced arrhythmia is also important with “sustained” AF being defined in large animal and human electrophysiological studies as lasting >30 s. Hence, AT/F data were analyzed based on susceptibility to both pacing modalities and grouped into duration of the induced arrhythmia lasting <10 s, between 10-30 s and >30 s. As expected, one month old WT mice were mostly insensitive to single stimulus-induced AT/F (4%, 1/25) compared to burst pacing (40%, 10/25, $P<0.05$) (**Fig.2.3**, Top). Carbachol increased the susceptibility to both single extrastimulus (33%, 4/12) and burst pacing (58%, 7/12). Muscarinic receptor activation also prolonged the duration of AT/F episodes with only 2 of 12 untreated mice having sustained AT/F, while 5 of the 12 had sustained AT/F after carbachol administration. The site of stimulation within the atrium also affected susceptibility to AT/F induction. For WT mice, burst pacing more readily induced AT/F from the MRA (40%, 10/25) compared to

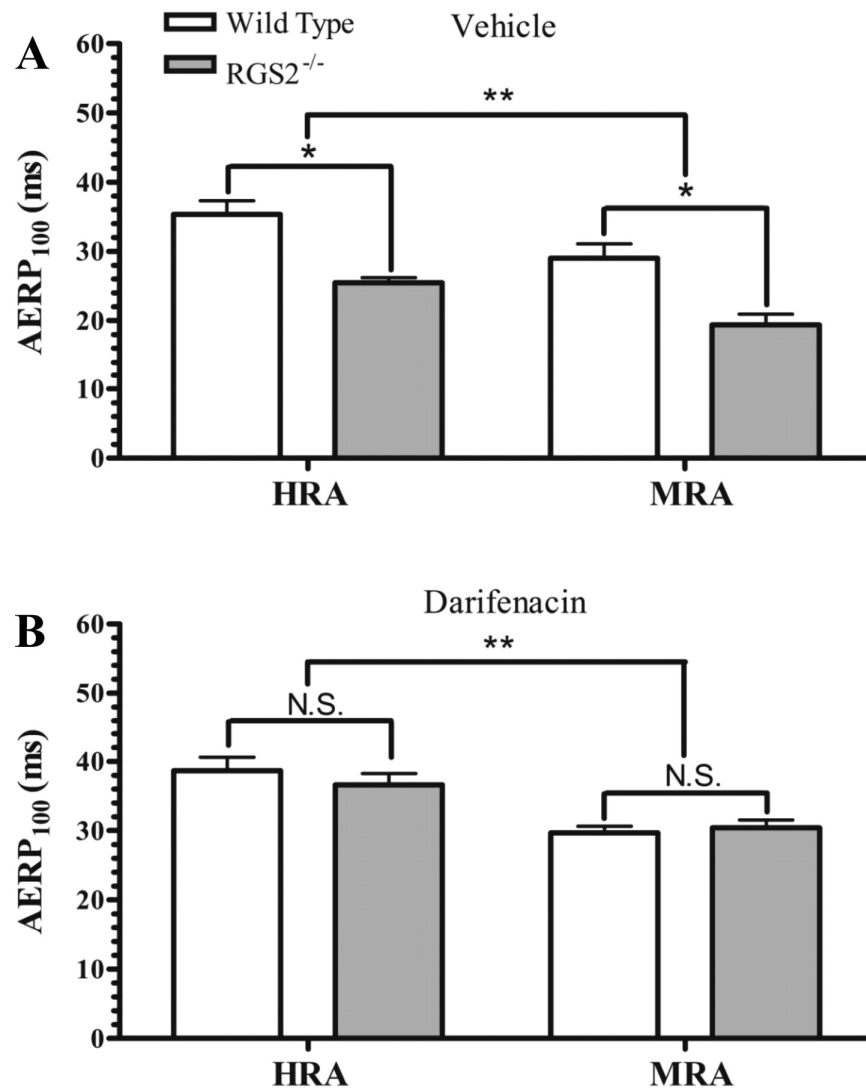


Figure 2.2: Atrial effective refractory period (AERP) was measured using programmed electrical stimulation (PES) with a 100ms drive train in 1 month old male wild type compared RGS2^{-/-} mice. AERP was measure in both the high right atrium (HRA) and mid right atrium (MRA) in the absence (A. Vehicle) and presence of darifenacin (B. Darifenacin). The AERP of the RGS2^{-/-} was significantly lower than that of wild type mice with vehicle control, but was normalized with darifenacin. * P<0.05, ** P<0.01.

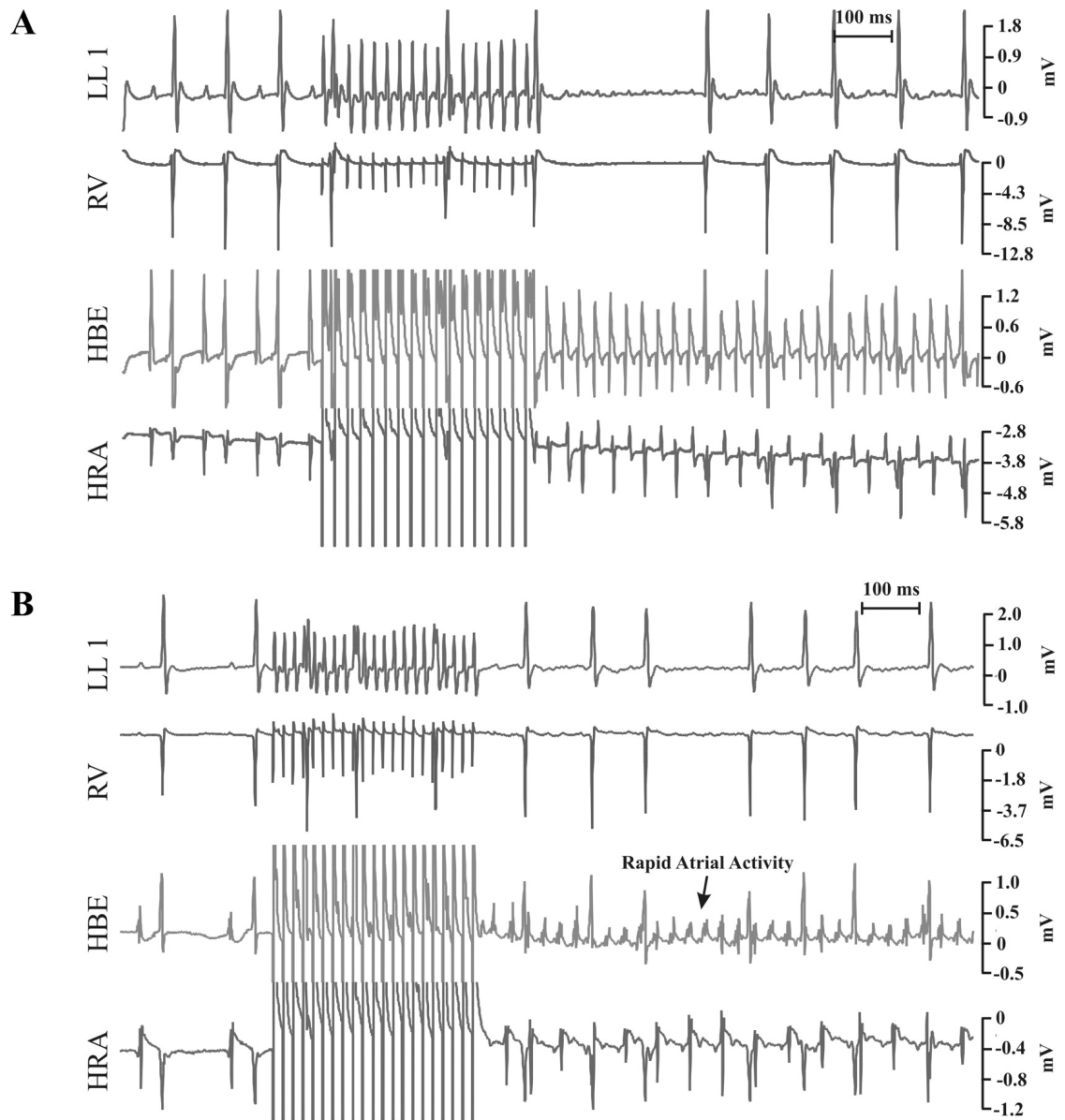


Figure 2.3: A. Atrial tachycardia/fibrillation (AT/F) induced with burst pacing (Burst) of the mid right atrium (MRA) in a 1 month old wild-type (WT) mouse. B. AT/F induced with burst pacing (Burst) of the MRA in a 1 month old *RGS2*^{-/-} mouse. Note the different tachycardia rates between the His bundle region electrogram (HBE) and the high right atrial electrogram (HRA) as well as the irregularly irregular ventricular response seen on limb lead I (LL1) and right ventricular electrogram (RV).

the HRA (8%, 2/25, $P < 0.05$) region. This is likely related to the relative AERPs, which were significantly shorter in the MRA compared to the HRA (**Table 2.1**). This electrical heterogeneity may be an important factor in providing a permissive substrate for wave break and re-entry initiation in the right atrium.

RGS2^{-/-} mice were more susceptible to PES induction of AT/F from the MRA (50%, 11/22) compared to the WT mice (4%, 1/25, $P < 0.05$) (**Table 2.2**). There was a trend for a greater percentage of RGS2^{-/-} mice to have sustained AT/F (>30 sec) with either pacing modality, but this did not reach significance ($0.1 > P > 0.05$) (**Table 2.2**).

2.3.3 Mechanism Of Arrhythmia (Evidence For Re-Entry)

Rapid focal activity has the potential to initiate rotors due to the interaction of a high frequency propagating wave fronts with the refractory tail of the previous wave^{17, 41}. Immediately after PES-initiated arrhythmia, local cycle lengths were often identical in the HRA and His bundle regions. However, sometimes at arrhythmia onset, heterogeneities in refractory periods were accompanied by a regional conduction block into the HRA (**Fig. 2.4, Top**). Also, heterogeneity in local cycle lengths were observed between the HRA and His bundle regions immediately following initiation of AT/F in an RGS2^{-/-} mouse (**Fig. 2.4, Bottom**). Immediately after induction, the local atrial electrogram from the His bundle region was shorter (22 ms) than that of the HRA (27 ms) region. However, 173 ms after initiation, local cycle length of the His bundle region converged with that of the HRA (25ms). This pattern suggests a drifting rotor that rapidly became anchored. However, this pattern may also indicate a tachycardia with a rapid rate at onset that slows down as the driving mechanism stabilizes. The rapid onset may combine with the regional ERP heterogeneity to produce a functional conduction block/slowing that recovers at a slower rate. In this and

Table 2.2: Incidence of AT/F induced by PES or burst pacing and maximum duration of induced AT/F with either PES or burst pacing induction.

	Wild Type	RGS2^{-/-}
<i>Inducibility</i>		
PES	4% (1/25)	50% (11/22)
Burst (50Hz, 400 ms pulse)	40% (10/25)	64% (14/22)
<i>Duration</i>		
No Response	60% (15/25)	36% (8/22)
<10 s	20% (5/25)	23% (5/22)
10-30 s	16% (4/25)	18% (4/22)
>30 s	4% (1/25)	23% (5/22)

χ^2 Analysis of discrete values revealed significant differences in atrial tachycardia/fibrillation (AT/F) susceptibility with programmed electrical stimulation (PES) ($P < 0.05$).

other mice (n=4) the cycle length during AT/F (27ms) was faster than the intrinsic AERP in the HRA region (32ms), suggesting the possibility of electronic interactions from a rotor core causing reduced refractoriness⁴¹.

2.3.4 Expression Of M2, M3 And M4 Receptors And RGS2 And RGS4 mRNA

Regional heterogeneity (left vs right atrium) in the expression of muscarinic receptors and/or their associated RGS proteins may contribute to arrhythmia. Therefore, we compared regional levels of mRNA encoding M2, M3 and M4 receptors, as well as RGS2 and RGS4, in 1 month old WT mice using the Relative Expression Software Tool (REST)³¹. There was no difference in M2, M3 and M4 receptor expression in WT compared to RGS2^{-/-} mice (data not shown). However, M2 receptor expression in WT mice was higher in the RA compared to the LA (P<0.05, ratio=0.763), while M3 receptor was higher in the LA (P<0.05, ratio=1.188) (**Fig. 2.5**). M4R, RGS2 and RGS4 did not differ between the two atria. In order to compare the expression levels of M2, M3 and M4 muscarinic receptors LinRegPCR analysis was used to determine both the PCR reaction efficiencies and the starting concentration of the amplicon (N0). As expected, the M2 receptor expression was substantially higher than both M3 and M4 receptors in atria and ventricles (**Fig2.6, Bottom**). RGS2 was more highly expressed than RGS4 in both right and left atria, while there was greater expression of RGS2 in the atrium than the ventricle (**Fig. 2.6, Top**).

2.3.5 Effects Of Body Temperature

Previously, with the exception of QTc, all electrophysiological parameters were found to be prolonged at lower body temperatures³. We extended these results to determine the effect of low body temperature (33.5 °C) on AERP and AT/F susceptibility. At 33.5 °C, AERPs were prolonged in both the HRA (34±3 vs 41±3, P<0.05) and MRA (24±3 vs 29±3, P<0.05) regions. The prolongation of AERP's reduced the susceptibility to AT/F induction.

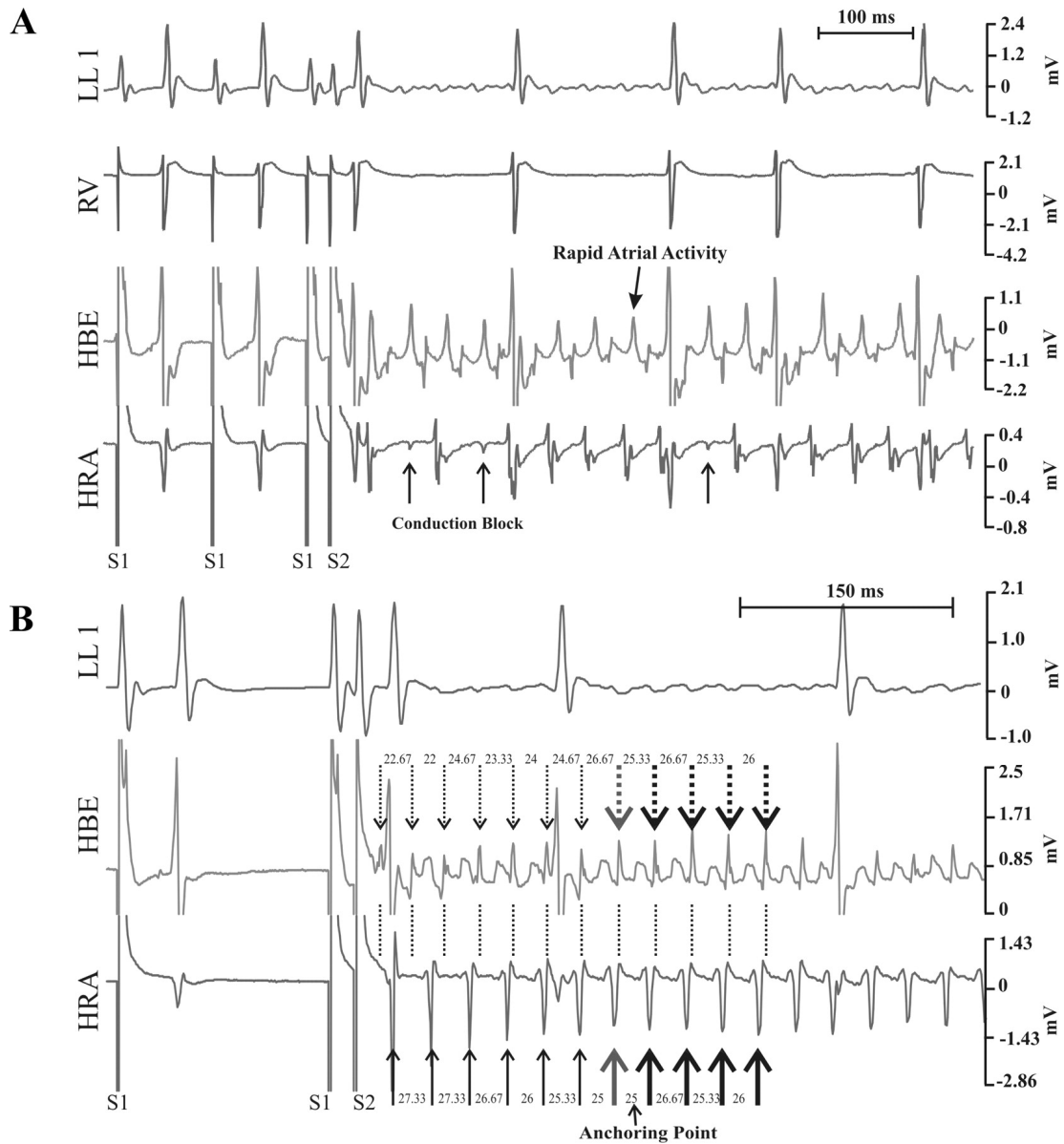


Figure 2.4: **A.** Programmed electrical stimulation (PES)-induced atrial tachycardia/fibrillation (AT/F) with a single extrastimulus (S2) in a 1 month old *RGS2*^{-/-} mouse. Note the conduction block into the high right atrial (HRA) region seen as far-field (low amplitude) potentials during block. The duration of the arrhythmia was >200 sec with an average atrial rate of ~1600 bpm. **B.** PES-induced AT/F using a single extrastimulus (S2) in a 1 month old *RGS2*^{-/-} mouse. Note the tachycardia cycle length variations between the high right atrial (HRA) and His bundle electrogram (HBE) regions, which regularize 173 ms after induction (anchoring point). LL1 limb lead 1. RV, right ventricular electrogram. HBE, electrogram from the His bundle region. HRA, recording from the high right atrium.

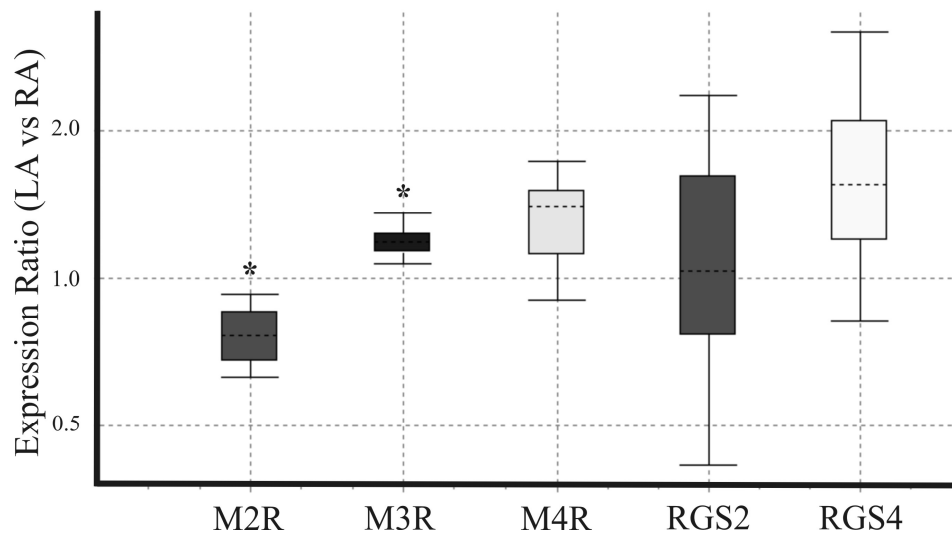


Figure 2.5: Quantitative real time reverse transcriptase polymerase chain reaction (qRT-PCR) determination of M2 and M3 receptor mRNA content in the atria of 1-month-old wild-type (WT) mice. Left vs right atrial mRNA expression ratios of were determined using the Relative Expression Software Tool (REST). There was greater expression of M2R in the RA, and greater M3R in the LA. * P<0.05.

Maintenance of body temperature is important as previous studies have stated that AT/F cannot be induced in mice without carbachol²². Our studies clearly show that AT/F can be induced without carbachol administration, and this difference is likely due to having maintained body temperature constant at 37 °C throughout the previous studies.

2.4 DISCUSSION

This study, to my knowledge, demonstrates for the first time a role for RGS proteins in atrial arrhythmia. The RGS2^{-/-} mice were more susceptible to PES-induced AT/F, and there was a greater percentage of RGS2^{-/-} mice with sustained AT/F. The greater susceptibility to AT/F was likely due to the abbreviated AERP in RGS2^{-/-} mice. This strain dependent difference was maintained in the presence of carbachol, while atropine abolished the strain dependent differences. These findings suggest an alteration in muscarinic receptor-gated K⁺ flux evidently due to an increase in muscarinic receptor response per se. The observed phenotypic difference cannot easily be attributed to increased parasympathetic release of acetylcholine, as chronic telemetry showed that while mean arterial pressure was increased by ~10 mm Hg in RGS2^{-/-} animals, heart rate was unchanged, indicating a resetting of the baroreceptor reflex¹². It follows that any observed cardiac electrophysiological phenotype would be due to the direct effect of RGS2 loss in the atria, rather than a baroreflex-mediated enhancement of vagal activity. Consistent with other studies, I found that RGS2 was highly expressed in the atria of mice. As RGS2 is a selective GAP for Gαq, while having limited potency on Gai/o¹, I hypothesized that Gαq-coupled M3Rs and not Gai/o-coupled M2Rs were involved in RGS2^{-/-} mediated reductions in AERP. The M3 muscarinic receptor activates a delayed rectifier potassium channel (I_{K, M3}) in the atrium³⁸. To date I_{K, M3} is the only identified atrial K⁺ channel activated by Gαq which is blocked by

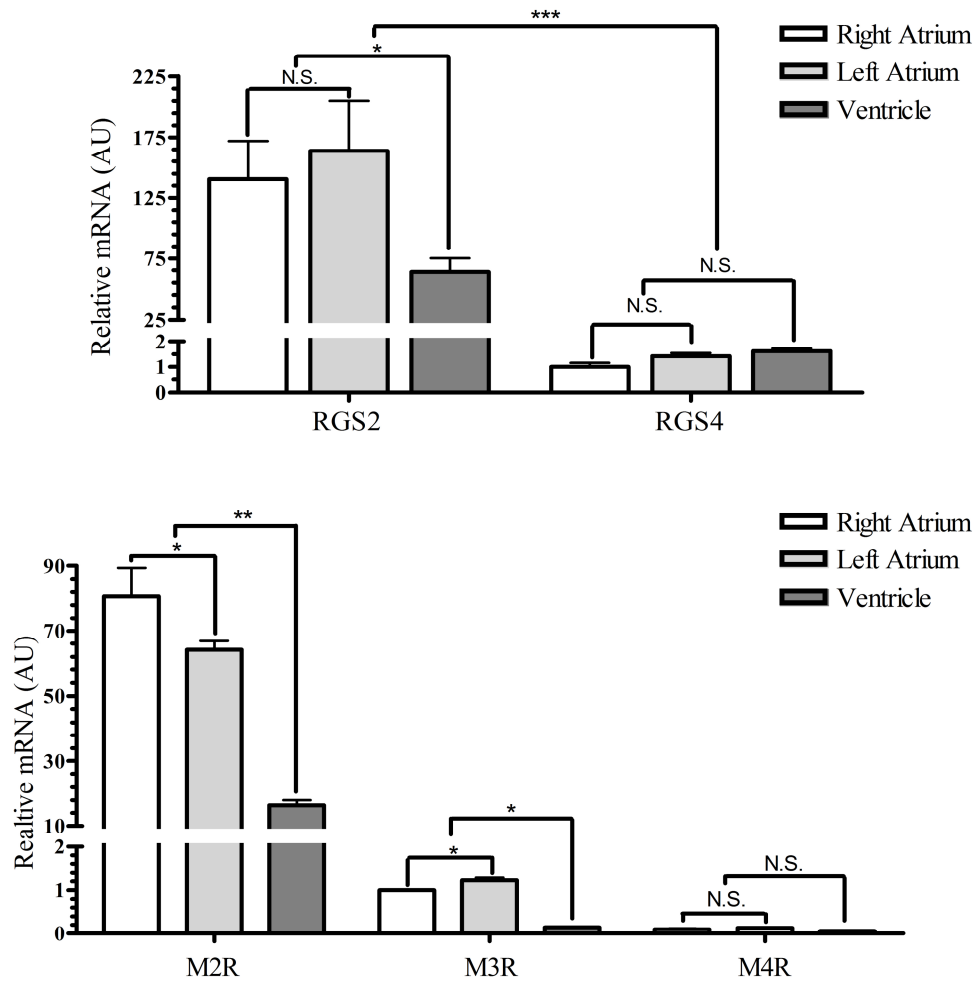


Figure 2.6: Relative mRNA expression as a ratio of the normalized gene of interest (GOI) relative to a house keeper gene (GAPDH) compared to either RGS4 (A) or M3R (B) in the left atrium, using the following equation: $[N0(GOI)/N0(GAPDH)]/[N0(M3R \text{ or } RGS4)]$.

atropine⁴³ and the M3 selective antagonist, darifenacin⁴². $I_{K, M3}$ has only been observed in canine atrial cells in the presence of 10 mM choline. However, while M2 deficient mice had a positive inotropic response to carbachol, M2/M3 double knockout mice were devoid of any inotropic response²¹. As the heart has been classically considered a “pure M2” organ²³, I examined the levels of M2, M3 and M4 muscarinic receptor mRNA in the RA, LA and ventricle. M2R expression was ~70 times higher than M3R with very little M4R detected in either atria or ventricle. To confirm the participation of M3R, I determined AERP in the absence and presence of darifenacin. This selective antagonist eliminated AERP differences between strains, confirming an M3R mediated phenotype.

AF can be maintained by either rapidly firing ectopic foci (e.g. from the pulmonary veins) or a functional re-entrant circuit (mother rotor). Reduced AERP in $RGS2^{-/-}$ mice would be expected to provide a vulnerable substrate for reentry by proportionally decreasing the wavelength of excitation. While it can be difficult to distinguish between AF mechanisms using whole animal intracardiac electrophysiological studies in animals the size of the mouse, I have made a number of observations that suggest a re-entrant mechanism of AT/F in the $RGS2^{-/-}$ mouse. 1) $RGS2^{-/-}$ mice were susceptible PES-induced AT/F, which, while not diagnostic in itself, is thought to more readily induced reentry than triggered activity¹⁶. 2) Myocardial regions with large heterogeneities in electrical properties are often more vulnerable to reentry², which can result from unidirectional conduction block in regions with longer refractoriness⁴. In the present study the atrial ERP was significantly longer in the HRA compared to the MRA region, and AT/F was more easily induced by pacing the MRA. 3) Computer modelling has been used to determine electrical and structural heterogeneities between the crista terminalis and right atrium as being key mechanisms underlying the initiation of reentry⁴. Rapid pacing in this area results in unidirectional conduction blockage

towards the crista terminalis and the initiation of reentry⁴. Consistent with this concept, I observed activation heterogeneities between the MRA and HRA region during and at the onset of AT/F (**Fig.2.4 Top**).

Initiation of rotors are suggested to be key in maintaining AF⁴¹. Once initiated, rotors have the potential to drift until they anchor around tissue heterogeneities (i.e. scars, coronary arteries, bands of connective tissue etc)⁴¹. Drifting rotors exhibit Doppler-like shifts in tachycardia cycle lengths such that the coupling interval is shorter in an area it drifts towards and longer in regions from which it moves away¹⁶. After anchoring, cycle lengths in the two regions should be identical. Due to the small size of the mouse heart, and the left atrial predominance of AF mechanisms, one could speculate that anchoring should occur rapidly with Doppler shifts observed relatively infrequently in the RA. However, I observed this complex activation pattern in an RGS2^{-/-} mouse (Fig.4 bottom). Rotors also enhance the repolarization of excited myocardium (reducing AERP) up to 1cm away due to a strong electrotonic current flow into the unexcited core^{16,41}. For this mouse, the local cycle length in the HRA during arrhythmia was faster than what would be allowed by the intrinsic ERP (32ms) further strengthening the argument for a re-entrant mechanism in AF in the RGS2^{-/-} mouse. Nevertheless, the suggestion of reentry supporting AF in the mouse requires techniques such as optical mapping to document the mechanism.

Both M2 and M3 muscarinic receptor-mediated K⁺ currents may be involved in the development of AF. In the canine heart, M2R-regulated I_{K, ACh} comprises >60 % of the total muscarinic mediated outward K⁺ current³⁷. However, with AF due to ventricular tachypacing-induced congestive heart failure, the contribution of I_{K, M3} increased to ~50% of the total outward K⁺ current³⁷. I_{K, ACh} channels also can participate in AF, as GIRK3.4

knockout (*GIRK4*^{-/-}) mice, which lack functional I_{K, ACh} channels, appear to be completely resistant to carbachol-induced AF²².

RGS protein regulation of M2R function likely contributes to AF. RGS4 was identified as an important regulator of I_{K, ACh} channels in the SA node; however, little RGS4 was detected in the surrounding right atrium⁶. Consistent with this observation, I found >150 fold higher expression of RGS2 than RGS4 in the mouse atria. Future studies may reveal a role for other RGS proteins in atrial arrhythmia.

2.5 CLINICAL RELEVANCE

With the aging of the population there is an increasing drive to identify novel treatments for AF. This will require increased understanding of the signalling pathways and molecular regulators involved in arrhythmia induction, perpetuation, and atrial remodelling. The clinical relevance is highlighted by the success of ACE inhibitors in preventing fibrosis and development of an AF substrate²⁶. Mutations in, or altered expression/function of a variety of RGS proteins could be involved in AF mechanisms in patients, and indeed changes in RGS2 have been identified in several human cardiovascular phenotypes. Targeting RGS proteins may be important for drug development³³. Also, our data suggests that selective M3R blockade, alone or in combination with other anti-arrhythmic agents, may be useful for patients with AF. However, in mice oral darifenacin exerted only transient binding to cardiac muscarinic receptors⁴⁵, its use may be limited.

2.6 LIMITATIONS

While these results indicate a role for RGS2 and the M3 muscarinic receptor in promoting AF in the mouse, additional studies will need to directly determine the role of

$I_{K, M3}$ activity. In the mouse, it may be difficult to distinguish atrial fibrillation from atrial tachycardia, particularly with an arrhythmia of short duration. However, using standard clinical criteria for atrial fibrillation: lack of regular P waves, irregularly irregular ventricular responses often it was possible to demonstrate characteristics of atrial fibrillation in the mouse. Nevertheless, this is difficult particularly with arrhythmias of short duration. Atrial vulnerability may also be due to a balance of autonomics^{20,36}. $RGS2^{-/-}$ mice have also been shown to have reduced renal sympathetic nerve activity compared to WT mice⁴⁰. Although, the lack of a heart rate difference between $RGS2^{-/-}$ and WT mice found in their earlier study¹² does not assist in establishing the role of the sympathetic nervous system in atrial susceptibility, the role of the balance between sympathetics and M3 responses remains to be determined. RNA expression provides an index of the relative importance of the proteins but may or may not parallel Bmax values of radioligand assessment of M2, M3 or M4 protein expression, distribution and function. One month old mice were chosen to avoid potential complexity due to the chronic effects of the hypertensive phenotype associated with $RGS2^{-/-}$ in the mouse. It is also recognized that it may not be possible to directly extrapolate from mouse experiments to the human.

2.7 REFERENCES

1. Abramow-Newerly M, Roy AA, Nunn C, Chidiac P. RGS proteins have a signalling complex: interactions between RGS proteins and GPCRs, effectors, and auxiliary proteins. *Cell Signal* 18:579-91. 2006.
2. Allesie MA, Bonke FI, Schopman FJ. Circus movement in rabbit atrial muscle as a mechanism of tachycardia. II. The role of nonuniform recovery of excitability in the occurrence of unidirectional block, as studied with multiple microelectrodes. *Circ Res* 39:168-77. 1976.
3. Appleton GO, Li Y, Taffet GE, Hartley CJ, Michael LH, Entman ML, Roberts R, Khoury DS. Determinants of cardiac electrophysiological properties in mice. *J Interv Card Electrophysiol* 11:5-14. 2004.

4. Aslanidi OV, Boyett MR, Dobrzynski H, Li J, Zhang H. Mechanisms of transition from normal to reentrant electrical activity in a model of rabbit atrial tissue: interaction of tissue heterogeneity and anisotropy. *Biophys J* 96:798-817. 2009.
5. Benjamin EJ, Wolf PA, D'Agostino RB, Silbershatz H, Kannel WB, Levy D. Impact of atrial fibrillation on the risk of death: the Framingham Heart Study. *Circulation* 98:946-52. 8-9-1998.
6. Cifelli C, Rose RA, Zhang H, Voigtlaender-Bolz J, Bolz SS, Backx PH, Heximer SP. RGS4 Regulates Parasympathetic Signaling and Heart Rate Control in the Sinoatrial Node. *Circ Res.* 24-7-2008.
7. Cladman W, Chidiac P. Characterization and comparison of RGS2 and RGS4 as GTPase-activating proteins for m2 muscarinic receptor-stimulated G(i). *Mol Pharmacol* 62:654-9. 2002.
8. Connolly MS, Lynch CB. Circadian variation of strain differences in body temperature and activity in mice. *Physiol Behav* 27:1045-9. 1981.
9. Doupnik CA, Xu T, Shinaman JM. Profile of RGS expression in single rat atrial myocytes. *Biochim Biophys Acta* 1522:97-107. 3-12-2001.
10. Dries DL, Exner DV, Gersh BJ, Domanski MJ, Waclawiw MA, Stevenson LW. Atrial fibrillation is associated with an increased risk for mortality and heart failure progression in patients with asymptomatic and symptomatic left ventricular systolic dysfunction: a retrospective analysis of the SOLVD trials. Studies of Left Ventricular Dysfunction. *J Am Coll Cardiol* 32:695-703. 1998.
11. Fisher JT, Vincent SG, Gomeza J, Yamada M, Wess J. Loss of vagally mediated bradycardia and bronchoconstriction in mice lacking M2 or M3 muscarinic acetylcholine receptors. *FASEB J* 18:711-3. 2004.
12. Gross V, Tank J, Obst M, Plehm R, Blumer KJ, Diedrich A, Jordan J, Luft FC. Autonomic nervous system and blood pressure regulation in RGS2-deficient mice. *Am J Physiol Regul Integr Comp Physiol* 288:R1134-R1142. 2005.
13. Haissaguerre M, Jais P, Shah DC, Takahashi A, Hocini M, Quiniou G, Garrigue S, Le Mouroux A, Le Metayer P, Clementy J. Spontaneous initiation of atrial fibrillation by ectopic beats originating in the pulmonary veins. *N Engl J Med* 339:659-66. 3-9-1998.
14. Hassall CJ, Burnstock G. Immunocytochemical localisation of neuropeptide Y and 5-hydroxytryptamine in a subpopulation of amine-handling intracardiac neurones that do not contain dopamine beta-hydroxylase in tissue culture. *Brain Res* 422:74-82. 29-9-1987.
15. Hoffmann E, Sulke N, Edvardsson N, Ruiter J, Lewalter T, Capucci A, Schuchert A, Janko S, Camm J. New insights into the initiation of atrial fibrillation: a detailed intraindividual and interindividual analysis of the spontaneous onset of atrial fibrillation using new diagnostic pacemaker features. *Circulation* 113:1933-41. 25-4-2006.

16. Jalife J, Delmar M, Davidenko JM, Anumonwo JM. *Basic Cardiac Electrophysiology for the Clinician*. Armonk, NY: Furura Publishing Company; 1999.
17. Jalife J, Pandit SV. Ionic mechanisms of wavebreak in fibrillation. *Heart Rhythm* 2:660-3. 2005.
18. Jones DL, Guiraudon GM, Skanes AC, Guiraudon CM. Anatomical pitfalls during encircling cryoablation of the left atrium for atrial fibrillation therapy in the pig. *J Interv Card Electrophysiol* 21:187-93. 2008.
19. Jones DL, Petrie JP, Li HG. Spontaneous, electrically, and cesium chloride induced arrhythmia and afterdepolarizations in the rapidly paced dog heart. *Pacing Clin Electrophysiol* 24:474-85. 2001.
20. Jones DL, Tuomi J, Ramsay D, Guiraudon CM, Armour JA, Cardinal R, Page P, Guiraudon GM. Left atrial neuroablation for atrial fibrillation: A feasibility study. *Canadian Journal of Cardiology* 23, 225C, 2007.
21. Kitazawa T, Asakawa K, Nakamura T, Teraoka H, Unno T, Komori S, Yamada M, Wess J. M3 muscarinic receptors mediate positive inotropic responses in mouse atria: a study with muscarinic receptor knockout mice. *J Pharmacol Exp Ther* 330:487-93. 2009.
22. Kovoov P, Wickman K, Maguire CT, Pu W, Gehrmann J, Berul CI, CLAPHAM DE. Evaluation of the role of I(KACh) in atrial fibrillation using a mouse knockout model. *J Am Coll Cardiol* 37:2136-43. 15-6-2001.
23. Krejci A, Tucek S. Quantitation of mRNAs for M(1) to M(5) subtypes of muscarinic receptors in rat heart and brain cortex. *Mol Pharmacol* 61:1267-72. 2002.
24. Larminie C, Murdock P, Walhin JP, Duckworth M, Blumer KJ, Scheideler MA, Garnier M. Selective expression of regulators of G-protein signaling (RGS) in the human central nervous system. *Brain Res Mol Brain Res* 122:24-34. 17-3-2004.
25. Lemola K, Chartier D, Yeh YH, Dubuc M, Cartier R, Armour A, Ting M, Sakabe M, Shiroshita-Takeshita A, Comtois P, Nattel S. Pulmonary vein region ablation in experimental vagal atrial fibrillation: role of pulmonary veins versus autonomic ganglia. *Circulation* 117:470-7. 29-1-2008.
26. Li D, Shinagawa K, Pang L, Leung TK, Cardin S, Wang Z, Nattel S. Effects of angiotensin-converting enzyme inhibition on the development of the atrial fibrillation substrate in dogs with ventricular tachypacing-induced congestive heart failure. *Circulation* 104:2608-14. 20-11-2001.
27. Li HG, Jones DL, Yee R, Klein GJ. Electrophysiologic substrate associated with pacing-induced heart failure in dogs: potential value of programmed stimulation in predicting sudden death. *J Am Coll Cardiol* 19:444-9. 1992.
28. Mawe GM, Talmage EK, Lee KP, Parsons RL. Expression of choline acetyltransferase immunoreactivity in guinea pig cardiac ganglia. *Cell Tissue Res* 285:281-6. 1996.

29. Morillo CA, Klein GJ, Jones DL, Guiraudon CM. Chronic rapid atrial pacing: structural, functional, and electrophysiological characteristics of a new model of sustained atrial fibrillation. *Circulation* 915:1588-95. 1995.
30. Oliveira-dos-Santos AJ, Matsumoto G, Snow BE, Bai D, Houston FP, Whishaw IQ, Mariathasan S, Sasaki T, Wakeham A, Ohashi PS, Roder JC, Barnes CA, Siderovski DP, Penninger JM. Regulation of T cell activation, anxiety, and male aggression by RGS2. *Proc Natl Acad Sci U S A* 97:12272-7. 24-10-2000.
31. Pfaffl MW, Horgan GW, Dempfle L. Relative expression software tool (REST) for group-wise comparison and statistical analysis of relative expression results in real-time PCR. *Nucleic Acids Res* 30:e36. 1-5-2002.
32. Riddle EL, Schwartzman RA, Bond M, Insel PA. Multi-tasking RGS proteins in the heart: the next therapeutic target? *Circ Res* 96:401-11. 4-3-2005.
33. Roman DL, Ota S, Neubig RR. Polyplexed Flow Cytometry Protein Interaction Assay: A Novel High-Throughput Screening Paradigm for RGS Protein Inhibitors. *J Biomol Screen*. 16-6-2009.
34. Ruijter JM, Ramakers C, Hoogaars WM, Karlen Y, Bakker O, van den Hoff MJ, Moorman AF. Amplification efficiency: linking baseline and bias in the analysis of quantitative PCR data. *Nucleic Acids Res* 37:e45. 2009.
35. Savelieva I, Camm AJ. Clinical trends in atrial fibrillation at the turn of the millenium. *J Intern Med* 250:369-72. 2001.
36. Scherlag BJ, Patterson E, Po SS. The neural basis of atrial fibrillation. *J Electrocardiol* 39:S180-S183. 2006.
37. Shi H, Wang H, Li D, Nattel S, Wang Z. Differential alterations of receptor densities of three muscarinic acetylcholine receptor subtypes and current densities of the corresponding K⁺ channels in canine atria with atrial fibrillation induced by experimental congestive heart failure. *Cell Physiol Biochem* 14:31-40. 2004.
38. Shi H, Wang H, Yang B, Xu D, Wang Z. The M3 receptor-mediated K⁽⁺⁾ current (IKM3), a G(q) protein-coupled K⁽⁺⁾ channel. *J Biol Chem* 279:21774-8. 21-5-2004.
39. Sokal RR, Rohlf FJ. *Biometry: The Principles and Practice of Statistics in Biological Research*. 2nd ed. San Francisco: W. H. Freeman and Company; 1981.
40. Tank J, Obst M, Diedrich A, Brychta RJ, Blumer KJ, Heusser K, Jordan J, Luft FC, Gross V. Sympathetic nerve traffic and circulating norepinephrine levels in RGS2-deficient mice. *Auton Neurosci* 136:52-7. 30-10-2007.
41. Vaquero M, Calvo D, Jalife J. Cardiac fibrillation: from ion channels to rotors in the human heart. *Heart Rhythm* 5:872-9. 2008.

42. Wang H, Lu Y, Wang Z. Function of cardiac M3 receptors. *Auton Autacoid Pharmacol* 27:1-11. 2007.
43. Wang Z, Shi H, Wang H. Functional M3 muscarinic acetylcholine receptors in mammalian hearts. *Br J Pharmacol* 142:395-408. 2004.
44. Wess J. G-protein-coupled receptors: molecular mechanisms involved in receptor activation and selectivity of G-protein recognition. *FASEB J* 11:346-54. 1997.
45. Yamada S, Maruyama S, Takagi Y, Uchida S, Oki T. In vivo demonstration of M3 muscarinic receptor subtype selectivity of darifenacin in mice. *Life Sci* 80:127-32. 14-12-2006.

CHAPTER 3: Atrial Tachycardia/Fibrillation in the Connexin 43 G60S Mutant (Oculodentodigital Dysplasia) Mouse

A version of this chapter has been published:

Tuomi JM, Tymi K, Jones DL. Atrial Tachycardia/Fibrillation in the Connexin 43 G60S Mutant (Oculodentodigital Dysplasia) Mouse. ” Am J Physiol Heart Circ Physiol. 2011 Apr;300(4):H1402-11. (Epub 2011 Jan 14)

3.0 CHAPTER SUMMARY

One of the greatest challenges in studying AF has been the impossibility of dissociating fibrillatory activation from its mechanism. Due to this most molecular data is correlative and does not describe the initial substrate state that lead to AF development. Studies in genetically manipulated mice may address both issues as induced pre-arrhythmia substrate remodelling allows for investigations of the initial state dissociated from fibrillatory activation thus yielding causative mechanistic insights. One particular challenge has been determining the role of altered connexins (Cx40 and Cx43) in promoting myogenic AF. Increases, decreases and no change in the expression of Cx40 and Cx43 have been observed in different patients and large animal models of AF. In each case, a change in Cx expression may be compensatory, lowering the substrate closer to threshold, or may promote permanent AF, raising the substrate further above threshold. In this chapter Cx40 deficient and Cx43^{G60S/+} mutant mice, with an 80% reduction in atrial phospho-Cx43, are studied to determine the role of altered connexin content in myogenic AF. Identification of a model of myogenic AF would allow testing of the hypothesis that "tonic autonomic influences play a role in all atrial arrhythmias". I found that while Cx40 deficient mice are protected from carbachol induced AF, the Cx43^{G60S/+} mutant mouse, is highly susceptible to AF that can be

terminated by darifenacin hydrobromide (a M3R blocker). Detailed electrogram analysis show disturbed right atrial conduction, while epicardial recordings found left to right atrial activation patterns consistent with clinical AF. Overall, these studies determined a role for the ICANS in myogenic AF while electrical recordings indicate that AF in the mouse is highly similar to that observed in the human.

3.1 INTRODUCTION

Atrial fibrillation (AF) is the most common cardiac arrhythmia seen by the general practitioner³. It is characterized by disorganized and rapid atrial electrical activation, which can drive rapid and irregular ventricular activation. AF requires a trigger for initiation, together with a dynamic susceptible or vulnerable substrate for maintenance. It has been shown to be triggered by either wavebreak²⁴ or ectopic foci²² arising from regions such as the pulmonary veins²⁰ or the posterior left or right atrium^{20,36}. Triggers combined with dynamic substrates of structural heterogeneities, reduced refractoriness, enhanced spatial dispersion of refractoriness and abnormal impulse conduction, to initiate and perpetuate the arrhythmia³⁸.

Gap junction channels are critical for the conduction of electrical impulses in the heart and may be involved in arrhythmia. They are composed of 4 transmembrane domain proteins, connexins (Cxs), which oligomerize in the Golgi apparatus to form hexamers called connexons³¹. Connexons from adjacent cells dock, primarily at intercalated disc, to form low resistance channels that allow rapid propagation of electrical signals⁷. While 4 primary isoforms of Cxs are found in the heart (mouse Cx30.2/ human Cx31.9, Cx40, Cx43, Cx45), only Cx40 and Cx43 are abundant in the working myocardium. The atrium expresses similar amounts of Cx40 and Cx43³³.

Remodelling of connexins can be functional (altered conductance) and structural (altered content/distribution) ¹⁴. The role of connexins in AF has been studied in animal models and patients with AF; however, the exact role of Cx40 and Cx43 is not clear ¹⁴. In wild type (WT) mice following the administration of carbachol, 7 of 8 mice were susceptible to atrial tachycardia/fibrillation (AT/F) lasting 139.2±402.1 seconds ⁵¹. However, studies in Cx40^{-/-} mice have reported that AT/F was not detected ¹, occurred infrequently (5 of 19) ⁴, had no difference in susceptibility compared to WT mice ⁴², or was short lived (5/10, <1 second) ^{4, 19, 49}. These reports demonstrate that relative to wild type (WT) mice in the presence of carbachol ⁵¹, Cx40^{-/-} mice have little susceptibility to sustained AT/F. However, somatic mutations in Cx40 ¹⁷ and Cx43 ⁴⁴ have been reported in patients with idiopathic AF. When expressed in N2A cell pairs, similarly mutated Cx40 had reduced junctional conductance (gj) and inhibited wild type (WT) Cx43 gj. These observations highlight an important distinction between functional and structural alterations of gap junction channels.

Arrhythmia studies in transgenic mice have primarily focused on Cx40 deficient (Cx40^{-/-}) mice as Cx43 deficient (Cx43^{-/-}) mice die peri-natally ⁴⁰. The cardiac selective Cx43 knockout mouse has only been used in studies of ventricular arrhythmia ¹⁸. To date, 62 mutations in Cx43 have been linked to *Oculodentodigital dysplasia (ODDD)*, a pleiotropic, autosomal dominant disorder in humans ^{39, 44} primarily affecting the eye, dentition, and digits of the hands and feet. Cardiac defects were reported in 177 individuals from 54 families with ODDD ³⁹. Both G138R ¹³ and I130T ²⁷ Cx43 mutant mice with the ODDD phenotype have increased susceptibility to ventricular arrhythmia; however, atrial arrhythmia susceptibility was not determined. The Cx43 G60S (Cx43^{G60S/+}) mutation in mice ³⁹ is dominant negative, causing connexons with mutant and WT Cx43 to be retained in the Golgi and targeted for degradation ³⁵. Cx43^{G60S/+} mutant mice have a 60% reduction in total atrial Cx43 protein

content, with a preferential down-regulation (~80%) of the highly phosphorylated form of Cx43³⁵. The Cx43^{G60S/+} mutation did not alter Cx40 or Cx45 expression. We took advantage of this well characterized Cx43^{G60S/+} mouse model to determine the role of Cx43 reductions in AT/F. Intracardiac electrophysiological pacing determined AT/F susceptibility in 6 month old male mice. As no atrial arrhythmias were reported in WT mice and a relatively low frequency of AT/F in Cx40^{-/-} mice, we compared Cx43^{G60S/+} mutant to age-matched Cx40^{-/-} mice to determine the role of reduced Cx43 and total loss of Cx40 in AT/F.

3.2. METHODS

3.2.1 Animals And Preoperative Procedures

Animal studies were approved by the Animal Use Committee of the University of Western Ontario (protocol #2006-121-12) and complied with the Guidelines of the Canadian Council on Animal Care and the Guide to the Care and Use of Laboratory Animals published by the US National Institutes of Health (NIH Publication No. 85-23, revised 1996). Six month old male Cx43^{G60S/+} mice were obtained from the colony maintained by Dr. Gerald Kidder which were originally developed by Dr. Janet Rossant (Centre for Modeling Human Disease, Toronto, ON, Canada)¹⁶. Comparisons were made to age matched male C57BL/6 littermate (Cx43^{+/+}), wild-type (WT) and Cx40^{-/-} mice originally derived from male mice provided by Dr. David Paul (Harvard University, Boston, MA)⁴³.

Mice were anesthetized with an intraperitoneal injection mixture of ketamine (150 mg/kg) and xylazine (10 mg/kg). Body temperature was monitored with a YSI-402 (Yellow Springs Instruments, Yellow Springs, Ohio) rectal probe inserted 1-1.5 cm beyond the anal sphincter, and maintained at 36.5-38 °C⁴⁵. A 23 ga Teflon® endotracheal tube was inserted and ligated in place to keep the airway open.

3.2.2 Surface Limb Lead Electrocardiograms (ECG)

Surface ECGs were obtained using 4 subcutaneous, 25 ga platinum electrodes (Grass Instrument Inc., Quincy, Mass.) placed at the base of each limb. ECG tracings were filtered between 0.05 to 100 Hz, digitized and sampled at 1.5 kHz, with an ECG100 preamplifier connected to a MP100 recording system (BIOPAC Systems, Biolyx, Montréal, PQ).

3.2.3 Blood Pressure And Conscious Restrained Heart Rates

Blood pressure and simultaneous heart rate was assessed non-invasively in conscious WT and Cx40^{-/-} mice using the CODA system¹⁵.

3.2.4 In Vivo Intracardiac Electrophysiology Studies

A 2F octapolar stimulation / recording / drug infusion catheter (CIB'ER Mouse®, NuMED Inc., Hopkinton, NY) was inserted through the right jugular vein and advanced into the right atrium and ventricle. Intracardiac electrograms were filtered between 100 to 5000 Hz (DA100 amplifier, BIOPAC Systems) and sampled at 1.5 kHz. All data was recorded using a personal computer running Acknowledge software (BIOPAC Systems). His bundle potentials were used to establish catheter positioning within the right atrium (RA) and ventricle (RV) with 2 pairs of bipolar electrodes located at the posterior septal mid right atrium (MRA) and high right atrial/superior vena cava region (HRA)⁴⁵.

3.2.5 Pacing Protocols

Bipolar pacing used 1 ms pulses at twice the diastolic threshold, delivered through a Grass stimulus isolation unit (SIU5), connected to a Grass SD9 stimulator, driven by a custom-built timer⁴⁵. Effective refractory periods (ERPs) from the right atrium (AERP), right ventricle (VERP), and AV node (AVNERP) were assessed with programmed electrical stimulation (PES)⁴⁵ using a drive train of 9 stimuli (S1) at a cycle length of 100 ms followed

by a progressively premature extra stimulus (S2). Atrial pacing with 1 ms decrements was used to determine the Wenkebach cycle length (WCL).

3.2.6 Arrhythmia Induction Protocols

Three pacing protocols were used to evaluate the susceptibility to electrically-induced AT/F: 1) a single atrial stimuli (SAS) delivered during sinus rhythm, timed to follow the P-wave (**Fig. 3.1A**); 2) programmed electrical stimulation (PES), with an increasingly premature extra stimulus (S2, **Fig. 3.1B**)²⁶, and 3) atrial burst pacing (1 ms pulses, 50Hz, 400 ms train)^{25, 45}. AT/F was characterized based on the susceptibility to the pacing modality and the arrhythmia duration: a) no response; b) lasting <10 s; c) lasting from 10 to 60 s, and d) >120 s. We previously determined that AT/F, when inducible in WT mice, is dependent on the pacing location in the right atrium, validated by using the His bundle potential as a landmark of catheter positioning⁴⁵. Previous murine studies of atrial arrhythmia frequently report low susceptibility to AT/F in WT mice in the absence of carbachol (CCh)⁵¹. As electrically-induced arrhythmia was rare in Cx40^{-/-} mice, additional provocation used the nonselective cholinergic agonist, carbachol (CCh, 50ng/g, intraperitoneal, Sigma, Mississauga, ON) in WT and Cx40^{-/-} mice⁴⁵.

3.2.7 Epicardial Left Atrial Recordings

A subgroup of Cx43^{G60S/+} mice were mechanically ventilated at a respiratory rate of 100 breaths per minute. The chest was open via a lateral thoracotomy between the first and second ribs. For epicardial recordings, Teflon insulated silver bipolar electrodes (0.2 mm spacing) were positioned on the surface of the left and right atrial appendages or the posterior left atrium²³.

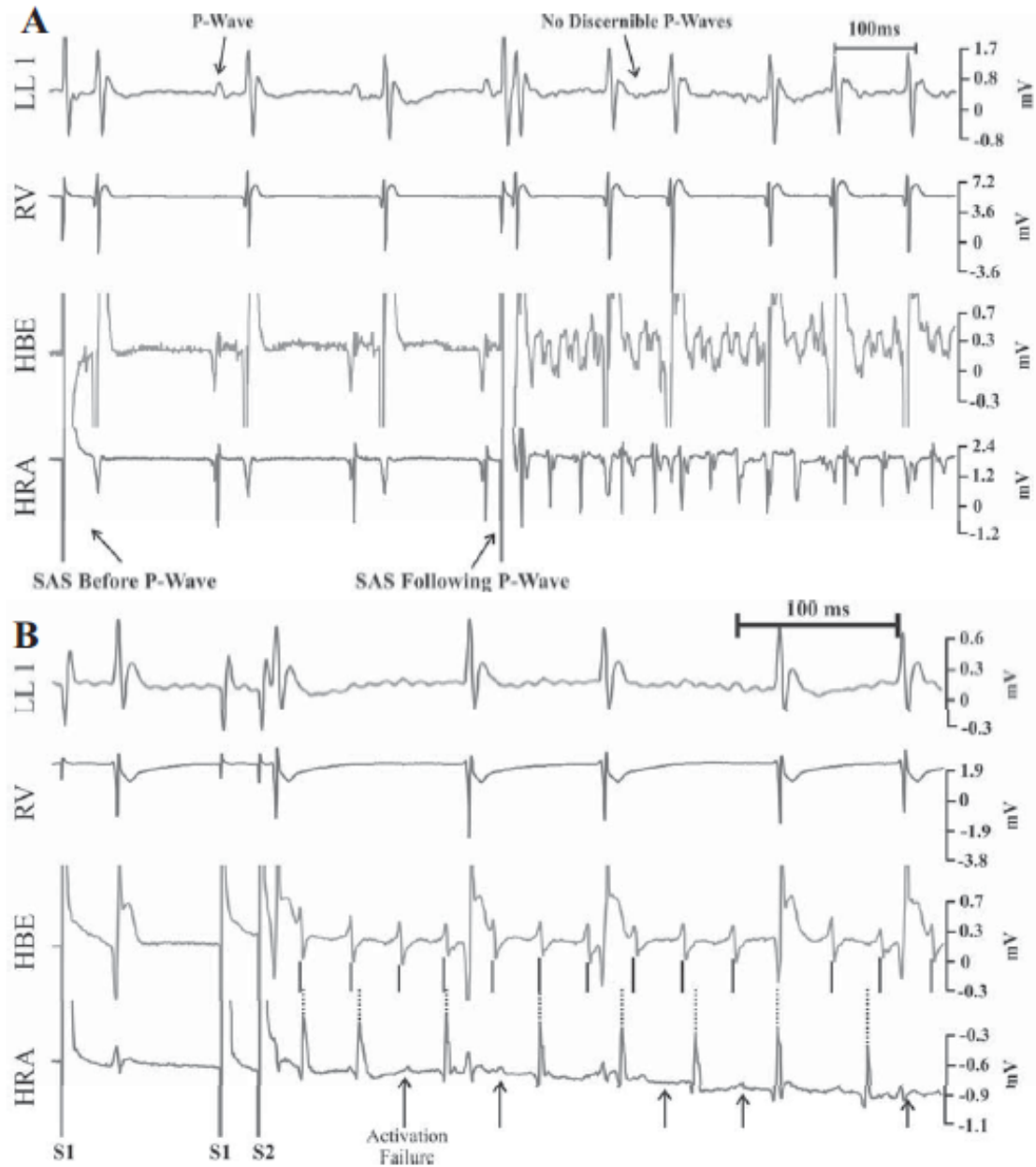


Figure 3.1 A: Induction of atrial fibrillation (AT/F) with a single atrial stimulus (SAS) delivered during sinus rhythm in a 6-mo-old male $Cx43^{G60S/+}$ mouse. Susceptibility to SAS induced AT/F indicates $Cx43^{G60S/+}$ mouse have an extremely vulnerable atrial substrate. **B:** Programmed electrical stimulation (PES)-induced AT/F with a single extrastimulus (S2) in a 6-mo-old male $Cx43^{G60S/+}$ mouse. LL1, limb lead I; RV, right ventricular electrogram; HBE, electrogram from the His bundle region; HRA, recording from the high right atrium.

3.2.8 Statistical Analysis

Drug and strain comparisons were analyzed with 2-way ANOVA, and the Bonferoni post-hoc test (Prism 4.0, GraphPad Software, La Jolla, CA). The Chi Square test was used to analyze discrete data. A probability of $P < 0.05$ was considered statistically significant. All data was expressed as the mean \pm SEM.

3.3 RESULTS

3.3.1 Standard Electrophysiological Parameters

Cx40^{-/-} mouse ECGs had prolonged P-wave and QRS durations, and QT and PQ intervals compared to age-matched WT mice (**Table 3.1**). Atrial-Hisian (AH) intervals were shorter during sinus rhythm and at a drive cycle length of 100 ms (AH₁₀₀), while His-ventricular (HV) intervals were prolonged compared to WT mice (**Table 3.1**). WCLs were also shorter in *Cx40*^{-/-} mice. *Cx43*^{G60S/+} mice had no differences in P-wave durations or PQ intervals compared to age matched littermates (*Cx43*^{+/+}); however, QRS durations and QT intervals were prolonged (**Table 3.2**). AH intervals recorded during sinus rhythm did not differ significantly, but with pacing, AH₁₀₀ was lower in the *Cx43*^{G60S/+} mice compared to *Cx43*^{+/+} mice. HV intervals were also shorter in the in *Cx43*^{G60S/+} mice (**Table 3.2**).

3.3.2 Effective Refractory Periods

PES consistently revealed regional heterogeneity in AERPs: longer in the high right (AHERP) than the mid right atrium (AMERP) (**Tables 3.1 & 3.2**), but did not differ between strains. CCh reduced sinus rate (~20%) and AERPs in *Cx40*^{-/-} and WT mice (**Table 3.1**). Interestingly, the ventricular ERP (VERP₁₀₀) was lower in *Cx43*^{G60S/+} compared to *Cx43*^{+/+} mice, consistent with results from isolated right ventricular myocytes of the conditional *Cx43* knockout mouse, which was found to have enhanced I_{K1} activity¹⁰. For *Cx40*^{-/-} mice, VERP

did not differ from those of WT mice; however, following CCh administration, VERP₁₀₀ in WT were even higher than those of Cx40^{-/-} mice (**Table 3.1**).

3.3.3 Cardiac Hypertrophy/Hypertension

Cardiac hypertrophy²⁹ and hypertension⁵⁰ were reported in Cx40^{-/-} mice. As both hypertension and heart failure are risk factors for developing AF, we documented these phenotypes in our mice. Cx40^{-/-} mouse hearts were visibly hypertrophic with a 54% increase in the ventricular weight to tibial length ratio (10.8 ± 0.8 vs. 7.0 ± 0.4 mg/mm, $P < 0.05$), while Cx43^{G60S/+} mouse hearts were normal (6.9 ± 0.5 vs. 7.2 ± 0.7 mg/mm, $P = \text{N.S.}$). Using tail cuff measurement, conscious Cx40^{-/-} mice had higher systolic (179.3 ± 4.8 vs 123.1 ± 5.6 mmHg, $P < 0.001$) and diastolic (140 ± 7.3 vs 94.3 ± 5.8 mmHg, $P < 0.001$) blood pressures and lower heart rates (594.1 ± 28 vs 701.2 ± 36 bpm, $P < 0.05$) compared to age matched WT mice. One Cx40^{-/-} animal died suddenly from unknown causes during tail cuff measurement. This death may have resulted from restraint stress-induced ventricular arrhythmia³⁷, as no WT but 2 Cx40^{-/-} mice had burst pacing induced ventricular tachycardia lasting ~13 seconds. Of note, atrial standstill was reported in patients that co-inherit a novel SCN5A mutation along with a Cx40 polymorphism³⁴. Blood pressures in Cx43^{G60S/+} mice were not determined.

3.3.4 Atrial Tachyarrhythmia Induction

Pacing-induced atrial arrhythmia had electrophysiological characteristics of AF²⁵, although distinguishing from rapid atrial tachycardia and validation of AF would require high density mapping. Thus, we labeled all atrial arrhythmias as AT/F⁴⁵.

C57BL/6 WT Mice were relatively insensitive to any duration of AT/F induction (0.1 sec to >120 sec) with PES (4 of 12, 17%), while they were inducible with burst pacing (9 of 12, 75%; Fig. 2A). CCh injection (50ng/g, I.P) caused a trend to increase susceptibility to AT/F

Table 3.1. Intracardiac electrophysiological values recorded in the absence and presence of carbachol in 6-mo-old male Cx40^{-/-} and C57BL/6 wild-type mice

	Vehicle				Carbachol			
	Wild type		Cx40 ^{-/-}		Wild type		Cx40 ^{-/-}	
	Value, ms	n	Value, ms	n	Value, ms	n	Value, ms	n
P wave	21 ± 1	12	23 ± 1	11*	21 ± 1	9	23 ± 1	9*
QRS	15 ± 1	13	20 ± 1	11‡	15 ± 1	9	19 ± 1	9‡
QT	27 ± 1	13	36 ± 2	11‡	29 ± 1	9	36 ± 1	9‡
PQ	43 ± 1	13	47 ± 1	12‡	42 ± 2	9	46 ± 2	9
AHERP ₁₀₀	30 ± 2	12	29 ± 2	13	28 ± 2	9	29 ± 3	9
AMERP ₁₀₀	25 ± 1	13	26 ± 1	11	22 ± 1	9	23 ± 1	9
WCL	91 ± 2	13	86 ± 1	13*	97 ± 2	9	95 ± 1	9
AVNERP ₁₀₀	64 ± 2	13	63 ± 2	13	73 ± 4	7	72 ± 2	8
AH ₁₀₀	33 ± 1	12	26 ± 1	12‡	40 ± 3	9	30 ± 2	9‡
AH	28 ± 1	13	23 ± 1	12‡	30 ± 1	9	26 ± 1	9*
HV	11 ± 1	13	20 ± 1	12‡	11 ± 1	9	19 ± 1	9‡
VERP ₁₀₀	46 ± 2	12	42 ± 2	12	59 ± 2	9	47 ± 3	7‡

Values are means ± SE; n, number of mice. AHERP, high right atrial effective refractory period; AMERP, mid-right atrial effective refractory period; WCL, Wenkebach cycle length; AVNERP, atrial-ventricular effective refractory period; AH, atrial-Hisian interval; HV, His-ventricular interval; VERP, right ventricular effective refractory period. Subscripts (100) indicate drive cycle lengths of 100 ms. *P < 0.05; †P < 0.01; ‡P < 0.001 for Cx40^{-/-} vs. wild-type mice within drug group.

Table 3.2. Intracardiac electrophysiological values recorded from 6-mo-old male Cx43^{G60S/+} and Cx43^{+/+} mice.

	Cx43 ^{+/+}		Cx43 ^{G60S/+}	
	Value, ms	n	Value, ms	n
P wave	19 ± 1	11	19 ± 2	12
QRS	15 ± 1	11	17 ± 1	12*
QT	28 ± 1	11	30 ± 1	12*
PQ	40 ± 1	11	38 ± 1	12
AHERP ₁₀₀	26 ± 2	11	28 ± 2	12
AMERP ₁₀₀	22 ± 2	11	20 ± 1	12
WCL	91 ± 2	10	87 ± 2	12
AVNERP ₁₀₀	67 ± 3	10	62 ± 2	12
AH ₁₀₀	34 ± 1	11	29 ± 1	12*
AH	27 ± 1	11	24 ± 1	12
HV	10 ± 1	11	9 ± 1	12*
VERP ₁₀₀	40 ± 1	10	34 ± 2	12*

Values are means ± SE; n, number of mice. *P < 0.05 for Cx43^{G60S/+} vs. Cx43^{+/+} mice.

induction with both PES (7 of 10, 70%, $X^2=2.93$, $P=0.08$) and burst pacing (9 of 10, 90%, $X^2=0.83$, $P=0.36$). SAS induction protocol was not performed in WT mice. However, CCh injection prolonged the duration of AT/F with only 1 of 12 untreated WT mice having sustained AT/F (>2 min) before, while 7 of 10 had sustained AT/F after CCh administration ($X^2=8.96$, $P=0.003$, **Fig. 3.2B**). Consistent with our previous studies⁴⁵, the site of stimulation within the atrium also influenced AT/F inducibility. In WT mice, CCh induced AT/F was more readily initiated from the mid-right septal atrium (MRA) (7 of 10, 70%) compared to the high right atrium/superior vena cava region (HRA) (1 of 10, 10%, $X^2=7.5$, $P=0.006$). This may have been due to the respective AERPs, which were shorter in the MRA compared to the HRA (**Table 3.1**). The requirement for pacing of the MRA to induce AT/F was consistent in all Cx40^{-/-}, Cx43^{G60S/+}, Cx43^{+/+} and WT mice.

Cx40^{-/-} mice were less susceptible to AT/F induction of all durations (0.1 sec to >120 sec) with burst pacing in the absence of CCh (2 of 13, 15%) compared to WT animals (9 of 12, 75%, $X^2=9.0$, $P=0.003$, Fig. 2A). In the absence of CCh, more WT mice were susceptible to short lived, non-sustained AT/F (<10 sec), compared to Cx40^{-/-} mice (9 of 12 vs. 1 of 13, $X^2=11.78$, $P<0.001$, **Fig 3.2B & C**). However, there was no difference between WT and Cx40^{-/-} mice in the susceptibility to sustained AT/F (>120 sec) (1 of 12 vs. 1 of 13, $X^2=0.003$, $P=0.95$, **Fig 3.2B & C**). Of note, the single Cx40^{-/-} mouse with sustained AT/F had a much shorter AERP in both HRA (14 ms) and MRA (12 ms) relative to average values (Table I). While the results of this and other studies indicate that Cx40^{-/-} mice do not appear to have an increase in susceptibility to AT/F compared to WT mice, it is possible that Cx40 deficiency would alter the substrate sufficiently to increase the susceptibility and sustainability of CCh-induced AT/F. As such we used CCh, to evaluate potentially increased susceptibility to AT/F

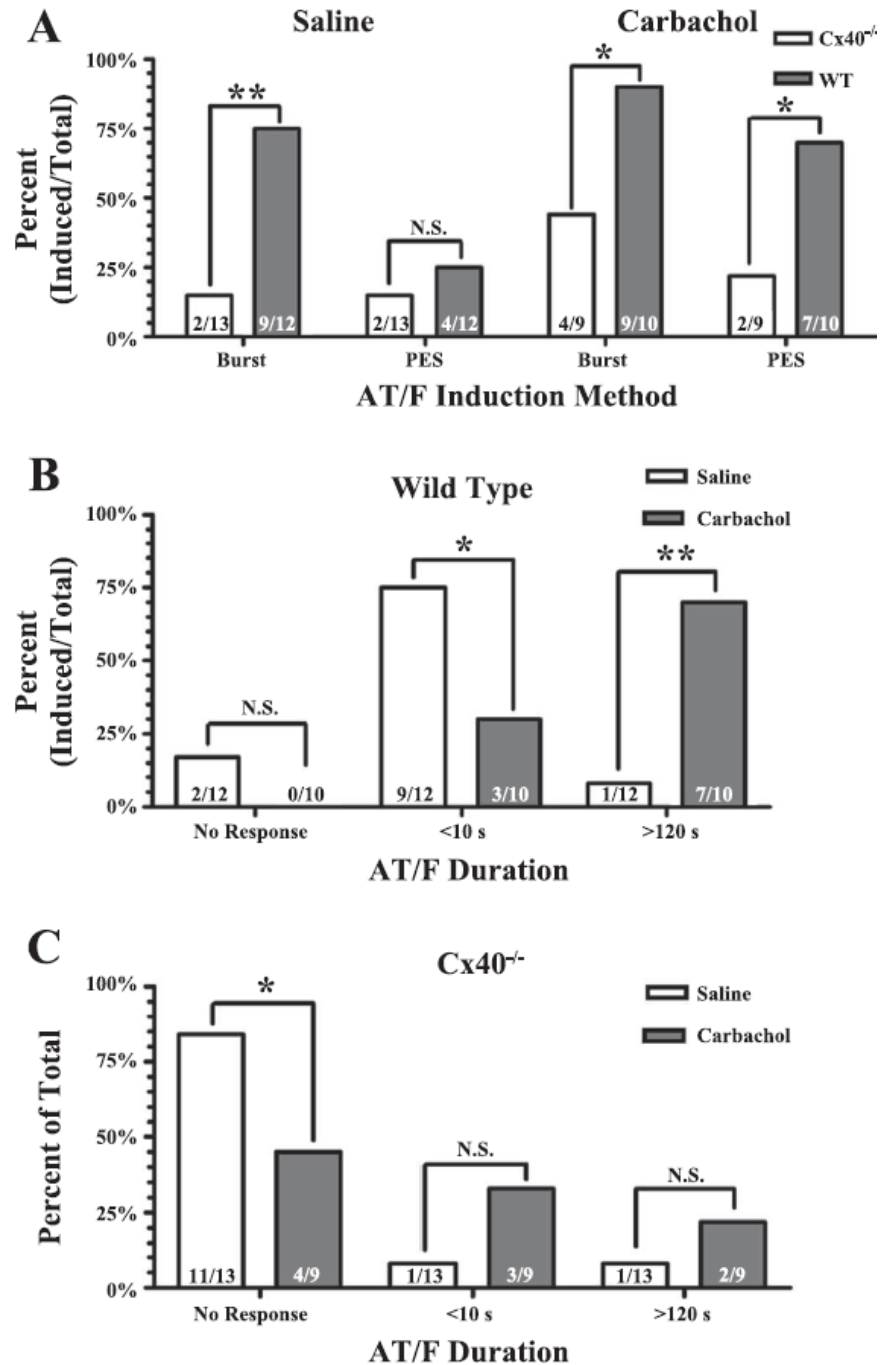


Figure 3.2. Incidence of AT/F-induced PES or burst pacing in 6-mo-old male wild-type (WT) and Cx40^{-/-} mice. AT/F was classified based on susceptibility (A) to each pacing protocol and the duration (B and C) of induced arrhythmias in both the absence and presence of carbachol.

in Cx40^{-/-} mice. However, unlike WT mice where CCh substantially increased susceptibility to sustained AT/F (Fig. 2B), administration of CCh did not increase susceptibility to sustained AT/F in Cx40^{-/-} mice (1 of 13 without vs 2 of 9 with CCh, $\chi^2=0.95$, $P=0.32$, **Fig. 3.2C**).

Cx43^{+/+} littermate mice were used as controls instead of WT mice to ensure strain background control for the G60S mutant strain. Similar to WT mice, Cx43^{+/+} mice were relatively insensitive to AT/F induction of any duration (0.1 sec to >120 sec) by either single atrial stimulation (SAS) (1 of 11) or PES (4 of 11), while 8 of 11 were inducible using burst pacing (**Fig. 3.3A**). Of those which were inducible, 3 had sustained AT/F (>120 sec), 1 was had AT/F of an intermediate duration (10 to 60 sec) while the other 4 were not sustained (<10sec, **Fig. 3.3B**).

Cx43^{G60S/+} mice were highly susceptible to the induction of AT/F with all 3 pacing modalities: SAS (12 of 12, Fig. 3A); PES (12 of 12, Fig. 3A), and burst pacing (12 of 12, Fig. 3A). Of these, 9 of 12 had sustained AT/F, while 3 of 12 had intermediate durations (10-60 sec, Fig. 3B). Cx43^{G60S/+} mice were more sensitive to induction of sustained AT/F compared to Cx43^{+/+} mice ($\chi^2=5.24$, $P=0.02$, Fig. 3B). Of the Cx43^{G60S/+} mice with sustained AT/F, the maximum arrhythmia duration allowed was >35 minutes before the arrhythmia was terminated using burst pacing; however, the majority were electrically terminated after 2 minutes in order to proceed with the electrophysiological studies. In a subset of the Cx43^{G60S/+} mice AT/F could be terminated using a single atrial stimulus delivered to the mid right atrium (n=5). In our previous study we found that RGS2^{-/-} mice had AT/F associated with enhanced M3 muscarinic receptor⁴⁵. Thus, we determined the efficacy of intravenous darifenacin hydrobromide (1 mg/kg), a selective M3 muscarinic receptor antagonist, to terminate the “new onset” sustained AT/F in 5 Cx43^{G60S/+}

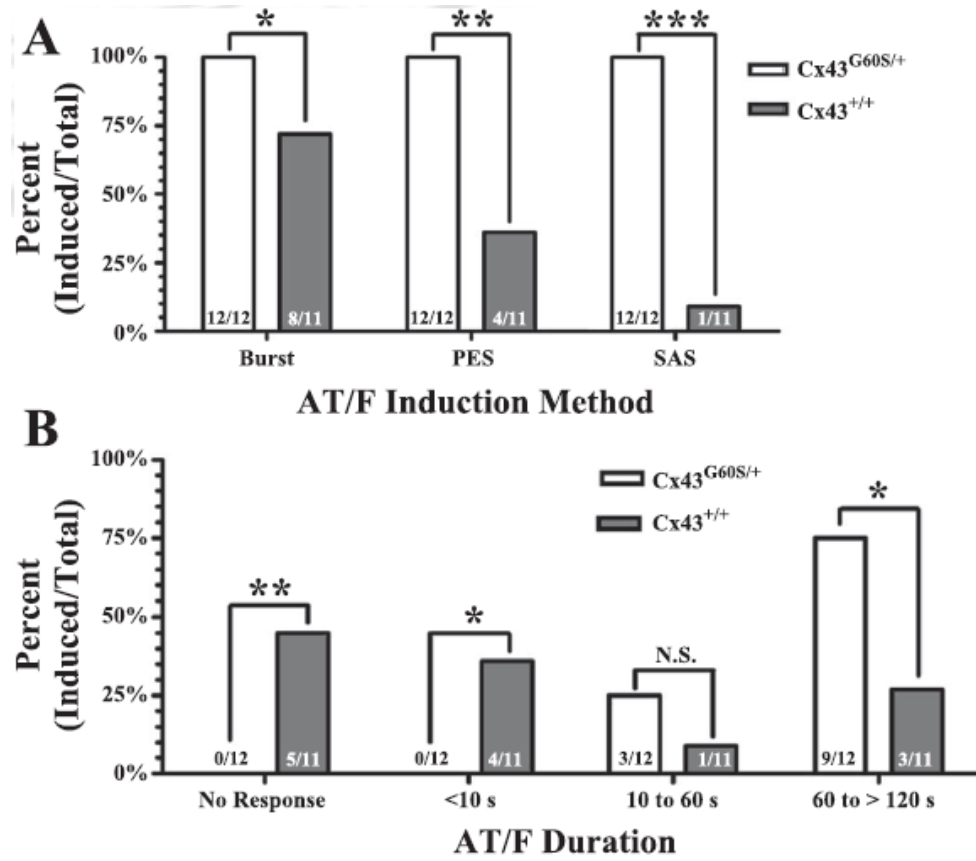


Figure 3.3. Incidence of AT/F induced by a SAS, PES, and burst pacing in 6-mo-old male Cx43^{+/+} littermate and Cx43^{G60S/+} mice. AT/F was classified based on susceptibility (A) to each pacing protocol and the duration (B) of induced arrhythmias.

mice. Intravenous injection of darifenacin terminated sustained AT/F in all 5 mice. Of note, AT/F was re-inducible with burst pacing 5 minutes after drug treatment.

3.3.5 Electrogram Analysis

The morphology of bipolar electrograms has been extensively studied in patients and animal models of AF^{11,30}. Normal unfractionated bipolar electrograms usually have a single monophasic or biphasic potentials, the morphology of which depends on the orientation of the electrode poles relative to the vector of the propagating electrical wave. Fractionated electrograms (FE) have multiple deflections within one cardiac cycle. As the study of electrogram fractionation in AT/F, to our knowledge, has not previously been performed in the mouse, we present the spectrum of electrograms that we have observed (**Fig. 3.4**). The simplest FE was a double potential, in which the time between peaks could be short (short double), or long (long double) (**Fig. 3.4**). Complex fractionated atrial electrograms (CFAE) have multiple peaks or may have continuous electrical activity throughout the entire cardiac cycle (**Fig. 3.4**). In humans, fractionated electrograms may be found: 1) in areas with slow conduction, such as the border zone of an infarct; 2) associated with a line of block (short/long double)¹¹; 3) around the pivot point of a micro re-entrant circuit, or 4) where waves collide³⁰. CFAEs have also been observed in myocyte monolayers, at sites of migrating rotors and wave break⁴⁶. As an index of conduction disturbance in-vivo, bipolar right atrial activation patterns observed in the MRA and HRA during AT/F were used, since optical mapping is not available in our laboratory, and in mice, optical mapping usually requires ex-vivo studies. We devised an index of electrogram patterns during AT/F, based on the degree of conduction disturbance: a) the lowest level was designated “fractionation only”, without a variable HRA cycle length compared to that recorded from the MRA; b) the intermediate had a variable HRA cycle length (CL) compared to the MRA CL, with or without intermittent

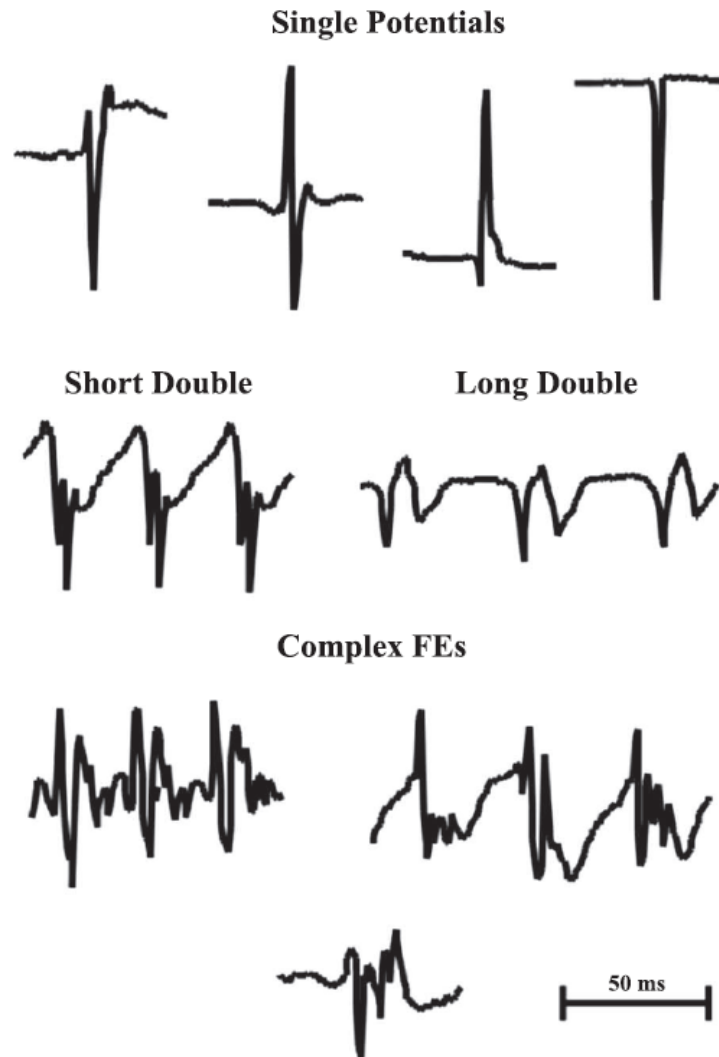


Figure 3.4. Morphology of fractionated bipolar electrograms (FEs) in mice recorded during sinus rhythm and electrically induced AT/F. Normal electrogram morphology had single sharp potentials. The simplest FEs had double potentials in which the time between peaks could be short (short double) or long (long double). Complex FEs had multiple peaks or continuous electrical activity throughout the entire cycle.

activation failure in the HRA, and c) the highest level had a pattern of 2:1 activation failure in the HRA compared to that recorded in the MRA. WT and Cx43^{+/+} mice commonly had unfractionated single potentials recorded from both the MRA and HRA electrodes during both sinus rhythm and AT/F. Fractionated double potentials, and complex electrograms were observed during AT/F in Cx43^{G60S/+} mice, commonly with double potential morphologies, which may have been due to functional conduction block along a zone of poor conduction.

In order to determine if the Cx43 G60S mutation-induced reduction in Cx43 was associated with disturbed conduction during AT/F (short cycle lengths or high rates), we compared electrograms recorded from Cx43^{G60S/+} to both Cx43^{+/+} and WT mice with induced AT/F. As there were no significant differences in the absence of carbachol, in the susceptibility to sustained AT/F between WT and Cx43^{+/+} mice (1 of 12 vs. 3 of 11, $X^2=1.43$, $P=0.23$), their responses to CCh-induced AT/F were grouped and compared to those of the Cx43^{G60S/+} mice. During AT/F, Cx43^{G60S/+} mice had a higher instance of disturbed RA conduction compared to Cx43^{+/+} and WT mice ($X^2=8.37$, $P=0.004$, **Fig. 3.5**). Importantly, tachycardia cycle lengths did not differ between the two groups (WT/Cx43^{+/+}, 33.2 ± 2 ms and Cx43^{G60S/+}, 35.9 ± 2.1 ms, $P=0.36$). The atrial activation rate during AT/F ranged from 1154 to 2609 per minute; an 8 fold maximal increase over the sinus rate of the anaesthetized mouse (325 ± 35 bpm) and a 4 fold increase over the sinus rate of the conscious “restrained” WT mouse (701.2 ± 36 bpm).

3.3.6 Left Atrial Recordings

As AF in patients frequently originates from the left atrium/pulmonary vein region, we performed epicardial left and right atrial appendage recording in a subset of mechanically ventilated Cx43^{G60S/+} mice (n=4). In all mice, atrial activation followed a left leading right atrial pattern, indicating that the arrhythmia driver was in the left atrium (n=4) (**Fig. 3.6A**).

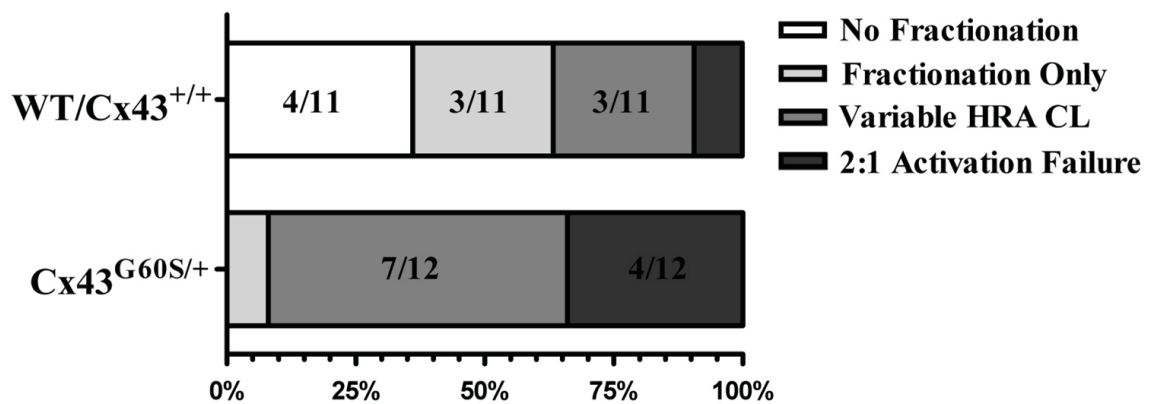


Figure 3.5. Classification of electrogram activation patterns during AT/F in Cx43^{G60S/+}, Cx43^{+/+}, and WT mice with carbachol-induced AT/F. Electrograms were grouped based on the degree of conduction disturbance, the least severe being “fractionation only”; intermediate being “variable HRA CL,” with or without intermittent activation failure in the HRA; and most severe being a pattern of “2:1 activation failure” of the HRA relative to the MRA.

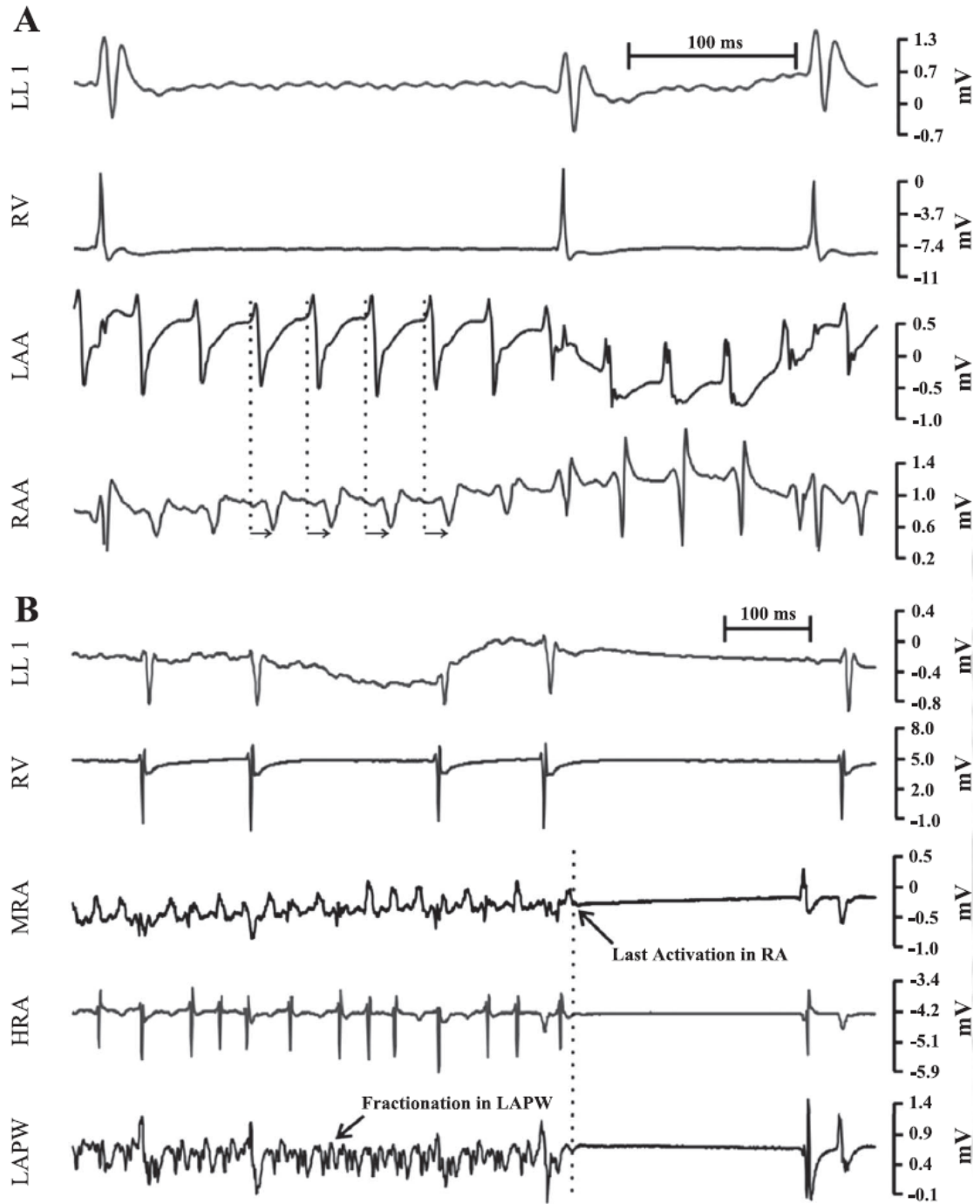


Figure 3.6. Recording from epicardial electrodes during AT/F in mechanically ventilated $Cx43^{G60S/+}$ mice. **A:** activation patterns recorded from the left (LAA) and right atrial appendages (RAA) demonstrating a left leading right activation pattern. **B:** recording from the left atrial posterior wall (LAPW) during AT/F demonstrating a complex fractionated left atrial electrogram pattern, while there is no fractionation in the right.

Spontaneous termination, when observed, occurred in the left with the last area of activation in the right atrium. Recordings from the posterior left atrium also revealed zones of high frequency complex fractionation (**Fig. 3.6B**), consistent with AF.

3.4 DISCUSSION

This main purpose of this study was to investigate the role of the Cx43 G60S mutation on the susceptibility to atrial tachy-arrhythmias in the mouse. Studies in the Cx40^{-/-} mouse also allowed direct comparisons on the role of reductions in each Cx isoform in AT/F. The results indicate that Cx43^{G60S/+} mice have increased susceptibility to AT/F while Cx40^{-/-} mice do not.

As gap junctions are critically important for cardiac impulse propagation it is not surprising that alterations of Cxs would be important in atrial arrhythmia. However, as Cx43 deficient mice die prematurely, comparative *in vivo* studies on the role of Cx40 and Cx43 in AT/F have not been performed. Interpretations of the significance of the results of past studies in Cx40^{-/-} mice have been hindered by the lack of definition of what constitutes a sustained atrial tachy-arrhythmia in the mouse. In the presence of CCh, WT mice had AT/F, averaging >139 s⁵¹. In the present study, we found long lasting (>2 min, and as long as 35 min), readily inducible (100% susceptibility) AT/F in Cx43^{G60S/+} mice. These observations provide a bench mark to define “sustained AT/F” in the mouse, allowing differentiation from transient arrhythmias.

We observed infrequent, primarily short runs of rapid atrial activity following burst pacing in the Cx40^{-/-} mice with only 1 incident of sustained AT/F, consistent with previous findings. After observing AT/F lasting >35 min in the Cx43^{G60S/+} mutant mice, it has become clear that short duration (<1 second) events are likely of limited physiological significance.

To evaluate if Cx40 deficiency could make the atrium more susceptible to AT/F in the presence of another provocative agent, we determined the susceptibility to CCh-induced AT/F in the Cx40^{-/-} mouse. However, we found that CCh did not significantly enhance inducibility of sustained AT/F in Cx40^{-/-} mice (>120 sec, Fig. 3C). This finding is consistent with those of dogs treated with n3-polyunsaturated fatty acids (PUFA) which had a reduced incidence of vagally induced AF, where protection was related to PUFA induced reductions in Cx40 protein expression⁴¹.

Three different pacing protocols were used to induce AT/F: burst pacing; PES with a single premature extra stimulus; and SAS with single atrial stimuli delivered during sinus rhythm timed to follow the p-wave and interact with the heterogeneous refractoriness of the atrial tissue. Both PES and SAS were thought to mimic physiological initiation of AT/F, as premature atrial beats often precede AT/F episodes²². Burst pacing, perhaps a non-physiological provocation, was found to more reliably induce AT/F by promoting cardiac electrical instability²⁵. Susceptibility to AT/F in the mouse induced by single stimuli delivered in sinus rhythm, an extremely mild pacing protocol, has not previously been reported in the mouse. AT/F induction with the SAS protocol indicates that the Cx43^{G60S/+} mice are extremely vulnerable to atrial arrhythmia. Detailed electrogram analysis showed that underlying heterogeneities in AERPs (in MRA vs HRA) on a background of reduced Cx43 content were associated with fibrillatory conduction with short cycle lengths (Fig. 5). Mechanistically, AF may result from a single source (mother rotor) resulting in fibrillation due to the breakup of high frequency wavefronts interacting with tissue heterogeneities²⁴. Thus reductions in Cx43 could promote AF initiation by promoting a wavebreak, coupled with conduction disturbances⁴⁸ to perpetuate AF. In an effort to compare murine AT/F to human AT/F, we determined if the mouse had left atrial predominance in AT/F mechanisms

as had been observed in man. Epicardial left atrial recordings in mechanically ventilated Cx43^{G60S/+} mice during AT/F had a left preceding right atrial activation pattern, and displayed zones of complex fractionation in the posterior left atrium. This result is consistent with clinical findings where the driver of AF is commonly observed in the posterior left atrium/pulmonary vein region^{20, 36}. While sustained AT/F occurred infrequently in the Cx40^{-/-} mice, genetic polymorphisms in Cx40 are associated with AF^{6, 8}. While a functional change in gap junctions caused by retaining mutant Cx40 at the intercalated disc may promote AF¹⁷, the present data show that complete removal of Cx40 (structural change) appears to provide resistance to CCh-induced AT/F. However, a large reduction (~80%) of phospho-Cx43 promotes enhanced AT/F susceptibility. While these results warrant further study, they are consistent with previously published results.

The atrium has equivalent expressions of Cx40 and Cx43. Thus atrial gap junctions may have varying stoichiometry (homomeric, heteromeric, homotypic or heterotypic), with unique gating and conductance properties⁹. In A7r5/Rin cell pairs, Cx40 and Cx43 can form homomeric/heterotypic and heteromeric/heterotypic gap junctions with unique gating and conductance properties⁹; however, junctional conductance is reduced relative to homomeric/homotypic channels. HeLa cell pairs co-expressing Cx40 and Cx43 also were reported to have substantial reductions (~56-66%) in junctional conductance compared to homotypic cell pairs⁴⁷. In addition, another study suggests that Cx40 and Cx43 hemichannels are potentially incompatible, as conduction was not detected²¹. It is reasonable to assume that Cx40^{-/-} and Cx43^{G60S/+} mice would have altered stoichiometry of connexon oligomerization which would alter conduction properties. However, the presence of, and functional consequence of gap junctions of mixed stoichiometry in the atrium has been reported to be uncertain¹².

A functional consequence of coexpression of Cx40 and Cx43 on junctional conductance (gj) in the mouse atrium has been studied using spermine, a compound that is reported to dose-dependently and selectively block Cx40 containing gap junctions³³. Spermine blockade in Cx40^{-/-} and Cx40^{+/+} atrial cell pairs indicated that Cx40 contributes to ~40% of wild type gj³³. Susceptibility to spermine inhibition also suggested that ~10-20% of atrial junctional conductance might be due to gap junctions of mixed stoichiometry³³. Also, junctional conductance was unaltered in myocyte pairs from Cx40^{-/-} mice (WT = 6.03±1.09 nS vs Cx40^{-/-} = 6.10±1.14 nS) (see Supplementary Material in Lu et al³³), suggesting an important role for channels of mixed stoichiometry or that Cx43 may compensate for the lack of Cx40.

Cx43^{G60S/+} mice have an ~80% reduction in ventricular phosphorylated Cx43 but only a ~50% decrease in ventricular myocyte gj. This suggests that myocytes biosynthesize larger amounts of Cx43 than is necessary to maintain normal cardiac gj function³⁵. This idea is consistent with the observation that in ventricular myocytes only 10% of the available cardiac gj channels are open to conduct current during a given action potential⁵². Both phosphorylation and pH are well known to regulate functional properties of gap junction channels. Ischemia results in acidification and closure of homomeric Cx40 and Cx43 containing gap junctions. However, coexpression of Cx40 and Cx43 in xenopus oocytes enhances the pH sensitivity of the channel, a phenomenon that requires the carboxy termini of both connexins⁵. Reductions in either Cx40 or Cx43 (reducing heterogeneity) would then likely decrease the pH sensitivity of the remaining gap junction channels.

In synthetic strands of neonatal atrial myocytes from Cx40^{-/-} and Cx43^{-/-} mice, conduction velocity was increased in Cx40^{-/-} strands, but was reduced in Cx43^{-/-} strands². The percent cell area occupied by the Cx40 immunosignal was smaller (2.0 ± 1.6% vs 1.0 ± 0.2%) in Cx43^{-/-} cultures, while the area of Cx43 immunosignal was larger (1.2 ± 0.9% vs 3.1

$\pm 3.6\%$) in Cx40^{-/-} cultures². This suggests that Cx40 may sterically limit the number of Cx43 containing gap junctions at the intercalated disc in WT atria. Removal of Cx40 would allow an increased insertion of Cx43 containing gap junctions into the intercalated disc region, to compensate for the reduced Cx40. Compensation may not be limited to those of neonatal myocytes, as optical mapping from adult Cx40^{-/-} mice revealed that morphologically normal hearts have no change in atrial conduction velocity³². Similar observations have been made in human myocardium, where there is a positive correlation between conduction velocity and the relative quantity of Cx immunolabelling (expressed as Cx40/[Cx40 + Cx43]), when Cx40 signal was higher or Cx43 signal was lower, conduction velocity was lower²⁸.

Taken together, these observations suggest the following theoretical model of the role of alterations of connexins in the atrium. As stated above, Cx40 may sterically limit Cx43 content at the intercalated disc region, thus loss of Cx40 would lead to compensatory increased Cx43 insertion; however, the reverse seems not to occur. Atrial gap junction channel conductance follows a hierarchy where Cx40/Cx40 > Cx43/Cx43 > Cx40/Cx43. Therefore, homogenous loss of Cx40 leads to increased junctional conductance (plus decreasing pH sensitivity of channels) and reduced heterogeneity as only Cx43/Cx43 gap junctions remain. As such increased heterogeneity of coupling might then promote AT/F. On the other hand, somatic mosaic mutation in either Cx40 or Cx43 in patients leads to AF. This is likely due to the resultant enhanced heterogeneity of the atrial tissue accentuated by the mosaic nature of the functional changes, whether or not there is an accompanying localization in the intercalated disc.

In conclusion, it is clear that alterations in gap junctions can have a role in AF mechanisms. However that role may not simply be due to reductions in Cx content¹⁴. Proper

interpretation of the role of Cxs in AT/F should consider the functional alterations, structural alterations, stoichiometric alterations, and the potential for compensation¹⁴. In this study we found that the Cx43^{G60S/+} mutant mouse had sustained AT/F. We also noted that Cx40^{-/-} mice were resistant to CCh-induced AT/F despite severe hypertension and cardiac hypertrophy; both risk factors for development of AF. As AF can be a silent disease, observed only after diagnostic (ECG) testing, it may be wise to monitor patients with Cx43 mutations causing *Oculodentodigital Dysplasia* as there are reports of cardiac phenotypes³⁹ in these patients and they may have additional age-related risk for developing AF.

3.5 LIMITATIONS

It may be difficult to distinguish AF from atrial tachycardia, when evaluating recordings from the mouse heart, particularly with arrhythmia of short duration⁴⁵. However, using the standard clinical criteria for identification of AF, lack of regular P waves on ECGs and irregularly irregular ventricular responses, often with left atrial predominance of AF mechanisms, in this study it was often possible to demonstrate these classical characteristics of AF in the mouse. In addition, it may not always be possible to extrapolate data obtained from the mouse to explain arrhythmia mechanisms in the human.

3.6 REFERENCES

1. Bagwe S, Berenfeld O, Vaidya D, Morley GE, Jalife J. Altered right atrial excitation and propagation in connexin40 knockout mice. *Circulation* 112:2245-53. 11-10-2005.
2. Beauchamp P, Yamada KA, Baertschi AJ, Green K, Kanter EM, Saffitz JE, Kleber AG. Relative contributions of connexins 40 and 43 to atrial impulse propagation in synthetic strands of neonatal and fetal murine cardiomyocytes. *Circ Res* 99:1216-24. 24-11-2006.
3. Benjamin EJ, Wolf PA, D'Agostino RB, Silbershatz H, Kannel WB, Levy D. Impact of atrial fibrillation on the risk of death: the Framingham Heart Study. *Circulation* 98:946-52. 8-9-1998.

4. Bevilacqua LM, Simon AM, Maguire CT, Gehrmann J, Wakimoto H, Paul DL, Berul CI. A targeted disruption in connexin40 leads to distinct atrioventricular conduction defects. *J Interv Card Electrophysiol* 4:459-67. 2000.
5. Bouvier D, Spagnol G, Chenavas S, Kieken F, Vitrac H, Brownell S, Kellezi A, Forge V, Sorgen PL. Characterization of the structure and intermolecular interactions between the connexin40 and connexin43 carboxyl-terminal and cytoplasmic loop domains. *J Biol Chem* 284:34257-71. 4-12-2009.
6. Burstein B, Comtois P, Michael G, Nishida K, Villeneuve L, Yeh YH, Nattel S. Changes in connexin expression and the atrial fibrillation substrate in congestive heart failure. *Circ Res* 105:1213-22. 4-12-2009.
7. Caspar DL, Goodenough DA, Makowski L, Phillips WC. Gap junction structures. I. Correlated electron microscopy and x-ray diffraction. *J Cell Biol* 74:605-28. 1977.
8. Chaldoupi SM, Loh P, Hauer RN, de Bakker JM, van Rijen HV. The role of connexin40 in atrial fibrillation. *Cardiovasc Res* 84:15-23. 1-10-2009.
9. Cottrell GT, Burt JM. Heterotypic gap junction channel formation between heteromeric and homomeric Cx40 and Cx43 connexons. *Am J Physiol Cell Physiol* 281:C1559-C1567. 2001.
10. Danik SB, Rosner G, Lader J, Gutstein DE, Fishman GI, Morley GE. Electrical remodeling contributes to complex tachyarrhythmias in connexin43-deficient mouse hearts. *FASEB J* 22:1204-12. 2008.
11. de Bakker JM, van Capelle FJ, Janse MJ, Tasseron S, Vermeulen JT, de JN, Lahpor JR. Fractionated electrograms in dilated cardiomyopathy: origin and relation to abnormal conduction. *J Am Coll Cardiol* 27:1071-8. 1996.
12. Desplantez T, Dupont E, Severs NJ, Weingart R. Gap junction channels and cardiac impulse propagation. *J Membr Biol* 218:13-28. 2007.
13. Dobrowolski R, Sasse P, Schrickel JW, Watkins M, Kim JS, Rackauskas M, Troatz C, Ghanem A, Tiemann K, Degen J, Bukauskas FF, Civitelli R, Lewalter T, Fleischmann BK, Willecke K. The conditional connexin43G138R mouse mutant represents a new model of hereditary oculodentodigital dysplasia in humans. *Hum Mol Genet* 17:539-54. 15-2-2008.
14. Duffy HS, Wit AL. Is there a role for remodeled connexins in AF? No simple answers. *J Mol Cell Cardiol* 44:4-13. 2008.
15. Feng M, DiPetrillo K. Non-invasive blood pressure measurement in mice. *Methods Mol Biol* 573:45-55. 2009.
16. Flenniken AM, Osborne LR, Anderson N, Ciliberti N, Fleming C, Gittens JE, Gong XQ, Kelsey LB, Lounsbury C, Moreno L, Nieman BJ, Peterson K, Qu D, Roscoe W, Shao Q, Tong D, Veitch GI, Voronina I, Vukobradovic I, Wood GA, Zhu Y, Zirngibl RA, Aubin

- JE, Bai D, Bruneau BG, Grynepas M, Henderson JE, Henkelman RM, McKerlie C, Sled JG, Stanford WL, Laird DW, Kidder GM, Adamson SL, Rossant J. A Gja1 missense mutation in a mouse model of oculodentodigital dysplasia. *Development* 132:4375-86. 2005.
17. Gollob MH, Jones DL, Krahn AD, Danis L, Gong XQ, Shao Q, Liu X, Veinot JP, TANG AS, Stewart AF, Tesson F, Klein GJ, Yee R, Skanes AC, Guiraudon GM, Ebihara L, Bai D. Somatic mutations in the connexin 40 gene (GJA5) in atrial fibrillation. *N Engl J Med* 354:2677-88. 22-6-2006.
 18. Gutstein DE, Morley GE, Tamaddon H, Vaidya D, Schneider MD, Chen J, Chien KR, Stuhlmann H, Fishman GI. Conduction slowing and sudden arrhythmic death in mice with cardiac-restricted inactivation of connexin43. *Circ Res* 88:333-9. 16-2-2001.
 19. Hagedorff A, Schumacher B, Kirchhoff S, Luderitz B, Willecke K. Conduction disturbances and increased atrial vulnerability in Connexin40-deficient mice analyzed by transesophageal stimulation. *Circulation* 99:1508-15. 23-3-1999.
 20. Haissaguerre M, Jais P, Shah DC, Takahashi A, Hocini M, Quiniou G, Garrigue S, Le Mouroux A, Le Metayer P, Clementy J. Spontaneous initiation of atrial fibrillation by ectopic beats originating in the pulmonary veins. *N Engl J Med* 339:659-66. 3-9-1998.
 21. Haubrich S, Schwarz HJ, Bukauskas F, Lichtenberg-Frate H, Traub O, Weingart R, Willecke K. Incompatibility of connexin 40 and 43 Hemichannels in gap junctions between mammalian cells is determined by intracellular domains. *Mol Biol Cell* 7:1995-2006. 1996.
 22. Hoffmann E, Sulke N, Edvardsson N, Ruitter J, Lewalter T, Capucci A, Schuchert A, Janko S, Camm J. New insights into the initiation of atrial fibrillation: a detailed intraindividual and interindividual analysis of the spontaneous onset of atrial fibrillation using new diagnostic pacemaker features. *Circulation* 113:1933-41. 25-4-2006.
 23. Jackson PE, Feng QP, Jones DL. Nitric oxide depresses connexin 43 after myocardial infarction in mice. *Acta Physiol (Oxf)* 194:23-33. 2008.
 24. Jalife J, Delmar M, Anumonwo J, Berenfeld O, Kalifa J. *Basic Cardiac Electrophysiology for the Clinician*. 2 ed. Hoboken, NY: Wiley-Blackwell; 2009.
 25. Jones DL, Guiraudon GM, Skanes AC, Guiraudon CM. Anatomical pitfalls during encircling cryoablation of the left atrium for atrial fibrillation therapy in the pig. *J Interv Card Electrophysiol* 21:187-93. 2008.
 26. Jones DL, Petrie JP, Li HG. Spontaneous, electrically, and cesium chloride induced arrhythmia and afterdepolarizations in the rapidly paced dog heart. *Pacing Clin Electrophysiol* 24:474-85. 2001.
 27. Kalcheva N, Qu J, Sandeep N, Garcia L, Zhang J, Wang Z, Lampe PD, Suadicani SO, Spray DC, Fishman GI. Gap junction remodeling and cardiac arrhythmogenesis in a

- murine model of oculodentodigital dysplasia. *Proc Natl Acad Sci U S A* 104:20512-6. 18-12-2007.
28. Kanagaratnam P, Rothery S, Patel P, Severs NJ, Peters NS. Relative expression of immunolocalized connexins 40 and 43 correlates with human atrial conduction properties. *J Am Coll Cardiol* 39:116-23. 2-1-2002.
 29. Kirchhoff S, Kim JS, Hagendorff A, Thonnissen E, Kruger O, Lamers WH, Willecke K. Abnormal cardiac conduction and morphogenesis in connexin40 and connexin43 double-deficient mice. *Circ Res* 87:399-405. 1-9-2000.
 30. Konings KT, Smeets JL, Penn OC, Wellens HJ, Allessie MA. Configuration of unipolar atrial electrograms during electrically induced atrial fibrillation in humans. *Circulation* 95:1231-41. 4-3-1997.
 31. Laird DW. The life cycle of a connexin: gap junction formation, removal, and degradation. *J Bioenerg Biomembr* 28:311-8. 1996.
 32. Leaf DE, Feig JE, Vasquez C, Riva PL, Yu C, Lader JM, Kontogeorgis A, Baron EL, Peters NS, Fisher EA, Gutstein DE, Morley GE. Connexin40 imparts conduction heterogeneity to atrial tissue. *Circ Res* 103:1001-8. 24-10-2008.
 33. Lin X, Gemel J, Glass A, Zemlin CW, Beyer EC, Veenstra RD. Connexin40 and connexin43 determine gating properties of atrial gap junction channels. *J Mol Cell Cardiol* 48:238-45. 1-1-2010.
 34. Makita N, Sasaki K, Groenewegen WA, Yokota T, Yokoshiki H, Murakami T, Tsutsui H. Congenital atrial standstill associated with coinheritance of a novel SCN5A mutation and connexin 40 polymorphisms. *Heart Rhythm* 2:1128-34. 2005.
 35. Manias JL, Plante I, Gong XQ, Shao Q, Churko J, Bai D, Laird DW. Fate of connexin43 in cardiac tissue harbouring a disease-linked connexin43 mutant. *Cardiovasc Res* 80:385-95. 1-12-2008.
 36. Morillo CA, Klein GJ, Jones DL, Guiraudon CM. Chronic rapid atrial pacing: structural, functional, and electrophysiological characteristics of a new model of sustained atrial fibrillation. *Circulation* 91:1588-95. 1995.
 37. Natelson BH, Cagin NA. Stress-induced ventricular arrhythmias. *Psychosom Med* 41:259-62. 1979.
 38. Nattel S, Allessie M, Haissaguerre M. Spotlight on atrial fibrillation-the 'complete arrhythmia'. *Cardiovasc Res* 54:197-203. 2002.
 39. Paznekas WA, Karczeski B, Vermeer S, Lowry RB, Delatycki M, Laurence F, Koivisto PA, Van ML, Boyadjiev SA, Bodurtha JN, Jabs EW. GJA1 mutations, variants, and connexin 43 dysfunction as it relates to the oculodentodigital dysplasia phenotype. *Hum Mutat* 30:724-33. 2009.

40. REAUME AG, DE SOUSA PA, Kulkarnik S, Langille BL, Zhu D, Davies TC, Juneja SC, Kidder GM, Rossant J. Cardiac malformation in neonatal mice lacking connexin43. *Science* 267:1831-4. 24-3-1995.
41. Sarrazin JF, Comeau G, Daleau P, Kingma J, Plante I, Fournier D, Molin F. Reduced incidence of vagally induced atrial fibrillation and expression levels of connexins by n-3 polyunsaturated fatty acids in dogs. *J Am Coll Cardiol* 50:1505-12. 9-10-2007.
42. Schrickel JW, Kreuzberg MM, Ghanem A, Kim JS, Linhart M, Andrie R, Tiemann K, Nickenig G, Lewalter T, Willecke K. Normal impulse propagation in the atrioventricular conduction system of Cx30.2/Cx40 double deficient mice. *J Mol Cell Cardiol* 46:644-52. 2009.
43. Simon AM, Goodenough DA, Paul DL. Mice lacking connexin40 have cardiac conduction abnormalities characteristic of atrioventricular block and bundle branch block. *Curr Biol* 8:295-8. 26-2-1998.
44. Thibodeau IL, Xu J, Li Q, Liu G, Lam K, Veinot JP, Birnie DH, Jones DL, Krahn AD, Lemery R, Nicholson BJ, Gollob MH. Paradigm of genetic mosaicism and lone atrial fibrillation: physiological characterization of a connexin 43-deletion mutant identified from atrial tissue. *Circulation* 122:236-44. 20-7-2010.
45. Tuomi JM, Chidiac P, Jones DL. Evidence for enhanced M3 muscarinic receptor function and sensitivity to atrial arrhythmia in the RGS2-deficient mouse. *Am J Physiol Heart Circ Physiol* 298:H554-H561. 2010.
46. Umapathy K, Masse S, Kolodziejaska K, Veenhuyzen GD, Chauhan VS, Husain M, Farid T, Downar E, Sevaptisidis E, Nanthakumar K. Electrogram fractionation in murine HL-1 atrial monolayer model. *Heart Rhythm* 5:1029-35. 2008.
47. Valiunas V, Gemel J, Brink PR, Beyer EC. Gap junction channels formed by coexpressed connexin40 and connexin43. *Am J Physiol Heart Circ Physiol* 281:H1675-H1689. 2001.
48. Vaquero M, Calvo D, Jalife J. Cardiac fibrillation: from ion channels to rotors in the human heart. *Heart Rhythm* 5:872-9. 2008.
49. Verheule S, van Batenburg CA, Coenjaerts FE, Kirchhoff S, Willecke K, Jongsma HJ. Cardiac conduction abnormalities in mice lacking the gap junction protein connexin40. *J Cardiovasc Electrophysiol* 10:1380-9. 1999.
50. Wagner C, de WC, Kurtz L, Grunberger C, Kurtz A, Schweda F. Connexin40 is essential for the pressure control of renin synthesis and secretion. *Circ Res* 100:556-63. 2-3-2007.
51. Wakimoto H, Maguire CT, Kover P, Hammer PE, Gehrman J, Tiedman JK, Berul CI. Induction of atrial tachycardia and fibrillation in the mouse heart. *Cardiovasc Res* 50:463-73. 2001.
52. Weingart R. Electrical properties of the nexal membrane studied in rat ventricular cell pairs. *J Physiol* 370:267-84. 1986.

CHAPTER 4: Junctional Tachycardia in the Mouse is Prevented by Pacemaker Channel (If) Blockade

4.0 CHAPTER SUMMARY

A central objective of this thesis was to determine how to systematically elicit and study atrial arrhythmia in the mouse. Here I investigate AV nodal conduction properties and two supraventricular arrhythmias, AV nodal reentry and Junctional Tachycardia (JT). Histological studies indicate that the mouse AV junction is highly similar to the human. I determined that the mouse and human AV junction also have similar electrophysiological properties including: dual AV nodal physiology; nodal reentry; functional longitudinal dissociation of the bundle of His; and susceptibility to JT. JT occurs in approximately 10% of children following cardiac surgery and increases the risk of mortality by 5.6-14%. I found that rapid ventricular pacing (RVP) induced JT in the mouse, which was distinguished from AVNRT using diagnostic pacing studies. RVP caused decreases ($46 \pm 2.6\%$) in the minimal end-diastolic blood pressure and enhanced nodal conduction following 10 bursts (pre-pacing $AH=31 \pm 1$ ms vs post-pacing $AH=28 \pm 1$ ms, $P < 0.001$, $n=14$) prior to JT initiation, suggesting involvement of a baroreflex response. Vagal nerve stimulation (5/5) and propranolol (7/7) prevented JT induction, confirming a role for the autonomics. These observations provide evidence for the hypothesis that there is a role for the autonomics in most atrial arrhythmias. Due to the impaired ventricular function in neonates following cardiac surgery, use of negative inotropic drugs for JT, such as propranolol, is counter indicated. Thus, there is a need for a novel antiarrhythmic for the treatment of JT. In this chapter I found that Ivabradine hydrochloride, a selective I_f channel blocker, with no negative inotropic effects, prevented JT

in 8 of 9 mice ($X^2=14.4$, $P<0.001$). As such ivabradine might be useful in patients with post-operative JT.

4.1 INTRODUCTION

The heart's atrioventricular node (AVN) plays 2 important functions; cardiac impulse conduction and impulse initiation. The AVN is normally the only electrical route for activation from the atria to the ventricles and acts to shield the ventricles from excessively fast atrial rates. Dysfunction of AV nodal conduction results in AV block or re-entrant tachycardia (AVNRT). The mechanism of AVNRT is well defined, involving the conversion of multiple non-discrete input pathways to the compact AV node, (the "fast" (FP), "intermediate" (IP), and "slow" (SP) pathways), into functional dual pathways allowing for reentrant conduction (**Fig. 4.1**)⁴⁹. Normal antegrade conduction to the ventricles is through the FP. The SP, which is composed of the posterior peripheral or inferior nodal extension (PNE or INE) of the compact AVN, is present in all normal hearts⁴⁹. However, differential refractoriness, local negative balances of current source and current sink along with increasing electrical load at the transition zone of the AVN are thought to result in the development of a "line of block" in one pathway and thus initiate reentry⁴⁹. The AV node is tightly regulated by the autonomic nervous system³², explaining why vagal manoeuvres are successful in terminating AVNRT⁴⁷. Knowledge of the mechanism of AVNRT has resulted in development of successful curative interventions using radiofrequency ablation of the SP.

The AVN is also an oscillator, acting as a backup pacemaker during sinoatrial nodal (SAN) failure. The SAN is the dominant pacemaker of the heart. Normally the AVN

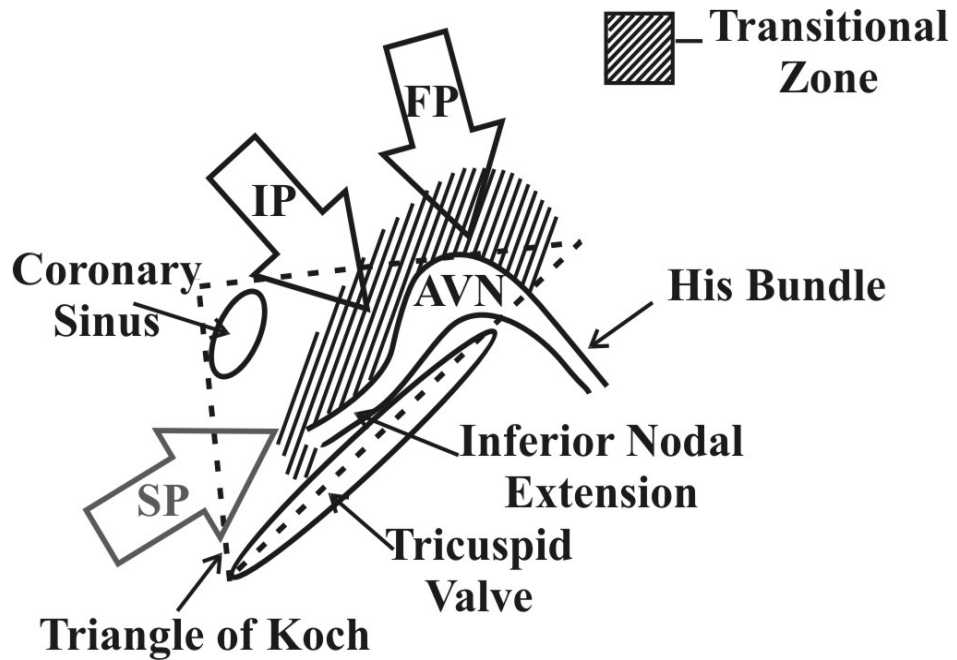


Figure 4.1: A diagrammatic representation of the structure of the atrial inputs to the AV node from optical mapping data adapted from Wu & Zipes⁴⁹. FP, fast pathway. IP, intermediate pathway. SP, slow pathway. AVN, compact AV node. Dashed lines represent the borders of the triangle of Koch.

pacemaker is much slower, thus it is kept quiescent by continual overdrive suppression by the faster SAN. In the heart, 2 pacemaking mechanisms have been proposed: that involve the activity of the hyperpolarization activated cyclic nucleotide gated (HCN4) pacemaker funny channel (I_f)²⁶, which produces a diastolic depolarization; and a "calcium clock", where oscillations in local Ca^{2+} release from the ryanodine receptor activate the electrogenic Na^+ - Ca^{2+} exchanger to accelerate the upstroke of the late diastolic depolarization²⁴. Genetic markers of pacemaking tissue (high: Cx30.2/Cx45/ HCN4/Tbx3, low: Cx40/Cx43/SCN5a) are expressed in both the mouse SA and AV node⁸. The I_f channel density is much greater in the SAN⁶, than the dominant AVN pacemaker region²⁶, located in the posterior nodal extension¹³. This indicates that I_f channel expression density correlates with intrinsic pacemaker rate. The human AVN also contains HCN4, with little HCN4 detected in the surrounding atrium⁵².

Dysfunction of AVN impulse initiation results in junctional tachycardia (JT, also called junctional "ectopic" tachycardia). JT is frequently observed in neonates following cardiac surgery^{4, 11, 19, 34}; although, a rare congenital form exists⁵⁰. The rapid rate and hemodynamic dysfunction during JT following cardiac surgery can be problematic, increasing the risk of mortality by 5.6%-14%^{4, 11, 19, 34}. It is suggested that the arrhythmia may be generated by injury to the AVN during surgery; however, JT can occur in patients where the AV node is not harmed. Thus, the mechanism(s) of JT have not yet been fully elucidated. Numerous clinical observations suggest a role for the autonomics. During JT the atria contract against closed AV valves, reducing the atrial component of ventricular filling, thus reducing cardiac output. This reduction coupled with the already reduced cardiac output due to post-surgical stunning, produces dangerous hypotension which may drive a positive feedback-like baroreflex response, potentiating the arrhythmia. Pre-operative treatment with propranolol, a

β -adrenergic receptor inverse agonist, can reduce the incidence of post-operative JT (control group (38%) vs. propranolol group (21%) $P < 0.042$)²⁸. Consistent with this finding, dopamine, an adrenergic agonist used for inotropic support after cardiac surgery in neonates^{4, 19}, is a risk factor for JT⁴. Amiodarone (generally considered a class III antiarrhythmic), used for treatment of JT, also has anti-sympathetic actions. Atrial sympathetic noradrenalin release is inhibited by pre-synaptic α -2 adrenergic receptor stimulation¹⁸. Post-operative use of Dexmedetomidine, a sedative and α -2 adrenergic receptor agonist, decreased JT rate from 197 ± 22 to 165 ± 17 bpm within 67 ± 75 min of administration⁹. Pacemaker function is tightly regulated by autonomic responses. Activation of β -adrenergic receptors (stimulatory) and M2 muscarinic receptors (inhibitory) regulate the formation of the cyclic AMP (cAMP) that directly regulates pacemaker channel and PKA activation. Cyclic AMP binding directly regulates I_f channels, causing a shift towards depolarization in the channel's activation curve. This coupled with the phosphorylation of various intracellular Ca^{2+} handling proteins (L-Type Ca^{2+} channels, RyR, Phospholamban) by PKA and CAMKII are also proposed to enhance the periodicity of the local Ca^{2+} release events of the "Calcium Clock" and pacemaker rate.

The development and 3-D architecture of the mouse atrioventricular conduction axis has high similarity to the human conduction system¹. Thus, I hypothesized that the mouse and human AV junction would have similar electrophysiological properties including: dual AV nodal physiology; nodal reentry; and functional longitudinal dissociation of the bundle of His. In addition, the mouse has been used for the study of AV nodal properties^{27, 37, 46} and arrhythmia²⁹ and as such may provide insights into the mechanisms of JT. I hypothesize that JT is caused by inappropriate (enhanced) AV nodal pacemaker activity initiated by abnormal autonomic (baroreflex) activity. In this chapter I determine normal AV nodal conduction

properties; determine the susceptibility of the mouse to induced JT; distinguish JT from AVNRT using diagnostic pacing studies; and study the mechanisms of JT pharmacologically in the mouse.

4.2 METHODS

4.2.1 Animals

Studies used 3-6 month old C57BL/6 mice from Charles River, unless otherwise stated. All studies were approved by the Animal Care and Use Committee of the University of Western Ontario (protocol #2006-121-12) and complied with the guidelines of the Canadian Council on Animal Care and the Guide to the Care and Use of Laboratory Animals published by the US National Institutes of Health (Institution #A5527-01). RGS2^{-/-} mice were provided by Dr. Peter Chidiac from his breeding colony.

Using routine procedures^{42,44}, mice were anesthetized with an i.p. injection mixture of ketamine (150 mg/kg) and xylazine (10 mg/kg). Body temperature was monitored with an YSI-402 (Yellow Springs Instruments, Yellow Springs, Ohio) rectal probe and maintained at 36.5 - 38 °C⁴². Through a cut-down, a 23 ga Teflon endotracheal tube was inserted and ligated in place to keep saliva and blood from the trachea and maintain it open. Limb lead ECGs were obtained using 4 subcutaneous 25 ga platinum electrodes (Grass Instrument Inc., Quincy, Mass.) placed at the base of each limb. ECG tracings were filtered between 0.05 to 100 Hz, digitized and sampled at 1.5 kHz, with an ECG100 preamplifier connected to an MP1000 recording system (BIOPAC Systems, Biolyntx, Montréal, PQ).

4.2.2 In Vivo Intracardiac Electrophysiology Studies

A 2F octapolar stimulation / recording / drug infusion catheter (CIB'ER Mouse®, NuMED Inc., Hopkinton, NY) (**Fig. 4.2a**) was inserted through the right jugular vein and

advanced into the right atrium and ventricle. Intracardiac electrograms were filtered between 100 to 5000 Hz (DA100 amplifier, BIOPAC Systems) and sampled at 1.5 kHz. All data were recorded using a personal computer running Acknowledge software (BIOPAC Systems). His bundle potentials (**Fig. 4.2b**) were used to establish catheter positioning within the right atrium (RA) and ventricle (RV) with 2 pairs of bipolar electrodes located at the mid right atrium (MRA) and the high right atrium region (HRA)⁴². The catheter positioning was verified using Computerized Tomography (CT, **Fig. 4.2c**).

Bipolar pacing used 1 ms pulses at twice the diastolic threshold, delivered through a Grass stimulus isolation unit (SIU5, Grass Equipment Ltd., Quincy, Mass), connected to a Grass S99 stimulator, driven by a custom-built timer⁴². Effective refractory periods (ERPs) from the right atrium (AERP), right ventricle (VERP), and AV node (AVNERP) were assessed with programmed electrical stimulation (PES)²⁵ using a drive train of 9 stimuli (S1) at a cycle length of 100 ms and 150 ms, followed by a progressively premature extra stimulus (S2). Atrial pacing with 1 ms decrements was used to determine the Wenkebach cycle length (WCL). Junctional Tachycardia was induced by repetitive (10-40) trains of ventricular burst pacing (train duration: 400ms, S1S1 coupling interval: 20ms). Single atrial stimuli delivered to the high right atrium at various phases of the tachycardia cycle were used to distinguish JT from AVNRT.

4.2.3 Blood Pressure

Blood pressure changes in response to ventricular burst pacing were assessed by cannulating the carotid artery with PE-10 tubing filled with heparinized saline. The tubing was connected to a COBE pressure transducer and recorded on the BioPac system.

4.2.4 Pharmacological Tests

Responses to cholinergic stimulation were determined using i.p. injections of the non-selective cholinergic agonist, carbamyl choline chloride, (carbachol, CCh, 0.05 mg/kg), and the non-selective cholinergic antagonist, atropine (1 mg/kg). Sympathetic blockade used i.v. injection of propranolol (1mg/kg) via a cannula inserted into the left jugular vein.

Ganglionic blockade used the nicotinic acetylcholine receptor blocker Hexamethonium bromide (30mg/kg, i.v.). Low dose Ivabradine hydrochloride (1 mg/kg, i.v.) examined the role of the pacemaker funny channel (I_f). Ruthenium Red (1 mg/kg, i.v.), a potent inhibitor of Ca^{2+} release from the ryanodine receptor and Caffeine (10mg/kg, i.v.) to stimulate Ca^{2+} release examined the function of the intracellular Ca^{2+} clock. DPCPX³⁵ (8-cyclopentyl-1, 3-dipropylxanthine, 100ug/kg, i.v.), a selective A1 adenosine receptor antagonist, tested the adenosine effect in the Caffeine response. Forskolin (1 mg/kg, i.v.), a direct activator of Adenylyl Cyclase, IBMX (0.5 mg/kg, i.v.) a nonselective phosphodiesterase inhibitor and Milrinone (1 mg/kg, i.v.) a selective PDE3 inhibition, investigated the role of cAMP in JT.

4.2.5 Statistical analysis

The Chi Square test was used to analyze discrete data. Student's t Test analyzed non-discrete data. A probability of $P < 0.05$ was considered statistically significant. All data was expressed as the mean \pm SEM.

4.3 RESULTS

4.3.1 Antegrade AV nodal conduction

Antegrade AV nodal conduction curves were examined for the presence of discontinuous conduction, an indication of functional dual AV nodal pathways²⁷.

Determination of what constitutes an adequate "jump" or sudden increase in A2H2 interval

with a decrease in A1A2 coupling interval, during programmed electrical stimulation, was made by examining for the presence of re-entrant atrial beats. Evidence for discontinuous conduction was taken as a >9 ms increase in A2H2 interval with a <5 ms decrease in A1A2

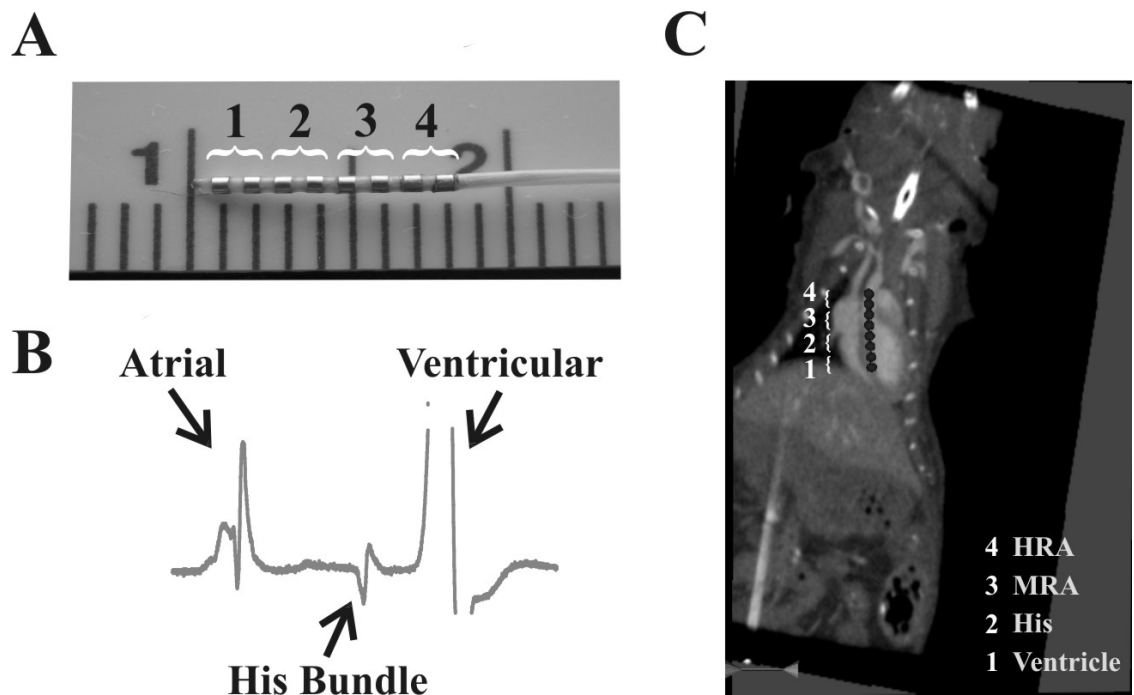


Figure 4.2. A) Photograph of the 2F octapolar recording catheter used for intracardiac pacing and recording experiments in the mouse. Numbers represent the bipolar electrode pairs used for recording sites within the heart: 1) ventricle 2) His bundle 3) mid-right atrium 4) high right atrium/superior vena cava. B) A representative electrogram from His bundle region. Electrode pair # 2 was the landmark used for determining of catheter position in the right atrium. C) Validation of catheter position using Computed Tomography (CT) imaging with the dots indicating the position of the electrode poles within the heart.

coupling interval. Using this criterion, discontinuous antegrade AVN conduction was observed in 8 of 19 mice (**Fig. 4.3**), with single re-entrant beats observed 3 of 19 (**Fig. 4.4**), but only one incidence multiple re-entrant events (1 of 19).

4.3.2 Functional Longitudinal Dissociation Of The His Bundle (FP vs SP conduction)

Functional longitudinal dissociation of the bundle of His has previously been observed during optical mapping studies in rabbit⁵¹ and human^{20, 23} AV junction preparations. This phenomenon was used to explain the His bundle electrogram (HBE) amplitude alterations^{2, 40} observed during SP vs FP activation of the His bundle. I examined mouse HBEs from antegrade conduction curves during discontinuous conduction (SP activation) and compared those electrograms to those recorded in the zone of continuous conduction (FP activation) on the same curve (**Fig.4.3b/Fig.4.4**, A1A2=59ms for FP vs A1A2=57ms for SP). His amplitudes during defined "slow pathway" conduction (0.15 ± 0.03 mV) was higher than during "fast pathway" conduction (0.12 ± 0.03 mV, $n=7$, $P<0.02$). This pattern of His amplitude alterations is indicative of functional longitudinal dissociation of the His. His amplitudes recorded during "Slow pathway" conduction were also significantly greater compared to those recorded during sinus rhythm (0.15 ± 0.03 mV vs 0.10 ± 0.02 mV, $n=7$, $P=0.01$) (**Fig 4.4**). As a control for motion artefact due to pacing rate during programmed electrical stimulation, HBE amplitudes from the continuous antegrade conduction curves were analyzed just prior to conduction failure (the AV node effective refractory period). There was no significant differences in HBE amplitudes from the last His bundle activation on the continuous conduction curves vs the His amplitude in the preceding cycle (0.10 ± 0.01 vs 0.10 ± 0.01 mV, $n=11$, $P=0.93$) or when compared to sinus rhythm (0.10 ± 0.01 vs

0.10±0.02, n=11, P=0.82). There was also no difference in HBE amplitudes recorded during sinus activation of the His for mice with discontinuous conduction curves (8/19) compared to the continuous conduction curves (11/19) (0.10±0.01 vs 0.10±0.02 mV, P=0.98). Detection of HBE amplitude alterations on antegrade conduction curves may be a useful diagnostic test for the presence of slow pathway conduction. The average change in HBE amplitude during SP activation was 0.04±0.01 mV. Therefore, a >0.03 mV change in HBE amplitude was set as an independent criterion for detection of SP conduction. To ensure there was no sample bias, raw data from individual antegrade conduction experiments were number coded, and randomized before re-analysis for HBE amplitude changes by an independent blinded observer. A >0.03mV change in HBE amplitude was detected in 1 of 11 animals with continuous conduction and 7 of 8 animals with discontinuous conduction curves.

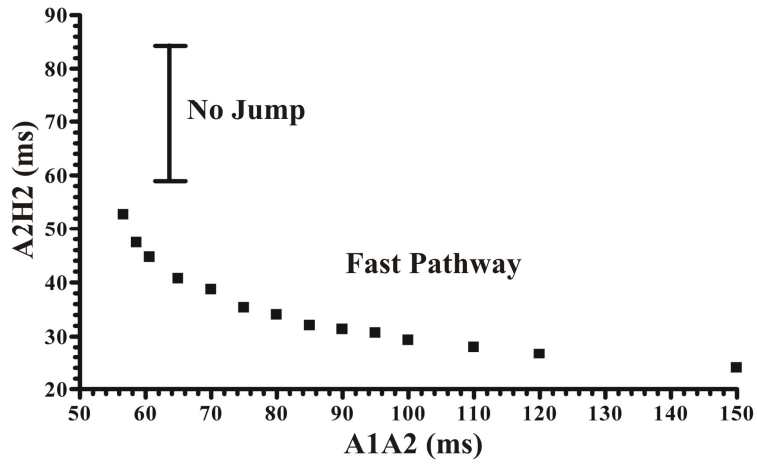
4.3.3 Junctional arrhythmia

Junctional arrhythmia (His-V-A activation pattern) lasting 1-60 seconds, was consistently induced following repetitive (10-40) trains of ventricular burst pacing (50 Hz, 400ms). The burst pacing protocol did not follow 1-1 with the pacing rate, but caused ventricular rate accelerations over 950 bpm. Junctional arrhythmia was induced in 74% of mice (14/19) producing a 32% increase in heart rate (325±15 vs 429±19 bpm, P<0.001). Spontaneous termination of the junctional arrhythmia was either sudden or occurred after the junctional rate arrhythmia slowed to a point that the arrhythmia was suppressed by a faster intrinsic SA nodal rate.

4.3.4 Diagnostic Pacing Studies

Diagnostic pacing studies were performed to determine the mechanism of the induced junctional arrhythmia and distinguish AVNRT from JT. A premature atrial stimulus delivered >30 ms before the next His activation, consistently advanced His activation

A



B

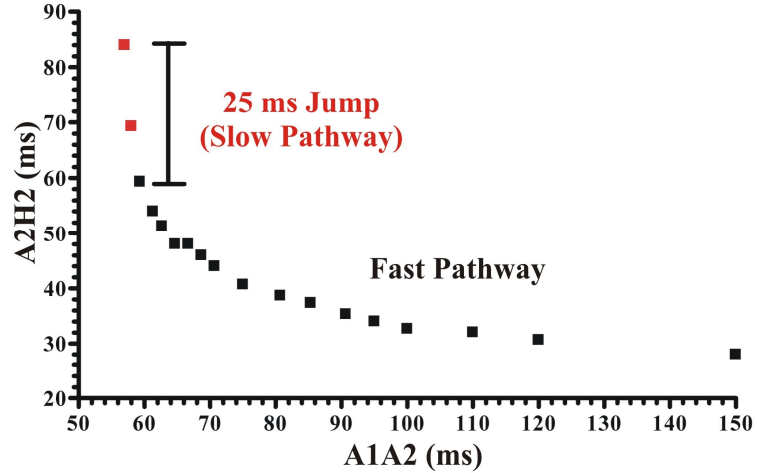


Figure 4.3. **A)** An antegrade AV nodal conduction curve in a mouse with apparent continuous (no Jump) AV nodal conduction. **B)** An antegrade AV nodal conduction curve in a mouse with discontinuous AV nodal conduction. An increase (jump) in A2H2 of >10 ms with a <4 ms decrease in A1A2 suggests conversion from the Fast to the Slow AV nodal pathway.

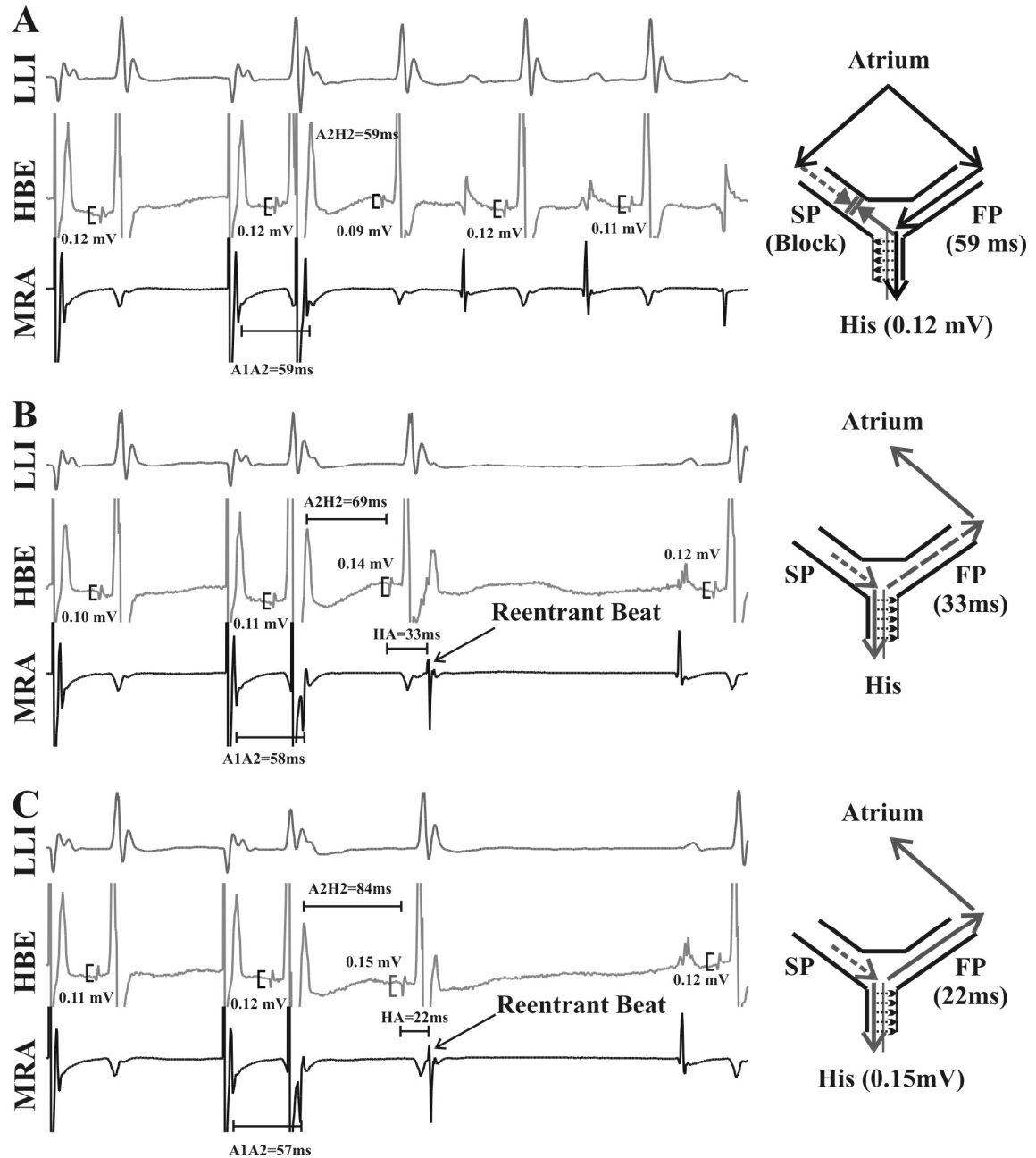


Figure 4.4. Single AV nodal reentrant beats were observed during recording of antegrade AV nodal conduction. **A)** An electrogram with normal fast pathway (FP) conduction to the His bundle during antegrade AV nodal conduction. **B)** After a 1 ms decrease in the A1A2 coupling interval, there was a 10 ms increase in A2H2 that initiated a reentrant atrial beat. **C)** With a further 1 ms decrease in A1A2, A2H2 increased 15 ms, and a reentrant atrial beat was recorded. Note, the HA interval (retrograde FP) during reentry in “C” is shorter (22ms) than in “B” (33ms), due to the prolonged SP conduction, allowing recovery of the FP. LLI, limb lead 1. HBE, His bundle electrogram. MRA, mid-right atrium. ** P<0.01.

(through the FP) without terminating the arrhythmia (0/14 were terminated, **Fig 4.5a**). Occasionally, premature FP activation transiently suppressed the junctional rhythm, but it resumed a few cycles later. Also, His-synchronous atrial activation did not advance the following ventricular cycle (0/14 were advanced). Both findings strongly indicate that the observed arrhythmia was JT and not AVNRT. Atrial effective refractory periods were commonly longer than the retrograde His to Atrium cycle length. Therefore, during His synchronous stimulation, retrograde activation of the atrium was blocked as the atrium was still refractory following the His synchronous stimulation. The mechanism of AVNRT involves the atrium as a critical component of the circuit, indicating this junctional arrhythmia is likely not AVNRT⁴⁹. In one mouse, retrograde Wenkebach block to the atrium that did not affect the V to V or His to His cycle length was observed, indicating that the atrium and retrograde pathway were not involved in the arrhythmia mechanism. These observations strongly suggest JT as the mechanism of the arrhythmia. Similarly, the induction using rapid ventricular pacing, and failure of AVNRT initiation in most animals using standard programmed electrical stimulation, also support JT as the arrhythmia mechanism.

4.3.5 Blood Pressure Measurements

Blood pressure measurements were obtained from the carotid artery cannula to determine a potential involvement of an autonomic baroreflex response in JT initiation. Ventricular rate during burst pacing produced transient 46 ± 2.6 % (n=4) reductions in the minimum end-diastolic blood pressure (**Fig 4.5b**). During JT, minimum end-diastolic blood pressure was also lower 22 ± 4 % (**Fig 4.5b**) than that during sinus rhythm, as the atria contracted against closed AV valves, decreasing the atrial component of ventricular filling. This was not a rate

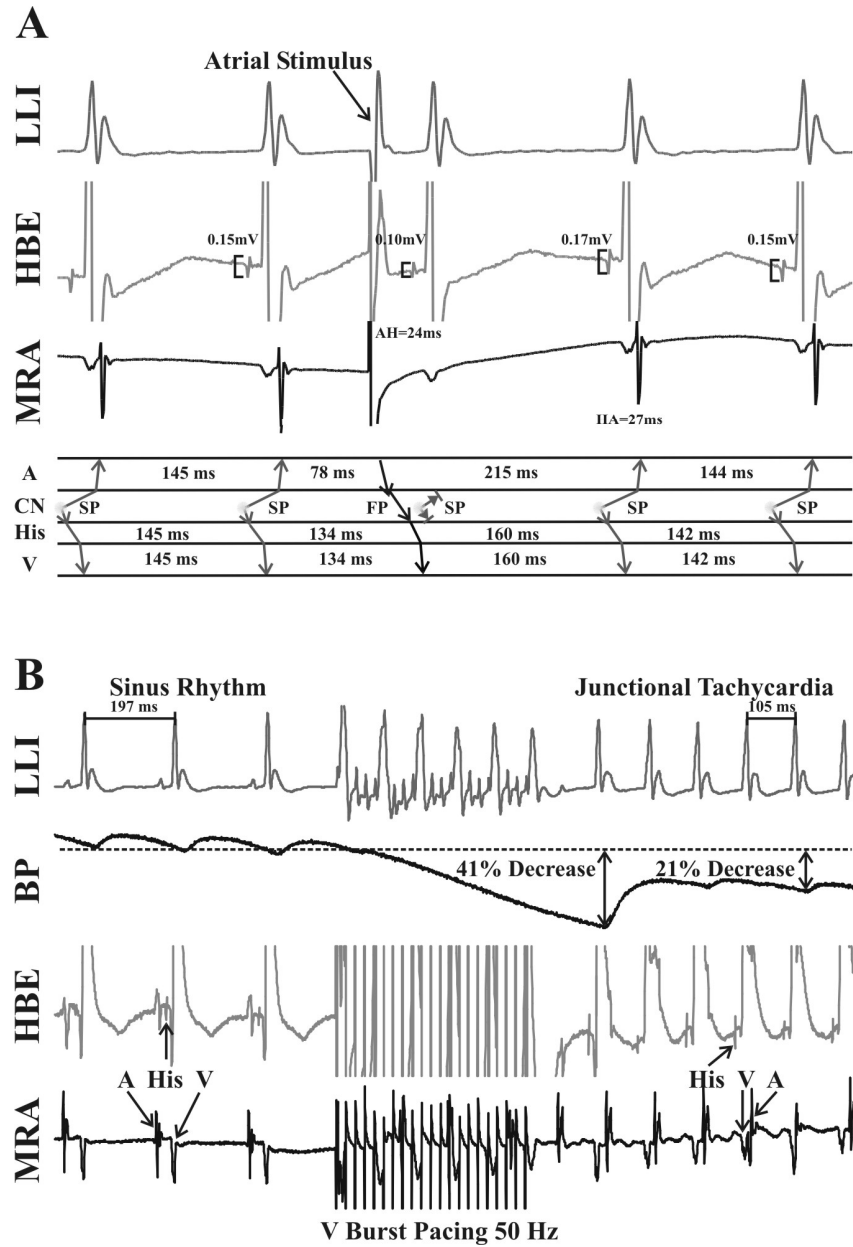


Figure 4.5. A) Top: Ventricular Burst Pacing induced Junctional Arrhythmia in a mouse. A single early atrial stimulus prematurely activated the fast pathway (FP). The junctional arrhythmia was not terminated by the atrial stimulus, demonstrating that the FP was not involved and confirming the arrhythmia was junctional tachycardia (JT). Bottom: A ladder diagram illustrating the hypothesized cardiac activation sequence during JT. **B)** Ventricular burst pacing (1 ms pulses at 50 Hz, 400 ms burst) induced junctional tachycardia (JT) in the mouse indicated by the His, then V, then A activation pattern. Diastolic blood pressure (BP), measured from the carotid artery, decreased 41% during burst pacing, suggesting that baroreflex sympathetic activation is involved in the arrhythmia. During JT, the atria and ventricles contract in synchrony associated with a 21 % reduced diastolic blood pressure. CN-compact node, ** P<0.05

Table 4.1: Basic electrophysiological values (in ms) in 6 month old male C57BL/6 mice recorded in the absence and presence of: Carbachol; Atropine, and Propranolol.

	Vehicle		Carbachol		Atropine		Propranolol	
AHERP ₁₅₀	28±1	19	26±2	10			25±1	7
AMERP ₁₅₀	25±1	19	22±1	10			18±1	7
AHERP ₁₀₀	30±2	19	27±2	10	53±2	10	25±1	7
AMERP ₁₀₀	22±1	19	23±1	10	42±1	10	18±1	7
WCL	91±2	19	98±2	10	89±1	10	99±2	7
AVNERP ₁₅₀	60±4	19	62±3	10			70±2	7
AVNERP ₁₀₀	66±3	19	75±4	10	61±2	10	80±2	7
AH ₁₅₀	26±2	19	27±2	10	28±1	10	38±2	7
AH ₁₀₀	33±2	19	35±2	10			44±2	7
VERP ₁₅₀	43±2	19	56±2	10	47±2	10	45±2	7
VERP ₁₀₀	47±2	19	60±1	10			48±2	7

dependent effect during JT as blood pressure increased when the atrium was paced at the same rate.

4.3.6 AV Nodal Conduction Times

AV nodal conduction times (AH interval) were analyzed before and after 10 rounds of burst pacing for evidence of a positive dromotropic response which would be indicative of a baroreflex response (withdrawal of parasympathetic and enhanced sympathetic drive). AV nodal conduction times were significantly decreased following 10 rounds of ventricular burst pacing (pre-pacing AH=31±1ms vs post-pacing AH=28±1ms, P<0.001, n=14) while there were no changes in sinus cycle length (185±12vs 188±10ms, P=0.39, n=14). However, following additional cycles of burst pacing, increased sinus rate was also observed.

4.3.7 Subthreshold Stimulation

Subthreshold stimulation of the slow pathway region has been shown to activate local autonomic nerves and produce transient accelerations in junctional rate^{21, 22}. Subthreshold stimulation of the right ventricle and His bundle region did not induce JT or alter nodal conduction times. Also, rapid atrial pacing (50Hz, 400 ms, 10-40 bursts) failed to induce JT. This argues against the possibility of JT induction due to time/voltage dependent effects on AV nodal autonomic nerves and sarcolemmal ion channel function.

4.3.8 Vagal Nerve Stimulation

Vagal nerve stimulation (20 Hz, 5 V, 10 ms pulse) was done simultaneously with ventricular burst pacing to further test the involvement of a baroreflex response in JT induction. Vagal nerve stimulation caused reductions in sinus rate and suppressed JT induction in 5 of 5 mice. Interestingly, JT initiated immediately following cessation of vagal nerve stimulation in all 5 mice.

4.3.9 Pharmacological Tests Of Baroreflex Involvement

Pharmacological tests using Carbachol (a parasympathetic agonist, 50ng/g i.p), atropine (a parasympathetic antagonist, 1mg/kg i.p) and propranolol (a sympathetic β -receptor inverse agonist, 1mg/kg i.v.) and hexamethonium (a nicotinic acetylcholine receptor (ganglionic) blocker, 30mg/kg, i.v.³) further examined the role of a baroreflex response in the induction of JT. While 8/10 mice were susceptible to JT at baseline, Carbachol reduced JT susceptibility (2/10) and atropine following carbachol restored, and slightly enhanced JT susceptibility (9/10). Propranolol completely abolished susceptibility to JT induction (0/7). It was initially hypothesized that hexamethonium would suppress JT susceptibility due to its sympathetic blockade; however i.v. administration mildly enhanced JT susceptibility (pre:5/8 vs post:7/8) and prolonged JT duration (6.1 ± 2.6 vs 14.8 ± 2.4 , $P<0.05$), as well as promoting JT in 2 animals that were not previously susceptible. This suggests that parasympathetic withdrawal may have the more prominent role in JT initiation.

4.3.10 His Bundle Electrograms Amplitude Alterations During JT vs Sinus Rhythm

His bundle electrograms were analyzed during JT and sinus rhythm for evidence of His amplitude alterations which would be indicative of functional longitudinal dissociation of the bundle of His⁵¹. Optical mapping studies of the AV junction have determined that the dominant site of junctional pacemaking activity is in the posterior nodal extension (the slow pathway region). Thus, His amplitude alterations might be observable when comparing JT (SP activation of the His) to sinus rhythm (FP activation of the His). His bundle electrogram amplitudes during JT were significantly greater compared to those of sinus rhythm (JT: 0.13 ± 0.01 mV vs sinus rhythm: 0.09 ± 0.01 mV, $n=14$, $P<0.05$). This pattern of activation was also observed during diagnostic pacing studies, where a premature atrial stimulus would activate the FP and His amplitude decreased to that observed during sinus rhythm activation (**Fig.**

4.5a). This result is consistent with His amplitude alteration observed during discontinuous antegrade AV nodal conduction curves and suggests that JT originated from the SP region.

4.3.11 Activation Patterns During JT

Activation patterns during JT were observed to shift from an “A-His-V” pattern with a short (5-10ms) AH interval and an inverted P wave morphology (2 of 14), to that of the more commonly observed “His-V-A” activation pattern (**Fig. 4.6**). This suggests that the dominant site of the focal arrhythmia could shift within the SP region, similar to how the dominant site of SA nodal pacemaking can shift along the crista terminalis in response to β -adrenergic stimulation¹². The A-His-V pattern of JT had a longer cycle length than the His-V-A pattern. This suggests that the dominant junctional pacemaker site of the His-V-A pattern was located closer to the compact AV node than the retrograde atrial exit site of the SP, while during the A-His-V pattern the site shifted closer to the retrograde exit site. This seems to be a likely interpretation however there are other explanations of this pattern.

4.3.12 Pharmacological Tests Of Pacemaking

To examine the role of the I_f channel in the induced JT, low dose Ivabradine Hydrochloride (1 mg/kg, i.v.⁴¹), a selective I_f channel blocker was used. Ivabradine produced a 12 ± 2 % decrease in heart rate and suppressed JT induction in 7 of 9 mice examined. Interestingly, in 2 mice, JT was not immediately suppressed, and activation patterns were observed to shift from the His-V-A to the A-His-V (short AH) pattern of JT. To examine the potential role of the Ca^{2+} clock in JT, Caffeine (10mg/kg, i.v.) and Ruthenium Red (1 mg/kg, i.v.) were used. Caffeine, known to stimulate the release of Ca^{2+} from intracellular stores, enhanced the rate of the induced JT in 5 of 5 mice. Caffeine also blocks A1 adenosine receptors, inhibits adenylyl cyclase activity, and A3 adenosine receptors which stimulate adenylyl cyclase activity. To differentiate the role of these two apparently antagonistic

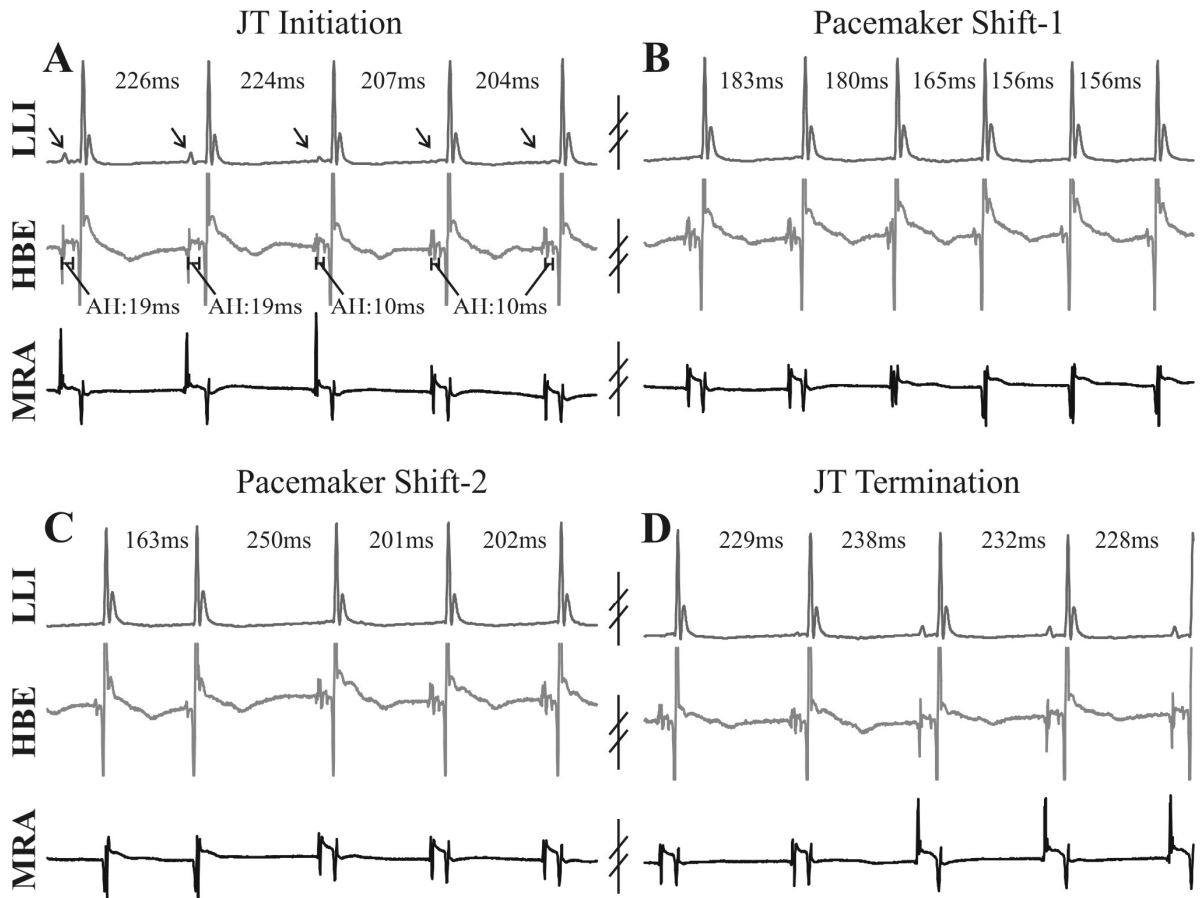


Figure 4.6. Evidence for a shifting junctional pacemaker locus along the slow pathway region in the mouse with burst pacing induced JT. **A)** The conversion from normal sinus activation of the His (AH = 19 ms) to a junctional arrhythmia with a short AH interval (AH = 10ms). **B)** The pacemaker locus shifts along the SP region to a more centralized location, converting the activation pattern from an A-His-V to a His-V-A pattern with an abbreviated cycle length (153 ms vs 204 ms). **C)** Reversion back to an A-His-V activation pattern of JT before **D)** the arrhythmia terminates and sinus rhythm resumes. Note: the isoelectric P-wave and altered forces in the mid-right atrial (MRA) electrogram in “A” and “D” during junctional rhythm indicating a low to high atrial activation.

actions, DPCPX (100µg/kg, i.v.) a selective A1 adenosine receptor antagonist was used. DPCPX had no effect on the rate or frequency of JT induction (3 of 3 mice). Ruthenium red binds ryanodine receptors and potently inhibits intracellular Ca²⁺ release. Ruthenium red (1mg/kg, i.v.) prevented JT induction in 5 of 5 mice. The coupled clock pacemaker system proposed by Lakatta et al.²⁴ suggests important interactions between sarcolemmal and intracellular events. Adenylyl cyclase produces cAMP which directly activates I_f channels but also activates PKA, which, through phosphorylation, affects intracellular Ca²⁺ handling. Regulation of cAMP compartmentalization by phosphodiesterases may also have a role in pacemaking²⁴ and JT; however, both IBMX, a non-selective PDE inhibitor, and Milrinone, a selective PDE3 inhibitor, suppressed JT (3 of 3 mice). This may have resulted from non-selective actions, which enhanced the sinus rate, suppressing the slower junctional rate. These compounds may also enhance contractility which could suppress JT by blunting the baroreflex response. Similarly, Forskolin (1mg/kg, i.v.), a direct activator of AC produced an enhancement of sinus rate and reduced JT susceptibility (4 of 4 mice). However, in 5, 12 month old C57BL/6 mice, Forskolin followed by caffeine caused spontaneous JT (not requiring rapid ventricular pacing) lasting >2 minutes. In all cases, the spontaneous JT was terminated by Ivabradine (1 mg/kg, i.v.).

4.3.13 RGS2 Deficient Mice

In biochemical assays, RGS2 has been found to interact with the C1 catalytic loop of adenylyl cyclase and inhibit its activity. RGS2 also inhibits forskolin-induced cAMP accumulation. The presence or absence of RGS2 in the AV node has not been determined, and is beyond this investigation. However, in the regulator of G-protein signalling 2 protein deficient (RGS2^{-/-}) mouse⁴¹, there was no difference in susceptibility to JT compared to age

matched littermates (unpublished). This suggests that RGS2 is either not present in the AV node or is not important in regulating JT susceptibility.

4.4 DISCUSSION

The objectives of this chapter were two-fold: first I examined normal AV conduction properties in the mouse and determine if the mouse AV junction had similar electrophysiological properties as the human, and second, I determined if junctional tachycardia (JT) could be induced and studied in the mouse. We found evidence of discontinuous antegrade conduction in 41%, reentrant nodal echo beats in 17%, and multiple reentrant events in 5% of the mice examined. These results were consistent to previous findings for the mouse²⁷. His bundle electrogram amplitude alterations during SP vs FP activation of the His suggests the presence of functional longitudinal dissociation of the mouse His bundle. This is a novel observation in the mouse. These electrophysiological findings are consistent with the histological observations suggesting the mouse AV conduction axis is highly similar to that of the human¹. As such, the mouse appears to be a suitable model to study AV nodal conduction properties and arrhythmia. Thus, we studied the mechanisms of JT in the mouse. Based on the literature, we proposed that JT is caused, in part, by inappropriate (enhanced) AV nodal pacemaker activity initiated by abnormal autonomic (baroreflex) activity.

I found that transient repetitive decreases in blood pressure induced JT in 74% of mice examined. The induced arrhythmia was prevented by parasympathetic activation (through vagal nerve stimulation or carbachol) and sympathetic blockade (propranolol). JT can often be difficult to distinguish from AVNRT during electrophysiological studies. However, it is possible to distinguish JT from AVNRT based on the response to single premature atrial

stimuli (SAS) delivered during different phases of the tachycardia cycle³¹. A SAS just before the His that advances the His without terminating the tachycardia indicates that the retrograde fast pathway is not essential for the circuit and confirms a diagnosis of JT. But any perturbation in His refractoriness following a His synchronous SAS indicates that anterograde slow pathway conduction is involved and confirms a diagnosis of AVNRT. This protocol has been used to distinguish JT from AVNRT with 100% specificity in adult patients³¹, and was successfully used to confirm JT in this study (**Fig 4.5a**).

Optical mapping observed junctional beats following administration of 1 $\mu\text{mol/L}$ isoproterenol in 9 of 347 (2.6%) of embryonic mouse hearts⁴⁵. However, to my knowledge, induction of JT has not been reported in the adult mouse. To further study the role of the autonomics I used both hexamethonium, a ganglionic blocker, and electrical vagal nerve stimulation. JT duration was mildly enhanced by hexamethonium and was blocked by, and then initiated immediately following removal of vagal nerve stimulation. Thus, I speculate that an imbalance in autonomic input to the AV node contributes to JT susceptibility. This hypothesis is supported by the literature where differential intracardiac sympathetic and parasympathetic innervation to the SA and AV nodes was observed in dogs^{15, 16}. AV junctional rhythm was observed by stimulating discrete autonomic nerves in the canine heart preparations¹⁴. Treatment with atropine and propranolol during nerve stimulation suggested that AV junctional rhythm was produced by sympathetic-parasympathetic imbalance. High level atrioventricular stimulation induced a junctional rhythm in the dog¹⁶. This is reminiscent of junctional rhythm observed clinically during SP ablations for AVNRT. Interestingly, it has also been observed that disruption of antegrade SP conduction is not necessary for termination of AVNRT¹⁷. In humans, stimulation of the fat pad which contains the parasympathetic ganglia supply of the AV node can alter right atrial effective refractory

periods up to 2 cm from the fat pad³². In another study, SP ablation decreased vulnerability to pacing induced AF, indicating SP ablation may modify parasympathetic inputs to the AV node and atrium³³. Frequently, there is also an improvement in FP conduction following SP ablation suggesting modification of the autonomic inputs^{5,30}. It has been hypothesized that that focal beats originating from the SP region may initiate AVNRT in patients²¹. Thus modifying the nervous inputs to the AVN may be important for successful AVNRT ablation, initially stimulating a junctional rhythm by a transiently suppressing parasympathetic inputs and then suppressing junctional beats which could initiate AVNRT by a complete ablation of the autonomic influence on pacemaker activity.

There are parallels in nodal function between species. Following removal of the SA node in the rabbit, AV junctional rhythm was initiated in the posterior nodal extension (the slow pathway region), which then spread to the compact node²². Based on the pattern of His amplitude alterations during JT compared to sinus rhythm and then comparing that of defined SP conduction compared to FP conduction, we suggest that JT in the mouse also originates from the SP region. As shown by optical mapping, the dominant site of the SA nodal pacemaker can shift along the crista terminalis in response to β -adrenergic stimulation¹², and in response to subthreshold pacing; the AVN pacemaker also shifted in 5% of cases²². I observed a similar pattern of shifting the AV nodal pacemaker along the SP region (**Fig. 4.6**) in JT during the conversion of an A-His-V (short AH:10 ms) to a His-V-A activation pattern in 2 of 19 mice examined (10%). Conversion to this A-His-V pattern occurred in 2 additional mice following the administration of Ivabradine. While these observations lack the sophistication of optical mapping, their consistency supports the hypothesis that JT is caused by enhanced junctional pacemaker activity initiated by autonomic influences.

The rapid rate of JT can be problematic and difficult to treat pharmacologically. In neonates following cardiac surgery, JT is associated with a mortality risk of 5.6 to 14%^{4, 11, 19, 34}. Pre-operative treatment with propranolol reduced the incidence of post-operative JET from 38 % without drug to 21 % in patients with propranolol²⁸. However, after surgery, patients may have reduced cardiac output requiring positive inotropic support to maintain blood pressure, often provided with dopamine, epinephrine or dobutamine⁷. Thus, β -adrenergic receptor blockade may be contra-indicated due to its negative inotropic effects. In addition, patients treated with propranolol to reduce the incidence of JT required more dopamine and dobutamine for inotropic support than non-blocked patients²⁸. Amiodarone has been used successfully to treat JT; however, it was found to have an 87% risk of adverse events in children including mortality, hypotension, and AV block³⁸. Thus, a novel non-inotropic treatment is required for the treatment/prevention of post-operative JT based on understanding its underlying mechanisms.

I propose that JT was caused by inappropriate junction pacemaker activity. Two central mechanisms of pacemaking in the heart have been proposed: diastolic depolarization's produced by the hyperpolarization activated cyclic nucleotide gated (HCN4) pacemaker funny channel (I_f); and rhythmic oscillations in local Ca^{2+} release from the ryanodine receptor which activates the electrogenic $Na^+ - Ca^{2+}$ exchanger to accelerate the upstroke of the late diastolic depolarization (Ca^{2+} clock). Both these proposed mechanisms have been observed in isolated nodal preparations. In the mouse, the intrinsic cycle length of the SA and AV node are 179 ± 2.7 ms and 258 ± 18.7 ms. Blocking I_f with $1 \mu\text{mol/L}$ ZD7288 increased the cycle length of both the SA (258 ± 18.7) and AV ($447 \pm 92.4 \text{ms}^{26}$). This indicates that I_f channel is important component of AV junctional pacemaking. The rate of the JT observed

(429±19 BPM) was 1.8 times that of the intrinsic rate of the AV nodal pacemaker observed in the previously discussed study²⁶.

The role of the Ca²⁺ clock has been investigated in the isolated rabbit junctional preparations³⁶. The rate of spontaneous activity was decreased by ryanodine and increased by isoprenaline. These changes were accompanied by respective changes in the slope of the preceding Ca²⁺ ramp. To determine the involvement of these mechanisms in the observed JT in our studies, I used Ivabradine hydrochloride (a selective I_f channel blocker), caffeine (to stimulate Ca²⁺ release), and ruthenium red (a potent inhibitor of intracellular Ca²⁺ release). Ryanodine, which depletes sarcoplasmic calcium stores by holding the Ryanodine receptor in a sub-conductance state, was not used due to the biphasic nature of the response, which would make the distinction between the effects difficult in whole animal studies. Both Ivabradine (8 of 9) and Ruthenium Red (5 of 5) prevented JT, while caffeine mildly potentiated the rate of the arrhythmia. To further investigate mechanisms I used Forskolin (an adenylyl cyclase activator), caffeine, DPCPX (an A1 adenosine receptor blocker), IBMX (a non-selective PDE inhibitor), and Milrinone (a selective PDE3 inhibitor)³⁹. The results of these studies are difficult to interpret as a number of competing and non-specific factors occur during in-vivo investigations. Despite this limitation, or perhaps as a result, I found in a subset of mice that Forskolin and caffeine together could induce a prolonged (>2 min) spontaneous (occurring without V burst pacing) junctional tachycardia. While the nature of this spontaneous JT is unknown, I speculate the involvement of an inappropriate phosphorylation cascade of various sarcolemmal ion channels and intracellular calcium handling proteins (RyR, Phospholamban) by PKA and CAMKII involved in pacemaking. This concept is an important component of the coupled-clock pacemaker system proposed by

Lakatta. In all cases (5 of 5) the spontaneous JT could be terminated by intravenous Ivabradine hydrochloride.

Ivabradine hydrochloride, blocks the intracellular side of the I_f channel in a use dependent manner¹⁰, a beneficial property for an anti-arrhythmic drug. Ivabradine has recently received FDA approval for the treatment of stable angina due to its pure heart rate reducing effects without compromising cardiac output (no negative inotropic effect). The fact that JT in the mouse could be prevented by Ivabradine suggests its potential therapeutic use in patients. This presumption is strengthened by clinical reports of successful termination of inappropriate sinus tachycardia with Ivabradine^{39,48}; although the mechanisms of junctional and sinus tachycardia may differ. Nevertheless, Ivabradine may be a beneficial therapeutic agent even if it merely slows the rate of JT, as the arrhythmia in post-surgical patients typically last no longer than 2 days and rate reducing strategies have previously been beneficial⁹.

4.5 REFERENCES

1. Aanhaanen WT, Mommersteeg MT, Norden J, Wakker V, de Gier-de VC, Anderson RH, Kispert A, Moorman AF, Christoffels VM. Developmental Origin, Growth, and Three-Dimensional Architecture of the Atrioventricular Conduction Axis of the Mouse Heart. *Circ Res.* 29-7-2010.
2. Agha AS, Castellanos AM, Sung RJ, Castillo CA, Myerburg RJ, Castellanos A. Bipolar catheter electrograms for study of retrograde atrial activation pattern in patients without pre-excitation syndromes. *Br Heart J* 38:641-5. 1976.
3. Aizawa-Abe M, Ogawa Y, Masuzaki H, Ebihara K, Satoh N, Iwai H, Matsuoka N, Hayashi T, Hosoda K, Inoue G, Yoshimasa Y, Nakao K. Pathophysiological role of leptin in obesity-related hypertension. *J Clin Invest* 105:1243-52. 2000.
4. Andreasen JB, Johnsen SP, Ravn HB. Junctional ectopic tachycardia after surgery for congenital heart disease in children. *Intensive Care Med* 34:895-902. 2008.

5. Basta MN, Krahn AD, Klein GJ, Rosenbaum M, Le FC, Yee R. Safety of slow pathway ablation in patients with atrioventricular node reentrant tachycardia and a long fast pathway effective refractory period. *Am J Cardiol* 80:155-9. 15-7-1997.
6. Brioschi C, Micheloni S, Tellez JO, Pisoni G, Longhi R, Moroni P, Billeter R, Barbuti A, Dobrzynski H, Boyett MR, DiFrancesco D, Baruscotti M. Distribution of the pacemaker HCN4 channel mRNA and protein in the rabbit sinoatrial node. *J Mol Cell Cardiol* 47:221-7. 2009.
7. Bromberg BI. Atrial Ectopic Tachycardia / Atrial Autonomic Tachycardia. In: Dick M, II, ed. *Clinical Cardiac Electrophysiology in the Young*. New York, New York: Springer Science & Business Media Inc.; 2006. p. 119-34.
8. Christoffels VM, Smits GJ, Kispert A, Moorman AF. Development of the pacemaker tissues of the heart. *Circ Res* 106:240-54. 5-2-2010.
9. Chrysostomou C, Beerman L, Shiderly D, Berry D, Morell VO, Munoz R. Dexmedetomidine: a novel drug for the treatment of atrial and junctional tachyarrhythmias during the perioperative period for congenital cardiac surgery: a preliminary study. *Anesth Analg* 107:1514-22. 2008.
10. DiFrancesco D. The role of the funny current in pacemaker activity. *Circ Res* 106:434-46. 19-2-2010.
11. Dodge-Khatami A, Miller OI, Anderson RH, Gil-Jaurena JM, Goldman AP, de Leval MR. Impact of junctional ectopic tachycardia on postoperative morbidity following repair of congenital heart defects. *Eur J Cardiothorac Surg* 21:255-9. 2002.
12. Efimov IR, Fedorov VV, Joung B, Lin SF. Mapping cardiac pacemaker circuits: methodological puzzles of the sinoatrial node optical mapping. *Circ Res* 106:255-71. 5-2-2010.
13. Efimov IR, Nikolski VP, Rothenberg F, Greener ID, Li J, Dobrzynski H, Boyett M. Structure-function relationship in the AV junction. *Anat Rec A Discov Mol Cell Evol Biol* 280:952-65. 2004.
14. Furukawa Y, Martin P, Levy MN. AV junctional rhythm induced by sympathetic-parasympathetic imbalance in dog hearts. *Am J Physiol (Heart Circ Physiol)* 259 (28):H839-H842. 1990.
15. Furukawa Y, Narita M, Takei M, Kobayashi O, Haniuda M, Chiba S. Differential intracardiac sympathetic and parasympathetic innervation to the SA and AV nodes in anesthetized dog hearts. *Jpn J Pharmacol* 55:381-90. 1991.
16. Furukawa Y, Wallick DW, Martin PJ, Levy MN. Chronotropic and dromotropic responses to stimulation of intracardiac sympathetic nerves to sinoatrial or atrioventricular nodal region in anesthetized dogs. *Circ Res* 66:1391-9. 1990.

17. Gianfranchi L, Brignole M, Delise P, Menozzi C, Paparella N, Themistoclakis S, Bonso A, Lolli G, Alboni P. Modification of antegrade slow pathway is not crucial for successful catheter ablation of common atrioventricular nodal reentrant tachycardia. *Pacing Clin Electrophysiol* 22:263-7. 1999.
18. Hein L, Altman JD, Kobilka BK. Two functionally distinct alpha2-adrenergic receptors regulate sympathetic neurotransmission. *Nature* 402:181-4. 11-11-1999.
19. Hoffman TM, Bush DM, Wernovsky G, Cohen MI, Wieand TS, Gaynor JW, Spray TL, Rhodes LA. Postoperative junctional ectopic tachycardia in children: incidence, risk factors, and treatment. *Ann Thorac Surg* 74:1607-11. 2002.
20. Hucker WJ, Fedorov VV, Foyil KV, Moazami N, Efimov IR. Images in cardiovascular medicine. Optical mapping of the human atrioventricular junction. *Circulation* 117:1474-7. 18-3-2008.
21. Hucker WJ, Nikolski VP, Efimov IR. Optical mapping of the atrioventricular junction. *J Electrocardiol* 38:121-5. 2005.
22. Hucker WJ, Nikolski VP, Efimov IR. Autonomic control and innervation of the atrioventricular junctional pacemaker. *Heart Rhythm* 4:1326-35. 2007.
23. Kurian T, Ambrosi C, Hucker W, Fedorov VV, Efimov IR. Anatomy and electrophysiology of the human AV node. *Pacing Clin Electrophysiol* 33:754-62. 1-6-2010.
24. Lakatta EG, Maltsev VA, Vinogradova TM. A coupled SYSTEM of intracellular Ca²⁺-clocks and surface membrane voltage clocks controls the timekeeping mechanism of the heart's pacemaker. *Circ Res* 106:659-73. 5-3-2010.
25. Li HG, Jones DL, Yee R, Klein GJ. Electrophysiologic substrate associated with pacing-induced heart failure in dogs: potential value of programmed stimulation in predicting sudden death. *J Am Coll Cardiol* 19:444-9. 1992.
26. Liu J, Noble PJ, Xiao G, Abdelrahman M, Dobrzynski H, Boyett MR, Lei M, Noble D. Role of pacemaking current in cardiac nodes: insights from a comparative study of sinoatrial node and atrioventricular node. *Prog Biophys Mol Biol* 96:294-304. 2008.
27. Maguire CT, Bevilacqua LM, Wakimoto H, Gehrman J, Berul CI. Maturation of atrioventricular nodal physiology in the mouse. *J Cardiovasc Electrophysiol* 11:557-64. 2000.
28. Mahmoud AB, Tantawy AE, Kouatli AA, Baslaim GM. Propranolol: a new indication for an old drug in preventing postoperative junctional ectopic tachycardia after surgical repair of tetralogy of Fallot. *Interact Cardiovasc Thorac Surg* 7:184-7. 2008.

29. Matthes J, Yildirim L, Wietzorrek G, Reimer D, Striessnig J, Herzig S. Disturbed atrioventricular conduction and normal contractile function in isolated hearts from Cav1.3-knockout mice. *Naunyn Schmiedebergs Arch Pharmacol* 369:554-62. 2004.
30. Murgatroyd FD, Klein GJ. AVNRT: "what goes around, comes around"--but where? *Pacing Clin Electrophysiol* 22:259-62. 1999.
31. Padanilam BJ, Manfredi JA, Steinberg LA, Olson JA, Fogel RI, Prystowsky EN. Differentiating junctional tachycardia and atrioventricular node re-entry tachycardia based on response to atrial extrastimulus pacing. *J Am Coll Cardiol* 52:1711-7. 18-11-2008.
32. Quan KJ, Lee JH, Van Hare GF, Biblo LA, Mackall JA, Carlson MD. Identification and characterization of atrioventricular parasympathetic innervation in humans. *J Cardiovasc Electrophysiol* 13:735-9. 2002.
33. Razavi M, Cheng J, Rasekh A, Yang D, Delapasse S, Ai T, Meade T, Donsky A, Goodman MJ, Massumi A. Slow pathway ablation decreases vulnerability to pacing-induced atrial fibrillation: Possible role of vagal denervation. *Pacing Clin Electrophysiol* 29:1234-9. 2006.
34. Rekawek J, Kansy A, Miszczak-Knecht M, Manowska M, Bieganowska K, Brzezinska-Paszke M, Szymaniak E, Turska-Kmiec A, Maruszewski P, Burczynski P, Kawalec W. Risk factors for cardiac arrhythmias in children with congenital heart disease after surgical intervention in the early postoperative period. *J Thorac Cardiovasc Surg* 133:900-4. 2007.
35. Reynolds SM, Docherty R, Robbins J, Spina D, Page CP. Adenosine induces a cholinergic tracheal reflex contraction in guinea pigs in vivo via an adenosine A1 receptor-dependent mechanism. *J Appl Physiol* 105:187-96. 2008.
36. Ridley JM, Cheng H, Harrison OJ, Jones SK, Smith GL, Hancox JC, Orchard CH. Spontaneous frequency of rabbit atrioventricular node myocytes depends on SR function. *Cell Ca* 44:580-91. 2008.
37. Saba S, London B, Ganz L. Autonomic blockade unmasks maturational differences in rate-dependent atrioventricular nodal conduction and facilitation in the mouse. *J Cardiovasc Electrophysiol* 14:191-5. 2003.
38. Saul JP, Scott WA, Brown S, Marantz P, Acevedo V, Etheridge SP, Perry JC, Triedman JK, Burriss SW, Cargo P, Graepel J, Koskelo EK, Wang R. Intravenous amiodarone for incessant tachyarrhythmias in children: a randomized, double-blind, antiarrhythmic drug trial. *Circulation* 112:3470-7. 29-11-2005.
39. Schulze V, Steiner S, Hennersdorf M, Strauer BE. Ivabradine as an alternative therapeutic trial in the therapy of inappropriate sinus tachycardia: a case report. *Cardiol* 110:206-8. 2008.

40. Sebag C, Motte G, Pariente P, Davy JM. [Fragmenting of the His potential after atrial stimulation]. *Arch Mal Coeur Vaiss* 74:705-17. 1981.
41. Stieber J, Wieland K, Stockl G, Ludwig A, Hofmann F. Bradycardic and proarrhythmic properties of sinus node inhibitors. *Mol Pharmacol* 69:1328-37. 2006.
42. Tuomi JM, Chidiac P, Jones DL. Evidence for enhanced M3 muscarinic receptor function and sensitivity to atrial arrhythmia in the RGS2 deficient mouse. *Am J Physiol Heart Circ Physiol* 298:H554-H561(Epub 2009 Dec 4). 1-2-2010.
43. Tuomi JM, Chidiac P, Jones DL. Evidence for enhanced M3 muscarinic receptor function and sensitivity to atrial arrhythmia in the RGS2-deficient mouse. *Am J Physiol Heart Circ Physiol* 298:H554-H561. 2010.
44. Tuomi JM, Tyml K, Jones DL. Atrial tachycardia/fibrillation in the connexin 43 G60S mutant (Oculodentodigital dysplasia) mouse. *Am J Physiol Heart Circ Physiol* 300:H1402-H1411. 2011.
45. Valderrabano M, Chen F, Dave AS, Lamp ST, Klitzner TS, Weiss JN. Atrioventricular ring reentry in embryonic mouse hearts. *Circulation* 114:543-9. 8-8-2006.
46. VanderBrink BA, Link MS, Aronovitz MJ, Saba S, Sloan SB, Homoud MK, Estes III NA, Wang PJ. Assessment of atrioventricular nodal physiology in the mouse. *J Interv Card Electrophysiol* 3:207-12. 1999.
47. Wen ZC, Chen SA, Tai CT, Chiang CE, Chiou CW, Chang MS. Electrophysiological mechanisms and determinants of vagal maneuvers for termination of paroxysmal supraventricular tachycardia. *Circulation* 98:2716-23. 15-12-1998.
48. Winum PF, Cayla G, Rubini M, Beck L, Messner-Pellenc P. A case of cardiomyopathy induced by inappropriate sinus tachycardia and cured by ivabradine. *Pacing Clin Electrophysiol* 32:942-4. 2009.
49. Wu J, Zipes DP. Mechanisms underlying atrioventricular nodal conduction and the reentrant circuit of atrioventricular nodal reentrant tachycardia using optical mapping. *J Cardiovasc Electrophysiol* 13:831-4. 2002.
50. Yangni NO, Brembilla-Perrot B. Clinical characteristics and management of paroxysmal junctional tachycardia in the elderly. *Arch Cardiovasc Dis* 101:143-8. 2008.
51. Zhang Y, Bharati S, Mowrey KA, Zhuang S, Tchou PJ, Mazgalev TN. His electrogram alternans reveal dual-wavefront inputs into and longitudinal dissociation within the bundle of His. *Circulation* 104:832-8. 14-8-2001.
52. 2009Zipes DP, Jalife J. Cardiac electrophysiology: from cell to bedside, 5th ed. 2009.

CHAPTER 5: DISCUSSION

This thesis set out to test the hypotheses and achieve objectives listed below. These goals were achieved as outlined in the following summary section of the major finding of this thesis.

Hypotheses

1. There is an interface of neuro-myogenic influences on arrhythmia mechanism. Therefore there is a role for the autonomics in most atrial arrhythmias.
2. RGS2^{-/-} mice have enhanced M3 muscarinic receptor signalling and an increased susceptibility to electrically induced atrial tachycardia/fibrillation.
3. Cx40 deficient mice will be protected from, but the Cx43^{G60S/+} mutant will have severe AT/F.
4. Junctional tachycardia is caused inappropriate activation of the AV nodal pacemaker initiated by abnormal autonomics.

Objectives

1. To determine what atrial arrhythmias are inducible in the mouse and how to systematically elicit and study those arrhythmias.
2. Determine the mechanisms of the induced atrial arrhythmias in the mouse to provide the basis for future investigations of potential therapeutic options for patients.
3. Develop the proposed "Threshold Model" of arrhythmogenesis and use it to analyze results and make relative comparisons of observations obtained from the different experiments performed in this thesis.

5.1 SUMMARY AND MAJOR FINDINGS

There were multiple objectives in this thesis. I sought to determine how to systematically elicit atrial arrhythmia in the mouse to study various molecular factors involved in arrhythmogenesis in the controlled context of "induced pre-arrhythmia substrate remodelling". As outlined in **Chapter 1**, a central goal of this discussion section is to develop the proposed "Threshold Model" of arrhythmogenesis and use it to put the results into perspective and make relative comparisons of observations from the different experiments in this thesis. Briefly, the Threshold Model proposes that a myocardial substrate that is susceptible to arrhythmia initiation by an appropriate trigger would be said to be above the threshold. If the atrial substrate is well below threshold a single arrhythmogenic perturbation would not initiate an arrhythmia. If the atrial substrate is well above the threshold, then an antiarrhythmic treatment might be ineffective in terminating the arrhythmia. This concept will be developed throughout this discussion and summary of the major findings of this thesis. In this discussion, I have summarized the importance of the various methodological considerations revealed during my investigations. I have also examined the central hypothesis of this thesis "that there is an interface of neuro-myogenic influences on arrhythmia mechanisms", and as such there is a role for the autonomics in most atrial arrhythmias. Finally, I present the Threshold Model as a useful tool to make predictions of clinical outcomes.

The first objective of this thesis was to determine how to systematically and reproducibly elicit and study atrial arrhythmia in the mouse. I found that atrial tachycardia/fibrillation (AT/F) as well as AV nodal reentry and junctional tachycardia (JT) are inducible in the mouse. Both AF and JT pose significant clinical challenges as there are many patients who do not respond to current clinical management strategies^{14,22}. Also, as the

population ages, AF will place an increasing burden on health care resources, not only for its treatment and ongoing therapeutic management, but also because of the 2 most serious complications of AF, heart failure and stroke⁶. JT results in a risk of death of 5.6 – 14 %^{2, 5, 8, 15} in neonates following cardiac surgery. AF is equally problematic with an increased risk of all-cause mortality (1.5-1.9 fold) compared to those without AF, regardless of the presence of symptoms³. This is suggested to be due to the effects of AF itself, drug toxicities associated with treatment, or co-morbidities such as hypertension, heart failure, and valvular disease^{14, 22}. Clearly, there is a great need for uncovering the mechanisms of these arrhythmias, so that novel targets for intervention can be identified.

While both AT/F and nodal re-entry have previously been studied in the adult mouse, the inducibility of JT is a novel observation. In this thesis, experimental description of AT/F was based on 2 criteria: the susceptibility to induction with different pacing methods (triggers), and its duration which describes a substrate susceptible to AT/F maintenance. The induction of AT/F required pacing of the mid-right septal atrium (MRA) validated by using His bundle electrograms as a landmark of catheter location. This may have been due to the observed electrical heterogeneity between the MRA and the high right atrium (HRA), as effective refractory periods were consistently shorter in the MRA than the HRA. The catheter placement may also allow for trans-septal pacing of the left atrium. This finding was independent of the strain of mouse used. This was a novel anatomical and methodological finding that allowed for the systematic and reproducible initiation of AT/F among groups of mice. The induction of AT/F requires a trigger and a substrate susceptible to arrhythmia maintenance. In this thesis, I used 3 different electrophysiological pacing methods (triggers) to induce AT/F including: burst pacing; programmed electrical stimulation (PES) with 1 extra stimulus, and a single atrial stimulus (SAS) timed to follow the P-wave and interact

with the heterogeneous refractoriness of the normal sinus depolarization. These pacing protocols can be subdivided based on their ability to modify the substrate. The drive train during PES can affect both action potential duration and amplitude as the pacing rate is greater than the intrinsic rate along the cardiac restitution curve. Burst pacing would have a similar substrate modifying effect, however the high frequency pacing (50 Hz) may also activate intrinsic nerves. The most physiological of these "triggers" may be the SAS protocol as premature beats often precede AF episodes⁹ and the SAS protocol would have no substrate modifying effects. Burst pacing is the least physiological as it not only acts as a trigger but contributes to substrate formation by promoting cardiac electrical instability¹⁰. The induction of AT/F with burst pacing only but not PES or SAS implies that the substrate is near the arrhythmia threshold and required the added substrate modifying effect of burst pacing induced electrical instability for arrhythmia initiation. This concept has important implications as in **Chapter 2**. I found that 1 month old RGS2^{-/-} mice had a greater susceptibility to PES induced AT/F but no difference in susceptibility to burst pacing induced AT/F when compared to wild type littermates. These results also provide evidence for the hypothesis that functional M3 muscarinic receptors are present in the atria and are involved in arrhythmogenesis.

The use of 3 different triggers to elicit AT/F is proposed to allow the examination of the degree of substrate vulnerability to arrhythmia initiation. In **Chapter 3**, all 3 pacing protocols were used to examine AT/F susceptibility in the 6 month old Cx43^{G60S/+} mutant and Cx43^{+/+} littermate mice (**Figure 3.3A**). While the Cx43^{G60S/+} mutant mouse was 100% susceptible to AT/F induction with each trigger, susceptibility in the Cx43^{+/+} littermates followed a pattern of burst pacing > PES > SAS induction. As such, a substrate vulnerable to SAS induction is very close to the Threshold for arrhythmia initiation, followed by PES induction, while, as

discussed before, susceptibility to burst pacing only implies a substrate that is further from the threshold.

The duration of the induced arrhythmia is also of critical importance as it defines a substrate's ability to maintain an arrhythmia once initiated. Clinically, a duration of greater than 30 seconds is used to indicate sustained arrhythmia. This classification appears to be relatively arbitrary; however, it is a standard value and was used in **Chapter 2** to define sustained AT/F. It was found that the $RGS2^{-/-}$ mouse had a greater propensity to sustain AT/F with any induction protocol; however, this was not significant. In **Chapter 3**, AT/F in the $Cx43^{G60S/+}$ mutant mouse lasted longer than 35 minutes; however, I expanded on this standard (in agreement with other published findings) and defined severe sustained AT/F in the mouse as lasting longer than 2 minutes. **Figure 3.3B** shows that 75% of the $Cx43^{G60S/+}$ mutant mice had AT/F lasting longer than 2 minutes which was significantly greater than the $Cx43^{+/+}$ littermate mice. These results indicate that $Cx43^{G60S/+}$ mutant mice have a substrate which is more susceptible to the maintenance of AT/F than the $RGS2^{-/-}$ mice. This suggests that RGS2 and M3 muscarinic receptors are more limited contributors to substrate formation while Cx43 reduction is a major contributor. This interpretation is consistent with findings in **section 3.3.4** showing that while darifenacin (a selective M3 receptor antagonist) could terminate new onset sustained AT/F in $Cx43^{G60S/+}$ mutant mice, AT/F was reinducible 5 minutes after termination. It may be that darifenacin only destabilized arrhythmia maintenance while not lowering the substrate very far below threshold for arrhythmia induction. However, it has also been reported that darifenacin exerted only transient binding to cardiac muscarinic receptors in mice²¹, which could also explain the reinduction. These observations also provide evidence that there is a nervous component to AT/F in $Cx43^{G60S/+}$ mutant mice. In **Chapter 4**, I found that junctional tachycardia (JT) was caused by

inappropriate (enhanced) AV nodal pacemaker function initiated by abnormal autonomic (baroreflex) influences. I presented evidence for a role of both enhanced calcium clock and membrane clock function by utilizing ruthenium red (a potent inhibitor of intracellular calcium release) and ivabradine hydrochloride (a selective I_f channel blocker). However, it must be recognized that ruthenium red binds and inhibits many ion channels in addition to the L-Type Ca^{2+} channel. Both ruthenium red and ivabradine prevented JT induction, indicating that interference with either pacemaking mechanism lowered the substrate below the threshold for arrhythmogenesis.

The study of arrhythmia mechanisms in the mouse and development of novel antiarrhythmic interventions was an objective of this thesis. I found that both darifenacin hydrobromide and ivabradine hydrochloride may be useful antiarrhythmics given that they are currently used clinically for other purposes. Darifenacin is used to treat overactive bladder syndrome while ivabradine is used in the treatment of stable angina due to its pure heart rate reducing effects. Darifenacin's use may be limited, although it was found to destabilize AT/F causing termination in $Cx43^{G60S/+}$ mutant mice, it did not prevent reinduction by burst pacing. Nevertheless, it may still be of use clinically, either alone, or in combination with current antiarrhythmics utilizing a single dose "pill in the pocket" anti-arrhythmic drug for rhythm control^{14, 22}. On the other hand, ivabradine has great potential for clinical application for JT management. Not only was low dose ivabradine found to terminate JT in 8 of 9 mice, it has no negative inotropic effects^{17, 19} and is currently FDA approved for other purposes.

The current clinical management of AF uses 2 strategies, controlling the ventricular rate during AF (rate control) and preventing AF from recurring (rhythm control). Rate control utilizes β blockers, Ca^{2+} channel blockers and digoxin to reduce AV nodal conduction and

slow the ventricular rate. Anticoagulation therapy with warfarin is necessary as AF is associated with a high rate of thromboembolic events. Rate control utilizes various Na⁺ channel and K⁺ channel blocking drugs to maintain sinus rhythm. Studies comparing the 2 strategies (AFFIRM¹) showed no difference in overall mortality between the rhythm and rate control arms. This may have been due to the fact that patients in the rhythm control arm were not always in sinus rhythm and patients in the rate control arm were not always in AF. There was also an increase in stroke in the rhythm control arm as patients stopped taking warfarin. The risk of stroke persists in high risk patients even after restoration of sinus rhythm. It is suggested that AF may cause, or be a marker of biochemical alteration at the endothelial and intra-atrial level that may increase stroke risk independent of mechanical considerations⁴. These observations highlight an increased need for the understanding of AF mechanisms which was a goal of this thesis. To this end, I have developed a novel Threshold Model of arrhythmogenesis that allows the relative comparison of the role of multiple physiological factors in promoting AF. I have also investigated the neuro-myogenic interface of arrhythmia mechanism and suggest that the intrinsic cardiac autonomic nervous system (ICANS) is involved in most atrial arrhythmias.

Both pharmacological and electrical atrial defibrillation are used to restore sinus rhythm (cardioversion). Some patients are refractory (not susceptible) to restoration of sinus rhythm using electrical cardioversion. The Threshold Model would suggest that the substrate is too far above threshold for electrical cardioversion to terminate AF. If the ICANS is involved in most atrial arrhythmias as suggested, then it is predicted that muscarinic receptor blockade would lower the substrate sufficiently close to threshold to allow electrical cardioversion to terminate AF in these refractory patients. Following this, a search of PubMed revealed a clinical study¹² demonstrating atropine facilitated electrical cardioversion of AF, consistent

with the previous predictions. In this study, 49 of 364 patients (13.5%) with persistent AF did not respond to electrical cardioversion. However, following 2 mg of atropine, 40 of 49 previously refractory patients were successfully restored to normal sinus rhythm. Other standard antiarrhythmic drugs are also successful in facilitating electrical cardioversion¹³.

As proposed in **Chapter 1**, a 2 media (physiological and electrical) perspective of the heart, where many dependent or independent physiological factors can promote the same electrical phenomena, yields a physiological substrate Threshold Model of arrhythmogenesis. The Threshold Model is useful as it allows the simple comparison of results of different investigations relative to each other and the basal substrate state. Relative comparison is used to normalize and compare the results of many studies using advanced techniques such as quantitative real time PCR. While not informative of the actual mechanism of arrhythmia (abnormal impulse initiation/propagation), it allows a simple analysis of the physiological substrate state that can promote abnormal rhythm in the electrical media, regardless of the electrical mechanism. As the results of different investigations in the intact mouse accumulate, this form of relative comparison will aid in distinguishing between major and minor contributors to arrhythmia susceptibility. The Threshold Model is not proposed to overthrow a previous theory of arrhythmogenesis, only add to the arsenal of tools used to conceptualize the importance of results of various investigations. Any model or scientific theory allows for testing of hypotheses generated from its use. As discussed above this seems to be the case with the Threshold Model which begins to demonstrate it as a robust tool for arrhythmia research.

5.2 LIMITATIONS

The use of mice to investigate human disease is a common tool allowing the study of various genetic causes of disease, in isolation, and potential therapeutic options for patients. However, as discussed in detail in **Chapter 1 Section 1.0**, utilizing the mouse for arrhythmia investigation has limitations including differences in the intrinsic rate of the SA node, ion channels and differences in action potential morphology and duration. It is recognized that the mouse is not a human; however, comparative analysis of the mouse and human genome have revealed that approximately 99% of all mouse genes can be linked with a human homologue²⁰.

In **Chapter 2**, the role of RGS2 in arrhythmogenesis was investigated. The results of these studies indicated a role for RGS2 and the M3 muscarinic receptor in promoting AT/F in the mouse; however, the potential role for other Gq coupled receptors influencing arrhythmogenesis was not determined. Also, direct patch clamp investigation of currents to directly determine if there was a role for the $I_{K, M3}$ channel in this phenotype was not performed. It is recognized that atrial vulnerability may also be due to the balance between autonomics, which were not explored in these studies^{11, 16}. This may be an important consideration as RGS2^{-/-} mice have been shown to have reduced renal sympathetic nerve activity compared to WT mice¹⁸. However, the lack of a heart rate difference between RGS2^{-/-} and WT mice found in their earlier study⁷ does not assist in establishing the role of the sympathetic nervous system in atrial susceptibility, therefore the role of the balance between sympathetics and M3 responses remains to be determined. Also in **Chapter 2**, RNA expression profiles were determined for the muscarinic receptors. While RNA expression provides an index of the relative importance of the proteins, it may not parallel Bmax values of radioligand assessment of M2, M3 or M4 protein expression, distribution and function.

Furthermore, AF propensity increases with aging. However in **Chapter 2**, one month old mice were chosen to avoid potential complexity due to the effects of the chronic hypertensive phenotype with $RGS2^{-/-}$.

The investigation of atrial fibrillation was the focus of both **Chapter 2** and **Chapter 3**. However, in the mouse, it may be difficult to distinguish atrial fibrillation from atrial tachycardia, particularly with an arrhythmia of short duration. However, with the use of the standard clinical criteria for identification of AF, lack of regular P waves on ECGs and irregularly irregular ventricular responses, and left atrial predominance, it was often possible to demonstrate these classical characteristics of AF in the mouse. In **Chapter 3** I sought to make a direct comparison of the role of Cx40 and Cx43 in AT/F susceptibility. This comparison has not been previously done and is of importance in understanding the role of the various connexin isoforms in atrial arrhythmia vulnerability. However, this investigation had complications as $Cx40^{-/-}$ is associated with cardiac morphological changes, hypertension, cardiac hypertrophy and altered kidney function. The $Cx43^{G60S/+}$ mouse was used as the $Cx43^{-/-}$ mouse dies perinatally. This G60S mutation produces a phenotype of ocludentodigital dysplasia in the mouse and may potentially have unforeseen systemic influences on cardiac function. While these studies were quite informative on the role Cx40 and Cx43 in atrial arrhythmogenesis, future analyses should be performed on cardiac selective knockout animals in order to avoid these non-specific effects.

In **Chapter 4**, AV nodal arrhythmia was investigated in the normal wild type mouse. Programmed electrical stimulation was used to map antegrade AV nodal conduction curves in order to observe slow pathway conduction. While the presence of an atrial echo beat when present, was helpful as it could be used as an index to determine when the minimal jump in A2H2 interval occurred revealing slow pathway conduction. It is recognized the absence of

an echo beat may not be indicative of a lack of slow pathway conduction which could sometimes be observed with an obvious jump. It is also recognized that the study of Junctional Tachycardia in the 6 month old mouse may not be indicative of human neonatal arrhythmia.

5.3 REFERENCES

1. AFFIRM Investigators. Atrial fibrillation follow-up investigation of rhythm management -- the AFFIRM study design. The Planning and Steering Committees of the AFFIRM study for the NHLBI AFFIRM investigators. *Am J Cardiol* 79:1198-202. 1-5-1997.
2. Andreasen JB, Johnsen SP, Ravn HB. Junctional ectopic tachycardia after surgery for congenital heart disease in children. *Intensive Care Med* 34:895-902. 2008.
3. Benjamin EJ, Wolf PA, D'Agostino RB, Silbershatz H, Kannel WB, Levy D. Impact of atrial fibrillation on the risk of death: the Framingham Heart Study. *Circulation* 98:946-52. 8-9-1998.
4. Cai H, Li Z, Goette A, Mera F, Honeycutt C, Feterik K, Wilcox JN, Dudley SC, Jr., Harrison DG, Langberg JJ. Downregulation of endocardial nitric oxide synthase expression and nitric oxide production in atrial fibrillation: potential mechanisms for atrial thrombosis and stroke. *Circulation* 106:2854-8. 26-11-2002.
5. Dodge-Khatami A, Miller OI, Anderson RH, Gil-Jaurena JM, Goldman AP, de Leval MR. Impact of junctional ectopic tachycardia on postoperative morbidity following repair of congenital heart defects. *Eur J Cardiothorac Surg* 21:255-9. 2002.
6. Dries DL, Exner DV, Gersh BJ, Domanski MJ, Waclawiw MA, Stevenson LW. Atrial fibrillation is associated with an increased risk for mortality and heart failure progression in patients with asymptomatic and symptomatic left ventricular systolic dysfunction: a retrospective analysis of the SOLVD trials. *Studies of Left Ventricular Dysfunction. J Am Coll Cardiol* 32:695-703. 1998.
7. Gross V, Tank J, Obst M, Plehm R, Blumer KJ, Diedrich A, Jordan J, Luft FC. Autonomic nervous system and blood pressure regulation in RGS2-deficient mice. *Am J Physiol Regul Integr Comp Physiol* 288:R1134-R1142. 2005.
8. Hoffman TM, Bush DM, Wernovsky G, Cohen MI, Wieand TS, Gaynor JW, Spray TL, Rhodes LA. Postoperative junctional ectopic tachycardia in children: incidence, risk factors, and treatment. *Ann Thorac Surg* 74:1607-11. 2002.

9. Hoffmann E, Sulke N, Edvardsson N, Ruiter J, Lewalter T, Capucci A, Schuchert A, Janko S, Camm J. New insights into the initiation of atrial fibrillation: a detailed intraindividual and interindividual analysis of the spontaneous onset of atrial fibrillation using new diagnostic pacemaker features. *Circulation* 113:1933-41. 25-4-2006.
10. Jones DL, Guiraudon GM, Skanes AC, Guiraudon CM. Anatomical pitfalls during encircling cryoablation of the left atrium for atrial fibrillation therapy in the pig. *J Interv Card Electrophysiol* 21:187-93. 2008.
11. 2007 Jones DL, Tuomi J, Ramsay D, Guiraudon CM, Armour JA, Cardinal R, Page P, Guiraudon GM. Left atrial neuroablation for atrial fibrillation: A feasibility study. *Canadian Journal of Cardiology* 23, 225C, 2007.
12. Kaluski E, Blatt A, Leitman M, Krakover R, Vered Z, Cotter G. Atropine-facilitated electrical cardioversion of persistent atrial fibrillation. *Am J Cardiol* 92:1119-22. 1-11-2003.
13. Marcus GM, Sung RJ. Antiarrhythmic agents in facilitating electrical cardioversion of atrial fibrillation and promoting maintenance of sinus rhythm. *Cardiol* 95:1-8. 2001.
14. Nixon JV. *The AHA Clinical Cardiac Consult*. 3 ed. Philadelphia: Lippincott Williams & Wilkins; 2011.
15. Rekawek J, Kansy A, Mischczak-Knecht M, Manowska M, Bieganowska K, Brzezinska-Paszke M, Szymaniak E, Turska-Kmiec A, Maruszewski P, Burczynski P, Kawalec W. Risk factors for cardiac arrhythmias in children with congenital heart disease after surgical intervention in the early postoperative period. *J Thorac Cardiovasc Surg* 133:900-4. 2007.
16. Scherlag BJ, Patterson E, Po SS. The neural basis of atrial fibrillation. *J Electrocardiol* 39:S180-S183. 2006.
17. Sulfi S, Timmis AD. Ivabradine -- the first selective sinus node I(f) channel inhibitor in the treatment of stable angina. *Int J Clin Pract* 60:222-8. 2006.
18. Tank J, Obst M, Diedrich A, Brychta RJ, Blumer KJ, Heusser K, Jordan J, Luft FC, Gross V. Sympathetic nerve traffic and circulating norepinephrine levels in RGS2-deficient mice. *Auton Neurosci* 136:52-7. 30-10-2007.
19. Tardif JC, Ponikowski P, Kahan T. Efficacy of the I(f) current inhibitor ivabradine in patients with chronic stable angina receiving beta-blocker therapy: a 4-month, randomized, placebo-controlled trial. *Eur Heart J* 30:540-8. 2009.
20. Waterston RH, Lindblad-Toh K, Birney E, Rogers J, Abril JF, Agarwal P, Agarwala R, Ainscough R, Alexandersson M, An P, Antonarakis SE, Attwood J, Baertsch R, Bailey J, Barlow K, Beck S, Berry E, Birren B, Bloom T, Bork P, Botcherby M, Bray N, Brent MR, Brown DG, Brown SD, Bult C, Burton J, Butler J, Campbell RD, Carninci P, Cawley S, Chiaromonte F, Chinwalla AT, Church DM, Clamp M, Clee C, Collins FS, Cook LL, Copley RR, Coulson A, Couronne O, Cuff J, Curwen V, Cutts T, Daly M,

David R, Davies J, Delehaunty KD, Deri J, Dermitzakis ET, Dewey C, Dickens NJ, Diekhans M, Dodge S, Dubchak I, Dunn DM, Eddy SR, Elnitski L, Emes RD, Esvara P, Eyraas E, Felsenfeld A, Fewell GA, Flicek P, Foley K, Frankel WN, Fulton LA, Fulton RS, Furey TS, Gage D, Gibbs RA, Glusman G, Gnerre S, Goldman N, Goodstadt L, Grafham D, Graves TA, Green ED, Gregory S, Guigo R, Guyer M, Hardison RC, Haussler D, Hayashizaki Y, Hillier LW, Hinrichs A, Hlavina W, Holzer T, Hsu F, Hua A, Hubbard T, Hunt A, Jackson I, Jaffe DB, Johnson LS, Jones M, Jones TA, Joy A, Kamal M, Karlsson EK, Karolchik D, Kasprzyk A, Kawai J, Keibler E, Kells C, Kent WJ, Kirby A, Kolbe DL, Korf I, Kucherlapati RS, Kulbokas EJ, Kulp D, Landers T, Leger JP, Leonard S, Letunic I, Levine R, Li J, Li M, Lloyd C, Lucas S, Ma B, Maglott DR, Mardis ER, Matthews L, Mauceli E, Mayer JH, McCarthy M, McCombie WR, McLaren S, McLay K, McPherson JD, Meldrim J, Meredith B, Mesirov JP, Miller W, Miner TL, Mongin E, Montgomery KT, Morgan M, Mott R, Mullikin JC, Muzny DM, Nash WE, Nelson JO, Nhan MN, Nicol R, Ning Z, Nusbaum C, O'Connor MJ, Okazaki Y, Oliver K, Overton-Larty E, Pachter L, Parra G, Pepin KH, Peterson J, Pevzner P, Plumb R, Pohl CS, Poliakov A, Ponce TC, Ponting CP, Potter S, Quail M, Reymond A, Roe BA, Roskin KM, Rubin EM, Rust AG, Santos R, Sapojnikov V, Schultz B, Schultz J, Schwartz MS, Schwartz S, Scott C, Seaman S, Searle S, Sharpe T, Sheridan A, Shownkeen R, Sims S, Singer JB, Slater G, Smit A, Smith DR, Spencer B, Stabenau A, Stange-Thomann N, Sugnet C, Suyama M, Tesler G, Thompson J, Torrents D, Trevaskis E, Tromp J, Ucla C, Ureta-Vidal A, Vinson JP, Von Niederhausern AC, Wade CM, Wall M, Weber RJ, Weiss RB, Wendl MC, West AP, Wetterstrand K, Wheeler R, Whelan S, Wierzbowski J, Willey D, Williams S, Wilson RK, Winter E, Worley KC, Wyman D, Yang S, Yang SP, Zdobnov EM, Zody MC, Lander ES. Initial sequencing and comparative analysis of the mouse genome. *Nature* 420:520-62. 5-12-2002.

21. Yamada S, Maruyama S, Takagi Y, Uchida S, Oki T. In vivo demonstration of M3 muscarinic receptor subtype selectivity of darifenacin in mice. *Life Sci* 80:127-32. 14-12-2006.
22. Yan GX, Kowey PR. *Management of Cardiac Arrhythmias*. 2 ed. New York: Humana Press; 2011.

APPENDIX I: Bias in the C_q value observed with hydrolysis probe based quantitative PCR can be corrected with the estimated PCR efficiency value.

A version of this appendix has been published: **Tuomi, J. M.**, F. Voorbraak, D.L. Jones, J.M. Ruijter. "Bias in the C_q value observed with hydrolysis probe based quantitative PCR can be corrected with the estimated PCR efficiency value." [Methods](#). 2010 Apr;50(4):313-22. Epub 2010 Feb 6.

1.0 SUMMARY

For real-time monitoring of PCR amplification of DNA, quantitative PCR (qPCR) assays use various fluorescent reporters. DNA binding molecules and hybridization reporters (primers and probes) only fluoresce when bound to DNA and result in the non-cumulative increase in observed fluorescence. Hydrolysis reporters (TaqMan® probes and QZyme™ primers) become fluorescent during DNA elongation and the released fluorophore remains fluorescent during further cycles; this results in a cumulative increase in observed fluorescence. Although the quantification threshold is reached at a lower number of cycles when fluorescence accumulates, in qPCR analysis no distinction is made between the two types of data sets. Mathematical modeling shows that ignoring the cumulative nature of the data leaves the estimated PCR efficiency practically unaffected but will lead to at least 1 cycle underestimation of the quantification cycle (C_q value), corresponding to a 2-fold overestimation of target quantity. The effect on the target-reference ratio depends on the PCR efficiency of the target and reference amplicons. The leftward shift of the C_q value is

dependent on the PCR efficiency and with sufficiently large C_q values, this shift is constant. This allows the C_q to be corrected and unbiased target quantities to be obtained.

1.1 INTRODUCTION

The fluorescence-based quantitative real time PCR (qPCR) has become the gold standard technique for analysis of nucleic acids in medical diagnostics and life sciences. The proliferation of qPCR over the last decade has resulted in a diversity of reagents, protocols, analysis methods and reporting formats [1-3]. To promote consistency, increase transparency, and ensure the integrity of scientific literature, guidelines for the minimum information required for publication of qPCR experiments were formulated (MIQE) [4]. Quantitative PCR data analysis is based on the principle that the more copies of template that are present at the start, the fewer cycles of amplification it takes to make a specified amount of product [5]. The implementation of this principle involves setting of a fluorescence threshold (N_q) and determining the fractional cycle number (C_q) that is required to reach this quantification threshold [6-8]. Using the inverse of Eq. 1 (section 4), an estimate of the target quantity (expressed in arbitrary fluorescence units) can be calculated from the observed C_q value, using the amplification efficiency and this threshold [9-11]. Almost all qPCR analyses are based on the exponential nature of PCR kinetics (Eq. 1), and rely on the determination of the PCR efficiency per assay and C_q values per sample. However, the chemistries available for qPCR result in different kinetics of fluorescent reporter increases, which can be either non-cumulative (e.g SYBR green) or cumulative (e.g. TaqMan® probes). Apart from the illustration of typical amplification curves obtained for amplicons detected using SYBR Green I and TaqMan chemistries [3] the cumulative nature of some monitoring chemistries is commonly ignored in qPCR data analysis.

In this paper, we outline how the cumulative nature of some reagents impacts on qPCR data analysis choices, the way the data is analyzed and the results. In short, mathematical modeling shows that ignoring the cumulative nature of the data leaves the estimated PCR efficiency practically unaffected but will lead to at least 1 cycle underestimation of the C_q value, corresponding to 2-fold overestimation of the target quantity. The effect on the target-reference ratio depends on the PCR efficiency of the target and reference amplicons. The leftward shift of the C_q value is dependent on the PCR efficiency and with sufficiently large C_q values, this shift is constant. This allows the C_q to be corrected and unbiased target quantities to be obtained.

1.2 STRUCTURE OF THIS PAPER

This paper will follow the different steps of qPCR analysis from the choice of the assay to the presentation of the final results (Fig. 1). The main stream of qPCR analysis is based on determination of the PCR efficiency from standard curves (section 2.3.1). Alternatively, PCR efficiency values can be derived from individual amplification curves (section 2.3.2). The calculation steps in the flow chart explicitly separate the calculation of the target quantity of the gene of interest and reference genes from the calculation of the gene expression ratio. Many qPCR algorithms immediately calculate the expression ratio, thereby simplifying the equations by leaving out the quantification threshold and the PCR efficiency values. These equations inadvertently suggest that differences in PCR efficiency values do not play a role and can be ignored. It should be kept in mind that such simplification of the equations can only be done when the PCR efficiencies are equal [11]. Even small differences in efficiency can have a large effect on gene expression ratios [7].

Each section of the text will focus on a step, review the aspects relevant in the comparison of cumulative and non-cumulative chemistries and detail how the chosen detection chemistry will impact on the procedure and affect the result. Most steps will be illustrated with experimental or simulated data and graphs showing the biasing effect of the use of accumulated fluorescence data. Recommendations or correction methods will be presented where possible. These sections will refer to a Methods section describing the qPCR experiment of which the data are shown to illustrate certain steps and to a Theory / Calculations section describing the basic and derived equations used in qPCR data analysis and in the correction of the biasing effects of cumulative fluorescence data.

1.3. Methods

1.3.1 Tissue samples

The tissue samples used in this study were taken from the hearts of three, one month old C57BL/6 mice. Atria were isolated, flash frozen in liquid nitrogen and stored at -80 °C for no more than 6 months prior to RNA isolation using a Trizol kit (Qiagen Inc., Invitrogen, Burlington, ON). RNA concentration was determined using a spectrophotometer (NanoDrop; Thermo Scientific), and quality was assessed by gel electrophoresis. A total of 500 ng of RNA was converted to cDNA using the High-Capacity cDNA Reverse Transcription Kit with random primers (Applied Biosystems Inc., Carlsbad, CA).

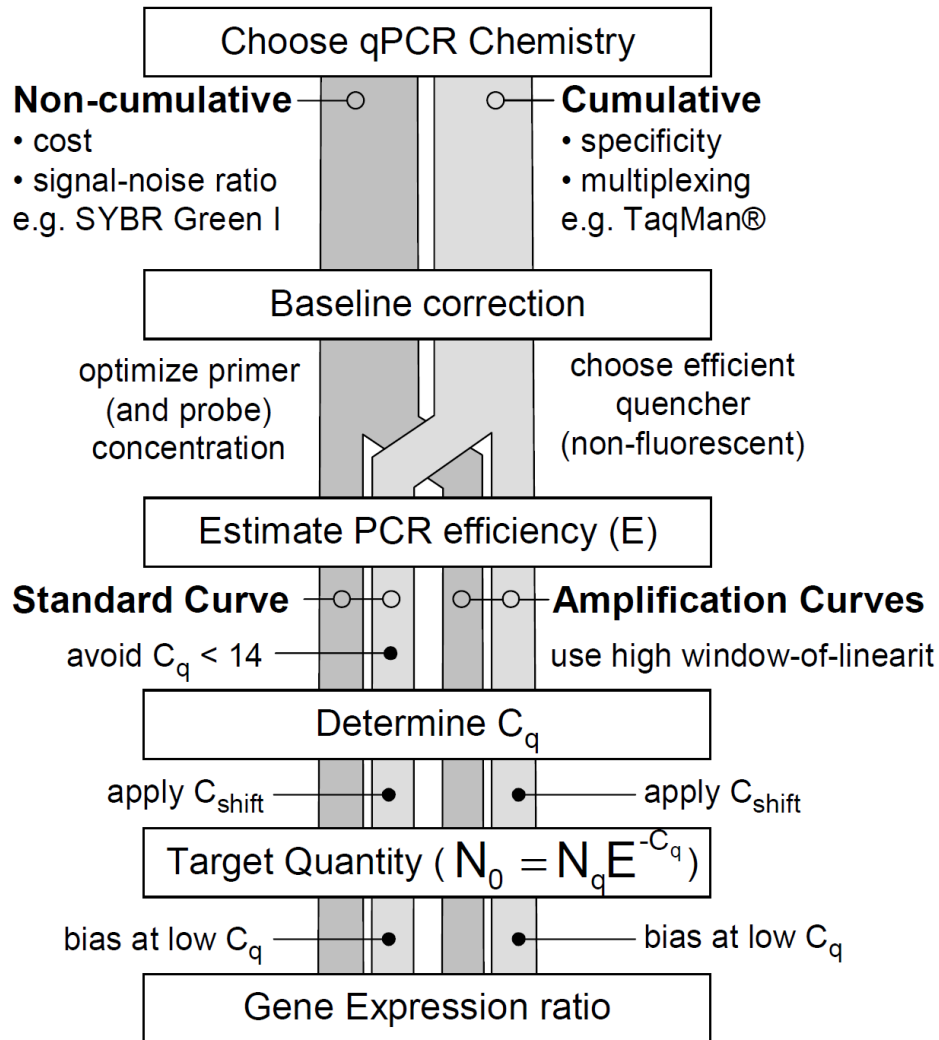


Figure 1. Flow chart.

Graphical illustration of the six decision and calculation steps in a quantitative PCR experiment that are described in this paper. The choice for a PCR monitoring chemistry results in the use of a non-cumulative or a cumulative reporter-fluorescence increase during PCR which has implications for the baseline subtraction. A second choice has to be made between PCR efficiency estimation with a standard curve or estimation from the amplification curves. Both methods can be applied to non-cumulative as well as cumulative fluorescence data. After determination of the C_q values and calculation of the target quantities, all data streams come together in the calculation of the gene expression ratio which is the final result of a qPCR experiment.

1.3.2 PCR reactions

C57BL/6 mouse atrial samples were amplified in 384-well plates on a BioRad cycler. The qPCR was performed using 15 µl reaction volumes. Specific primers for SYBR-green qPCR were developed using Primer-BLAST (NCBI) and examined for secondary structures using the oligonucleotide calculator [62]. Custom oligo (Invitrogen) primers for β -actin reference (Forward: CTGGAACGGTGAAGGCGACAG; Reverse: GCTTTTGGGAGGGTGAGGGAC; product: 182 bp), M2 Muscarinic Receptor (M2R) (Forward: TAGCACCATCAACCCTGCCTGC; Reverse: TCCCAAGACACACTCGACCAC; product: 151 bp), M3 Muscarinic Receptor (M3R) (Forward: CACAAGCGAGTGCCTGAGC; Reverse: GAATGGCCTCCACCTGC; product: 115 bp) were used at a 1 µmol/l concentration in SYBR green Mastermix (Quanta). The amplification protocol was identical for all primer sets: 10 min 95°C, 50x (15 s 95°C, 30s 60°C, 30s 72°C). Hydrolysis probe-based studies used TaqMan® gene expression Assays-on-Demand from Applied Biosystems and AmpliTaq Gold® 360 PCR Master Mix (ABI). Sequence information for primer and probe assays are proprietary to ABI and thus not available for publication. β -actin, M2 muscarinic receptor and M3 muscarinic receptor used a FAM reporter (excitation=495 nm, emission=515 nm) and TAMRA quencher (excitation=565 nm, emission=580 nm). These samples were measured in 3 parallel reactions using the following amplification protocol: 10 min 95°C, 50x (15 s 95°C, 30 s 60°C, 30 s 72°C).

1.3.3 Mathematical modeling

The basic equation for the kinetics of the exponential phase of PCR amplification (Eq. 1; section 4) was used to derive an equation of the kinetics that would be observed when the fluorescence accumulates from cycle to cycle (Eq. 2). These two models served to derive an equation for the distance between the cumulative and non-cumulative amplification curves on a log (fluorescence) scale. These equations were used in a spreadsheet program to calculate PCR efficiency values, target gene quantities and gene expression ratios. In these calculations, the PCR efficiency was derived from the slope of 4 data points (window-of-linearity method) [34]. A quantification threshold (N_q) was set at 1 cycle below the upper limit of this window. PCR efficiency and C_q values were then used to calculate the target quantity, N_0 [24]. The calculations were done with windows resulting in C_q values ranging from 10 to 40 cycles.

1.3.4 Theory / Calculations

The basic equation for PCR kinetics is:

$$N_c = N_0 \times E^C \quad [\text{Eq. 1}]$$

where the amount of amplicon after C cycles (N_c) is the starting concentration of the amplicon (N_0) times the PCR efficiency (E) to the power C . The PCR efficiency in this equation is defined as fold increase per cycle (2 indicates 100% efficiency). Because the fluorescence is linearly related to the amount of the amplicon, Eq. 1 also describes the increase in fluorescence for a non-cumulative DNA binding fluorochrome or hybridization reporter. When the fluorescent reporter of a hydrolysis probe is released during elongation, it remains fluorescent in subsequent cycles and accumulates. Because the amount of fluorescence released per cycle depends on the amount of amplicon present at the start of each cycle, cumulative fluorescence increases according to:

$$\Sigma N_c = \sum_{n=1}^c (N_0 \times E^n) \quad [\text{Eq. 2}]$$

The practically constant vertical distance between Eq. 1 and Eq. 2 at large cycle numbers, when plotted on a logarithmic axis (Fig. 2A), is written as ΔN , which can be calculated by:

$$\Delta N = \lim_{c \rightarrow \infty} (\Sigma N_c - N_c) = \log(1/(1 - (1/E))) \quad [\text{Eq. 3}]$$

Appendix A shows the derivation of Eq. 3. The horizontal distance, C_{shift} , between the cumulative and non-cumulative amplification curves then follows from the fact that on a logarithmic axis the slope of both lines can be considered to be given by $\log(E)$:

$$C_{\text{shift}} = \Delta N / \log(E) \quad [\text{Eq. 4}]$$

When the accumulation of fluorescence is ignored, biases will occur in the estimation of the starting target quantity (N_0) or target / reference ratios in starting quantities. The bias in the target quantity, calculated as $N_0 = N_q / E^{C_q}$, is given by:

$$\frac{N_{0,\text{observed}}}{N_{0,\text{real}}} = E^{C_{\text{shift}}} = 1/(1 - (1/E)) \quad [\text{Eq. 5}]$$

and the bias in the gene expression ratio by:

$$\frac{R_{\text{observed}}}{R_{\text{real}}} = \frac{E^{C_{\text{shift},\text{target}}}}{E^{C_{\text{shift},\text{reference}}}} \quad [\text{Eq. 6}]$$

Derivation of the latter two equations is shown in Appendices B and C.

1.4 QUANTITATIVE PCR ANALYSIS STEPS

1.4.1 Choice of detection chemistry

An impressive variety of monitoring chemistries are available for qPCR. The available non-cumulative fluorescent detection technologies depend on 2 principle mechanisms: 1) where a dye fluoresces upon binding with double stranded DNA (e.g SYBR

green), and 2) where fluorescence increases upon hybridization of the reporter to a specific oligonucleotide sequence. Examples of the latter include hairpin probe hybridization (LUX, Light Upon eXtension, Invitrogen), hairpin loop hybridization (Molecular beacons [12], Sigma Aldrich/IDT), and dual probe hybridization (Light Cycler, Roche) [2]. As the structure of these fluorescent reporters remains intact during the PCR reaction, the resulting increase in signal intensity is directly proportional to the amount of amplification product.

Cumulative reporter technologies depend on a hydrolysis step that irreversibly separates a fluorescent reporter from a quencher molecule. The close proximity of reporter and quencher, maintained until hydrolysis, results in suppression of the reporter molecule fluorescence (see Section 2.2). Examples of hydrolysis based chemistries include TaqMan® probes (Applied Biosystems), and the QZyme™ assay (Clontech laboratories, Inc.). As of Dec 2009, a PubMed search for TaqMan® probe-based assays yielded 4180 hits, while application of the QZyme™ assay has not yet gained popularity yielding only 2 PubMed hits. During the annealing/extension phase of PCR, the TaqMan® probe hybridizes to the template and the double stranded DNA-specific 5'-3' exonuclease activity of thermostable Taq or Tth polymerase degrades the probe and releases the reporter. The increased specificity due to the requirement for matching 3 independent nucleotide sequences (forward and reverse primers and probe), and the ability to multiplex reactions using different fluorophores in TaqMan® assays underlies the popularity of this system [2,13].

The cumulative fluorescence of hydrolysis reporters leads to observed fluorescence values that are higher than the kinetic equation of PCR predicts. Assuming the same fluorescence characteristics for a cumulative and a non-cumulative signal, Fig. 2A shows a simulation of the amplification curves of the same target, monitored with non-cumulative fluorescent dye binding (Eq. 1) and with a cumulative fluorescent probe (Eq. 2). The PCR

efficiency and target quantity N_0 was the same for both lines. At high cycle numbers, the lines become practically parallel on a logarithmic scale. The almost constant distance between the lines approximates a limit, written as ΔN . The mathematical derivation (see Appendix A) of this limit leads to Eq. 3, showing that ΔN is only dependent on the PCR efficiency. The distance between the non-cumulative and cumulative fluorescence curves for different PCR efficiency values is plotted in Fig. 2B. The horizontal lines represent the respective ΔN values calculated with Eq. 3. The graph shows that for a PCR efficiency of 1.4, parallelism can be considered to be reached after 20 cycles whereas at maximum PCR efficiency as little as 11 cycles are sufficient to reach parallelism. This means that for most quantitative PCR applications, on a semi-logarithmic plot the curves can be considered to be parallel at the level of the quantification threshold.

1.4.2 Baseline correction

Baseline fluorescence is defined as the level of fluorescence measured before any specific amplification can be detected. The word ‘baseline’ is used to avoid confusion with the ‘background’ which in PCR systems is often used to address the fluorescence of the internal reference dye (e.g. ROX or Fluorescein) or the signal observed outside the reaction wells. Similarly, the fluorescence baseline should not be confused with background defined as the amplification resulting from a ‘non-template’, ‘minus RT’ or ‘water’ control samples [14]. Fluorescence baseline has been described as constant, linearly dependent on cycle number [15-17] or as a non-linear saturation curve [18,19]. The definition of a constant baseline ranges from the minimum observed fluorescence [20], the mean of the 5 lowest observations [21], the mean of a fixed set of cycles [22,23] and the mean value of a dynamically

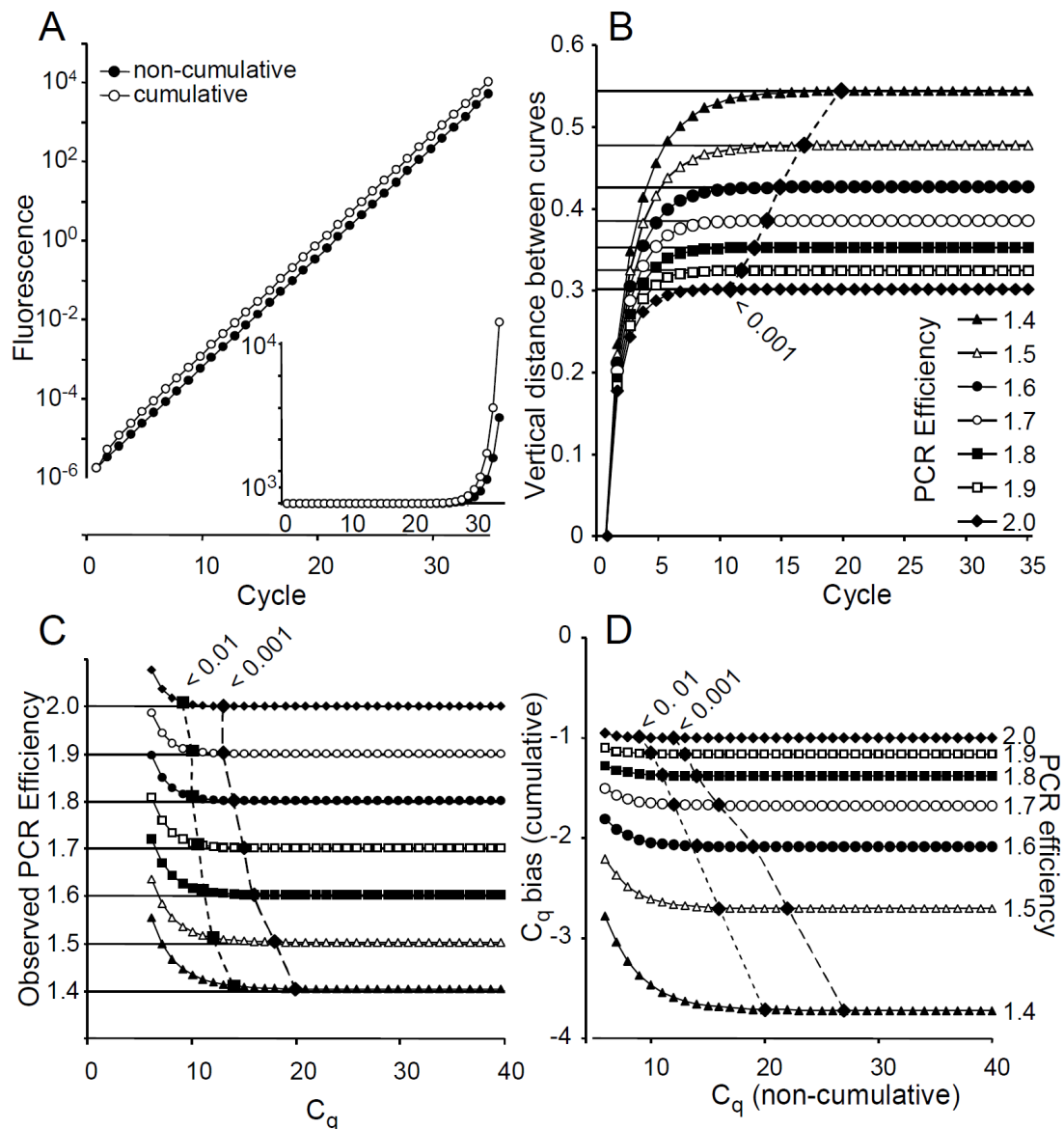


Figure 2. PCR efficiencies derived from non-cumulative and cumulative fluorescence curves.

A. Graphical representation of Eq. 1 and Eq. 2 (section 4) showing that on a logarithmic fluorescence axis, the curves resulting from a non-cumulative and a cumulative monitoring chemistry become virtually parallel. The inset shows the same data on a normal Y-axis. Parameters: N_0 : 0.000001, PCR Efficiency: 1.9 for both curves.

B. Demonstration that the vertical distance between the logarithmic curves closely approaches ΔN after a number of cycles that depends on the PCR efficiency. For each efficiency value, the black diamond indicates when the actual distance is less than 0.001 from ΔN .

C. PCR efficiencies derived from a subset of 4 cumulative fluorescence data points according to the window-of-linearity approach [34]. The PCR efficiencies are plotted against a C_q value obtained by placing a quantification threshold one cycle below the upper limit of the data

window. In windows that include early cycles the observed PCR efficiencies show a positive bias. The large black squares and diamonds indicate the C_q cycles above which this bias is less than 1% and 0.1%, respectively. Parameters: N_0 : 0.000001, PCR Efficiency: 1.4 - 2.0.

D. Bias in observed quantification cycle (C_q) for cumulative fluorescence data. C_q values in the simulated cumulative dataset were determined for quantification thresholds that lead to integer C_q values in a simulated non-cumulative data set. The large diamonds indicate the cycles at which the biases differ less than 0.001 from the C_{shift} predicted by Eq. 4 for each of the included PCR efficiency values. Parameters: N_0 : 0.000001, PCR Efficiency: 1.4 - 2.0.

determined set of ground phase cycles [15]. Most qPCR systems currently use a linear baseline trend.

It was described previously that a 2% underestimation of the baseline leads to a 2% underestimation of the PCR efficiency determined from the amplification curves whereas a similar overestimation of the baseline leads to such an overestimation of the PCR efficiency. Because of the exponential nature of PCR, such errors in the PCR efficiency can lead to a 10 fold error in reported gene expression ratios. To avoid these baseline estimation errors a new estimation algorithm was described [24]. This baseline estimation algorithm is based on the kinetic model of PCR amplification (Eq. 1) and assumes that the observed fluorescence at each data point up till the start of the plateau phase is the sum of baseline fluorescence and an exponential increasing amplicon concentration dependent fluorescence. The constant PCR efficiency in the exponential phase means that, in a semi-logarithmic plot, the data points in the exponential phase of the PCR reaction are on a straight line. The correct baseline value isolates the exponentially increasing part of the observed fluorescence values and results in the longest straight line of data points downwards from the plateau phase [24].

Experimental data from mouse atrium samples were analyzed using both SYBR green as well as TaqMan® assays (see section 3). The raw fluorescence data show that the baseline-to-plateau distance in SYBR green fluorescence data is larger than in Taqman® data (Fig. 3A). A similar difference in baseline-to-plateau distance between the two monitoring chemistries has been illustrated in other papers [3]. After baseline correction [24], both data sets show an exponential phase ranging over approximately 10 cycles (Fig. 3B).

An important factor influencing the baseline estimation is the baseline-to-plateau distance (ΔR_n) in the raw, i.e. not baseline corrected, data. This distance is determined by intrinsic properties of the fluorescent reporter and on the primer and probe concentrations

[24]. For non-cumulative fluorescence data, a large part of the baseline fluorescence results from the fluorescence of the unbound fluorochrome or fluorescent probe. For example, the unbound molecule of the DNA binding dye SYBR green is already fluorescent but at only 1/1000 of the fluorescence of the bound molecule [25]. High ΔR_n values are typical of SYBR green chemistry [3]. ΔR_n values recorded with hydrolysis probes, however, are reported to be significantly lower due to the use of FRET based chemistries that display inefficient quenching. For these chemistries it is important to choose a reporter/quencher pair that gives the largest baseline-to-plateau difference. This will facilitate the estimation of the correct baseline value and thus reduce the variation in observed PCR efficiency values (Fig. 3F) [24].

Criteria for selection of reporter/quencher pairs that display efficient quenching have been described. Briefly, 3 mechanisms of quenching reporter fluorescence include; 1) fluorescent resonance energy transfer (FRET); 2) static or contact quenching, and 3) quenching by the nucleotide proximal to the fluorophore (Guanine for FAM, Adenine for Alexa-488 dyes) [26]. In order to achieve efficient FRET, the reporter and quencher must be close to one another, and the absorption spectrum of the quencher must overlap the emission spectrum of the reporter fluorophore [27,28]. Reporter and quencher molecules can bind to form a ground-state complex [29]. Such coupling of the reporter and quencher's excited-state energy levels results in different electronic properties of the ground state complex that inhibits fluorescence [29]. The efficiency of contact quenching was revealed to always be greater than the efficiency of quenching by FRET [27,29].

Conventional TaqMan® probes use the reporter fluorophore, fluorescein (FAM), and a quencher, tetramethylrhodamine (TAMRA), which is also fluorescent. FAM/TAMRA based probes display relatively efficient quenching, over 90% [29]; however, the remaining

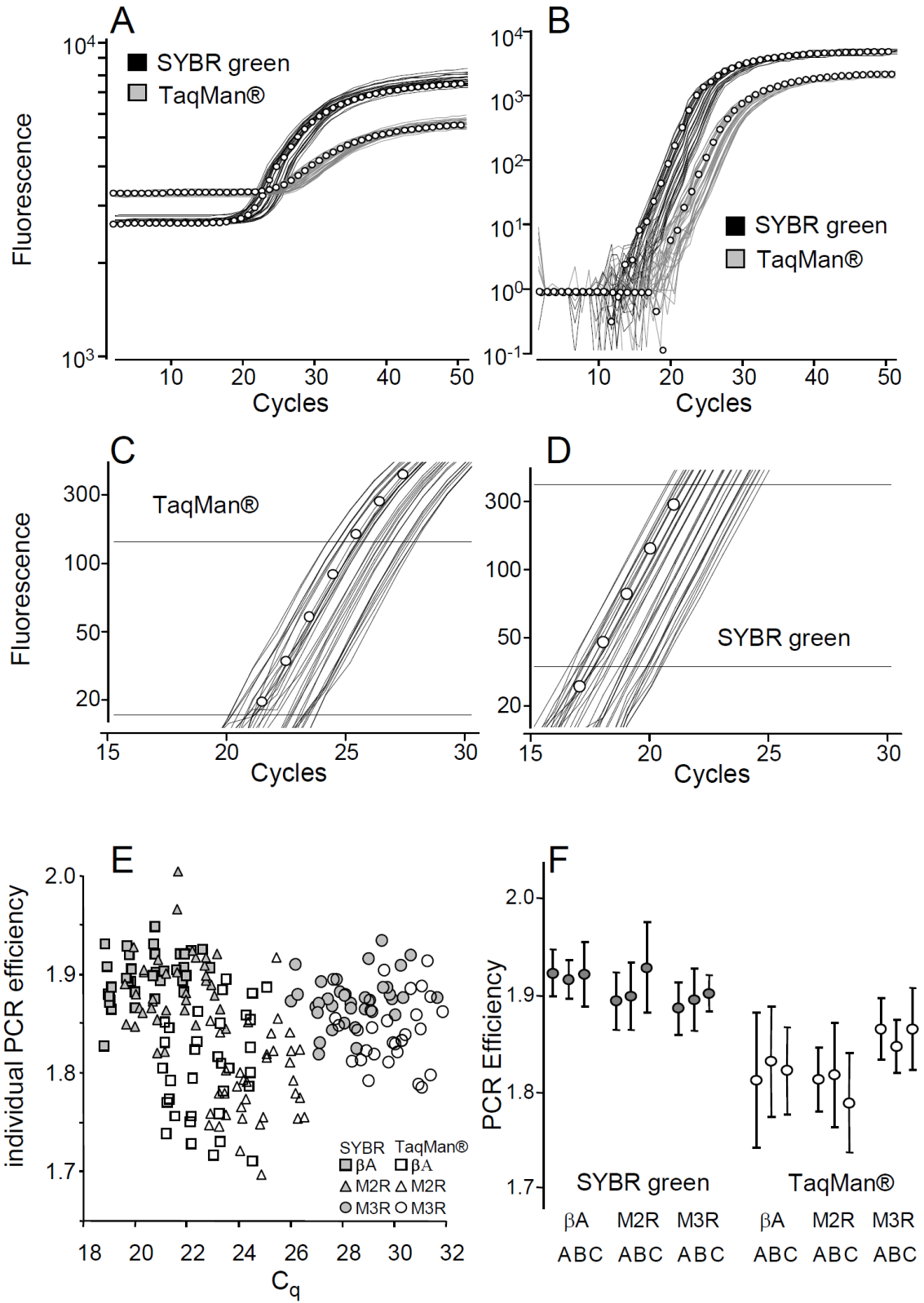


Figure 3. qPCR analysis with SYBR green and TaqMan® hydrolysis probe assays.

Amplification curves resulting from an experiment in which 3 amplicons (β -actin, M2 muscarinic receptor and M3 muscarinic receptor) were amplified with a non-cumulative SYBR green assay and a cumulative TaqMan® hydrolysis probe assay. Details on biological samples, experimental design and reaction conditions are given in the Methods section.

A. Raw fluorescence data resulting from PCR amplification of the M2 muscarinic receptor. The data are plotted on a logarithmic fluorescence axis and show that SYBR green fluorescence results in a larger baseline-to-plateau distance than TaqMan®.

B. Data from panel A were baseline corrected [24] and plotted on a logarithmic fluorescence axis.

C. Detail of the part of the TaqMan® amplification curves that is used for determination of the PCR efficiency per sample. The horizontal lines indicate the window-of-linearity [24]. Note that, although the window is at the top of the exponential phase, the amplification curves at the bottom of the window are diverging.

D. As C but for SYBR green amplification curves. Within the window virtually all amplification curves are parallel.

E. PCR efficiencies and C_q values determined for both assays and the 3 amplicons. The plot of PCR efficiency against C_q value shows no correlation between these two parameters.

F. Mean PCR efficiency (with 1 times standard deviation; N=12 per amplicon per sample) observed for a SYBR green and a TaqMan® hydrolysis probe assay. The graph shows that PCR efficiencies per sample overlap per amplicon, indicating the PCR efficiency is not sample dependent. Although the PCR distributions overlap for all amplicons in the SYBR Green assay and between β -actin and the M2 muscarinic receptor for the TaqMan® assay, those of the M3 muscarinic receptor in the TaqMan® assay are significantly higher.

Therefore, PCR efficiencies should be considered to differ between amplicons and between monitoring chemistries.

unquenched FAM and fluorescent TAMRA contribute significantly to baseline fluorescence and decrease ΔR_n . Non-fluorescent 'dark' quenchers absorb light and emit only heat [30]. These dark quenchers, trademarked black hole quenchers (BHQ®; Biosearch Technologies) can greatly increase signal to noise ratios in qPCR.

1.5 PCR EFFICIENCY ESTIMATION

For the transformation of qPCR data into (relative) target gene quantity, almost all qPCR data analyses are based on estimating PCR efficiencies, setting an N_q threshold and determining the C_q value per sample [17,31]. The calculation of the target gene quantity N_0 , uses the inverse of Eq. 1 ($N_0 = N_q/E^{C_q}$) and a PCR efficiency E , for which several estimation methods have been proposed in the literature.

Some qPCR data analysis algorithms, such as the comparative C_q method [32], use equations that do not account for specific PCR efficiency values. However, the derivation of these equations requires the efficiency values for all amplicons to be equal or even equal to 2. The MIQE guidelines do not mention an acceptable range of PCR efficiency values [4]. For the comparative C_q method a validation method to test the equality of target and reference efficiency was described [6]; at a PCR efficiency of 1.8, an observed efficiency up to 1.83 meets this criterion. Recently a range of 1.93 to 2.05 for the standard curve derived efficiency was described to reflect an optimized assay [3]. Note, however, that at a C_q of 30 cycles, treating an actual PCR efficiency of 1.9 as if maximal amplification was reached leads to an approximately 5-times overestimation of the target quantity [7]. When a small over- or underestimation of the PCR efficiency occurs independently in the target and reference genes, a 10-fold error in the gene expression ratio can easily result [24]. It may be for this

reason that the comparative C_q method is described as the most popular but not necessarily the most appropriate method [4].

Several reports showed that the assumption that the amplification efficiencies of the amplicon of interest and the reference gene were similar enough to ignore the differences, resulted in over- as well as under estimations of the biological effects [11,24,32-35]. To avoid this bias analysis should be based on a PCR efficiency value per amplicon [9-11,36,37].

1.5.1 PCR efficiency derived from a standard curve

The PCR efficiency per amplicon is most often derived from a dilution series, also known as standard curve [38] which is a plot of C_q values versus the known Log-concentration of a series of known concentrations or a serial dilution of a standard sample [3,6,32,36,39,40]. The simplicity and general use of the standard curve has led to its implementation in qPCR software which has obscured the mathematical principles upon which the analysis is based [8]. The regression line fitted to the data points is described by the equation $C_q = \text{Log}(N_q)/\text{Log}(E) - 1/\text{Log}(E) \cdot \text{Log}(N_0)$ which is the Log-transformed Eq. 1, rearranged to show the linear dependence of C_q on $\text{Log}(N_0)$.

Determining the efficiency value from a standard curve has been described as simplified because the PCR efficiency may vary with input concentration [15]. The requirement that the efficiency is constant for each included sample is rarely achieved and verified [41]. Studies on the reproducibility of the standard curve derived PCR efficiency with replicate standard curves show a large variation in values derived from these data sets [8,11,24,34].

The C_q values used to construct the standard curve result from a dilution series. For a typical dilution series (10 times dilution per step; 4 steps) the expected C_q values, at a PCR efficiency of 2, range over approximately 14 cycles. As will be shown in section 2.4, at high C_q values, all C_q are negatively biased when the observed fluorescence is cumulative. The resulting standard curve will be parallel and the slope of the curve will result in the same PCR efficiency as when the amplification was monitored with a non-cumulative reporter.

However, when the C_q values for the least diluted samples are too low, the negative bias in these samples is less (see section 2.4). These slightly overestimated C_q values will lead to a standard curve with a steeper slope and the derived efficiency will be too low. Because only the lowest C_q value of a dilution series will be affected, and C_q values below 10 cycles are very rarely used in a standard curve, this bias will have had minimal effects. In practice, the standard curve-derived efficiency can, therefore, be considered to be independent of the fluorescent chemistry used to monitor the PCR reaction. Similarly, the use of a concentration series as calibration curve to look-up the concentration of an unknown sample from its C_q is not affected because both calibration curve and sample C_q are similarly biased.

1.5.2 PCR efficiency derived from amplification curves

Alternatively, the PCR efficiency can be derived from a subset of data points in the exponential phase of the amplification curve of each individual sample. Such an efficiency value was used in the first radioactively monitored quantitative PCR experiments [42]. For data obtained by fluorescent monitoring of PCR amplification [43], several authors advocated the determination of the PCR efficiency from the slopes of individual amplification curves on a semi-logarithmic scale [34,44,45] or by non-linear fit of Eq. 1 to

data points in the exponential phase [15,41,46]. Similarly, mean efficiency values per amplicon can be estimated by calculating the common slope of the data points in the exponential phase for a group of samples [47]. Although good agreement between results obtained with a standard curve derived efficiency value and the mean of the efficiencies derived from individual amplification curves has been reported [48] other studies show that PCR analysis with the comparative C_q method or with standard curve derived efficiency values give precise (low within group variation) but significantly biased results [9,11,49]. In contrast, qPCR analysis based on the PCR efficiencies derived from individual amplification curves per sample resulted in unbiased target quantities but gave high variation within groups [9,49]. The average of these efficiency value for all samples per amplicon was shown to result in unbiased gene expression results with low variation [9,11,24,45,50]. The estimation of the PCR efficiency from the slope of the exponential phase of the amplification curve, plotted on a log (fluorescence) scale is directly derived from the logarithmic transformation of the basic kinetic equation of PCR (Eq. 1) [34]. The application of this method seems, therefore, to be limited to non-cumulative fluorescence data [24].

However, the simulation of the estimation of the PCR efficiency from cumulative fluorescence data shows that the estimated PCR efficiencies are only positively biased when they are derived from subsets with low cycle numbers (Fig. 2C). Even with a low PCR efficiency of 1.4, already after 14 cycles, the estimation error is below 1%. With maximum PCR efficiency, this number of cycles is sufficient to reduce the bias to 0.1%.

Comparison of the observed PCR efficiency values between different heart tissue samples shows that the PCR efficiency distributions overlap per amplicon and sample (Fig. 3F). The PCR efficiencies estimated from the individual samples can, therefore, be considered to be independent of the tissue sample; observed PCR efficiencies seem to be

drawn from a random distribution around the actual PCR efficiency of the amplicon [9,24]. Moreover, comparison of Figs. 2C and 3F shows that the predicted bias at low cycles is small compared to this experimental variation.

Estimation of the PCR efficiency from individual sample curves requires the observable exponential phase to be as long as possible (see section 2.2). When the subset of data used for estimation of the PCR efficiency is scrutinized, the TaqMan® data show more variable slopes than the SYBR green data (compare Figs. 3C and 3D). This variability is reflected in the increased variance of the resulting PCR efficiencies (Fig. 3F). Note that plotting the data on a logarithmic scale is required to judge this efficiency variance from the individual amplification curves. Identical ‘slopes’ on a normal fluorescence axis [3] merely indicate that the transition into the plateau phase occurs in parallel.

These results show that when the PCR efficiency is derived from the slope of the amplification curves per sample the resulting PCR efficiency will be correct when the data points used are beyond cycle 15. With low PCR efficiency and high abundance samples, one should be aware that in early cycles, the cumulative fluorescence curve has a steeper slope than the non-cumulative curve, and this will lead to an overestimation of the derived PCR efficiency.

1.6 C_q DETERMINATION

The second parameter that has to be derived from the qPCR data set is the quantification cycle (C_q) which is the fractional number of cycles needed to reach the quantification threshold (N_q). C_q values have been the mainstay of qPCR data analysis since the introduction of fluorescence monitoring of the PCR reaction [6,43]. The C_q value marks the position of the amplification curve on the cycle axis and is proportional to the logarithm

of the initial target concentration at constant amplification efficiency. C_q values are also referred to as C_t or C_p but this is discouraged in the MIQE guidelines [4].

Recommendations for placing the quantification threshold vary in literature. Some authors place the threshold at the level where amplicon DNA just becomes detectable [8,35] or at least at the low end of the exponential phase [6,10,20]. Other papers describe the threshold setting as arbitrary [44,49] or recommend specific positions like the midpoint of the exponential phase [45]. High threshold settings have mostly been avoided because of the variation in plateau phase levels. However, it was also recommended to avoid the lower end, and even the middle, of the exponential phase, because this region is still influenced by baseline noise [41]. Because the threshold is used in calculation based on the exponential amplification of DNA, the threshold should intersect with the exponential phase of the amplification curve [19]. Note that the threshold level is sometimes called ‘noise band’ [6], ‘benchmark’ [50] or ‘detection threshold’ [51] thereby adding to the confusion on the issues of baseline, background, threshold and variation in qPCR data analysis.

Alternatively, a C_q value has been derived from individual amplification curves by determining the fractional cycle at which a second derivative of a smoothed curve fitted to a subset of the observed data points reaches its maximum [38,52]. This second derivative maximum (SDM) marks the cycle at which exponential amplification no longer can be sustained and the curve begins to taper into the plateau phase [53]. This method gained popularity because it does not involve any decision by the user [52]. However, although the fluorescence level at the second derivative maximum typically will be similar for a given set of reaction conditions, this method is based on the assumption that information in the curve shape is more predictive of the target quantity than the fluorescence levels at each cycle. A

comparison of different C_q determination methods showed that in assays with variable baseline and plateau conditions the threshold method showed superior precision [53] .

The validity of the use of the C_q value is tightly linked to the exponential nature of the PCR amplification. Obviously the quantification threshold will be reached in an earlier cycle when the monitored fluorescence accumulates. This effect can clearly be seen when the C_q values that are observed with a cumulative fluorescent probe are plotted against the C_q values resulting from non-cumulative monitoring of the same simulated samples (Fig. 2D). At high C_q the negative bias in the C_q becomes constant and is then given by Eq. 4. This C_{shift} is especially large when the PCR efficiency is low. At low efficiencies it also takes a large number of cycles to reach this constant C_{shift} . This is why the standard curve-derived efficiency will be biased when at low PCR efficiencies such low C_q values are included (see section 2.3.1).

The relation between PCR efficiency and C_q value that is present in Fig. 2C is not observed in the analysis results of the quantitative PCR data (Fig. 3E). The non-cumulative SYBR green data, as well as the cumulative TaqMan® data show no correlation between PCR efficiency and C_q values.

Because of the cumulative nature of the fluorescence resulting from hydrolysis probes, the C_q values observed with these probes are lower than expected from their PCR kinetics. This shift is minimally 1 cycle when the PCR efficiency is 2, but lower PCR efficiency leads to a larger C_{shift} (Fig. 2D). The magnitude of this bias is similar to the error observed in C_q values between replicate measurements of the same sample, which is generally described to be low, especially when compared to operator, kit and probe differences [54]. Replicate measurements on the same sample show C_q differences of 0.2 [49] or 0.4 cycles [55]. Intra-assay coefficients of variation for replicate C_q values were

reported in the order of 1% [20], 7 % [56] and 10% [36]. The last percentage translates into a standard deviation of 2 cycles. This comparison of the C_{shift} bias with random experimental error is partly flawed because random error is averaged out whereas a systematic bias does not, and may go unnoticed when no reference is available.

1.6 CORRECTION OF C_{SHIFT}

Because ΔN and C_{shift} are fully dependent on the slope of the amplification curve in the exponential phase, a correction for this bias can be based on the constant PCR efficiency during this phase (Fig. 4). This PCR efficiency can be derived from a standard curve or from a subset of data points in the exponential phase of the amplification curves [34]. On a logarithmic fluorescence scale, the slope of the amplification curve is the logarithm of the PCR efficiency. Therefore, the known PCR efficiency can be used to calculate ΔN and C_{shift} . The sum of the observed C_q and C_{shift} results in a corrected C_q value, representing the value that would have been found when the same fluorescent dye had behaved non-cumulatively. This corrected C_q value can then be used to calculate the correct N_0 value. Note that in qPCR analysis algorithms that assume that the PCR efficiencies of all amplicons are equal, or at least similar enough to allow the difference to be ignored, like the comparative C_q method, the C_{shift} correction will have no effect on the result of the analysis.

The correction principle is illustrated in Fig. 4 and has to be applied to individual PCR samples. In case the PCR efficiency is derived from the individual amplification curves, the mean of all individual PCR efficiencies per amplicon has to be used to calculate the required C_{shift} . The latest version of the qPCR analysis program LinRegPCR (<http://LinRegPCR.HFRC.nl>) [24] implements this correction.

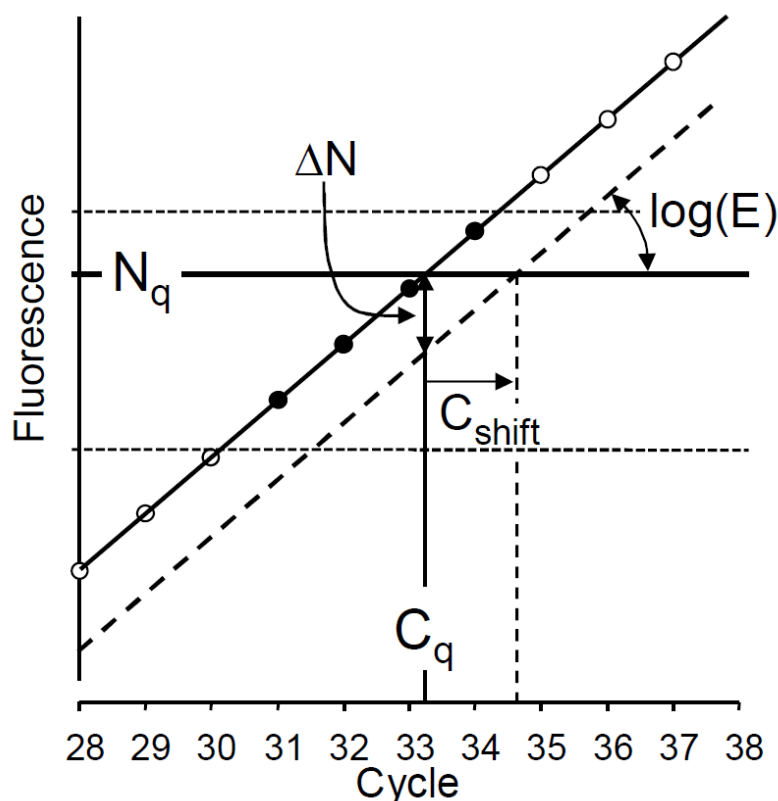


Figure 4. Correction of C_q values determined from cumulative fluorescence curves.

The circles represent the data points originating from monitoring the PCR reaction with a cumulative fluorescent probe. After setting the quantification threshold N_q (horizontal solid line) the C_q value can be determined. Using the estimated PCR efficiency value (E), the vertical distance to the equivalent non-cumulative fluorescence curve (dashed curve) can be calculated (Eq. 3). Because the slope of both curves is equal to $\log(E)$, simple geometry suffices to calculate the horizontal distance (C_{shift}) between the curves. The observed C_q value of the cumulative fluorescence curve can then be corrected to the C_q value (vertical dotted line) that would have been observed when the fluorochrome had not accumulated. The figure also illustrates the setting a window-of-linearity [34] (horizontal dotted lines) which is used to determine the PCR efficiency of the current sample by linear regression using the data points in the window (black circles). Parameters: N_0 : 1, PCR efficiency: 1.8. C_{shift} is 1.38 in this example.

1.7 CALCULATE TARGET QUANTITY (N_0) AND GENE EXPRESSION RATIO

Although papers describing qPCR results often only report C_q values it is clear that interpretation of these results cannot be done without knowledge of the PCR efficiency values [57]; C_q values should not be compared as such but converted into and reported as target quantities [58]. Because of the exponential nature of PCR, small differences in PCR efficiency between amplicons can lead to large differences in C_q value whereas similar C_q values for different amplicons can represent very different target quantities when the PCR efficiencies differ between amplicons [11,24]. As stated above, an observed C_q of 30 cycles can represent a 5-fold difference in target quantity when the PCR efficiency of two amplicons differs only as much as from 1.9 to 2. . Thus, restricting qPCR analysis to assays with a PCR efficiency above 1.9 will not prevent the variance introduced by ignoring the actual PCR efficiency. To avoid the tedious interpretation of C_q values it is recommended to use the estimated PCR efficiency, quantification threshold and C_q value to calculate a target quantity with the inverse of Eq. 1. The resulting N_0 value is an estimate of the target quantity in arbitrary fluorescence units.

Target quantities were calculated for simulated data sets monitored with non-cumulative and cumulative fluorescent chemistries (Fig. 5A). This simulation shows that the expected bias is dependent on the PCR efficiency because the vertical distance ΔN of the parallel curves is associated with a horizontal shift, C_{shift} , at the level of the quantification threshold (Eq. 4; Fig. 4). When the C_{shift} is ignored in PCR data analysis, biases will arise in the estimated target quantities (Eq. 5, Fig. 5A) and gene expression ratios (Eq. 6, Fig. 5B). The magnitude of these biases depends on the PCR efficiencies of the target and the reference genes. This effect is direct through the use of the efficiency value in calculating N_0 with the inverse of Eq. 1 and indirectly through the contribution of the efficiency to the C_{shift} .

Fig. 5A shows that the bias in estimated N_0 values approaches the value calculated with Eq. 5 at high C_q . With low PCR efficiency, low C_q values show the largest bias. This is because in these circumstances, the non-cumulative and cumulative curves are not yet completely parallel and biased efficiency values will be estimated (Fig. 2C). Moreover, a low PCR efficiency results in a smaller ΔN but larger C_{shift} (Fig. 2D). With high PCR efficiencies, the bias in N_0 is constant and minimal at the maximum efficiency of 2.

To study the effectiveness of the C_{shift} correction on the observed target quantity, its effect was simulated and the relative error in the resulting N_0 value was calculated (Fig. 6). This calculation shows that after the C_{shift} correction, for an amplicon with a PCR efficiency of 2, the N_0 values are within 0.5% of the given value already at a C_q of 12. With lower efficiency values, higher C_q values are required to reach the same small error. The dependence of the remaining error in N_0 on the C_q value results from the fact that at lower cycle numbers, the non-cumulative and cumulative amplification curves are not yet fully parallel (Fig. 2B). However, the observed remaining errors are well within the experimental and biological variation of quantitative PCR experiments [59,60].

Even when the accumulation of fluorescence is ignored, the gene expression ratio is unbiased when the PCR efficiencies of the target and the reference amplicon are equal (Fig. 5B). In that situation, the C_{shifts} cancel each other, resulting in unbiased gene expression ratios. For optimized PCR reactions, with efficiency values of 1.8 or higher, the bias in gene expression ratio will be limited to 12% (Fig. 5B). However, biases from 0.57 to 1.75 can be observed when these efficiencies range from 1.4 to 2. In this calculation of the bias in a gene expression ratio (Appendix C; Eq. 6), a single reference gene is used. When the geometric mean of the expression levels of multiple reference genes is used for normalization of the target quantity [61], the resulting bias depends on the efficiency values of the individual

reference genes. When these efficiencies are distributed around the PCR efficiency of the target amplicon, bias will be reduced.

Also the bias in the gene expression ratio can be removed by applying the described C_{shift} correction. Depending on the PCR efficiency and the C_q values, the C_{shift} correction procedure will completely remove the bias. When the PCR efficiencies of target and reference amplicons differ, some bias in the gene expression ratio may remain when C_q values are low.

The bias in the gene expression per sample as predicted by Eq. 6 is independent of the C_q values of the target and reference genes in the sample. This means that in a comparison of the relative difference of the gene expression ratios between different samples in an experiment the bias due to ignoring cumulative fluorescence cancels out; the same fold-difference between samples would be obtained with or without C_{shift} correction. However, this result is only unbiased when the PCR efficiency values of target and reference amplicons were included in the calculations. Moreover, for the calculation of unbiased absolute differences between samples in an experiment the C_{shift} correction is required.

2.7 Conclusions

Although monitoring PCR amplification with a cumulative fluorescent reporter gives higher observed fluorescence data, a correct PCR efficiency can be derived from the exponential phase from such a cumulative curve or from a standard curve based on C_q values derived from these data. The downward shift in C_q values is dependent on the PCR efficiency and can be corrected when this efficiency is known. When the accumulation of fluorescence is ignored, target quantities are at least two-fold too high. However, the error in the target/reference ratio of starting quantities is small when the PCR efficiencies of the target and reference amplicons are similar. When PCR efficiencies are derived from the exponential

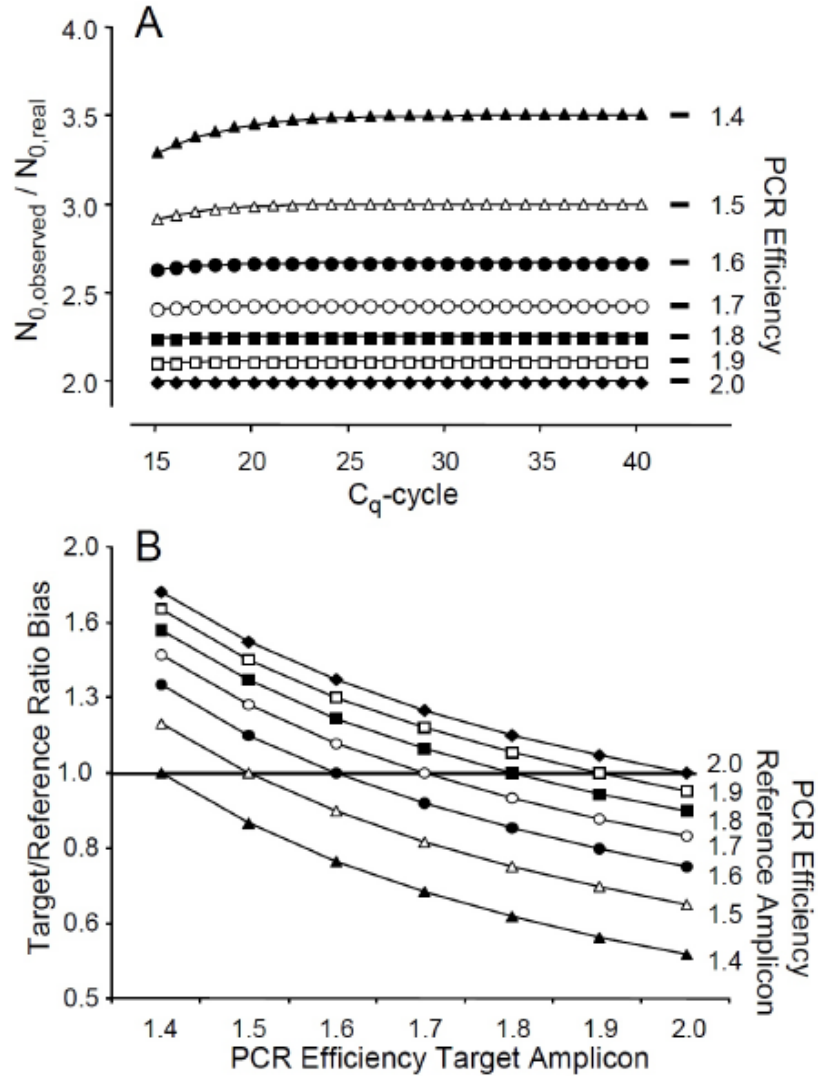


Figure 5. Results are biased when the accumulation of fluorescence is ignored.

A. Although Eq. 5 (section 4) predicts that the bias in the estimated target quantity (N_0) is independent of C_q , in practice N_0 is negatively biased when the C_q value, and thus the subset of data points used to calculate the PCR efficiency, is in the early cycles. To generate this graph, the C_q values and PCR efficiency values shown in Fig. 2C were used to calculate the observed N_0 . The relative error in N_0 was then calculated as the ratio between observed and given N_0 value. This relative error is independent of N_0 . Parameters: N_0 : 0.000001, PCR Efficiency: 1.4 - 2.0.

B. The bias in the gene expression ratio, calculated by dividing the starting amount of a target gene by that of a reference gene in the same sample depends on difference between the PCR efficiencies of the target and reference amplicon (Eq. 6). When the PCR efficiencies of both amplicons are equal, the gene expression ratio is unbiased. However, when the PCR efficiencies differ, positive and negative biases can occur. The parameters used in the calculation are the same as in Fig. 5A.

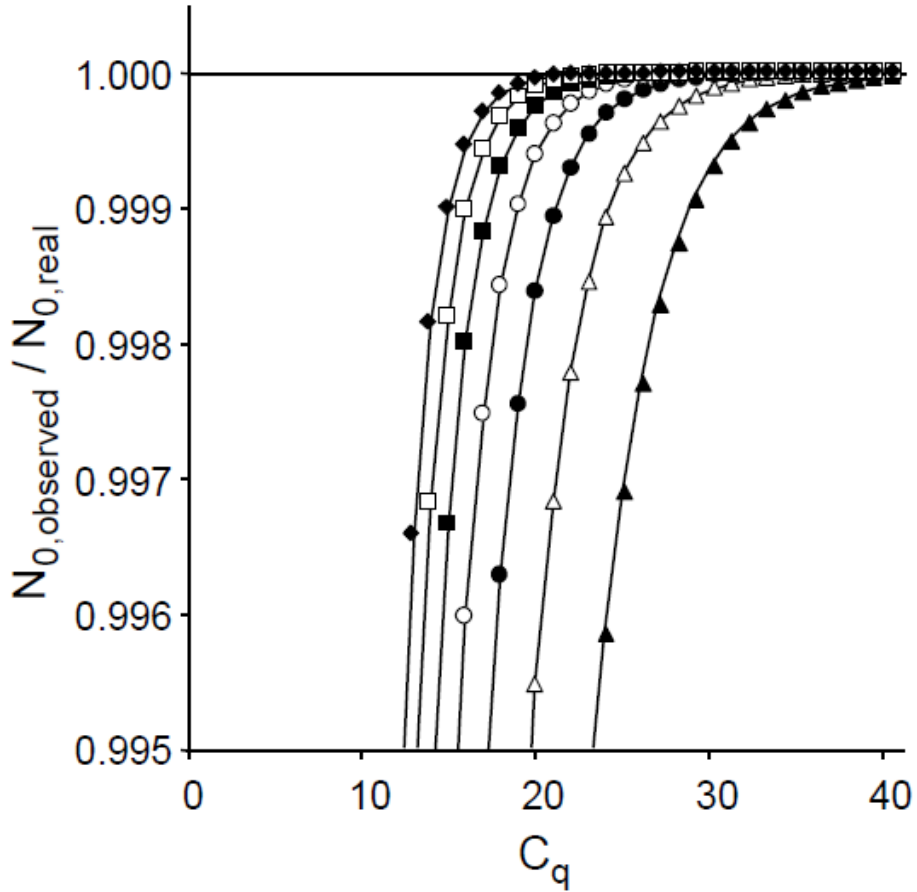


Figure 6. C_{shift} correction does not remove all bias in N_0 .

The fact that the bias in N_0 is dependent on the C_q value (see Fig. 5A) makes that the C_{shift} correction illustrated in Fig. 4 is not removing the bias in all situations. After application of the correction to the data of Fig. 5A a small error in the estimated N_0 values remains present. The graph shows the remaining bias in these estimated N_0 values. The C_q values that have to be observed to restrict this bias to at most 0.5% are plotted for a range of PCR efficiency values. The graph shows that, to limit the error to 0.5%.

phase of the amplification curves, the researcher should select a fluorophore-quencher pair with a high ΔR_n value to facilitate baseline estimation and thus reduce the variation in the estimated PCR efficiency.

3.8 APPENDICES

Appendix A. Derivation of ΔN

Appendix B. Derivation of bias in N_0 when C_{shift} is ignored

Appendix C. Derivation of bias in the gene expression ratio when C_{shift} is ignored

3.9 REFERENCES

- [1] S.A.Bustin, V.Benes, T.Nolan, M.W.Pfaffl, *J. Mol. Endocrinol.* 34 (2005) 597-601.
- [2] H.D.VanGuilder, K.E.Vrana, W.M.Freeman, *BioTechniques* 44 (2008) 619-626.
- [3] T.Nolan, R.E.Hands, S.A.Bustin, *Nat. Protoc.* 1 (2006) 1559-1582.
- [4] S.A.Bustin, V.Benes, J.A.Garson, J.Hellemans, J.Huggett, M.Kubista, R.Mueller, T.Nolan, M.W.Pfaffl, G.L.Shipley, J.Vandesompele, C.T.Wittwer, *Clin. Chem.* 55 (2009) 611-622.
- [5] N.J.Walker, *Science* 296 (2002) 557-559.
- [6] K.J.Livak, *User Bulletin 2*, PE Applied Biosystems (1997).
- [7] W.M.Freeman, S.J.Walker, K.E.Vrana, *BioTechniques* 26 (1999) 112-115.
- [8] R.G.Rutledge, C.Cote, *Nucleic Acids Res* 31 (2003) e93.
- [9] Y.Karlen, A.McNair, S.Perseguers, C.Mazza, N.Mermod, *BMC. Bioinformatics.* 8 (2007) 131.
- [10] M.W.Pfaffl, *Nucleic Acids Res* 29 (2001) e45.
- [11] J.H.Scheffe, K.E.Lehmann, I.R.Buschmann, T.Unger, H.Funke-Kaiser, *J. Mol. Med.* 84 (2006) 901-910.
- [12] S.Tyagi, D.P.Bratu, F.R.Kramer, *Nat. Biotechnol.* 16 (1998) 49-53.
- [13] T.Wang, M.J.Brown, *Anal. Biochem.* 269 (1999) 198-201.
- [14] J.Peccoud, C.Jacob, *Biophys. J.* 71 (1996) 101-108.
- [15] A.Tichopad, M.Dilger, G.Schwarz, M.W.Pfaffl, *Nucleic Acids Res* 31 (2003) e122.
- [16] A.Batsch, A.Noetel, C.Fork, A.Urban, D.Lazic, T.Lucas, J.Pietsch, A.Lazar, E.Schomig, D.Grundemann, *BMC. Bioinformatics.* 9 (2008) 95.
- [17] D.V.Rebrikov, D.I.Trofimov, *Appl Biochem Microbiol* 42 (2006) 455-463.
- [18] J.Wilhelm, A.Pingoud, M.Hahn, *Anal. Biochem* 317 (2003) 218-225.
- [19] J.Wilhelm, A.Pingoud, *Chembiochem.* 4 (2003) 1120-1128.
- [20] A.Larionov, A.Krause, W.Miller, *BMC. Bioinformatics.* 6 (2005) 62.
- [21] T.Bar, A.Stahlberg, A.Muszta, M.Kubista, *Nucleic Acids Res* 31 (2003) e105.
- [22] R.G.Rutledge, *Nucleic Acids Res* 32 (2004) e178.
- [23] R.G.Rutledge, D.Stewart, *BMC. Biotechnol.* 8 (2008) 47.

- [24] J.M.Ruijter, C.Ramakers, W.M.Hoogaars, Y.Karlen, O.Bakker, M.J.van den Hoff, A.F.Moorman, *Nucleic Acids Res.* 37 (2009) e45.
- [25] B.Kaltenboeck, C.Wang, *Adv Clin Chem* 40 (2005) 219-259.
- [26] J.E.Noble, L.Wang, K.D.Cole, A.K.Gaigalas, *Biophys. Chem.* 113 (2005) 255-263.
- [27] S.A.Marras, *Mol. Biotechnol.* 38 (2008) 247-255.
- [28] R.P.Haugland, J.Yguerabide, L.Stryer, *Proc. Natl. Acad. Sci. U. S. A* 63 (1969) 23-30.
- [29] M.K.Johansson. Choosing Reporter_Quencher Pairs for Efficient Quenching Through Formation of Intramolecular Dimers. *Methods in Molecular Biology* . 2006.
Ref Type: In Press
- [30] E.Reynisson, M.H.Josefsen, M.Krause, J.Hoorfar, *J. Microbiol. Methods* 66 (2006) 206-216.
- [31] S.Cikos, J.Koppel, *Anal. Biochem.* 384 (2009) 1-10.
- [32] K.J.Livak, T.D.Schmittgen, *Methods* 25 (2001) 402-408.
- [33] D.Klein, *Trends Mol. Med.* 8 (2002) 257-260.
- [34] C.Ramakers, J.M.Ruijter, R.H.Lekanne Deprez, A.F.M.Moorman, *Neurosci. Lett.* 339 (2003) 62-66.
- [35] M.L.Wong, J.F.Medrano, *BioTechniques* 39 (2005) 75-85.
- [36] M.W.Pfaffl, G.W.Horgan, L.Dempfle, *Nucleic Acids Res* 30 (2002) e36.
- [37] J.Meijerink, C.Mandigers, L.van de Locht, E.Tonnissen, F.Goodsaid, J.Raemaekers, *J. Mol. Diagn.* 3 (2001) 55-61.
- [38] R.Rasmussen, in: S. Meuer, C. Wittwer, and K. Nakagawara (Eds.) *Rapid Cycle Real-Time PCR: methods and applications* Springer Heidelberg 2001 pp. 21-34.
- [39] O.Nordgard, J.T.Kvaloy, R.K.Farmen, R.Heikkila, *Anal. Biochem* 356 (2006) 182-193.
- [40] M.Simard, E.Boucher, P.R.Provost, Y.Tremblay, *Anal Biochem* 362 (2007) 142-144.
- [41] S.Zhao, R.D.Fernald, *J. Comput. Biol.* 12 (2005) 1047-1064.
- [42] R.J.Wiesner, *Nucleic Acids Res* 20 (1992) 5863-5864.
- [43] C.T.Wittwer, M.G.Herrmann, A.A.Moss, R.P.Rasmussen, *BioTechniques* 22 (1997) 130-138.
- [44] A.Gentle, F.Anastasopoulos, N.A.McBrien, *BioTechniques* 31 (2001) 502, 504-506, 508.
- [45] S.N.Peirson, J.N.Butler, R.G.Foster, *Nucleic Acids Res* 31 (2003) e73.
- [46] W.Liu, D.A.Saint, *Anal Biochem* 302 (2002) 52-59.
- [47] P.Cook, C.Fu, M.Hickey, E.S.Han, K.S.Miller, *BioTechniques* 37 (2004) 990-995.
- [48] E.J.Walsh, C.King, R.Grimes, A.Gonzalez, *Biomed. Microdevices.* 8 (2006) 59-64.
- [49] J.H.Marino, P.Cook, K.S.Miller, *J. Immunol. Methods* 283 (2003) 291-306.
- [50] S.Cikos, A.Bukovska, J.Koppel, *BMC. Mol. Biol.* 8 (2007) 113.
- [51] E.J.Kontanis, F.A.Reed, *J. Forensic Sci.* 51 (2006) 795-804.
- [52] V.Luu-The, N.Paquet, E.Calvo, J.Cumps, *BioTechniques* 38 (2005) 287-293.
- [53] J.D.Durtschi, J.Stevenson, W.Hymas, K.V.Voelkerding, *Anal. Biochem.* 361 (2007) 55-64.
- [54] S.A.Bustin, *J. Mol. Endocrinol.* 29 (2002) 23-39.
- [55] P.Y.Muller, H.Janovjak, A.R.Miserez, Z.Dobbie, *BioTechniques* 32 (2002) 1372-1379.
- [56] M.W.Pfaffl, M.Hageleit, *Biotechnol. Lett.* (2001).

- [57] S.A.Bustin. Why the need for qPCR publication guidelines?-The case for MIQE, *Methods* (2010). This Issue.
- [58] S.A.Bustin, R.Mueller, *Clinical Science* 109 (2005) 365-379.
- [59] A.Tichopad, R.Kitchen, I.Riedmaier, C.Becker, A.Stahlberg, M.Kubista, *Clin. Chem.* 55 (2009) 1816-1823.
- [60] J.D.Combes, G.Grelier, M.Laversanne, N.Voirin, S.Chabaud, R.Ecochard, C.Lasset, C.Moyret-Lalle, *Anal. Biochem.* 393 (2009) 29-35.
- [61] J.Vandesompele, P.K.De, F.Pattyn, B.Poppe, R.N.Van, P.A.De, F.Speleman, *Genome Biol.* 3 (2002) RESEARCH0034.
- [62] W.A.Kibbe, *Nucleic Acids Res.* 35 (2007) W43-W46.

Appendix A. Derivation of ΔN (Eq. 3)

ΔN is defined as the distance between the logarithmic curves resulting from cumulative and non-cumulative fluorescence monitoring of PCR amplification. At high cycle numbers this distance approaches a limit of $\log(1/(1-(1/E)))$, because the distance at cycle number C is equal to the geometric series of $1/E$ up to $C-1$:

$$\begin{aligned} \log\left(N_0 \sum_{n=1}^C E^n\right) - \log(N_0 E^C) &= \log\left(N_0 \sum_{n=1}^C E^n / N_0 E^C\right) \\ &= \log\left(\sum_{n=1}^C E^n / E^C\right) \\ &= \log\sum_{n=0}^{C-1} (1/E)^n \end{aligned}$$

and: $\lim_{C \rightarrow \infty} \log\sum_{n=0}^{C-1} (1/E)^n = \log(1/(1-(1/E)))$

The latter equation requires that the PCR efficiency $E > 1$ which is always the case in quantitative PCR.

Appendix B. Derivation of the bias in N_0 when C_{shift} is ignored (Eq. 5)

The observed N_0 value, calculated with the C_q value of a cumulative fluorescence curve will be biased because the observed C_q value is too low due to the C_{shift} (Eq. 4). The starting

concentrations N_0 can be estimated from the quantification threshold (N_q), the PCR efficiency and the number of cycles (C_q) required to reach the threshold.

When the observed N_0 is give by: observed $N_0 = N_q / E^{C_q - C_{shift}}$

and the real N_0 is give by: real $N_0 = N_q / E^{C_q}$

and the bias in defined as the observed N_0 divided by the real N_0 then the bias is:

$$\begin{aligned} \text{bias} &= \text{observed } N_0 / \text{real } N_0 \\ &= N_q / E^{C_q - C_{shift}} / N_q / E^{C_q} \\ &= E^{C_q} / E^{C_q - C_{shift}} \\ &= E^{C_{shift}} \end{aligned}$$

With Eq. 4 for C_{shift} this bias simplifies to $1/(1-(1/E))$.

Appendix C. Derivation of the bias in the gene expression ratio when C_{shift} is ignored

(Eq. 6)

The gene expression ratio is defined as the ratio of the estimated starting concentrations of a

$$\text{target and a reference gene: } \text{Ratio} = \frac{N_{0,target}}{N_{0,reference}} = \frac{N_q / E_{target}^{C_{q,target}}}{N_q / E_{reference}^{C_{q,reference}}} = \frac{E_{reference}^{C_{q,reference}}}{E_{target}^{C_{q,target}}}$$

The observed gene expression ratio, calculated with the C_q value of the cumulative fluorescence curves of target and reference genes will be biased because the C_q values are too low due to the C_{shift} (Eq. 3).

$$\text{When the observed gene expression ratio is: } \text{observed Ratio} = \frac{E_{reference}^{C_{q,reference} - C_{shift,reference}}}{E_{target}^{C_{q,target} - C_{shift,target}}}$$

and the real gene expression ratio is: $real\ Ratio = \frac{E_{reference}^{C_{q,reference}}}{E_{target}^{C_{q,target}}}$

then the bias, defined as observed ratio divided by the real ratio is:

$$\begin{aligned} \frac{observed\ Ratio}{real\ Ratio} &= \frac{E_{reference}^{C_{q,reference}-C_{shift,reference}}}{E_{target}^{C_{q,target}-C_{shift,target}}} \bigg/ \frac{E_{reference}^{C_{q,reference}}}{E_{target}^{C_{q,target}}} \\ &= \frac{E_{reference}^{C_{q,reference}-C_{shift,reference}}}{E_{reference}^{C_{q,reference}}} \bigg/ \frac{E_{target}^{C_{q,target}-C_{shift,target}}}{E_{target}^{C_{q,target}}} \\ &= E_{target}^{C_{shift,target}} \bigg/ E_{reference}^{C_{shift,reference}} \end{aligned}$$

APPENDIX II

Subject: eSirius Notification - New Animal Use Protocol is APPROVED2006-121-12::5

*** THIS IS AN EMAIL NOTIFICATION ONLY. PLEASE DO NOT REPLY ***

AUP Number: 2006-121-12.

AUP Title: Transgenic Mouse Model Of Human Cardiac Disease

Official Notice of Animal Use Subcommittee (AUS) Approval: Your new Animal Use Protocol (AUP) entitled "Transgenic Mouse Model Of Human Cardiac Disease

" has been APPROVED by the Animal Use Subcommittee of the University Council on Animal Care. This approval, although valid for four years, and is subject to annual Protocol Renewal.2006-121-12::5

1. This AUP number must be indicated when ordering animals for this project.
2. Animals for other projects may not be ordered under this AUP number.
3. Purchases of animals other than through this system must be cleared through the ACVS office. Health certificates will be required.

The holder of this Animal Use Protocol is responsible to ensure that all associated safety components (biosafety, radiation safety, general laboratory safety) comply with institutional safety standards and have received all necessary approvals. Please consult directly with your institutional safety officers.

Submitted by: Copeman, Laura S
on behalf of the Animal Use Subcommittee
University Council on Animal Care

CURRICULUM VITAE

Jari Tuomi

Current Laboratory Address

Physiology and Pharmacology
Medical Sciences Building 261, UWO
1151 Richmond St.
London, Ontario, Canada
N6A 5C1

Post Secondary Education

- 2011-2015 M.D. Northern Ontario School of Medicine, Sudbury Ontario.
- 2006-2011 Ph.D. in Physiology and Pharmacology. Department of Physiology and Pharmacology. The University of Western Ontario. Thesis Title: Mechanisms of Atrial Arrhythmia: Investigations of the Neuro-Myogenic Interface in the Mouse
- 2002-2006 Bachelor of Medical Sciences Degree Honors Physiology. Department of Physiology and Pharmacology. The University of Western Ontario.

Honors and Awards

Scholarships and Awards

- 2010-2011 European Cardiac Arrhythmia Society 3rd Place Poster Presentation
- 2010-2011 CIHR CGS-D Banting and Best Doctoral Research Award
- 2010-2011 OGSST (declined in favour of CIHR)
- 2009-2010 OGSST scholarship recipient
- 2009-2010 OGSST scholarship recipient
- 2008-2009 Award Best Cardiovascular Poster Department Research Day
- 2008-2009 Passed Ph.D. comprehensive exams with Distinction
- 2007-2008 OGS scholarship recipient
- 2008-2009 CPS Travel Award
- 2008-2009 Mogensen Trust travel award
- 2007-2008 CPS Travel Award

Teaching Awards

- 2009-2010 Nominated for a Society of Graduate Students Teaching Award
- 2008-2009 Nominated for a Society of Graduate Students Teaching Award

Work Experience in Science

2006-2011 Teaching Assistant in the Department of Physiology and Pharmacology

Other Experiences and Volunteer Activities

2010 VROC/Smarter Science Mentorship Program
2009-2010 TA Union Food Bank Committee
2008-2009 TA Union Needs Based Bursary Committee
2007-2008 Departmental Seminar Committee
2006 Lets Talk Science elementary school challenge group leader
2006-2011 Involvement in the Virtual Researcher On-Call High School Program

Publications

Peer-reviewed publications

Published

Tuomi, J. M., P. Chidiac, D.L. Jones. "Evidence for enhanced M3 muscarinic receptor function and sensitivity to atrial arrhythmia in the RGS2 deficient mouse." *Am J Physiol Heart Circ.Physiol* 298(2): H554-H561(Epub 2009 Dec 4).

Tuomi, J. M., F. Voorbraak, D.L. Jones, J.M. Ruijter. "Bias in the Cq value observed with hydrolysis probe based quantitative PCR can be corrected with the estimated PCR efficiency value." [Methods](#). 2010 Apr;50(4):313-22. Epub 2010 Feb 6.

Tuomi, J. M., K. Tysl, D.L. Jones. "Atrial Arrhythmia in the Connexin 43 G60S Mutant Mouse: A Model of Oculodentodigital Dysplasia" *Am J Physiol Heart Circ Physiol*. 2011 Apr;300(4):H1402-11. (Epub 2011 Jan 14)

In preparation

Tuomi, J. M., D.L. Jones "Junctional Tachycardia in the Mouse can be Prevented by Pacemaker Channel (If) Blockade." In preparation, will be submitted in July 2011.

National/International Meetings and Presentation Abstracts

Tuomi, J. M., D. L. Jones (2011). "Junctional Tachycardia in the Mouse can be Prevented by Pacemaker Channel (If) Blockade." *J Interv Card Electrophysiol* (2011) 30:87-198
[Reviewed Abstract]

- Tuomi, J. M.,** D. L. Jones (2011). "Atrial Tachycardia/Fibrillation in the Connexin 43 G60S Mutant (Ocludentodigital Dysplasia) Mouse" *J Interv Card Electrophysiol* (2011) 30:87-198 [Reviewed Abstract]
- Tuomi, J. M.,** D. L. Jones (2011). "Junctional Tachycardia in the Mouse can be Prevented by Pacemaker Channel (If) Blockade." *Physiol Can. CPS Annual Meeting*. Feb 11-13 (2011)
- Tuomi, J. M.,** P. Chidiac, DL Jones. (2009). "Enhanced M3 receptor activity and susceptibility to atrial fibrillation in RGS2 deficient mice." *Circulation* 120(18, Sup. 2): S712. [Reviewed Abstract]
- Tuomi, J. M.,** K. Tyml, DL Jones. (2009). Abstract 2895: Atrial Arrhythmia in Connexin 40 Deficient and Connexin 43 Mutant Mice. *Circulation* 120: S712-b- [Reviewed Abstract]
- JM Tuomi,** K Tyml, DL Jones. Atrial Arrhythmia in Connexin 40 Deficient and Connexin 43 Mutant Mice. *Canadian Journal of Cardiology*, Vol 25, (Suppl. B): 693. [Reviewed Abstract]
- JM Tuomi,** P Chidiac, DL Jones. Atrial Arrhythmia in the RGS2 Deficient Mice. *Canadian Journal of Cardiology*, Vol 25, (Suppl. B): 576, 2009. [Reviewed Abstract]
- Jones, D. L., Chidiac, P., Sims, S. and **Tuomi, J. M.** Cardiac electrophysiology and arrhythmia in the mouse: effects of temperature and knock out of RGS2. *J. Physiol. Sci.* 59 (Suppl. 1): 123, 2009.
- Tuomi, J.** and Jones, D. L. Atrial arrhythmia in the RGS2 deficient mouse. Margaret Moffat Research Day, #58, March 26, 2009.
- J. Tuomi,** P Chidiac, D.L. Jones. RGS2 Knock out Reveals M3 Mediated Cardiac Electrophysiology in the Mouse. *Acta Physiologica Sinica* 60 (Suppl 1): 81, 2008
- Jones, D. L., **Tuomi, J.**, Ramsay, D., Guiraudon, C. M., Cardinal, R., Page, P., and Guiraudon, G. M. Left atrial neuroablation for atrial fibrillation therapy: a feasibility study. *J. Interv. Card. Electrophysiol.* 21: 171-172, 2008.
- Tuomi, J. M.** and Jones, D. L. Cardiac electrophysiology and arrhythmia in the mouse. *Physiol. Can.* <http://www.cps.cfbs.org/program.html>, pg 24-25, 2008.
- Jones DL, **Tuomi J,** Sims S. Electrophysiology, Calcium Handling, and Gap Junctions in Transgenic Mice Overexpressing the Human Mutant PRKAG2 Gene. *Physiology Canada*. 2007.
- Jones, D. L., **Tuomi, J.**, Ramsay, D., Guiraudon, C. M., Armour, J. A., Cardinal, R., Page, P., and Guiraudon, G. M. Left atrial neuroablation for atrial fibrillation: a feasibility study. *Can. J. Cardiol.* 23 (Suppl. C): 72C-73C, 2007. [Reviewed abstract]

Jones, D. L., **Tuomi, J.**, Ramsay, D., Guiraudon, C. M., Armour, J. A., Cardinal, R., Page, P., and Guiraudon, G. M. Left atrial neuroablation for atrial fibrillation: a feasibility study. *Can. J. Cardiol.* 23 (Suppl. C): 225C, 2007. [Reviewed abstract]

Tuomi, J. M., Chidiac, P. and Jones, D. L. The regulator of G-protein signalling 2 (RGS2) modulates AV nodal function: removing the brake on G α q reveals a role for M3 muscarinic receptors. *Proc. 8th Annual Joint Great Lakes GPCR Retreat & Club de Récepteur à Sept Domaine Transmembranaires du Québec.* Abst #72, 2007.